Real-time Process Monitoring for Froth Flotation Processes using Image Processing and Dynamic Fundamental Models

by

Khushaal Popli

A thesis submitted in partial fulfillment of the requirements for the degree of

Doctor of Philosophy

in

Process Control

Department of Chemical and Materials Engineering

University of Alberta

Abstract

Froth flotation is a crucial and complex process, which has been used in various industries for the purpose of separation and beneficiation. Various classes of factors including chemistry, operational, or equipment influence the process outputs. Its complex nature makes it difficult to control and monitor the process. For instance, a small disturbance in any of these classes of factors propagates to the final process output by affecting various micro-scale sub-processes. In addition to this, process measurements are either accurate with slower sampling time, or less accurate and expensive for faster sampling times. The overall objective of this thesis is to develop a monitoring scheme aided with soft sensor models for online measurements for process outputs. Systematic study was undertaken in this thesis to develop monitoring schemes for mechanical cell flotations, starting from pure galena mineral flotation to synthetic mixtures of galena and quartz, and finally extending it to the real industrial Pb-Zn sulfide ore.

A dynamic process model is required for the monitoring purposes. It was proposed that a fundamental model, providing the in-depth understanding of the process would perform better than empirical models to capture the disturbances in the process. For this purpose, a framework was developed for dynamic fundamental modeling that incorporates the mathematical relationships between micro-scale sub-processes and macro-scale transportation. All the significant sub-processes such as bubble-particle attachment, detachment, entrainment, and drainage, were included in the framework . Both pulp and

froth phases were considered in the model development phase.

Relationship between the froth visuals and process performance were explored to develop soft sensors for online measurements for the process outputs, which are, grade and recovery. A commercial package, VisioFroth, by Metso® Minerals was used to extract real-time images and its features. Image features were used to develop soft sensor models for process outputs. Soft sensor model were developed based on machine learning algorithms, such as, Principal Component Regression, Partial Least Squares Regression, Random Forest, and Support Vector Machines. Soft sensor study was also extended to oil sands extraction process to demonstrate its applicability in other industries that use flotation on a regular basis. With bitumen being darker in color, it was more challenging problem as compared to the mineral flotation. However, set of robust soft sensor models, that were valid on various flotation conditions showed a promising potential in other real-time objectives such as model predictive control or real-time optimization.

Finally, real time measurements were reconciled with the dynamic modeling framework for state and parameter estimation using extended Kalman filter. Estimation of model parameters that represent flotation sub-processes, provides real-time information about the process performance. Heuristics were developed for monitoring the process and identifying the disturbances though monitoring of parameter estimates. Various classes of disturbances were artificially created in batch flotation experiments in mechanical cell flotation. This included variation in feed particle size, reagent dosages, air flow rate, and impeller speed. Estimated parameters were successfully able to track the disturbances and identify its root for remedial actions. Developed scheme was also used to monitor the entrainment sub-process by decoupling the total recovery and identifying different components. Entrainment monitoring further helps in increasing the product grade while maintaining the desired recovery of the minerals. All the monitoring heuristics and soft sensor models were implemented and developed using batch flotation in a mechanical flotation cell.

Preface

The work in this thesis is based on the research carried under the supervision of Dr. Vinay Prasad and Dr. Qi Liu. It is a paper based thesis, and contribution and details of each chapter/paper are discussed below.

Chapter 2 of this work is accepted as Popli, K.; Sekhavat, M.; Afacan, A.; Dubljevic, S.; Liu, Q.; Prasad, V., 2015 "Dynamic Modeling and Real-Time Monitoring of Froth Flotation". *Minerals*. Myself and Mr. Sekhavat conducted the experimental investigations on batch flotation and performed the dynamic modeling simulations. I performed the investigations on image processing and correlating those measurements to recovery. Dr. Prasad, Dr. Liu and Mr. Afacan guided in the design of the experimental investigations Dr Vinay Prasad and Dr. Dubljevic supervised the development of the modeling and soft sensing-based monitoring efforts. Under the guidance of Dr Vinay Prasad, I wrote the initial drafts of the manuscripts, and all authors contributed to the editing of the final manuscript.

Chapter 3 of this work is submitted as Popli, K.; Afacan, A.; Liu, Q.; Prasad, V., 2017 "Monitoring the Feed Particle Size in Froth Flotation using Parameter Estimation with Fundamental Dynamic Models ". *Chemical Engineering Science*. I performed the batch flotation experiments, induction time measurements, developed modeling framework, and performed simulations. I investigated the image features and developed the soft sensor models. Dr. Liu and Mr. Afacan helped in the designing of experiments. Dr. Prasad guided the soft sensor development and its implementation for monitoring. I wrote the first draft of the manuscript, which was subsequently edited by other authors.

Chapter 4 of this work is submitted as Popli, K.; Liu, Q.; Afacan, A.; Prasad, V., 2017 "Real-time Monitoring of Entrainment using Fundamental Models and Froth Images ". *Minerals Engineering*. I conducted the batch flotation experiments. I developed the entrainment modeling framework and simulations. I also studied the image features, their correlation to process outputs and applied it to the developed entrainment monitoring scheme. Mr. Afacan, Dr. Prasad, and Dr. Liu helped in the experimental designing and batch flotation experiments. Dr. Prasad supervised the soft sensor development, modeling structure development, and state estimation. I drafted the initial version of the manuscript and all authors contributed to the final version.

Chapter 5 of this work is submitted as Popli, K.; Liu, Q.; Afacan, A.; Prasad, V., 2017 "Development of Online Soft Sensors and Dynamic Fundamental Model-Based Process Monitoring for Complex Sufide Ore Flotation ". *Minerals Engineering*. I conducted the batch flotation experiments using mechanical flotation cell under the guidance of Dr. Liu and Mr. Afacan. Using Support Vector Regression, I trained and developed soft sensor models for online process outputs. I developed the modeling framework and combined it with image based measurements for state and parameter estimation. I also studied the image features, their correlation to process outputs and applied it to the developed entrainment monitoring scheme. Dr. Prasad was involved in the model development and soft sensor development using machine learning. I wrote the initial version of the manuscript, which was subsequently edited by all authors.

Chapter 6 of this work is submitted as Popli, K.; Maries, Victor.; Afacan, A.; Liu, Q.; Prasad, V., 2017 "Development of a Vision-Based Online Soft Sensor for Oilsands Flotation Using Support Vector Regression and its Application in the Dynamic Monitoring of Bitumen Extraction ". *The Canadian Journal of Chemical Engineering*. I performed the bitumen extraction experiments using oil sands ores. Mr. Maries helped in deciding the experimental conditions and developing experimental design. Mr. Afacan was involved in validating the experimental design. Under the guidance of Dr. Liu and Dr. Prasad, I analyzed the product samples, performed Dean Stark measurements, and developed image based soft sensor. I prepared the initial draft and all authors contributed to its editing for the final version.

To mom and dad, for their continuous love and motivation

Acknowledgements

Firstly, I am sincerely thankful to my professors, Dr. Vinay Prasad and Dr Qi. Liu, for providing me with this opportunity and continuous supervision. I would like to thank Dr. Vinay Prasad for his continuous support and guidance that kept me motivated throughout this journey. It was my extreme pleasure to learn various aspects of control and modeling under his guidance.

I would also like to express my gratitude to Dr. Qi Liu for supporting me throughout and guiding me with his immense mineral processing knowledge. My mineral processing knowledge has reached a higher level following many discussions with him. I also thank Artin Afacan for helping me throughout with all the experimentation knowledge. Various discussions regarding the flotation process and academic career were always helpful and interesting. I take this opportunity to sincerely thank Dr Stevan Dublejevic for sharing his expertise on differential equations and always motivating me to reach higher level. I also thank Dr Manisha Gupta for her encouragement and motivation.

I am very grateful to all the researchers and staff that helped me with my experiments and research. I would like to thank Dr Kaipeng Wang for his help with flotation experiments and laboratory etiquette. I would like to appreciate the efforts by the staff at National Institute of Nanotechnology, Brittany, Lisa, and Dr Xiaoli for their continuous help with analytical instruments. I would also like to thank Dr Qingxia Liu for providing me access to induction timer instrument and training. I also thank Dr Arno de Klerk for allowing me to use XRF instrument in his lab.

I would like to thank my colleagues and group-mates for the scientific discussions and continuous support. This journey would have been way more difficult without the support of my lovely friends. Thank you all for all the good memories and uninterrupted motivation and support. No words can describe my appreciation for my dear family. Thank you Mummy, Papa, Uncle, Aunt, and Dheeraj for being there. Special thanks to my sisters Dimple and Tina for their love and support.

Lastly, I would like to acknowledge the funding from Canadian Centre for Clean Coal/Carbon and Mineral Processing Technologies (C5MPT), and The Natural Sciences and Engineering Research Council of Canada (NSERC). I would also like to thank our industrial partners, Teck Minerals and Canadian Natural Resources Ltd., for their continuous services and support.

Contents

List of Tables

List of Figures

Chapter 1

Introduction

1.1 An introduction to froth flotation

Froth flotation is the most commonly used separation process in the mineral industry. Since the inception of the flotation process in industry in 1905, various researchers have contributed to the continuous innovation and development in the understanding of the process (Fuerstenau et al., 2007). Flotation has also been applied to achieve concentration and separation in other industries, such as coal, paper recycling, wastewater treatment, and oil sands extraction (Rao and Liu, 2013; Rubio et al., 2002; Xing et al., 2015, 2017). Among the various types of mineral ores, sulfide, copper, and zinc ores are extensively beneficiated using froth flotation (Fuerstenau et al., 2007). Froth flotation is primarily driven on the basis of differences in surface properties of the valuable and the gangue minerals present in the ore. Flotation can be described as the sequence of following physio-chemical events: i) grinding the ore to obtain sufficient liberation between desired minerals and gangue minerals, ii) mixing the ore slurry with the required dosage of different reagents to impart surface hydrophobicity to the desired minerals and maintain selectivity, iii) attachment of the desired hydrophobic mineral surface to the rising bubbles, and iv) upward motion of the air bubble-particle aggregate to the top of the cell and eventually skimming the desired mineral-rich froth layer (Dewitt, 1940; Ata, 2012; Yianatos et al., 2009).

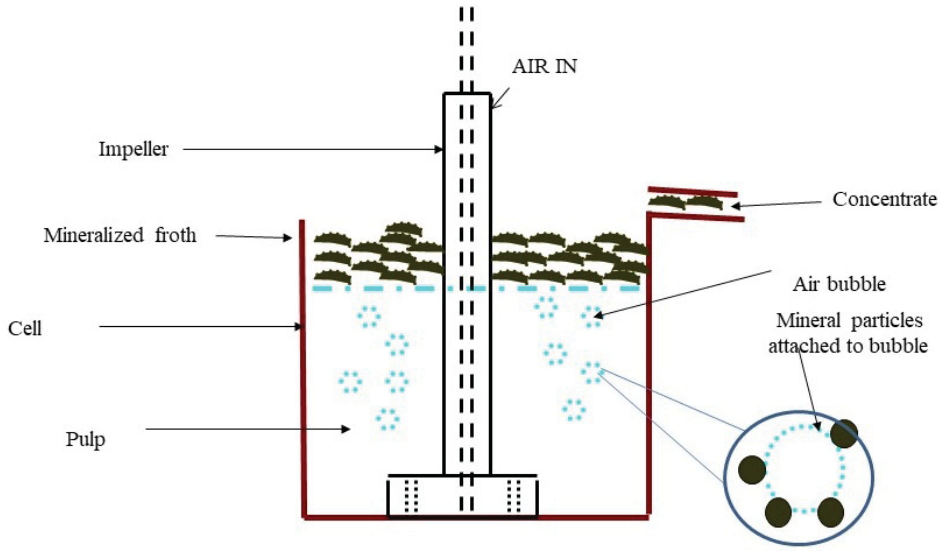

Figure 1.1: A schematic representation of flotation process

A schematic diagram of a flotation cell is given in Figure 1.1 that demonstrates the basic flotation principle. It shows that the particles attached to the bubbles in the pulp are rising up the slurry against gravity to reach the froth layer. As seen in Figure 1.1, the flotation cell creates two different sections, pulp and froth, based on the air present in the cell. Various sub-processes happen in the flotation cell to recover the valuable mineral while maintaining a desired quality or grade. These sub-processes are discussed below.

Attachment and detachment The attachment sub-process is defined as the successful capture of the particle with hydrophobic surface layer by the rising bubble and forming a bubble-particle aggregate (Derjaguin and Dukhin, 1993). Detachment, on the other hand, is the dislodging of the particles from the formed aggregate when the kinetics energy exceeds or equals the detachment energy (J. Ralston and Mischuk, 1999).

True flotation, entrainment, and drainage These sub-processes affect the particle movement across the pulp-froth interface. A mineral particle is said to be recovered by true flotation when it rises up the froth while being attached to the bubble. On the contrary, entrainment is defined as the non-selective mechanical transfer of suspended mineral particles (hydrophobic and hydrophilic) from the pulp to the froth section, and subsequently to the concentrate (Wang et al., 2016; Gong et al., 2010). Drainage is the fall-back of the free particles from the froth to the pulp section through the plateau border, defined as the hydrodynamic layer between the intersecting bubbles. Phenomena such as bubble burst and coalescence in the froth section lead to the detachment of particles from bubbles and further possibility of re-attachment, transfer to concentrate, or drainage to the pulp section.

Flotation is a complex process with many physical and chemical sub-processes and the presence of multiple phases (solid, liquid, and gas). Various factors are responsible to achieve the desired separation and maintain the favorable conditions for the flotation. These factors can be classified as being related to chemistry (reagents), equipment (cell sizing and design, air flow, mixing rate), and operation (feed properties, feed rate, liberation, particle size, pulp density, pH)(Kawatra, 2002).

Reagents have a crucial role in the process to enable the separation. The different types of reagents are collectors, frothers, activators, depressants, and pH regulators (Dewitt, 1940). Collectors are organic chemicals responsible for developing a hydrophobic layer, selectively on the valuable mineral for bubble-particle attachment. Frothers are used to stablize the froth by lowering the surface tension of the liquid and increasing the film strength of the gas bubbles (Bulatovic, 2007; McFadzean et al., 2016). A stable froth leads to a higher mineral recovery. Activators and depressants influence the selective interaction of a mineral particle with the collector. The activator improves the conditions for interaction and strengthens the attachment process. In contrast, depressants modify the mineral particle-collector interaction to inhibit the mineral hydrophobization and make the mineral hydrophilic with respect to the attachment sub-process (Bulatovic, 2007). Finally, pH regulators also improve the mineral particle-collector interaction by controlling the hydrogen ion concentration and consequently, the pH of the pulp.

Equipment factors play an important role in maintaining the conditions required for the mineral separation. The air flow rate affects the mineral recovery and product grade through its relationship with bubble size, plateau border area, air hold-up, flotation rate constant, and attachment sub-process (Fuerstenau et al., 2007; Laplante et al., 1983). The impeller provides the turbulent energy and its speed has an impact on the attachment and detachment sub-processes. Operational factors such as feed rate, liberation, pulp density, and particle size also have relationships with various flotation sub-processes and directly affect process outputs (mineral recovery and grade). For instance, feed particle size controls the mineral liberation and affects attachment and detachment kinetics. It should be emphasized that all the flotation process factors discussed above should be considered for a smooth and upset-free operation. Disturbance in any of the factors have an influence on other factors, making it difficult to identify the root cause of a disturbance. The interdependence of the factors causes difficulty in flotation predictive modeling and its validation (Klimpel, 1995; Rao et al., 1995).

1.2 Motivation: Disturbances, modeling, control, and measurements

The main objective of the flotation process is the maximization of grade and recovery while maintaining stable operation (Fuerstenau et al., 2007). However, highly varying feed properties and other related operating parameters, potentially leading to poor froth stability, can result in reduced grade and/or recovery of the desired mineral. With the depletion in easily separable ore and high processing costs, it is of utmost importance to identify and reject any disturbance causing a drop in quality or mineral recovery. A robust monitoring scheme would aid in identifying the root cause of various disturbances in the process.

A complete understanding of the system based on its dynamic modeling will lead to better process control, thereby increasing the profitability. Dynamic modeling can be approached in different ways: empirical modeling (based on experimental data), fundamental modeling (based on first principles) and semi-empirical (based on both data and first principles). Flotation modeling began with an in-depth understanding of the pulp phase. However, various researchers explored the importance of froth phase and its modeling in the 1960 (Arbiter and Harris, 1962; Harris et al., 1963; Harris and Rimmer, 1966). The froth phase is considered to be significant and needs to be studied in detail for better understanding of the flotation process (Vera et al., 2002). In most of the modeling studies, a flotation cell has been divided into two phases: pulp and froth. Several empirical and semi-empirical models have been developed to describe the flotation processes by studying impeller speed and air flow rate (Gorain et al., 1998). Woodburn conducted the first ever research to use the air recovery for flotation modeling (Woodburn, 1970). Later on, Hadler et al. (Hadler et al., 2012) studied the relationship between air rate, froth depth and air recovery and found that the recovery was higher with deeper froth (Hadler et al., 2012).

Several kinetic models have also been developed to study the flotation rate with pulp and froth phase dynamics (Vera et al., 2002). Hanumanth et al. (Hanumanth and Williams, 1992) developed a three-phase model by adding an additional phase to the froth section. Froth cell was divided into three sections, the pulp phase, primary froth phase (just above the interface), and the secondary froth phase (rest of the froth) (Hanumanth and Williams, 1992). Most of the modeling studies on entrainment were focused towards developing a empirical relationship between water recovery and entrainment recovery (Cilek and Umucu, 2001; Bisshop J.P. & White, 1976; Warren, 1985; Kirjavainen, 1992). One such model is given in equation 1.1 (Cilek and Umucu, 2001).

$$R_g = x^{0.2684} - 0.0276T_f(R_w^{-1.10311} - 0.1186V_a) \tag{1.1}$$

where, R_g is entrainment recovery, x is solids %, V_a is the aeration rate, T_f is the froth thickness, and R_w is the water recovery.

Recently, population balance based modeling has been explored to capture dynamic changes in bubbles in the froth phase (Bhole et al., 2008; Cruz, 1997). These changes include bubble bursting and coalescence. Sawyerr et al. (Cruz, 1997) have developed bubble population balances on two statistically homogeneous zones: the impeller zone and the bulk zone, as shown in Figure 1.2. It considers that there is no bubble breakage in the bulk zone, which is mainly characterisized by bubble coalescence. During the last 25 years, a few researchers have been involved with models for column flotation (Vazirizadeh et al., 2015a,b; Bouchard et al., 2014; Tuteja et al., 1994; Cruz, 1997). These models connect the hydrodynamic process conditions to the mineral recovery and improve the theoretical understanding of column flotation.

Currently, empirical models are employed in various process control applications in the mineral process industry (Ding and Gustafsson, 1999). Empirical models are often linear and perform well around certain operating conditions at which they were identified. Also, they do not provide much useful information about the fundamental understanding of the process.

In summary, several attempts have been made to understand the flotation process through modeling and present a structure for applications such as process optimization,

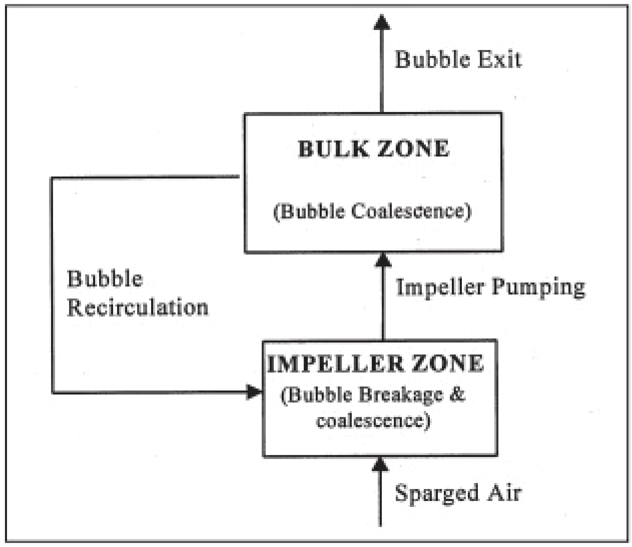

Figure 1.2: Different zones considered for bubble population modeling: reproduced from (F. Sawyerr D.A. Deglon and O'Connor, 1998)

design, and control. The developed theoretical models can be mainly classified as micro-scale models that explain sub-processes such as bubble-particle collision, attachment, or detachment in depth (Derjaguin and Dukhin, 1993; Parkinson and Ralston, 2011; Yoon and Mao, 1996; Dobby and Finch, 1987; Bascur, 2000). These models provide fundamental explanations using surface forces and Derjaguin-Landau-Verwey-Overbeek(DLVO) theory (Dobby and Finch, 1987; Yoon and Mao, 1996). On the other hand, macro-scale kinetic models provide information about mineral transfer from feed to the concentrate through flotation rate constants (Vera et al., 2002; Hanumanth and Williams, 1992). These models typically use experimental data to identify the model parameters and do not connect it to the microscopic level sub-processes. In the absence of a complete modeling framework that connects these two scales of operation, there is no way of determining which of multiple possible disturbances has affected the process.

Laurila et al. (Laurila et al., 2002) construct a hierarchy for process control in flotation processes, as shown in Figure 1.3; this consists of four levels and aims at maximizing profit for the industry. Instrumentation, or measurements are vital components for developing control schemes. Basic process control for flotation deals with controlling the primary variables, which are pulp level, air flowrate, and reagent dosages (Shean and Cilliers, 2011). Controlling these variables at the desired set points indirectly controls the main process outputs, mineral grade and recovery. However, advanced process control (APC) directly controls the main process outputs using modern control techniques such as model predictive control with real-time optimization. APC works toward developing a robust system which is unaffected by changes in process conditions. The majority of the APC systems in flotation are designed to control mass pulls, specific stream grade, and recovery. Mass pull, or the amount of concentrate collected, is measured using density and flowrate of the concentrate streams (Shean and Cilliers, 2011). At industrial scale, mineral separation is achieved thorough a flotation circuit that consists of various flotation cells. Controlled variables in each cell are connected and controlled by manipulating the respective input variables for the cell. Each cell is also characterized by individual operational constraints that have to be considered for control schemes (Bergh and Yianatos, 2011). Circuit-wide control for flotation, which is frequently applied in mineral industries, makes it difficult to target disturbance in any given cell (Singh et al., 2003; Bergh and Yianatos, 2013). It is therefore necessary to design control schemes that are developed for individual cells and are easily scalable to the whole circuit. New monitoring and control schemes should be able to identify and reject the disturbances while informing about the root cause and maintaining desired grade and recovery.

As stated, instrumentation and measurements are the basic block for any control scheme for froth flotation. Flow sensors are employed to measure the flow rates for different streams, which are further used for pulp level control purposes (Laurila et al., 2002). Other similar sensors employed are pH meters, temperature sensors, reagent flows, and interface detection sensor. Grade and recovery, being the most important

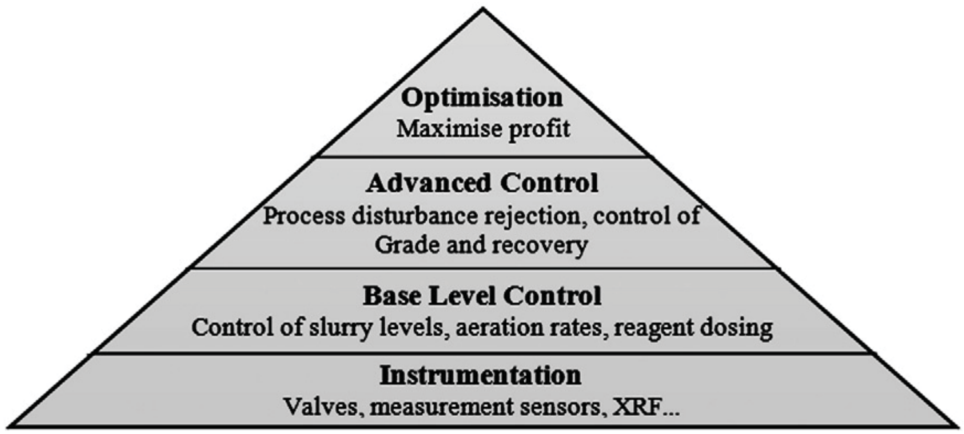

Figure 1.3: Hierarchy levels for process control in froth flotation operation: reproduced from (Laurila et al., 2002)

process variables, are measured through elemental assaying. Typically, XRF is used to measure the contents for the process streams in two ways: a) Offline laboratory analysis through XRF, and b) Online sample analyzer (OSA). Offline measurements through XRF suffer the drawback of long delays that make it challenging to use them for control or monitoring applications (Laurila et al., 2002). A typical on-stream XRF analyzer is presented in Figure 1.4. It consists of multiple sampling points with different flow rates and requires frequent calibration. Online sample analyzers have an advantage of low sampling time of 15 seconds to 1 minute, with cycle time of 5 to 15 minutes (Laurila et al., 2002). However, OSA instruments are expensive to maintain, hard to calibrate and, have lesser accuracy than the offline laboratory measurements (Jahedsaravani et al., 2017; Holtham and Nguyen, 2002). As a consequence, we need a better alternative for online measurements for mineral grade and recovery. The alternative method should be fast, accurate, robust, inexpensive, and require lesser efforts on calibration.

Various researchers have tried to explore the relationship between froth surface visuals and mineral content (Aldrich et al., 2010; Barbian et al., 2007; Bonifazi et al., 2000; Holtham and Nguyen, 2002; Leiva et al., 2012; Moolman et al., 1996; Duchesne, 2010;

Liu et al., 2004; Bartolacci et al., 2006; Mehrabi et al., 2014). Machine vision research has been primarily in the field of developing algorithms for extracting maximum froth visual features (Mehrabi et al., 2014; Jahedsaravani et al., 2017; Aldrich et al., 2010; Ventura-Medina and Cilliers, 2002; Wang and Stephasson, 1999; Wang et al., 2003) and controlling the mass pull through froth velocity (Holtham and Nguyen, 2002). In other research, some researchers have tried to develop a mathematical correlation for grade using few image features such as color, bubble size, froth stability, or froth velocity (Supomo et al., 2008; Runge et al., 2007; Marais and Aldrich, 2010; Bonifazi et al., 2000; Hargrave and Hall, 1997). One such study by Runge et al. (Runge et al., 2007) developed a correlation between copper grade and average bubble size for a particular flotation test (Runge et al., 2007). The results, reproduced in Figure 1.5, demonstrate that although there is a good correlation, a better model before being applied in a control and monitoring framework. Combining information from all the possible visual features would be a better input set for measuring real-time grade and recovery. Despite various studies related to machine vision, operators rely on their experience and eye vision apart from XRF for qualitative assessment before taking any control decisions. It is therefore necessary to provide a replacement supplement to OSA that could also estimate grade and recovery in real-time.

1.3 Thesis contribution

It is challenging to develop a monitoring scheme for froth flotation with many variable interactions and process variables affecting the outputs, which are mineral grade and recovery. This thesis addresses some of the challenges described in previous sections. The thesis provides original contributions in three important areas for the improvement in froth flotation understanding and monitoring. These include *dynamic modeling, online*

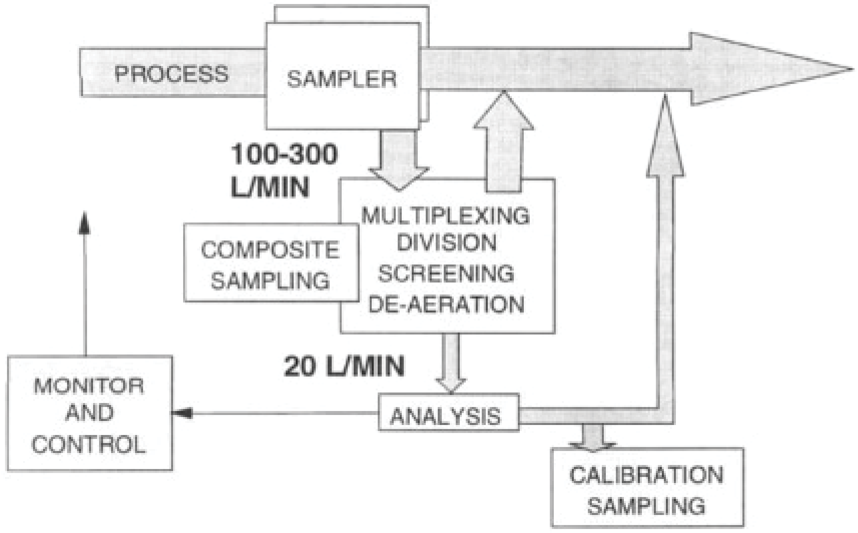

Figure 1.4: Use of a typical online XRF analyzer for process monitoring and control: reproduced from (Laurila et al., 2002)

measurements, and monitoring scheme. The overall scheme is developed to solve the following practical concerns and objectives in batch mechanical cell-based flotation:

- Establish a method to inferentially measure the mineral grade and recovery in real-time
- Demonstrate the validity of the proposed method of measuring real time grade and recovery for other applications of froth flotation
- Identify the disturbances in equipment-based variables such as impeller speed and air flow rate
- Identify the disturbances in feed particle size and its effect on flotation performance
- Decouple the overall flotation recovery into recovery by *true flotation* and recovery by *entrainment*

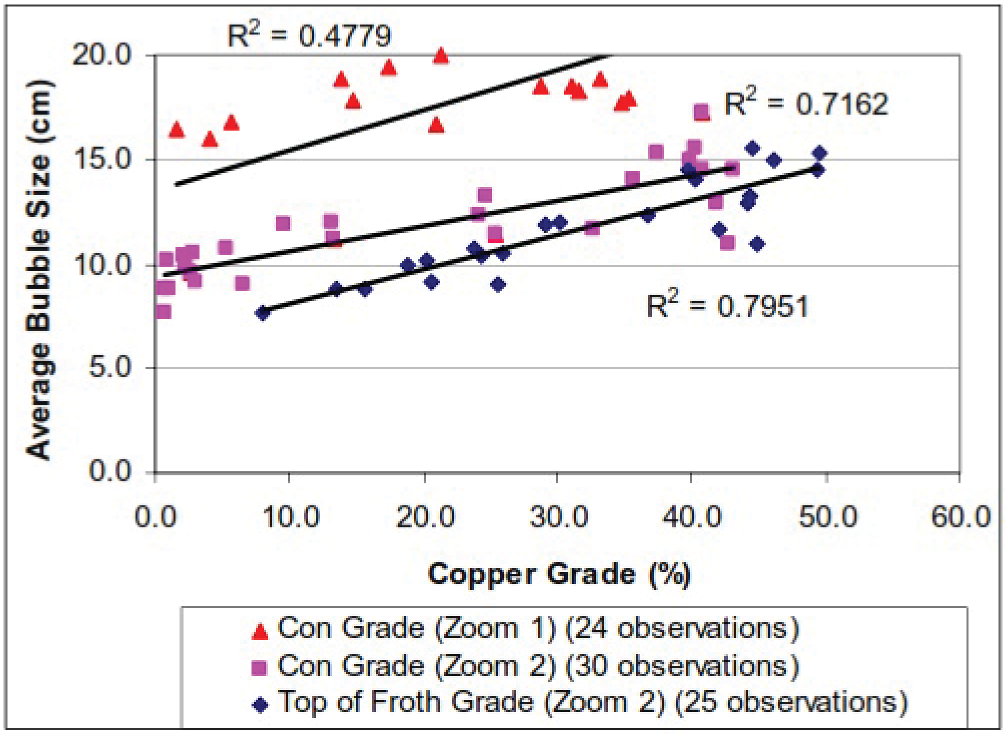

Figure 1.5: Correlation between average bubble size (cm) and copper grade (%) in a flotation test: reproduced from (Runge et al., 2007)

- Identify the disturbances in collector reagents and its effect on flotation performance
- Implement the sensing and monitoring scheme on froth flotation for benefication of real industrial ore

The three areas of theoretical developments as mentioned above and their implementation using mechanical cell flotation are briefly explained in the following subsections.

1.3.1 Development of a dynamic modeling framework to connect sub-processes to process outputs

A multi-scale modeling structure was developed to combine micro-scale and macro-scale phenomena to the overall flotation process. A compartment-based set of models were explored further to include sub-processes in the flotation. Different sets of compartments were used with two compartments of gas phase and slurry phase in each pulp and froth section. The modeling framework utilized the fact that a mineral particle could be present in any one of the compartments at any given instant of time. Ordinary differential equations (ODE's) were used to represent the states of mineral particles and their transfer from one compartment to another. Intra-phase and inter-phase sub-processes were considered in the set of ODEs. These sub-processes include attachment, detachment, entrainment, drainage, and transfer from froth to concentrate. A fundamental description of the micro-scale sub-processes were incorporated to the overall modeling framework. For instance, the attachment rate constant, a parameter in the attachment sub-process, is a crucial parameter for mineral separation. Its dependence on factors such as particle size, bubble size, impeller energy was included in the model through micro-scale description of probabilities of collision, attachment, and stability. In conclusion, a fundamental modeling framework was developed to establish the relationship of various process parameters to the overall process outputs through the respective sub-processes at the micro-scale.

1.3.2 Development of a inferential image based model to obtain the online measurements of mineral grade and recovery

The commercial froth image package VisioFroth by Metso® Minerals was used to capture froth surface images and extract image features. These features extract sufficient information in the form of 22 variables, ranging from static features such as different color components, bubble size and froth width to dynamic features such as froth velocity, stability and collapse rate. Bubble segmentation, which is used in the analysis, is shown in Figure 1.6. VisioFroth uses a watershed algorithm to obtain the required segmentation. Image features were used to develop online soft sensors using various machine learning techniques. Principal component analysis (PCA) was used to study the correlation among the image features and understand the data collinearity. Supervised machine learning regression algorithms were used for the correlation of image features to the process outputs. These algorithms included principal component regression (PCR), partial least square regression (PLSR), random forest, and support vector regression (SVR). Also, a mass balance approach was applied to estimate the mineral recovery using image-based sensing of online grade and solids recovery for multi-component flotation. Soft sensor model development considered the necessary robustness for the image based methods and showed the applicability at diverse various process conditions without the need of re-calibration. The VisioFroth package was chosen as it is already installed at various mineral and oil sands industries across Canada. However, it is not fully utilized to its potential as it is mainly used to control mass pull for the concentrate stream, and this work expands its potential use. Additionally, soft sensors are easy to maintain and do not require extra capital for the installation.

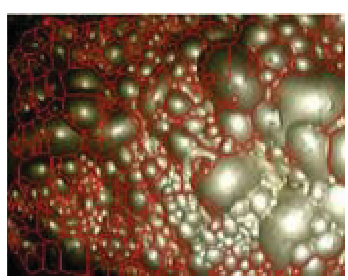

Figure 1.6: Bubble segmentation for a sample image extracted through VisioFroth

1.3.3 Monitoring and disturbance identification

The model framework described in section 1.3.1 is used to develop a state-space system of equations. The model was reconciled with online process measurements as described in section 1.3.2. Various model parameters were used to characterize the sub-processes and concentration of mineral particles in different compartments were considered as the states of the model. Based on the observability analysis and available process measurements, the model was updated in real-time using online measurements and state estimation. Parameters were augmented to the states for parameter estimation. An extended Kalman filter (EKF) was used for the state and parameter estimation. The estimated parameters were used to track the dynamics of the process and identify disturbances by comparing the dynamic trend to the normal operating conditions. Heuristics could be developed for various possible disturbances in the flotation process. Also, updated model and parameter estimates could be used to inferentially measure the contribution of entrainment to the overall mineral recovery. Moreover, entrainment estimation is very useful to target the reduction in entrainment of a specific mineral to improve the product grade while maintaining its optimum recovery. The overall proposed scheme can be implemented at the flotation circuit level while being applied in individual cells. In the case of a drop in mineral recovery or grade, it is then possible to track the cell that is causing the disturbance and identify its root cause to provide a remedy for the upset.

1.3.4 Diverse process scenarios and implementation of monitoring scheme and soft sensors

It was required to develop the monitoring schemes and soft sensors for varied process and feed conditions. A JK Teck flotation cell was used for the batch flotation with controllable impeller speed and air flow rate. VisioFroth system was installed on the mechanical cell for image features for all the flotation studies. Following types of flotation scenarios were explored for this study:

- Pure galena (lead sulfide, PbS) flotation
- Flotation for synthetic ore comprising of galena and quartz (silica, SiO_2)
- Flotation for real industrial ore mainly consisting of galena and sphalerite (zinc sulfide, ZnS) among other gangue minerals
- Oil sands extraction using batch flotation to obtain concentrated bitumen

Diverse process conditions were used to show the applicability of the developed methods and their robustness. Experiments were designed to artificially create the disturbances in order to develop and validate heuristics for monitoring and disturbance identification. Flotation conditions were used to represent the industrial scale flotation. Oil sands flotation was used to understand the relationship between froth images and bitumen grade and recovery. Darker surface images for the oil sands flotation with lesser variation compared to the mineral processing application provided a challenging environment for the soft sensor development. Inclusion of oil sands flotation in the study shows the potential of the image-based soft sensor development to other flotation applications.

1.4 Thesis outline

The thesis is organized as the collection of five primary chapters and a chapter on conclusions, aside from this introductory chapter. Batch flotation experiments were conducted for different studies and designed based on the requirements. The chapters are described as follows.

Chapter 2: *Dynamic Modeling and Real-Time Monitoring of Froth Flotation*
The chapter focusses on the batch flotation of pure galena mineral. A compartmental model is expanded to include sub-processes with the help of model parameters. Considering the feed is pure mineral, froth images were correlated to the mineral recovery using PCR and PLSR. It demonstrates the application of EKF algorithm for parameter estimation with attachment and detachment rate constant as the selected parameters. A diverse range of experiments is used to create and track disturbances in air flow rate and impeller speed. This chapter provides a solid proof of concept of the developed monitoring algorithm for froth flotation.

Chapter 3: *Monitoring the feed particle size in froth flotation using parameter estimation with fundamental dynamic models*
This chapter extends the study for pure mineral flotation to understand the effect of feed particle size. It is not uncommon for disturbances to occur in the feed particle size. The work in this chapter focuses on proposing a method for feed particle size tracking based on feedback control that can replace the traditional feedforward control approach for feed particle size. A dynamic model framework similar to that of Chapter 2 is used to study the system with inclusion of the effect of feed particle size. Two feed particle size tracking methods are proposed and compared using batch flotation experiments for different particle size distributions. Additionally, a random forest machine learning method is implemented and proposed for inferential sensing of pure mineral recovery through froth images.

Chapter 4: *Realtime entrainment monitoring using fundamental models and froth images*
The crucial issue of entrainment is addressed in this chapter. It is of great importance to

reduce entrainment for increasing mineral grade in the concentrate. The chapter expands on the entrainment and drainage sub-processes in the dynamic model. Experiments are conducted with a synthetic mixture of galena and quartz used as feed to represent a mixture of hydrophobic and hydrophilic minerals, respectively. Support vector machine algorithms are utilized for image- based sensing of grade and recovery for both the minerals using froth images. The image-based models extends the previously developed algorithms from single component feed to a two-component mixture. Parameter estimation for entrainment and drainage related model parameters are used to decouple the recovery components to *true flotation* and *entrainment* recovery. Additionally, the effects of feed particle size on entrainment are demonstrated in this chapter. The individual recovery estimation allows the control algorithms to specifically target the gangue mineral entrainment and improve the process efficiency.

Chapter 5: *Development of online soft sensors and fundamental model based process monitoring for complex sulfide ore flotation*

This chapter extends the study towards a real industrial complex sulfide ore obtained from Alaska red dog mine. The ore consists of galena and sphalerite as the desired minerals and pyrite, quartz, and barium oxide as the gangue minerals. Soft sensor model development solves the challenge associated with developing image-based soft sensors for multi-stage flotation processes through support vector machine algorithms. Flotation conditions including the grinding size and reagent dosages are obtained from industrial standards to represent a realistic flotation scenario. It establishes a methodology for online measurements on grade and recovery for both the stages of flotation of complex sulfide ores, which are the lead rougher and zinc rougher stages. A fundamental modeling framework is used for multiple stages to monitor the flotation process. Additionally, heuristics are developed for disturbances in reagent dosages. Monitoring and soft sensing is demonstrated for a full scale multi-stage flotation of a complex sulfide ore.

Chapter 6: *Development of a vision-based online soft sensor for oil sands flotation using support vector regression and its application in the dynamic monitoring of bitumen extraction*

Other applications of froth flotation are explored in this chapter. The primary objective is to develop and demonstrate that the online soft sensing method can be extended to other industries that use flotation. The oil sands industry, based on its relevance to the Canadian economy and the difficulty it presents in froth image sensing is chosen for the study. Different types of oil sands ore obtained from the Athabasca field. A soft sensing method is developed for bitumen grade and recovery using support vector regressions. Calibration is performed against the off-line measurements obtained using the Dean-Stark method. The developed soft sensor could be introduced for the purpose of dynamic monitoring and advanced process control applications. The applicability of the single model for different types of ore confirms its robustness at different process conditions and for different feeds with varying bitumen content.

Chapter 6: Conclusions and future work

This chapter summarizes the research in this thesis and provides conclusions for the findings and developments. It also presents the recommendations for the future research path and extension of the study to other flotation systems.

It is noted that the thesis is based on the paper-format and follows the rules set by Faculty of Graduate Studies and Research at University of Alberta. Therefore, to maintain the paper-format and ensure completeness, some part of the chapters might contain repetitions, especially in the methodology sections. The overlap was not removed in order to provide smooth flow of the thesis to the readers and ease the understanding for the material.

1.5 References

Aldrich, C., Marais, C., Shean, B.J., Cilliers, J.J., 2010. Online monitoring and control of froth flotation systems with machine vision: A review. International Journal of Mineral Processing 96, 1–13.

Arbiter, N., Harris, C., 1962. Flotation kinetic, in: Fuerstenau, D. (Ed.), Froth Flotation. AIME, New York, pp. 215–262.

Ata, S., 2012. Phenomena in the froth phase of flotation A review. International Journal of Mineral Processing 102-103, 1–12.

Barbian, N., Cilliers, J.J., Morar, S.H., Bradshaw, D.J., 2007. Froth imaging, air recovery and bubble loading to describe flotation bank performance. International Journal of Mineral Processing 84, 81–88.

Bartolacci, G., Jr., P.P., Jr., J.T., Duchesne, C., Bossé, P.A., Fournier, J., 2006. Application of numerical image analysis to process diagnosis and physical parameter measurement in mineral processesPart I: Flotation control based on froth textural characteristics. Minerals Engineering 19, 734–747.

Bascur, O.A., 2000. An interactive dynamic flotation model framework. Developments in Mineral Processing 13, C8a–21–C8a–31.

Bergh, L., Yianatos, J., 2011. The long way toward multivariate predictive control of flotation processes. Journal of Process Control 21, 226–234.

Bergh, L., Yianatos, J., 2013. Control of rougher flotation circuits aided by industrial simulator. Journal of Process Control 23, 140–147.

Bhole, M.R., Joshi, J.B., Ramkrishna, D., 2008. CFD simulation of bubble columns incorporating population balance modeling. Chemical Engineering Science 63, 2267–2282.

Bisshop J.P. & White, M.E., 1976. Study of particle entrainment in flotation froths. Transactions of the Institution of Mining and Metallurgy 85.

Bonifazi, G., Giancontieri, V., Meloni, A., Serranti, S., Volpe, F., Zuco, R., Koivo, H., Hätönen, J., Hyötyniemi, H., Niemi, A., Sipari, P., Kuopanporrti, H., Ylinen, R., Heikkila, I., Lahteenmaki, S., Miettunen, J., Stephasson, O., Wang, W., Carlsson, L.E., 2000. Characterization of the flotation froth structure and color by machine vision (ChaCo). Elsevier. volume Volume 13 of *Developments in Mineral Processing*. pp. C8a–39–C8a–49.

Bouchard, J., Desbiens, A., del Villar, R., 2014. Column flotation simulation: A dynamic framework. Minerals Engineering 55, 30–41.

Bulatovic, S.M., 2007. Handbook of flotation reagents : chemistry, theory and practice. Elsevier.

Cilek, E.C., Umucu, Y., 2001. A statistical model for gangue entrainment into froths in flotation of sulphide ores. Minerals Engineering 14, 1055–1066.

Cruz, E.B., 1997. A comprehensive dynamic model of the column flotation unit operation. Phd. Virginia Polytechnic Institute and State University.

Derjaguin, B.V., Dukhin, S.S., 1993. Theory of flotation of small and medium-size particles. Progress in Surface Science 43, 241–266.

Dewitt, C.C., 1940. Froth Flotation Concentration. Industrial & Engineering Chemistry 32, 652–658.

Ding, L., Gustafsson, T., 1999. Modelling and control of a flotation process: Control and optimisation in minerals, metals and materials processing, in: Proceedings of an international symposium held at the 38th annual conference of metallurgists of CIM in Quebec, Canadian Institute of Mining, Metallurgy and Petroleum, Quebec. pp. 285–298.

Dobby, G.S., Finch, J.A., 1987. Particle size dependence in flotation derived from a fundamental model of the capture process. International Journal of Mineral Processing 21, 241–260.

Duchesne, C., 2010. Multivariate Image Analysis in Mineral Processing, in: Sbarbaro, D., del Villar, R. (Eds.), Advanced Control and Supervision of Mineral Processing Plants. Springer, pp. 85–139.

F. Sawyerr D.A. Deglon, O'Connor, C.T., 1998. Prediction of bubble size distribution in mechanical flotation cells. Journal of The South African Institute of Mining and Metallurgy 98, 179–185.

Fuerstenau, M.C., Jameson, G.J., Yoon, R.H., 2007. Froth Flotation: A Century of Innovation. SME.

Gong, J., Peng, Y., Bouajila, A., Ourriban, M., Yeung, A., Liu, Q., 2010. Reducing quartz gangue entrainment in sulphide ore flotation by high molecular weight polyethylene oxide. International Journal of Mineral Processing 97, 44–51.

Gorain, B.K., Harris, M.C., Franzidis, J.P., Manlapig, E.V., 1998. The effect of froth residence time of the kinetics of flotation. Minerals Engineering 11, 627–638.

Hadler, K., Greyling, M., Plint, N., Cilliers, J.J., 2012. The effect of froth depth on air recovery and flotation performance. Minerals Engineering 3638, 248–253.

Hanumanth, G.S., Williams, D.J.A., 1992. A three-phase model of froth flotation. International Journal of Mineral Processing 34, 261–273.

Hargrave, J., Hall, S., 1997. Diagnosis of concentrate grade and mass flowrate in tin flotation from colour and surface texture analysis. Minerals Engineering 10, 613–621.

Harris, C., Jowett, A., Ghosh, S., 1963. Analysis of data from continuous flotation testing. Transactions of the American Institute of Mining and Metallurgical Engineers , 444–447.

Harris, C., Rimmer, H., 1966. Study of two-phase model of the flotation process. Transactions of the Institution of Mining and Metallurgy , 153–162.

Holtham, P.N., Nguyen, K.K., 2002. On-line analysis of froth surface in coal and mineral flotation using JKFrothCam. International Journal of Mineral Processing 64, 163–180.

J. Ralston, S.S.D., Mischuk, N.H., 1999. Bubble-particle attachment and detachment in otation. International Journal of Mineral Processing 56, 133–164.

Jahedsaravani, A., Massinaei, M., Marhaban, M., 2017. Development of a machine vision system for real-time monitoring and control of batch flotation process. International Journal of Mineral Processing 167, 16–26.

Kawatra, S.K., 2002. Froth Flotation - Fundamental Principles. Technical Report. Michigan Technical University.

Kirjavainen, V.M., 1992. Mathematical model for the entrainment of hydrophilic particles in froth flotation. International Journal of Mineral Processing 35, 1–11.

Klimpel, R., 1995. The Influence of Frother Structure on Industrial Coal Flotation, in: HighEfficiency Coal Preparation (Kawatra, ed.), Society for Mining, Metallurgy, and Exploration, Littleton. pp. 141–151.

Laplante, A.R., Toguri, J.M., Smith, H.W., 1983. The effect of air flow rate on the kinetics of flotation. Part 1: The transfer of material from the slurry to the froth. International Journal of Mineral Processing 11, 203–219.

Laurila, H., Karesvuori, J., Tiiili, O., 2002. Strategies for Instrumentation and Control of Flotation Circuits, in: Mineral processing plant design, practice, and control, Vancouver. pp. 2174–2195.

Leiva, J., Vinnett, L., Yianatos, J., 2012. Estimation of air recovery by measuring froth transport over the lip in a bi-dimensional flotation cell. Minerals Engineering 3638, 303–308.

Liu, J.J., MacGregor, J.F., Duchesne, C., Bartolacci, G., 2004. Monitoring of Flotation Processes Using Multiresolutional Multivariate Image Analysis (MR-MIA). IFAC Proceedings Volumes 37, 53–58.

Marais, C., Aldrich, C., 2010. The estimation of platinum flotation grade from froth image features by using artificial neural networks., in: International Platinum Conference, Platinum in transition Boom or Bust', The Southern African Institute of Mining and Metallurgy.

McFadzean, B., Marozva, T., Wiese, J., 2016. Flotation frother mixtures: Decoupling the sub-processes of froth stability, froth recovery and entrainment. Minerals Engineering 85, 72–79.

Mehrabi, A., Mehrshad, N., Massinaei, M., 2014. Machine vision based monitoring of an industrial flotation cell in an iron flotation plant. International Journal of Mineral Processing 133, 60–66.

Moolman, D.W., Eksteen, J.J., Aldrich, C., van Deventer, J.S.J., 1996. The significance of flotation froth appearance for machine vision control. International Journal of Mineral Processing 48, 135–158.

Parkinson, L., Ralston, J., 2011. Dynamic aspects of small bubble and hydrophilic solid encounters. Advances in Colloid and Interface Science 168, 198–209.

Rao, F., Liu, Q., 2013. Froth treatment in Athabasca oil sands bitumen recovery process: A review. Energy & Fuels 27, 7199–7207.

Rao, T., Govindarajan, B., Barnwal, J., 1995. A Simple Model for Industrial Coal Flotation Operation, in: High-Efficiency Coal Preparation (Kawatra, ed.), Society for Mining, Metallurgy, and Exploration, Littleton. pp. 177–185.

Rubio, J., Souza, M., Smith, R., 2002. Overview of flotation as a wastewater treatment technique. Minerals Engineering 15, 139–155.

Runge, K., McMaster, J., Wortley, M., Rosa, D.L., Guyot, O., 2007. A Correlation Between Visiofroth Measurements and the Performance of a Flotation Cell. Ninth Mill Operators' Conference , 79–86.

Shean, B., Cilliers, J., 2011. A review of froth flotation control. International Journal of Mineral Processing 100, 57–71.

Singh, A., Louw, J., Hulbert, D., 2003. Flotation stabilization and optimization. South African Institute of Mining and Metallurgy 103, 581–588.

Supomo, A., Yap, E., Zheng, X., Banini, G., Mosher, J., Partanen, A., 2008. PT Freeport Indonesia's mass-pull control strategy for rougher flotation. Minerals Engineering 21, 808–816.

Tuteja, R.K., Spottiswood, D.J., Misra, V.N., 1994. Mathematical models of the column flotation process: A review. Minerals Engineering 7, 1459–1472.

Vazirizadeh, A., Bouchard, J., del Villar, R., 2015a. On the relationship between hydrodynamic characteristics and the kinetics of column flotation. Part I: Modeling the gas dispersion. Minerals Engineering 74, 207–215.

Vazirizadeh, A., Bouchard, J., del Villar, R., Ghasemzadeh Barvarz, M., Duchesne, C., 2015b. On the relationship between hydrodynamic characteristics and the kinetics of flotation. Part II: Model validation. Minerals Engineering 74, 198–206.

Ventura-Medina, E., Cilliers, J.J., 2002. A model to describe flotation performance based on physics of foams and froth image analysis. International Journal of Mineral Processing 67, 79–99.

Vera, M.A., Mathe, Z.T., Franzidis, J.P., Harris, M.C., Manlapig, E.V., O'Connor, C.T., 2002. The modelling of froth zone recovery in batch and continuously operated laboratory flotation cells. International Journal of Mineral Processing 64, 135–151.

Wang, L., Peng, Y., Runge, K., 2016. Entrainment in froth flotation: The degree of entrainment and its contributing factors. Powder Technology 288, 202–211.

Wang, W., Bergholm, F., Yang, B., 2003. Froth delineation based on image classification. Minerals Engineering 16, 1183–1192.

Wang, W., Stephasson, O., 1999. A robust bubble delineation algorithm for froth images, in: International Conference on Intelligent Processing and Manufacturing of Materials, pp. 471–476.

Warren, L.J., 1985. Determination of the contributions of true flotation and entrainment in batch flotation tests. International Journal of Mineral Processing 14, 33–44.

Woodburn, E.T., 1970. Mathematical modelling of flotation processes. Miner.Sci.Eng 2, 3–17.

Xing, Y., Gui, X., Liu, J., Cao, Y., Lu, Y., 2015. Effects of Energy Input on the Laboratory Column Flotation of Fine Coal. Separation Science and Technology 50, 2559–2567.

Xing, Y., Gui, X., Pan, L., Pinchasik, B.E., Cao, Y., Liu, J., Kappl, M., Butt, H.J., 2017. Recent experimental advances for understanding bubble-particle attachment in flotation. Advances in Colloid and Interface Science 246, 105–132.

Yianatos, J., Contreras, F., Díaz, F., Villanueva, A., 2009. Direct measurement of entrainment in large flotation cells. Powder Technology 189, 42–47.

Yoon, R.H., Mao, L., 1996. Application of Extended DLVO Theory, IV: Derivation of Flotation Rate Equation from First Principles. Journal of colloid and interface science 181, 613–626.

Chapter 2

Dynamic Modeling and Real-Time Monitoring of Froth Flotation[1]

A dynamic fundamental model was developed linking processes from the microscopic scale to the equipment scale for batch froth flotation. State estimation, fault detection, and disturbance identification were implemented using the extended Kalman filter (EKF), which reconciles real-time measurements with dynamic models. The online measurements for the EKF were obtained through image analysis of froth images that were captured and analyzed using the commercial package VisioFroth (Metso® Minerals). The extracted image features were then correlated to recovery using principal component analysis and partial least squares regression. The performance of real-time state estimation and fault detection was validated using batch flotation of pure galena at various operating conditions. The image features that were strongly representative of recovery were identified, and calibration and validation were performed against off-line measurements of recovery. The EKF successfully captured the dynamics of the process by updating the model states and parameters using the online measurements. Finally, disturbances in the air flow rate and impeller speed were introduced into the system, and the dynamic behavior of the flotation process was successfully tracked and the disturbances were identified using state

[1]A version of this chapter has been published as Popli, K.; Sekhavat, M.; Afacan, A.; Dubljevic, S.; Liu, Q.; Prasad, V., 2015 "Dynamic Modeling and Real-Time Monitoring of Froth Flotation". Minerals

estimation.

2.1 Introduction

Froth flotation is the most common method in the minerals industry for the selective recovery of value mineral(s) from finely ground ores. It is based on the differences in the surface hydrophobicity of valuable and gangue minerals. The chemical (e.g., collector, frother, etc.) and physical conditions (e.g., feed rate, pulp density, agitation speed, air flow rate, etc.) are inter-related in froth flotation processes. The main objective of froth flotation is to maximize the grade and recovery of the value mineral(s) while maintaining upset-free operation (Fuerstenau et al., 2007). In typical froth flotation operations, large variations in the feed composition and various disturbances affecting the system result in a decrease in the grade and recovery. Control strategies applied to flotation systems typically target bias, froth depth, and gas hold up using feedback control by manipulating variables such as air and water flow rates, and reagent addition (Bouchard et al., 2005; Villar et al., 1999; Maffei and de Oliveira Luz, 2000). Typically, empirical models are used in the design of these feedback controllers. These empirical models are usually linear and only valid in narrow operating zones, thus making them inaccurate in larger operating ranges. Furthermore, since they do not provide any physical insight into the process and its behavior, they do not have any diagnostic utility outside of their use in control. Fundamental models, on the other hand, incorporate physical understanding of the process and can be used for predictions of grade and recovery and the diagnosis and monitoring of process behaviour in the presence of disturbances and process uncertainty. The fundamental models developed by (Neethling and Cilliers, 2002; Neethling et al., 2003; Neethling and Cilliers, 2009) that are based on attachment of solids to bubbles using first order rate constants have been accepted widely in mineral processing. However, these models cannot be used for dynamic purposes such as fault detection and real-time process monitoring. Therefore, there is a requirement for dynamic fundamental models in froth flotation.

Dynamic models must be coupled with real-time measurements and a model-updating scheme for process monitoring. However, the complexity and harshness of the process environment in froth flotation present considerable challenges for the deployment of hardware sensors in the real-time measurement of important process variables. Soft sensing is an alternative to hard sensing and refers to the use of inferential relations to provide estimations of variables of interest. Various estimators are used in chemical processes to estimate the states of the system. These include the Kalman filter (KF), the extended Kalman filter (EKF), the ensemble Kalman filter (EnKF), and the particle filter (PF) (Geetha et al., 2014; Höckerdal et al., 2011; Prasad et al., 2002) . The EKF works for nonlinear systems and has been used effectively for fault detection purposes (Benkouider et al., 2009).

The EKF minimizes the error covariance between the measured and the predicted output (grade and/or recovery for froth flotation). Conventionally, X-ray fluorescence (XRF) is used to determine the composition of the process streams. However, employing an online XRF is expensive, and calibrating it is difficult due to matrix effects in the samples. It is also known that both grade and recovery in the concentrate are strongly related to froth structure (Moolman et al., 1996). Therefore, observing froth images can provide information about the grade of the concentrate product, which can then be correlated to the recovery using the grades of the feed and tailing streams. In general, control decisions are made by operators using basic inferences based on visual observation without any further analysis of the images (Runge et al., 2007). Quantifying the dynamic information obtained from the images using machine vision is essential for their use in control and monitoring, and different image processing algorithms are available for bubble segmentation and velocity calculations. These algorithms include edge detection and watershed algorithms for bubble segmentation as well as Fourier and wavelet transforms for velocity calculations (Aldrich et al., 2010). Some of the commonly used image processing software for froth flotation are: (1) VisioFroth (Metso® Minerals, Orleans Cedex, France), (2) METCAM FC (SGS, Lakefield, ON, Canada), (3) FrothMaster^{TM}(Outotec, Burlington, ON, Canada) (Leiva et al., 2012) and (4) PlantVision^{TM} (KnowledgeScape Inc, Salt Lake City, UT, USA). Several researchers have tried to correlate individual variables such as bubble size, color, and texture to grade and/or recovery; however, the majority of the studies do not provide quantitative relations suitable for calibration of these variables against the grade/recovery (Moolman et al., 1996).

In this study, we develop a dynamic fundamental model for batch flotation incorporating information from multiple scales, develop a method to obtain quantitative information about recovery in flotation from dynamic images using principal component analysis (PCA) and partial least squares (PLS) regression, develop a soft sensor for real-time updating of the model using extended Kalman filtering (EKF), and then demonstrate the efficacy of the soft sensor in identifying and tracking unknown disturbances in batch flotation tests on galena conducted at different operating conditions.

2.2 Experimental Section

Batch flotation experiments are conducted using a mechanical flotation cell to train and validate the aforementioned real-time estimation algorithm. Flotation of high purity galena single mineral is chosen to demonstrate the fault detection strategy and represent a proof of concept for monitoring using fundamental models. In future work, the methods will be demonstrated on more complex sulphide ores. For these tests, the effects of the air flow rate, impeller speed, collector, and frother dosage on recovery are investigated. The experiments are carried out in a JK Tech batch flotation cell (Julius Kruttschnitt Mineral Research Centre, University of Queensland, Indooroopilly, Australia) with a capacity of 1.6 L. The cell is equipped with a bottom-drive mechanical stirrer and air supply is provided from the bottom of the cell.

The batch flotation was monitored with a VisioFroth system (Metso® Minerals) to capture the images at the top of the froth surface as shown in Figure 2.1. Hardware components of the VisioFroth system include a single IP camera, a laser, and LED lights. These images are then analysed using the software component of VisioFroth the so-called optimizing control system (OCS), to measure several image features. This image processing package is used to measure the angle and magnitude of the froth velocity, bubble distributions, color, froth texture, and stability as well as the height of the froth overflowing over the lip.

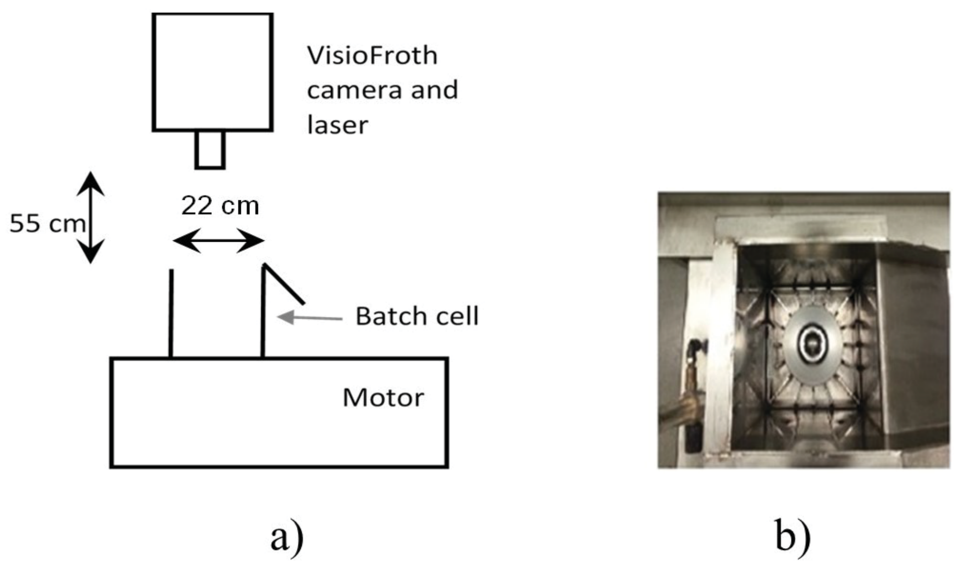

Figure 2.1: (a) Schematic diagram for batch flotation process equipped with VisioFroth, (b) top view of the batch flotation cell.

The laser is used to find the height of the overflowing froth using the change in the horizontal position of the laser line on top of the froth as shown in Figure 2.3. The reference froth height level corresponds to the laser being at the baseline and is at the initial time. As the froth height increases, the laser line moves a new position (d). This difference in laser line positions is used to deduce the horizontal distance from the baseline. The laser angle is set at the time of installation. The froth height (b) is calculated as:

$$b = a - f.tan(c) \tag{2.1}$$

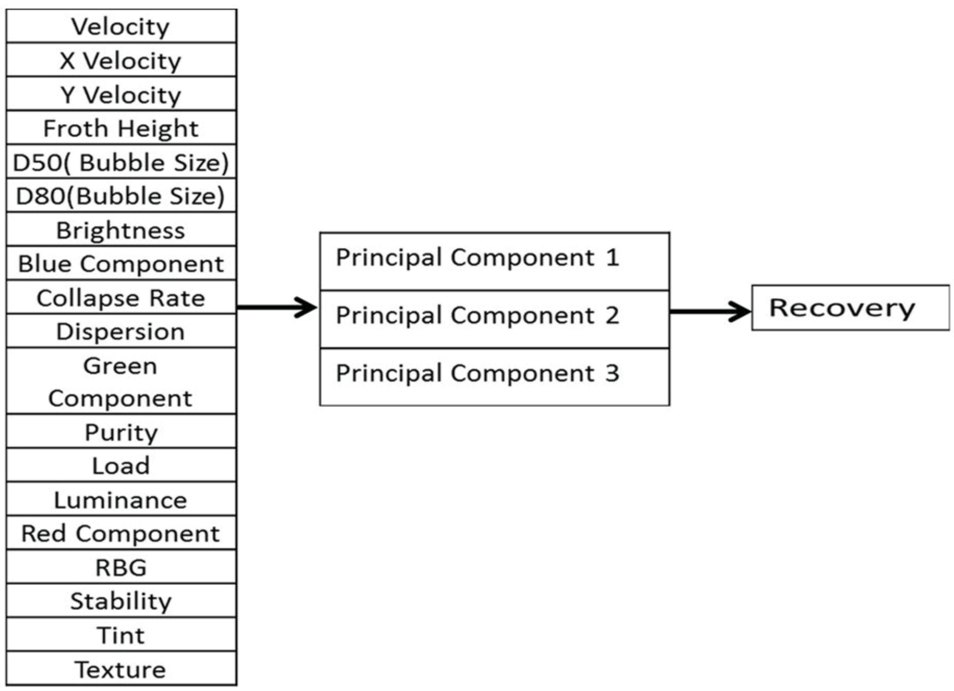

Figure 2.2: Illustration of dimension reduction using principal component analysis (PCA) with three principal components.

Table 2.1 lists the various VisioFroth measurements and algorithms.

Statistical techniques, including principal component analysis (PCA) and partial least square (PLS) regression, are used to identify the important features of the images and develop a correlation for the recovery using offline measurements. The use of PCA results

Table 2.1: VisioFroth measurements and algorithms.

Variable	Algorithm
Velocity	Modified Fourier transforms to calculate the displacement between two consecutive images.
Bubble size measurement	Watershed techniques are used to outline bubbles and hence calculate the bubble surface area.
Collapse rate	Calculated based on change in bubble surface area.

in dimension reduction of the data for better understanding of the given information (Jolliffe, 2005). The basic principle of this method is to represent the input matrix of data X in terms of scores (T) and loadings (P):

$$X = TP^T + E \tag{2.2}$$

Dimension reduction and correlation is illustrated in Figure 2.2 for the case of three principal components. The scores represent the projection of the original data samples onto the transformed space of reduced dimension, and the loadings represent the weights or contributions of the original variables to each principal component. Only the principal components that contribute significantly to explaining the variance in the original data are retained, and dimension reduction is obtained by truncating the number of variables based on this principle. In Equation 2.2, E represents the error in the representation after truncation. Thus, variables that have high loadings on the most significant principal components contribute significantly to explaining the variance in the data, and can be considered to be significant. To obtain a correlation between the input and output data, principal component regression (PCR) is employed. In PCR, regression of the score matrix from PCA is performed against the output measurement (recovery). PLSR (partial least squares regression) is also used to develop the correlation between images and recovery (Geladi and Kowalski, 1986).

Potassium ethyl xanthate (KEX) and methyl isobutyl carbinol (MIBC) were used as

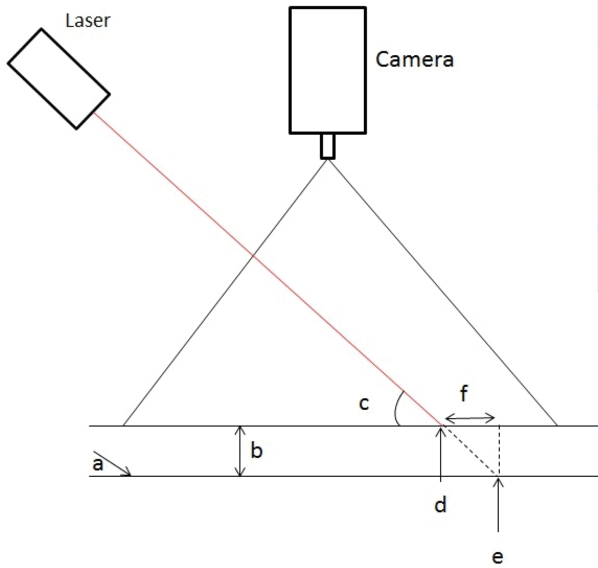

a	**Reference froth height**
b	**Calculated froth height**
c	**Laser angle**
d	**Laser line**
e	**Baseline**
f	**Distance from baseline**

Figure 2.3: Field of view and demonstration of froth height measurement using the laser light.

collector and frother, respectively. Galena was obtained from Boreal Science Company in Canada in cleaved form. The galena was crushed and dry ground to -106 μm. The particle size distribution of the ground galena sample is presented in Table 2.2.

Table 2.2: Particle size distribution for galena feed.

Passing Size (μm)	Cumulative Weight (%)
106	100
75	96
45	37
38	30

The output of the flotation process, recovery, is dependent on the air flow rate, impeller speed, collector dosage, and frother dosage. In order to capture a wide range of these operating conditions, a fractional factorial design was used to generate different operating conditions and levels of these factors, as summarized in Table 2.3. In each run, after selecting a desired operating condition, galena was mixed with water in the concentration of 50 g galena/1.5 L water. First, the slurry was conditioned with collector and frother for 2 and 6 min, respectively. Then, air was supplied to the cell and froth was collected at intervals of 10 s up to 100 s, and at 50 s intervals for the next 200 s. The collected froth was dried after vacuum filtration and weighed for recovery calculation. Also, images of top surface of the froth were extracted at sample time intervals of 1 s.

Table 2.3: Operating conditions used in the factorial experimental design.

Runs	Air Flow rate (L/min)	Impeller Speed (rpm)	Frother (MIBC) Dosage (mol/L slurry)	Collector (KEX) Dosage (mol/L slurry)
1	8	500	0.042	10^{-5}
2	14	500	0.042	10^{-3}
3	8	1100	0.042	10^{-3}
4	14	1100	0.042	10^{-5}
5	8	500	0.1	10^{-3}
6	14	500	0.1	10^{-5}
7	8	1100	0.1	10^{-5}
8	14	1100	0.1	10^{-3}

For testing the fault detection algorithm, an operating condition was selected and a step disturbance was introduced either in the air flow rate or the impeller speed. For the first disturbance test, the conditions of run 8 (described in Table 2.3) were used initially, and the air flow was then decreased from 14 to 8 L/min at time t = 5 s. For the second disturbance test, the conditions of run 1 were used initially, and the impeller speed was changed from 500 to 1100 rpm at time t = 5 s.

2.3 Model Development

A flotation cell consists of two distinct phases: a pulp phase and a froth phase with various inter and intra-phase processes involved in the transport of material. The proposed framework in this research is based on a multi-scale approach, where attachment processes are coupled to equipment scale and inter-phase processes. This was achieved by formulating population balance, hydraulic force balance, mass transfer and kinetic rate equations for attachment and detachment and entrainment/drainage of mineral particles.

A mineral particle can be present at any of these three states, i.e., (1) attached to the bubbles in the pulp phase, (2) free in the pulp phase, or (3) attached to the bubbles in the froth phase. Particles could also be free in the froth phase, in water films and plateau borders, although the number of such particles may be small. However, in order to focus on the attachment and detachment, these particles were ignored in this study. The modeling framework that has been proposed is represented in Figure 2.4.

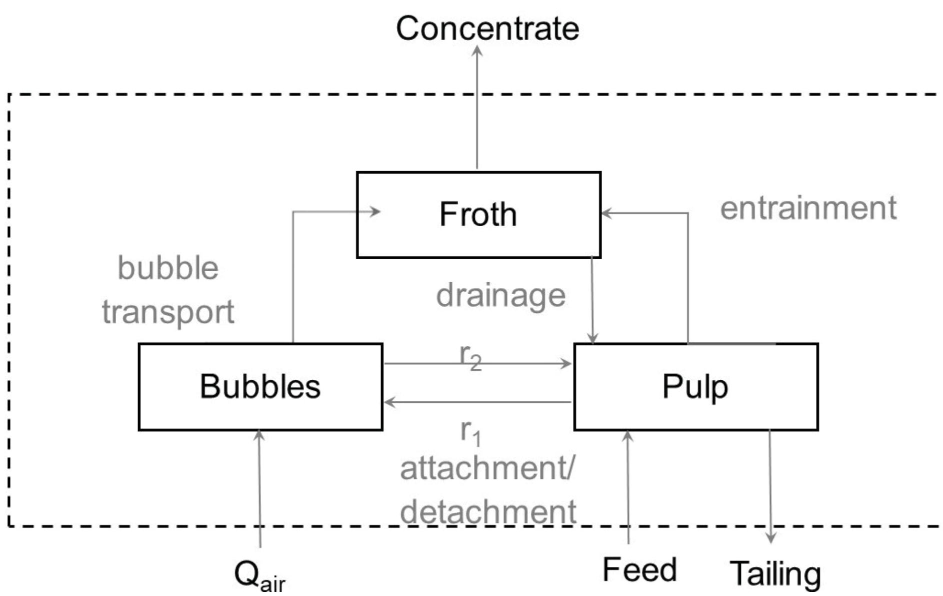

Figure 2.4: Schematic representation of the flotation modeling framework.

There are several mass transfer and kinetic processes between the three phases in the cell; they are summarized below:

- Selective attachment of mineral particles to the bubbles in the pulp phase (first order rate process, r_1).
- Detachment of particles from bubbles in the pulp phase (first order rate process, r_2).
- Transfer of particles that are attached to bubbles into the froth phase.

- Transfer of free particles from the pulp phase to the froth phase by entrainment and transfer of liquid (water) from the froth back to the pulp phase.

- Drop-back of particles from the froth to the slurry. These particles could be free particles in the froth phase, or attached particles that were detached at some point in the froth phase. At our level of modeling, we have opted for simplicity and do not distinguish between these two types of particles.

These sub-processes and recovery can be mathematically described using the following equations. The ordinary differential Equations 2.3, 2.4, and 2.5 represent the mass balances for valuable mineral particles attached to the bubbles in the pulp phase, the particles that are free in the pulp phase and the particles that are attached to the bubbles in the froth phase, respectively, and Equation 2.6 represents the recovery of the valuable mineral particles.

$$\frac{d}{dt}(\epsilon V_p x_b) = k_1(1-\epsilon)V_p x_p - k_2\epsilon V_p x_b - Q_{air} x_b \tag{2.3}$$

$$\frac{d}{dt}((1-\epsilon)V_p x_p) = k_2\epsilon V_p x_b - k_1(1-\epsilon)V_p x_p - Q_E x_p + Q_{E'} x_c \tag{2.4}$$

$$\frac{d}{dt}(\epsilon_f V_f x_c) = -k_3 V_f x_c + Q_{air} x_b + Q_E x_p - Q_{E'} x_c \tag{2.5}$$

$$y = \frac{\epsilon_f V_f t_{samp} k_3 x_c}{m_{init}} \tag{2.6}$$

Here, y is the instantaneous recovery of galena, m_{init} is the amount of galena in the feed, x_b is the concentration of particles on the surface of the bubbles in the pulp, x_p is the concentration of particles free in the pulp, x_c is the concentration of particles attached in the froth, k_1 is the first order rate constant for attachment, k_2 is the first order rate constant for detachment, k_3 is the rate of removal of material in the concentrate product, ϵ is the volume fraction of air in the pulp, ϵ_f is the volume fraction of air in the froth, V_p is the volume of the pulp phase, V_f is the volume of the froth phase, Q_{air} is the air flow rate, Q_E is the volumetric flow rate of slurry from the pulp to the froth layer, $Q_{E\prime}$ is the volumetric flow rate of liquid drainage from the froth layer to the pulp phase.

The attachment rate constant, k_1, and the detachment rate constant, k_2, are further dependent on various probabilities as discussed in the subsequent sections.

2.3.1 Attachment Phenomena in the Pulp Phase

Various studies have shown that the flotation process can be conceptualized as a chemical reaction (Bloom and Heindel, 2003; Jameson et al., 1977). The most general expression was proposed by Ahmed and Jameson (Ek, 1992):

$$\frac{dn_P^f(t)}{dt} = -k\prime(n_B^f(t))^m(n_P^f(t))^n \tag{2.7}$$

where $n_B^f(t)$ and $n_P^f(t)$ are the concentrations of free bubbles and particles, t is the flotation time, $k\prime$ is the pseudo-rate constant and m and n are the orders of the reaction with respect to bubbles and particles, respectively. The pseudo-rate constant can be expressed in terms of micro-process probabilities (Bloom and Heindel, 1997, 2002; Heindel and Bloom, 1999; Amand, 1999; Schulze, 1992; Schulze and Hecker, 1984; Schulze, 1991) based on the following assumptions: (1) the reaction is first order (Nguyen et al., 1998; Woodburn, 1970; Yoon and Mao, 1996) (2) the bubble concentration is constant, and (3) the volume of the removed particles is negligible (Ek, 1992). Therefore, Equation 2.7 can be written as:

$$\frac{dn_P^f(t)}{dt} = -kn_P^f(t) \tag{2.8}$$

where k is the rate constant and can be defined as:

$$k = ZP_cP_{asl}P_{tpc}P_{stab}n_B^f(t) \tag{2.9}$$

where Z is the bubble-particle collision frequency, P_c is the probability of bubble-particle collision, P_{asl} is the probability of bubble-particle attachment by sliding, P_{tpc} is the probability of forming a three-phase contact, P_{stab} is the probability of bubble-particle aggregate remaining stable during the transfer from the pulp phase to the froth phase (Bloom and Heindel, 2003).

The number of bubble-particle collisions is defined (Bascur, 2000) as:

$$Z = 5N_PN_Bd_B^2U_t \tag{2.10}$$

where Z is the number of collisions per unit time per cell volume, N_p is the number of particles ready for collision, N_B is the number of bubbles ready for collision, d_B is the mean size of the aggregates and U_t is the turbulent aggregate velocity.

Heindel and Bloom (Heindel and Bloom, 1999) proposed the probability of bubble-particle collision to be

$$\begin{aligned} P_c = \frac{1}{1+|G|}\Bigg\{ &\frac{1}{2\left[\frac{R_P}{R_B}+1\right]^3}\left[2\left(\frac{R_P}{R_B}\right)^3 + 3\left(\frac{R_P}{R_B}\right)^2\right] \\ &+\frac{2Re_B^*}{\left[\frac{R_P}{R_B}+1\right]^4}\left[\left(\frac{R_P}{R_B}\right)^3 + 2\left(\frac{R_P}{R_B}\right)^2\right]\Bigg\} + \frac{|G|}{1+|G|} \end{aligned} \tag{2.11}$$

where R_p and R_B are the particle and bubble radius, respectively, and G is the dimensionless particle settling velocity and is defined as

$$G = \frac{\nu_{PS}}{\nu_B} \tag{2.12}$$

where v_{ps} is the particle settling velocity and v_B the bubble rise velocity (Bloom and Heindel, 2003).

The probability of attachment by sliding is expressed as (Heindel and Bloom, 1999):

$$P_{asl} = exp\Big\{ -2\Big(\frac{\bar{\lambda}}{C_b}\Big)\Big(\frac{R_P}{R_P + R_B}\Big)\Big(\frac{g(r) - G}{|k(r)| - G}\Big)\Big(\frac{h_o}{h_{crit}} - 1\Big)\Big\} \tag{2.13}$$

where

$$g(r) = \Big(1 - \frac{3R_B}{4r} - \frac{R_B^3}{4r^3}\Big) + Re_B^*\Big(\frac{R_B}{r} + \frac{R_B^3}{r^3} - \frac{2R_B^4}{r^4}\Big) \tag{2.14}$$

$$k(r) = \Big\{\Big(1 - \frac{3R_B}{2r} + \frac{R_B^3}{2r^3}\Big) + 2Re_B^*\Big(\frac{R_{B^4}}{r^4} - \frac{R_B^3}{r^3} - \frac{R_B^2}{r^2} + \frac{R_B}{r}\Big)\Big\} \tag{2.15}$$

$$\bar{\lambda} = \frac{6\pi\mu_l R_p}{f} \tag{2.16}$$

where r is approximately equal to $R_B + R_P$, f is the fluid friction factor, C_B is a constant representing the bubble surface mobility, h_o is the initial thickness of the film at the time the sliding process begins and the particle starts to contact the bubble, and h_{crit} is the liquid film thickness at the time that the film starts to rupture (Bloom and Heindel, 2003).

The probability of forming a three-phase contact, P_{tpc}, is assumed to be equal to unity, as it is considered to be a highly probable event (Bloom and Heindel, 2002). The probability of bubble-particle aggregate stability, P_{stab}, is defined (Schulze, 1992) as

$$P_{stab} = 1 - exp\left(1 - \frac{1}{Bo\prime}\right) \tag{2.17}$$

where

$$Bo\prime = \frac{4R_P^2\left(\Delta\rho g + \frac{1.9\rho\varepsilon^{2/3}}{(R_P+R_B)^{1/3}}\right) + 3R_B\left(\frac{2\sigma}{R_B} - 2R_B\rho_l g\right) sin^2\left(\pi - \frac{\theta}{2}\right)}{\left|6\sigma sin\left(\pi - \frac{\theta}{2}\right) sin\left(\pi + \frac{\theta}{2}\right)\right|} \tag{2.18}$$

where ε is the Kolmogorov turbulent energy density, g is the acceleration due to gravity, θ is the contact angle, ρ_p is the particle density and $\Delta\rho = (\rho_p - \rho_l)$ (Bloom and Heindel, 2003).

2.3.2 Detachment Phenomena in the Pulp Phase

Bloom and Heindel (Bloom and Heindel, 2003, 1997) developed a population balance model to include both attachment and detachment phenomena that can be considered as the equivalents of forward and reverse reactions.

$$\frac{dn_P^f(t)}{dt} = -k_1 n_P^f(t) + k_2 n_B^a(t) \tag{2.19}$$

where $n_B^a(t)$ is the concentration of the bubbles to which particles are attached on their surface, k_1 is the attachment rate constant and k_2 is the detachment rate constant. The first term in Equation 2.19 represents attachment phenomena by the formation of bubble-particle aggregates and the second term represents detachment phenomena in which the aggregates become unstable and do not reach the froth layer. The detachment rate constant, k_2, is expressed as

$$k_2 = Z' P_{destab} = Z'(1 - P_{stab}) \tag{2.20}$$

where $Z\prime$ is the detachment frequency and P_{destab} is the probability of the bubble-particle aggregate becoming unstable in the pulp phase. The detachment frequency can be expressed as

$$Z' = \frac{\sqrt{C_1 \varepsilon^{1/3}}}{(d_P + d_B)^{2/3}} \tag{2.21}$$

where C_1 is an empirical constant taken to be 2.

The dependence of the attachment and detachment rate constants on the probabilities of bubble-particle collision, attachment by sliding, forming a three-phase contact and aggregate stability during transfer from the pulp to the froth are summarized in Figure 2.5. These relations are used in the interpretation of the online estimates of parameters and disturbances affecting the system.

2.3.3 State Space Model

For parameter estimation and online updating of the proposed model, the three differential equations (Equations 2.3 - 2.5) are expressed in state-space form. The states and the output are given by

$$\frac{dx}{dt} = Ax(t) + Bu(t) \tag{2.22}$$

$$\begin{bmatrix} \dot{x_1} \\ \dot{x_2} \\ \dot{x_3} \end{bmatrix} = \begin{bmatrix} -a_1 & a_2 & 0 \\ a_3 & -a_4 & a_5 \\ a_7 & 0 & -(a_8 + a_9) \end{bmatrix} \begin{bmatrix} x_1(t) \\ x_2(t) \\ x_3(t) \end{bmatrix} + \begin{bmatrix} 0 \\ a_6 \\ 0 \end{bmatrix} \tag{2.23}$$

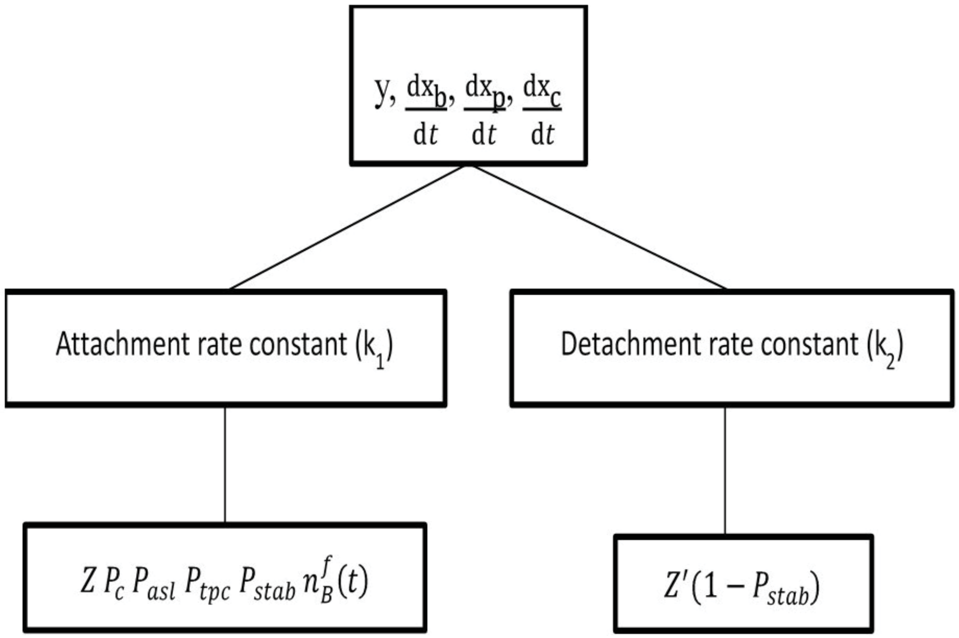

Figure 2.5: States and outputs of models and their dependence on model parameters. y represents the output (recovery), x_b is the concentration of particles on the surface of the bubbles in the pulp, x_p is the concentration of particles free in the pulp, x_c is the concentration of particles attached in the froth, Z is the number of collisions per unit time per cell volume, P_c is the probability of bubble-particle collision, P_{asl} is the probability of attachment by sliding, P_{tpc} is the probability of forming a three-phase contact, P_{stab} is the probability of bubble-particle aggregate stability during transfer from the pulp to the froth phase, n_B^f is the concentration and $Z\prime$ is the detachment frequency of particles.

$$y(t) = \begin{bmatrix} 0 & 0 & \frac{\epsilon V_f t_{samp} k_3}{m_{init}} \end{bmatrix} \begin{bmatrix} x_1(t) \\ x_2(t) \\ x_3(t) \end{bmatrix} \tag{2.24}$$

where y is the instantaneous recovery of galena, m_{init} is the initial mass of material in the batch flotation cell, k_3 is the rate of removal of material in the concentrate product, x_1 is the first state, i.e., the mass of solids attached to the bubbles per unit volume of pulp phase, x_2 is the second state, i.e., the mass of solids free in the pulp phase per unit volume of the pulp phase, and x_3 is the third state, i.e., the mass of solids attached to the bubbles in the froth phase. The input for the state-space model is the air flow rate. The parameters of the proposed state space model are defined in Table 2.4.

Table 2.4: Parameters used in the state space model.

Parameter	Definition
a_1	$k_2 + \frac{Q_{air}}{\epsilon V_p}$
a_2	$\frac{k_1(1-\epsilon)}{\epsilon}$
a_3	$\frac{k_2\epsilon}{1-\epsilon}$
a_4	k_1
a_5	$\frac{Q_E}{(1-\epsilon)V_P}$
a_6	$\frac{\dot{m}}{(1-\epsilon)V_P}$
a_7	$\frac{Q_{air}}{\epsilon V_f}$
a_8	$\frac{Q_E}{\epsilon V_f}$
a_9	$\frac{k_3}{\epsilon}$

2.4 State and Parameter Estimation

2.4.1 Offline Estimation: Model Parameters

Model parameters were estimated by minimizing the errors between the predicted recovery and the measured recovery obtained from batch experiments for different operating conditions. Offline parameter estimation was performed by minimizing the sum of errors between the model predicted and measured recovery over the time of the batch flotation runs by using the parameter estimates (k_1, k_2, k_3 and ϵ) as decision variables. These offline estimates were used as initial guesses for online estimation.

2.4.2 Online Estimation: State and Parameter Estimation

The extended Kalman filter was used for online estimation of states and parameters. The EKF works in a predictor-corrector format and on the principle of optimality by minimization of the estimated error covariance. Its linear variant, the Kalman filter, is the optimal linear estimator, while the EKF provides a suboptimal estimate for nonlinear systems (Prasad et al., 2002; Kalman, 1960; Haddad, 1976).

A nonlinear state space model with states x and outputs y is of the form

$$\dot{x} = f(x, u) + w(t), w(t) \sim N(0, Q) \tag{2.25}$$

$$y = g(x) + v(t), w(t) \sim N(0, R) \tag{2.26}$$

where w and v represent process and measurement noise, respectively. Set of differential equations are converted to the linear discrete difference equations using discretization and Jacobian computations:

$$x_k = Ax_{k-1} + Bu_{k-1} + w_{k-1} \tag{2.27}$$

$$y_k = Hx_k + v_k \tag{2.28}$$

where,

$$A = \frac{\partial f}{\partial x}(\widehat{x}_{k-1}, u_{k-1}, 0) \tag{2.29}$$

$$H = \frac{\partial f}{\partial y}(x_{k-1}, 0) \tag{2.30}$$

Prediction step for the EKF are given as:

$$\widehat{x_k^-} = f(\widehat{x}_{k-1}, u_{k-1}, 0) \tag{2.31}$$

$$P_k^- = A_k P_{k-1} A_k^T + Q \tag{2.32}$$

Correction step is given as:

$$K_k = P_{k|k-1} G_k^T (G_k P_{k|k-1} G_k^T + R)^{-1} \tag{2.33}$$

$$\hat{x}_{k|k} = \hat{x}_{k|k-1} + K_k (y_k - g(\hat{x}_{k|k-1})) \tag{2.34}$$

$$P_{k|k} = (I - K_k G_k) P_{k|k-1} \tag{2.35}$$

The EKF estimate at the end of each time step is given by $\hat{x}_{k|k}$, and $\hat{P}_{k|k}$ represents the covariance of the state estimates. K_k is the Kalman gain at each time step t_k. Details on the augmentation of the parameters to be estimated to the state vector has been explained by Prasad et al. (Prasad et al., 2002).

Parameters can be estimated by treating them as augmented states with no dynamics and forming new augmented state matrices (Prasad et al., 2002). However, observability considerations limit the maximum number of parameters to be estimated in this manner to be equal to the number of outputs; therefore, only one parameter was estimated online. However, by running multiple EKFs in parallel, each independently estimating a different parameter, the performance of the state and output estimation based on the updating of each parameter was compared. Heuristics were developed for fault detection by observing the changes in the estimates of these parameters and states in real time during the process operation, and this is described in the next section.

2.5 Results and Discussions

2.5.1 Correlation of Image Features to Recovery

Several image features were extracted using VisioFroth and correlated to the recovery measured offline using PCR and PLSR. Figure 2.6 shows a representative result for the experiments performed using the operating conditions for run 5 shown in Table 2.3. The images inset in the figure demonstrate that the image features vary with varying recovery. PCA indicates that three principal components were sufficient to capture 90% of the variance. This indicates the various extracted image features are well-correlated to each other. Features such as the velocity in the x-direction (flowing out of the cell) and the mean bubble diameter have high loadings with respect to principal component 1, and can be considered to be important variables.

PCR and PLSR were performed using five components in the input space to obtain better correlation between the image features and the recovery. A comparison of the correlated recovery against the experimental values is presented in Figure 2.7.

Both PLSR and PCR provide good agreement with the measured recovery values at different times; thus, either technique can be used along with image analysis to replace the assay measurement and be used online in real time. It can be concluded that froth features can provide a good description of process conditions in the form of predicting recovery. Additionally, the advantages of this technique over other methods such as online XRF include the ability to sample at shorter intervals, ease of calibration and being relatively inexpensive.

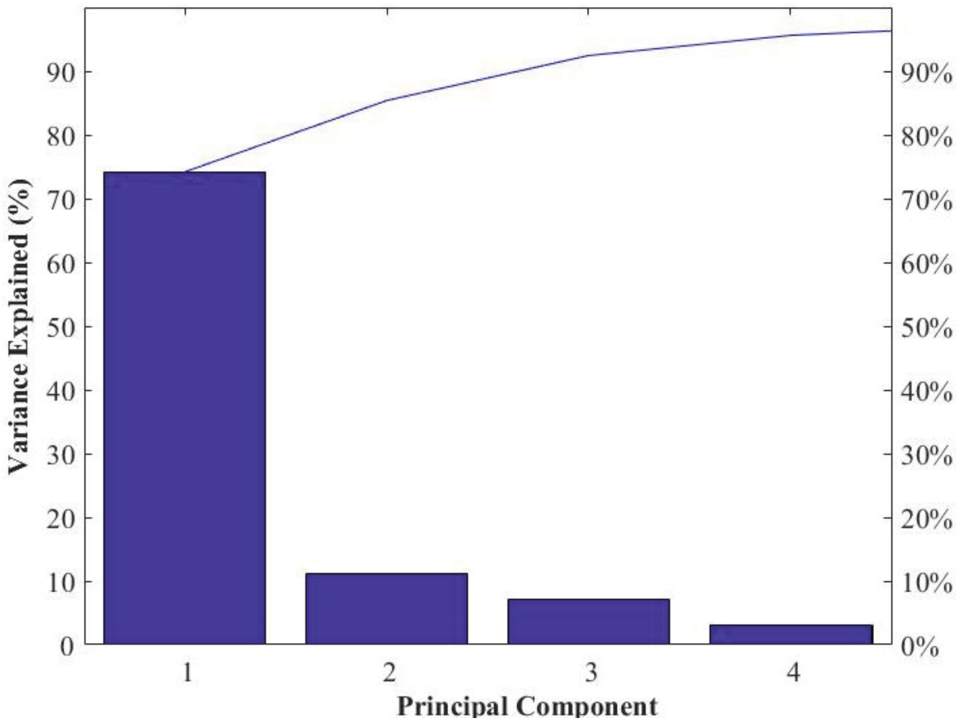

Figure 2.6: Percentage variance (bars) and cumulative percentage variance (solid line) of the image features captured by the principal components.

2.5.2 Offline Parameter Estimation

This section describes the offline fitting of the proposed model to the experimental data obtained from the batch flotation tests. In each run, the operational conditions of the experiments are input into the model and the states and the recovery were calculated and then the results are compared with the experimental data. The parameter estimates were based on obtaining the lowest error between the model predictions and experimental values for the recovery. The results for run 1 (operating conditions given in Table 2.3 are shown in Figure 2.8 with estimated values for k_1, k_2 and k_3 as 40, 20 and 40 s^{-1}, respectively. These parameter estimates are taken as the initial values for the online estimation using the EKF. Similar fits were obtained for the other operating conditions. The coefficient of determination (R^2) was greater than 86% for all the tests (Sekhavat,

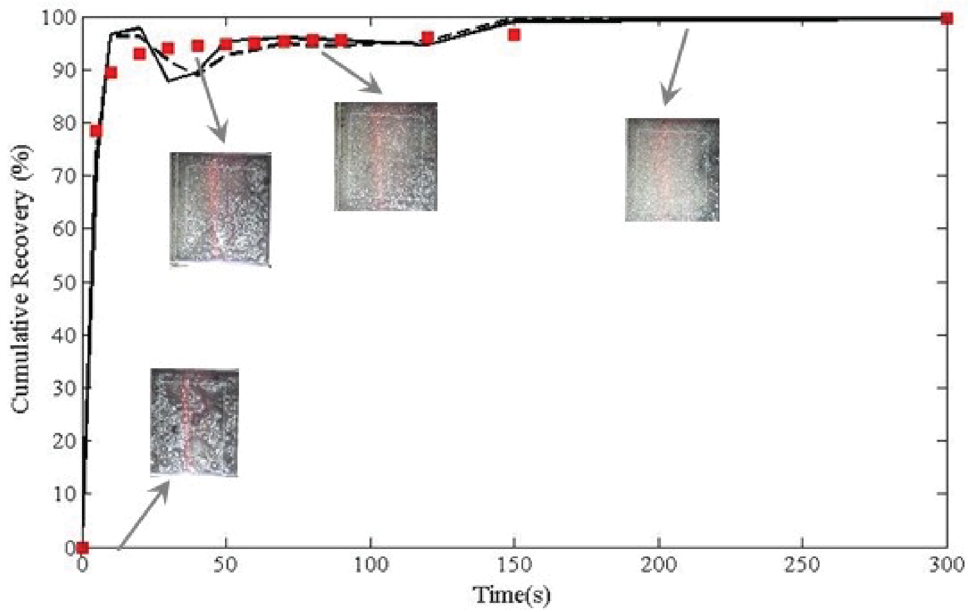

Figure 2.7: Comparison of principal component regression (PCR, solid line) and partial least squares regression (PLSR, dashed line) with experimental values of recovery (marker).

2014). This indicates that the fundamental model is able to capture the dynamics of the batch process, and can be used for process monitoring and control.

2.5.3 Online Estimation: State and Parameter Estimation

Online estimation using the EKF is also demonstrated for the operating conditions of run 1. Three EKFs were run in parallel, and the corresponding sets of results are presented with parameter estimation for k_1, k_2, and k_3, respectively. Figure 2.9 shows the performance of the EKF-based model in predicting recovery in real-time for the case when parameter k_1 is being estimated. Similar results were obtained for the cases when parameters k_2 and k_3 were being estimated, respectively. Figure 2.10 shows the online estimates obtained for each of the parameters being updated independently. It is observed that the rate constant of attachment (k_1) increases and that of detachment (k_2)

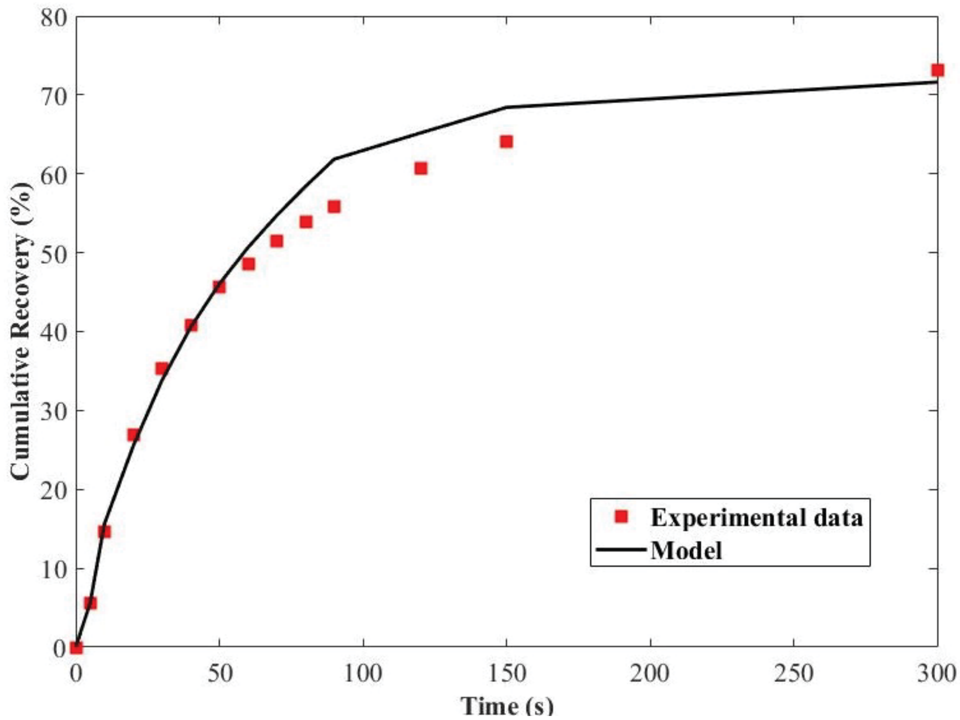

Figure 2.8: Comparison of model predictions of cumulative recovery based on offline parameter estimation with experimental data for the batch flotation of galena.

decreases with time due to the changing dynamics of the system. The rate of removal of material in the concentrate product (k_3) decreases with time and reaches a steady value of 13.3 s^{-1}. The final estimates are summarized in Table 2.5. With the model being updated in real-time, the updates in estimated values of the parameters highlight that the dependence of these dynamically varying parameters (k_1, k_2 and k_3) on process conditions is changing with time. This indicates that online estimation is essential for real-time monitoring, in order to be able to capture the dynamics of the changes in the parameters.

The results from online estimation are also consistent with the models for attachment and detachment described in Sections 2.3.1 and 2.3.2. The images of the froth surface revealed that the bubble size increased with time in the batch flotation run described

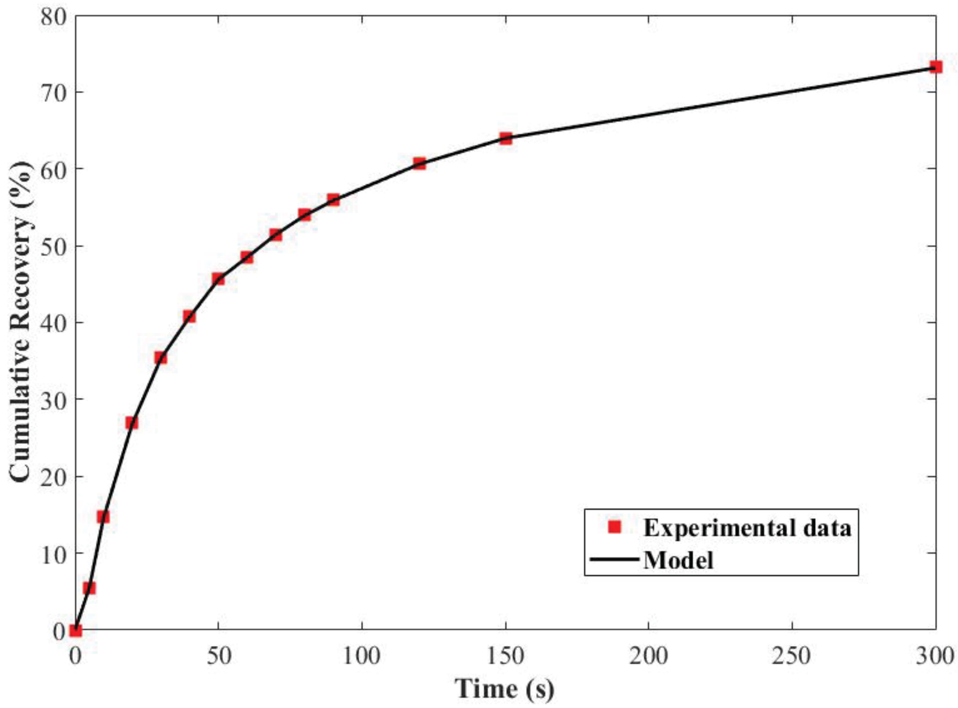

Figure 2.9: Comparison of real-time model predictions based on the extended Kalman filter (EKF) with experimental data for cumulative recovery when parameter k_1 is being updated.

Table 2.5: Values of estimated (k_1, k_2 and k_3) and constant model parameters.

Symbols	Parameters	Values	Remarks
$Q_{air}(L/min)$	Air flow rate	8	Constant
$V_p(m^3)$	Volume of pulp phase	$1.4x10^{-3}$	Constant
$V_f(m^3)$	Volume of froth phase	$0.26x10^{-3}$	Constant
ϵ	Volume fraction of air	0.4	Constant
$k_1(s^{-1})$	Rate constant for attachment	Final value = 45.8	Estimated and updated (trend shown in Figure 2.10)
$k_2(s^{-1})$	Rate constant for detachment	Final value = 17.1	Estimated and updated (trend shown in Figure 2.10)
$k_3(s^{-1})$	Rate of removal of material in the concentrate product	Final value = 13.3	Estimated and updated (trend shown in Figure 2.10)

above. While the number of particles decreased with time as more mineral was recovered, leading to a reduction in the number of bubble-particle collisions and the probabilities of bubble-particle collision and attachment by sliding reduce slightly as the bubble size increases (Equations 2.9 - 2.10 and 2.13, the probability that the bubble-particle aggregate remains stable during the transfer from the pulp phase to the froth phase increases with the increase in the bubble size. This increase in P_{stab} is the dominant effect, and leads to an increase in k_1 (Equation 2.9) and decrease in k_2 (Equations 2.17 and 2.18).

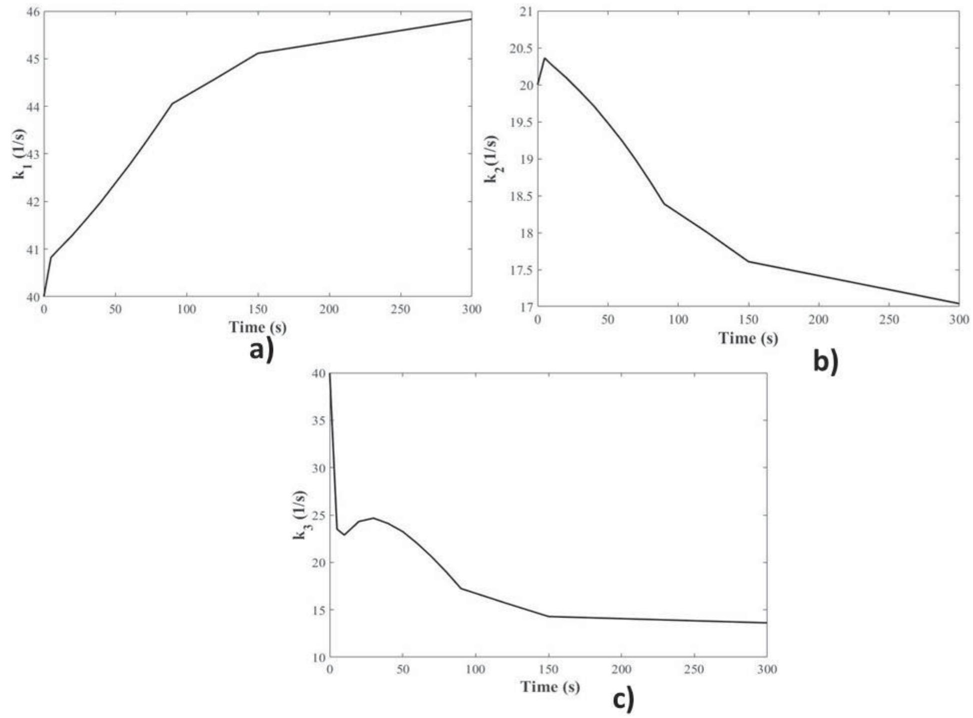

Figure 2.10: EKF estimates of model parameters in real-time: (a) parameter k_1 being estimated, (b) parameter k_2 being estimated, and (c) parameter k_3 being estimated.

2.5.4 Disturbance Identification

The ability of the EKF estimator to track changes in operation and modifying parameter estimates was also tested for two case studies with disturbances. In the first case study, a disturbance in the air flow rate was introduced at time t = 5 s in the batch cell with initial operating conditions for run 8 (shown in Table 2.3). At this time, the air flow rate was decreased from 14 to 8 L/min. There is a significant decrease in the cumulative recovery due to a sudden decrease in the air flow rate; this is shown in Figure 2.11. This is expected as lowering the air flow rate leads to lowering of the flow rate of the valuable mineral (galena) in the concentrate and hence to lower recovery. Despite the presence of the disturbance in the system, the EKF was able to track the changes by updating the states and parameters as new measurements arrive and capture the dynamics of the system satisfactorily, as seen in Figure 2.11.

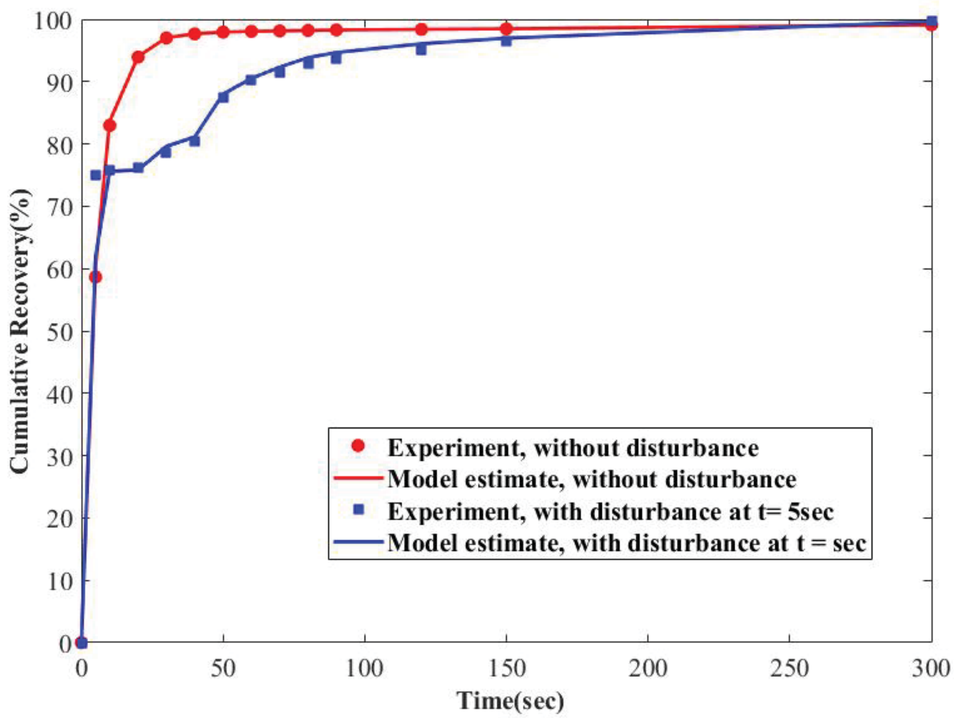

Figure 2.11: Comparison of cumulative recovery profiles for run 8 (conditions defined in Table 2.3) with a step disturbance applied in the air flow rate (from 14 to 8 L/min) at time t = 5 s.

Figure 2.12 shows the EKF-based parameter estimates for each of the parallel estimators (estimating k_1, k_2 and k_3, respectively), with and without the disturbance. When the disturbance was applied to the system, parameter k_1, which is related to the attachment of particles, and parameter k_2, which is related to the detachment of particles, did not change significantly in comparison to the condition when there was no disturbance. However, parameter k_3, which is related to the rate of transfer of particles to the concentrate from the froth phase, decreased because lowering the air flow rate resulted in a decrease in the number of the particles that are brought from the pulp phase to the froth phase; consequently, the rate of transfer of particles to the concentrate product would be decreased as well.

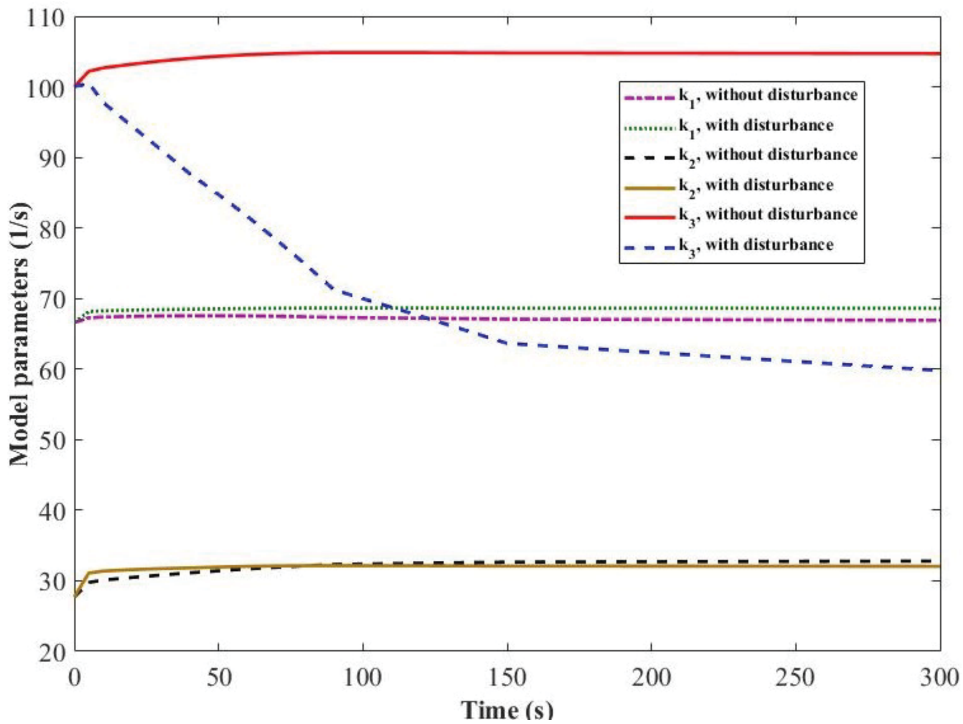

Figure 2.12: Comparison of real-time parameter estimates (k_1, k_2 or k_3 being estimated) for run 8 with the step disturbance in the air flow rate.

Additionally, the estimated states of the system are shown in Figure 2.13. As is expected, the only system state that changes with a disturbance in the air flow is the concentration of the particles attached in the pulp. This slight increase is observed due to a decrease in the transfer of particles from the pulp to the froth.

The second case study was based on the initial operating conditions for run 1 (given in Table 2.3), with the impeller speed being increased from 500 to 1100 rpm at time t = 5 s to create a step disturbance. Increasing the impeller speed in the pulp phase increases the bubble count and the bubble-particle interactions. This leads to an increase in the probability of bubble-particle collision and therefore attachment (Equations 2.9 and 2.10),

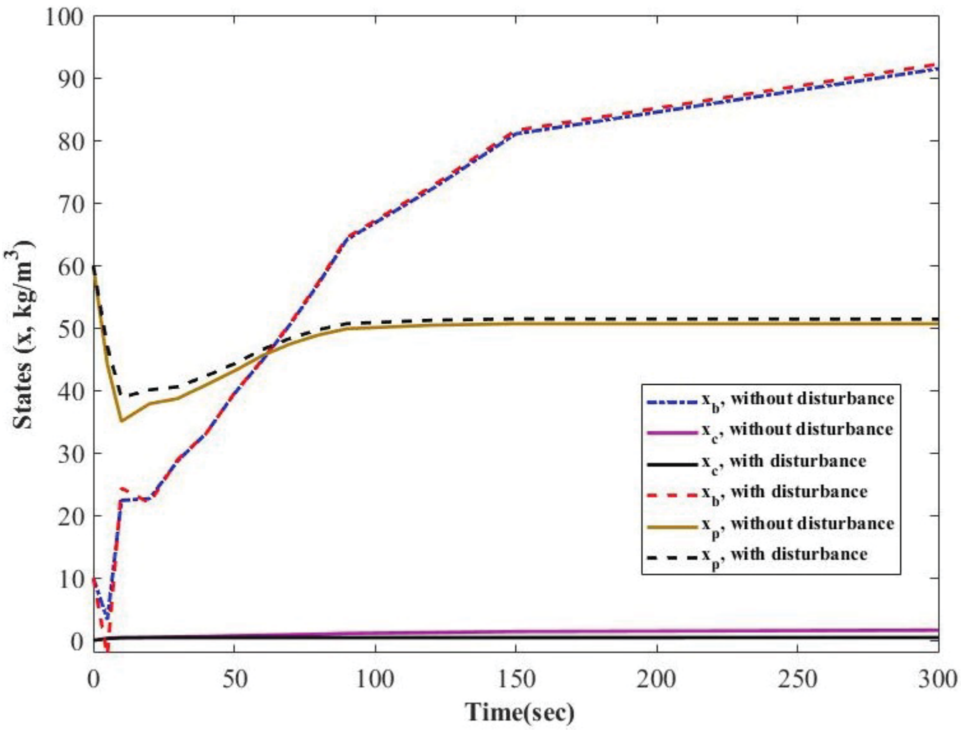

Figure 2.13: Real-time state estimates using the EKF for run 8 with the step disturbance in the air flow rate (x_b: concentration of particles on the surface of the bubbles in the pulp, x_p: concentration of particles free in the pulp, x_c: concentration of particles attached in the froth).

leading to an increase in the particles brought into the froth phase and consequently in the concentrate. Figure 2.14 shows the EKF estimates for each of the parallel estimators for the three parameters of the system (k_1, k_2 and k_3), with and without the disturbance. The estimates of parameters k_2 and k_3 did not change significantly but k_1, the rate of attachment, decreased initially due to the increased turbulence, and then increased due to the larger number of interactions between bubbles and particles.

The changes in the estimated states for the case with the disturbance in the impeller speed are similar to those for the case with the air flow disturbance, as is shown in Figure 2.15. This indicates that monitoring of the parameters, and not the states, is preferred for tracking these types of disturbances in the system, since the estimates of the parameters are more sensitive to the presence, size, and type of disturbances present in the system. These results provide a proof of concept that heuristics related to online parameter estimation using parallel EKFs (negative step changes in the air flow rate being detected by a reduction in the value of the parameter estimate for k_3, and positive step changes in the impeller speed being detected by a decrease and then an increase in the parameter estimate for k_1) can be developed and used for process monitoring and fault diagnosis in froth flotation processes, and are consistent with the fundamental processes involved in attachment and detachment of particles to bubbles, their transfer from the pulp to the froth and their eventual recovery in the concentrate. Our future work aims to extend this proof of concept to more complex ores and continuous flotation processes, and to develop rigorous algorithms for process monitoring under any operating conditions and disturbances.

2.6 Conclusions

A fundamental model for batch froth flotation was developed based on descriptions of bubble-particle collision, attachment, and detachment coupled with bubble and liquid transport. Real-time measurements of froth bubble size and velocity utilizing image processing techniques were injected into the model. Offline parameter estimation was used to verify the validity of this model for describing the dynamics of batch froth flotation processes. Statistical methods such as principal component regression and partial least squares regression were used to calibrate the real-time froth surface images against the recovery measured offline. Both the methods described the recovery well in real time and were successful in reducing the dimension of image features significantly without any substantial loss of information or prediction capability. Methods based on advanced state and parameter estimation techniques (extended Kalman filtering) were used to update the

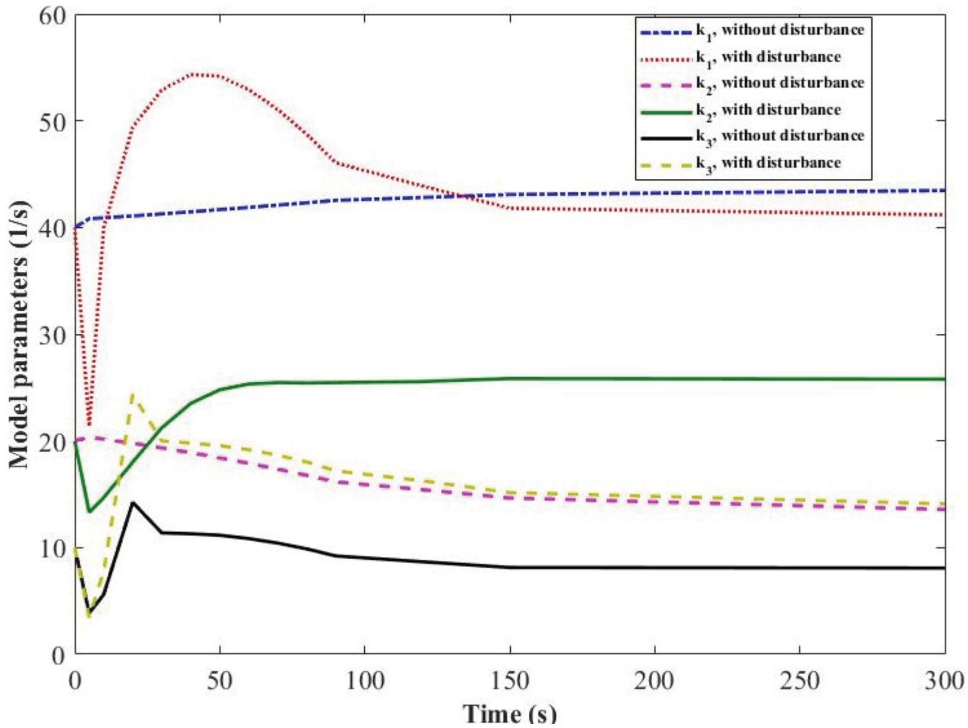

Figure 2.14: Comparison of parameter estimates (k_1, k_2 or k_3 being estimated) for run 1 with a step disturbance applied in the impeller speed from 500 to 1100 rpm at time t = 5s.

models and their parameter estimates in real time based on the online measurements. Validation with experiments confirmed that process dynamics were captured both in normal operations as well as in the presence of disturbances affecting the batch flotation process. Disturbances in the air flow rate and impeller speed were induced in the system. Based on the updated parameter estimates (using the EKF), heuristics were developed and validated that could discriminate between various disturbances affecting the system, thus providing a proof of concept that monitoring using real-time updated fundamental models provides physical insight into the batch flotation process.

2.7 References

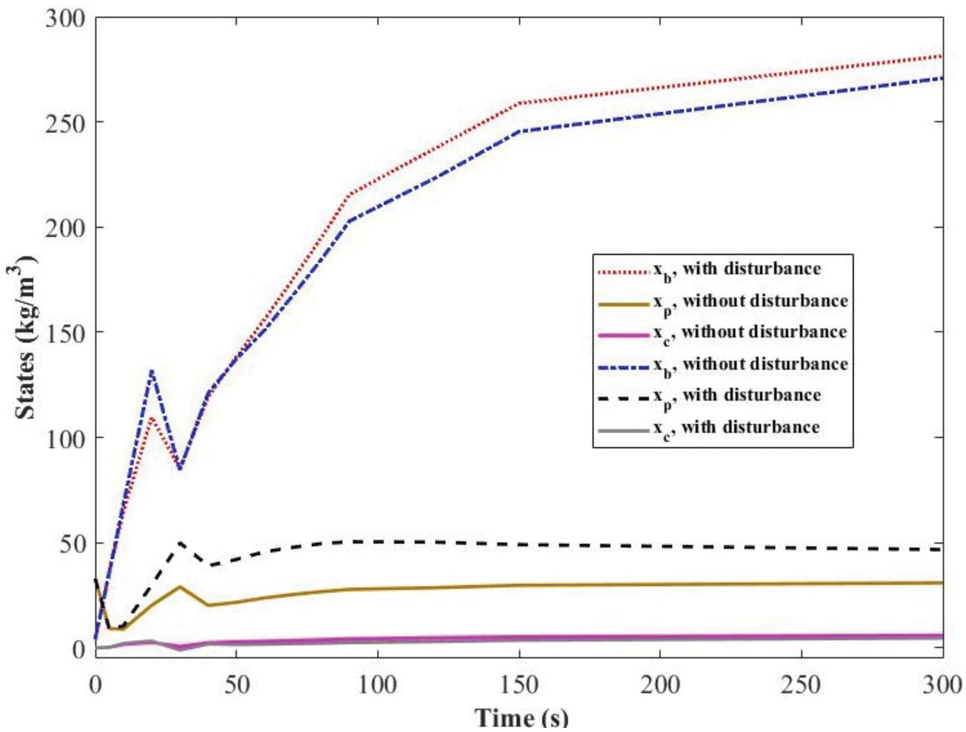

Figure 2.15: Real-time state estimates using the EKF for run 1 with the step disturbance in the impeller speed (x_b: concentration of particles on the surface of the bubbles in the pulp, x_p: concentration of particles free in the pulp, x_c: concentration of particles attached in the froth).

Aldrich, C., Marais, C., Shean, B.J., Cilliers, J.J., 2010. Online monitoring and control of froth flotation systems with machine vision: A review. International Journal of Mineral Processing 96, 1–13.

Amand, F.J.S., 1999. Hydrodynamics of deinking flotation. International Journal of Mineral Processing 56, 277–316.

Bascur, O.A., 2000. An interactive dynamic flotation model framework. Developments in Mineral Processing 13, C8a–21–C8a–31.

Benkouider, A.M., Buvat, J.C., Cosmao, J.M., Saboni, A., 2009. Fault detection in semi-batch reactor using the EKF and statistical method. Journal of Loss Prevention in the Process Industries 22, 153–161.

Bloom, F., Heindel, T.J., 1997. Mathematical modelling of the flotation deinking process. Mathematical and Computer Modelling 25, 13–58.

Bloom, F., Heindel, T.J., 2002. On the structure of collision and detachment frequencies in flotation models. Chemical Engineering Science 57, 2467–2473.

Bloom, F., Heindel, T.J., 2003. Modeling flotation separation in a semi-batch process. Chemical Engineering Science 58, 353–365.

Bouchard, J., Desbiens, A., del Villar, R., 2005. Recent advances in bias and froth depth control in flotation columns. Minerals Engineering 18, 709–720.

Ek, C., 1992. Flotation kinetics. Innovation in Flotation Technology 5, 183–210.

Fuerstenau, M.C., Jameson, G.J., Yoon, R.H., 2007. Froth Flotation: A Century of Innovation. SME.

Geetha, M., Kumar, P.A., Jerome, J., 2014. Comparative Assessment of a Chemical Reactor Using Extended Kalman Filter and Unscented Kalman Filter. Procedia Technology 14, 75–84.

Geladi, P., Kowalski, B.R., 1986. Partial least-squares regression: a tutorial. Analytica Chimica Acta 185, 1–17.

Haddad, A., 1976. Applied optimal estimation. volume 64. The MIT Press, Cambridge.

Heindel, T.J., Bloom, F., 1999. Exact and Approximate Expressions for Bubble Particle Collision. Journal of colloid and interface science 213, 101–111.

Höckerdal, E., Frisk, E., Eriksson, L., 2011. EKF-based adaptation of look-up tables with an air mass-flow sensor application. Control Engineering Practice 19, 442–453.

Jameson, G.J., Nam, S., Young, M.M., 1977. Physical factors affecting recovery rates in flotation. Miner.Sci.Eng 9, 103–118.

Jolliffe, I., 2005. Principal Component Analysis. Encyclopedia of Statistics in Behavioral Science. .

Kalman, R.E., 1960. A New Approach to Linear Filtering and Prediction Problems .

Leiva, J., Vinnett, L., Yianatos, J., 2012. Estimation of air recovery by measuring froth transport over the lip in a bi-dimensional flotation cell. Minerals Engineering 3638, 303–308.

Maffei, A.C., de Oliveira Luz, I.L., 2000. Pulp-froth interface control in the flotation column. Developments in Mineral Processing 13, C3–1–C3–7.

Moolman, D.W., Eksteen, J.J., Aldrich, C., van Deventer, J.S.J., 1996. The significance of flotation froth appearance for machine vision control. International Journal of Mineral Processing 48, 135–158.

Neethling, S.J., Cilliers, J.J., 2002. Solids motion in flowing froths. Chemical Engineering Science 57, 607–615.

Neethling, S.J., Cilliers, J.J., 2009. The entrainment factor in froth flotation: Model for particle size and other operating parameter effects. International Journal of Mineral Processing 93, 141–148.

Neethling, S.J., Lee, H.T., Cilliers, J.J., 2003. Simple relationships for predicting the recovery of liquid from flowing foams and froths. Minerals Engineering 16, 1123–1130.

Nguyen, A.V., Ralston, J., Schulze, H.J., 1998. On modelling of bubbleparticle attachment probability in flotation. International Journal of Mineral Processing 53, 225–249.

Prasad, V., Schley, M., Russo, L.P., Bequette, B.W., 2002. Product property and production rate control of styrene polymerization. Journal of Process Control 12, 353–372.

Runge, K., McMaster, J., Wortley, M., Rosa, D.L., Guyot, O., 2007. A Correlation Between Visiofroth Measurements and the Performance of a Flotation Cell. Ninth Mill Operators' Conference , 79–86.

Schulze, H.J., 1991. The fundamentals of flotation deinking in comparison to mineral flotation. .

Schulze, H.J., 1992. Probability of particle attachment on gas bubbles by sliding. Advances in Colloid and Interface Science 40, 283–305.

Schulze, H.J., Hecker, M., 1984. Physico-chemical elementary processes in flotation: an analysis from the point of view of colloid science including process engineering considerations. Elsevier Amsterdam.

Sekhavat, M., 2014. Real-Time Updating of a Dynamic Fundamental Model for Froth Flotation Process.

Villar, R.D., Grégoire, M., Pomerleau, A., 1999. Automatic control of a laboratory flotation column. Minerals Engineering 12, 291–308.

Woodburn, E.T., 1970. Mathematical modelling of flotation processes. Miner.Sci.Eng 2, 3–17.

Yoon, R.H., Mao, L., 1996. Application of Extended DLVO Theory, IV: Derivation of Flotation Rate Equation from First Principles. Journal of colloid and interface science 181, 613–626.

Chapter 3

Monitoring the Feed Particle Size in Froth Flotation using Parameter Estimation with Fundamental Dynamic Models[1]

In this work, a fundamental dynamic model was updated in real-time to monitor the feed particle size in froth flotation using direct and indirect estimation. Direct estimation was performed by expanding the model using descriptions of micro-scale sub-processes such as attachment and detachment with mean particle size as a parameter, whereas indirect estimation was performed by estimating the rate constants and inferring the particle size based on the micro-scale models. Froth images and their features were acquired using Visiofroth, a commercial vision package by Metso® Minerals. A random forest-based soft sensor was developed to obtain online recovery measurements using these image features. Models were updated in real-time using an extended Kalman filter with the online output measurement (recovery) being obtained from the developed image-based soft sensor. Batch flotation experiments were performed with pure galena to calibrate the soft sensor as well as to validate the estimation of the particle size. Four different

[1]A version of this chapter is submitted as Popli, K.; Afacan, A.; Liu, Q.; Prasad, V., 2017 "Monitoring the Feed Particle Size in Froth Flotation using Parameter Estimation with Fundamental Dynamic Models ". Chemical Engineering Science

feed particle size distributions, with mean particle size ranging from 12 to 112 microns, were employed with same operating conditions (air flow rate, impeller speed, reagent and frother concentrations). Changes in particle size were captured better by direct estimation as compared to indirect estimation. Fundamental effects of particle size on attachment and detachment were also analyzed using real-time process monitoring.

3.1 Introduction

Froth flotation is a process where multiple factors such as chemical (collector, frother), physical (air flow, agitator) and operational variables (feed rate, feed size, pulp density) influence the process performance (Kawatra, 2002). It is characterized by various sub-processes in the pulp and the froth phase. Along with the intra-phase processes, there is an interphase transportation of material as well. Bubbles collide with particles in the pulp phase and form continuously moving bubble-particle aggregates in the froth phase. However, some of the attached particles in the froth phase do not enter the outlet due to bubble bursting or bubble coalescence (K. Runge R. Crosbie, 2010). It is very likely that a small disturbance in any of the sub-process could propagate to other sub-processes and affect the type and quantity of solids entering the concentrate.

Grinding circuits can often produce undersize or oversize particles and it is crucial to analyze the effect of changes in feed particle size in real-time. With various flotation cells in the overall circuit, it is also important to know the source cell of the disturbance. This can be accomplished by continuously monitoring the various sub-processes in both pulp and froth phases. A successful monitoring scheme aids in identifying possible faults and understanding the complex behavior of froth flotation processes. Historically, plant operators relied on their experience-based heuristics to determine the process status based on the froth appearance. Later, sophisticated classification systems were developed based on machine vision of the froth (Cipriano et al., 1998; Aldrich et al., 1997). Most earlier studies were conducted to control certain operational variables using froth vision (Kaartinen and Koivo, 2002; Brown et al., 2001; Liu and MacGregor, 2008; Aldrich et al., 2010; Popli et al., 2015). However, according to the authors' best knowledge, no study has been performed to investigate real-time monitoring for feed particle size using a vision-based system.

The effect of particle size on flotation has been studied extensively and an optimal particle size range has been suggested for optimal recovery depending on the type of minerals (Glembotsky, 1953; Trahar, 1981). Fine particles are difficult to float, medium sized particles have higher chances of floating and coarse particles float depending on the operating conditions (Trahar, 1981). Apart from this, the recovery and grade depend on the liberation achieved at each particle size range. Different particle size ranges respond differently to the physio-chemical conditions in the flotation cell. Collectors enhance the bubble-particle attachment by making the mineral surface hydrophobic. The same collector concentration performs differently for each particle size range in spite of having similar chemical conditions in the cell (Gaudin et al., 1931; Glembotsky, 1953). Fundamentally, froth flotation kinetics depend on the probability of collision, the probability of attachment and the probability of detachment between bubble and particles (Popli et al., 2015). For better performance, particles should have a high probability of collision and attachment and low probability of detachment along with sufficient mineral liberation. These probabilities are further influenced by the particle size. A change in particle size in the feed stream propagates to the final recovery by creating a disturbance or a change in the rate constants or probabilities for collision, attachment and detachment. Therefore, it is very important to understand the relationship between particle size and these rate constants.

There are a few first principles-based steady-state models and other simulators (JK-

SimFLoat, MODSIM) developed for flotation processes that can be used for optimizing the process conditions (Neethling and Cilliers, 2002; Neethling et al., 2003; Neethling and Cilliers, 2009; King, 2012; Schwarz and Alexander, 2006). However, these models can not be used for dynamic monitoring and process control; also, the flotation models used for process control are primarily empirical (Bouchard et al., 2005). In this work, we build on our earlier work (Popli et al., 2015) to develop a set of dynamic fundamental models that connect micro-scale sub-processes (attachment, detachment) to macro-scale sub-processes (mass transfer, intraphase transfer).

In this paper, a feed particle size monitoring scheme is developed and tested using batch flotation experiments for pure galena. Induction time measurements are used along with the fundamental models to understand the effect of particle size on various sub-processes. An extended Kalman filter (Prasad et al., 2002; Kalman, 1960; Haddad, 1976) is used to update the fundamental model in real-time by estimating its states and parameters using online recovery measurements. A statistical ensemble regression method (random forest) is used to develop a soft sensor to measure online recovery based on the froth images and their features. The monitoring scheme developed is validated to estimate the mean particle size for a flotation run with an unknown feed particle size distribution.

3.2 Experimental Section

3.2.1 Materials: Ore samples and reagents

Pure galena (lead sulfide, PbS) obtained from Boreal Science, Canada was used as the feed. These samples were ground to different particle size ranges using a combination of a jaw crusher and a disc pulveriser. Four different feed particle size distributions were obtained using sieve analysis. Three of these were used to develop and study the monitoring algorithm, and a fourth mixed distribution was used to test the estimates of the feed particle size. Representative samples were obtained using a sample splitter for particle size measurements. Particle size distributions were measured using a Malvern Mastersizer 3000 and are summarized in Table 3.1 and represented in Figure 3.1.

Table 3.1: Particle size distribution parameters for different feed samples.

Distribution	D10(μm)	D50(μm)	D90(μm)	Mean(μm)
Distribution I	3.3	8.61	29.7	12.13
Distribution II	3.95	21.6	66.5	28
Distribution III	70	100.2	150	113
Test distribution	6.48	22.3	123	45.4

A collector and a frother were added as chemical reagents. Collectors were used to increase the selectivity for improved attachment between the mineral and bubbles in the cell (Kawatra, 2002), while the frother was used to improve bubble stability and produce a stable froth in the cell (Kawatra, 2002). In this study, potassium ethyl xanthate ($C_3H_5KOS_2$, KEX) and methyl isobutyl carbinol ($C_6H_{14}O$, MIBC) were employed as the collector and frother, respectively.

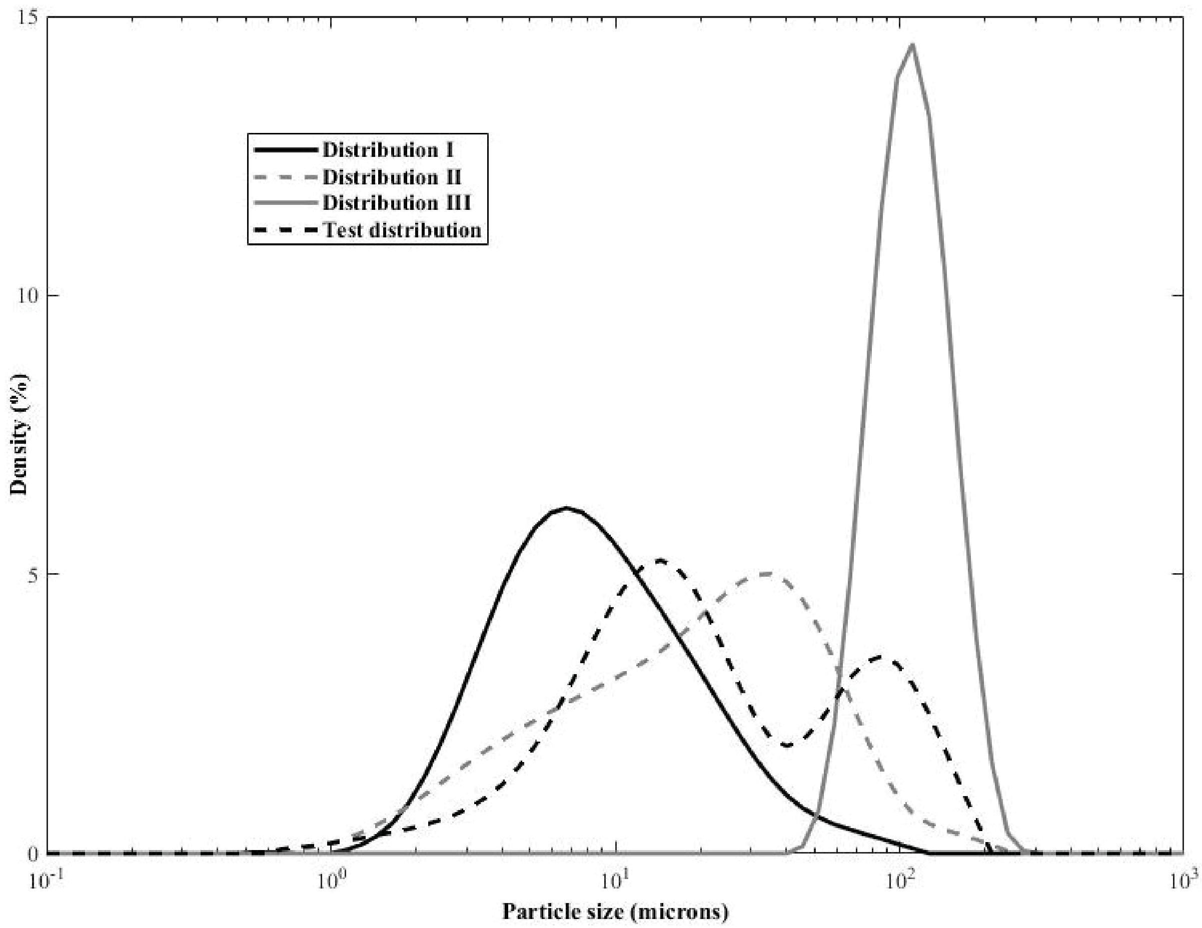

Figure 3.1: Particle size distribution for different feed samples (logarithmic scale).

3.2.2 Batch flotation

A batch flotation cell was used for the flotation of pure galena. The batch cell was equipped with the Visiofroth system by Metso® Minerals that consists of a camera, laser, and LED light. It was used to capture the images of the top surface of the froth in real-time. This has been elaborated in our previous work (Popli et al., 2015) and the schematic diagram is depicted in Figure 3.2. The image features extracted from Visiofroth are listed in Table 3.2.

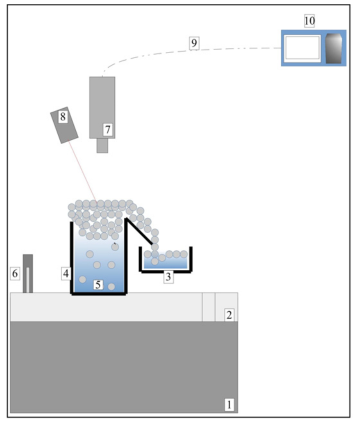

Figure 3.2: Schematic diagram for a JKTech batch flotation machine with the VisioFroth setup, where, 1: motor, 2: impeller control, 3: collection pan, 4: batch cell, 5: impeller, 6: air control and rotameter, 7: camera with LED, 8: laser light, 9: data transfer via network wire, 10: monitoring of realtime data.

Table 3.2: Image features extracted from the top surface of the froth using the Visiofroth system.

Image features	Image features
Velocity	Green component
X velocity	Purity
Y velocity	Load
Froth height	Luminance
D50 (Bubble size)	Red component
D80 (Bubble size)	RBG
Brightness	Stability
Blue component	Tint
Collapse rate	Texture
Cell value	a- component lab model
Dispersion	b- component lab model

Batch experiments were designed to perform flotation for different feed particle size distributions. Design specifications were obtained from our previous work, based on the conditions for high flotation performance (Popli et al., 2015). These are summarized in Table 3.3.

Table 3.3: Flotation conditions maintained in the cell.

Design parameter	Value
Volume of slurry (l)	1.6
Solids concentration (g/l)	31.25
Air flow rate (cm/s)	2.67
Impeller speed (rpm)	1100
Frother dosage (ml/l)	0.1
Collector dosage (mol/l)	10^{-3}

The slurry of galena was mixed with the collector (KEX) and the impeller speed was set at 1100 rpm for 8 minutes for conditioning. The frother (MIBC) was added at the end of the 8 minutes and mixing was continued for 2 more minutes. The air flow rate was set to 14 lpm to start the flotation process. The images were captured at 5 seconds time intervals using the Visiofroth system. Table 3.2 shows various features of captured images based on real-time. Froth was collected at intervals of 10 seconds for a minute, followed by 50 second intervals, until the completion of the flotation process. The samples collected were then dried and weighed to obtain data for soft sensor development and calibration.

3.2.3 Induction time measurement

The induction time is a measure of bubble-particle attachment. It is defined as the contact time needed for the attachment of particles to the bubble (Gu et al., 2003), and is used to understand the qualitative relationship between attachment and particle size. We have used an induction timer apparatus for measurement that is similar to the set-ups described in (Gu et al., 2003; Ye et al., 1989; Yoon and Yordan, 1991). In our work, bubbles were generated in a capillary tube and their movement was controlled by a speaker drum. Bubbles and particles were kept in contact for different time durations. For a successful attachment, the film between interacting phases should undergo thinning and rupture to form a stable attachment. This process consists of the three sub-processes described below:

- Thinning to a critical level of thickness (t_t)
- Rupture of film and formation of three phase contact line (also called TPC) (t_r)
- TPC expansion for stable attachment (t_e)

$$t = t_t + t_r + t_e \tag{3.1}$$

The total time, t, is defined as the induction time.

The induction time was measured for all feed distributions. All the samples were mixed with a specific dosage of potassium ethyl xanthate (KEX) as a collector agent. The concentration of the collector agent per m^2 of the galena particles was kept constant at 0.00187 mol/m^2. Various contact times were set ranging from 5ms to 5000 ms to find the probability of attachment. The bubble was dropped on to the particle bed and stayed in contact for the specified contact time, and was then lifted upwards. The outcome of each attempt was observed on the monitor, and multiple trials were performed at each contact time. A contact time that led to more than 50% probability of attachment was taken as the induction time. A sample calculation is demonstrated in Figure 3.3, where the probability of successful attachment attempts is plotted against the contact time. A power function ($y = Ax^b$) is plotted to fit the probability curve and the time corresponding to the probability of 0.5 is the induction time. Induction time values for the samples are reported in Section 3.4 and attachment trends are compared qualitatively with the predictions of the attachment equations in Section 3.3.2. The induction time is used as an offline estimate for the probability of attachment with particle size.

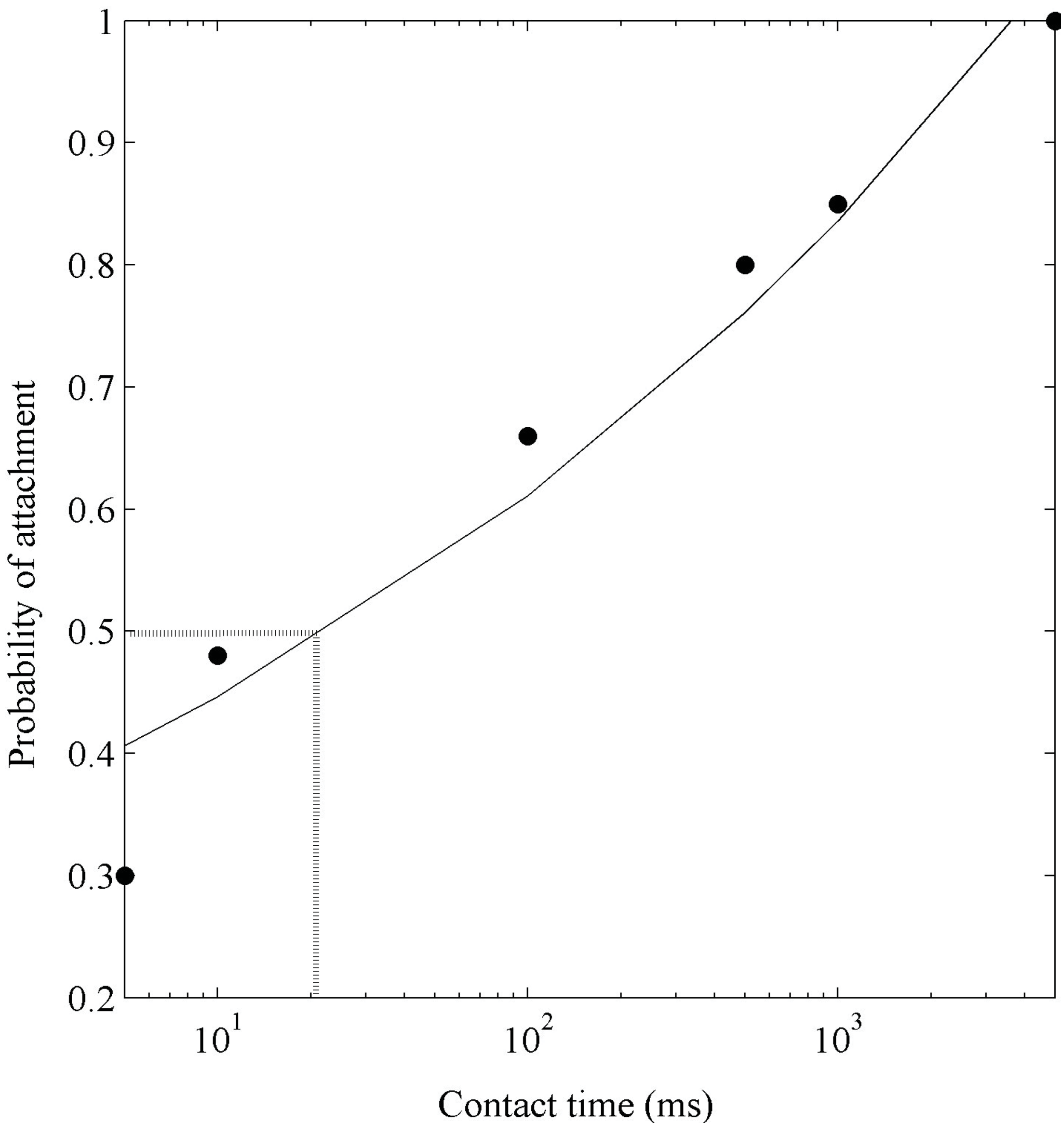

Figure 3.3: Sample calculation for induction time measurement based on attachment probability of 0.5 after fitting the probability with a power function (y = Ax^b).

3.3 Monitoring scheme: Image-based soft sensor, fundamental model, and real-time estimation

A monitoring scheme was developed based on updating the model using an extended Kalman filter (EKF), with online measurements being obtained from the image-based soft sensor. The monitoring scheme is illustrated in Figure 3.4. The model was supplied with initial guesses for the states along with the model inputs. The outputs of the model were then compared with the output of the soft sensor to update the state estimates for the model based on extended Kalman filtering. The particle size was then estimated and monitored in real-time with the EKF. The following subsections explain the image-based *soft sensor development*, *fundamental model*, and *state estimation*.

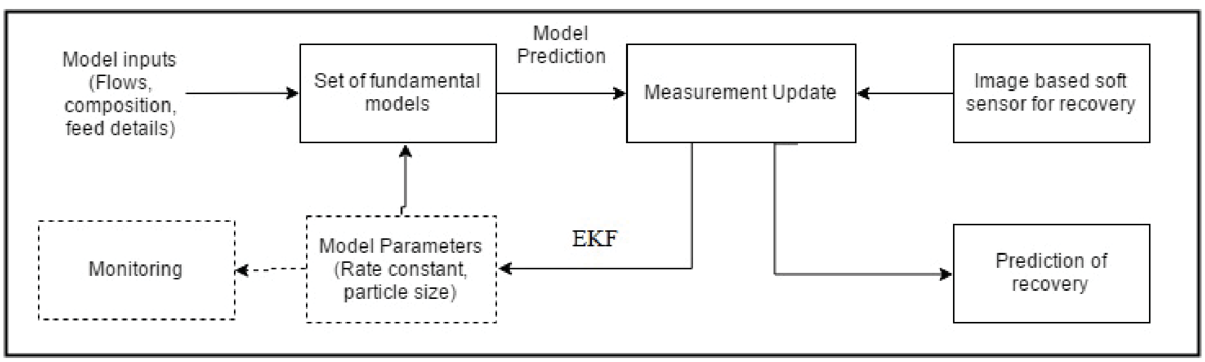

Figure 3.4: Monitoring scheme based on state estimation using the extended Kalman filter (EKF).

3.3.1 Development of image-based soft sensor for online recovery

It is very difficult to devise online measurements of grade and recovery for ore flotation. Conventional methods such as (offline) X-ray fluorescence (XRF) spectroscopy have higher sampling times and online methods such as the in-line XRF are expensive and often difficult to calibrate (Popli et al., 2015). Image-based soft sensors explore the relationship between froth appearance and froth composition to develop an online estimate of grade and consequently, recovery (Moolman et al., 1996). In this work, the image features listed in Table 3.2 were used as real-time inputs to obtain the online recovery inferentially.

In this case of pure mineral flotation, we proposed that the image was linked to the cumulative recovery or the amount of mineral entering the concentrate. For example, image features at time of t = 10 s were correlated to the total/cumulative recovery from time of t=0 s to t=10 s. While we have developed a soft sensor using froth images previously (Popli et al., 2015), we have improved it in this work by using ensemble regression methods. Specifically, we have used random forest-based regression, which is based on a nearest neighbor approach; we have found it to provide a more accurate image-based soft sensor.

Random forests, introduced by Breiman (Breiman, 2001), are based on the bagging ensemble algorithm, where a series of regression trees are developed independently, and the average of all the outputs from different trees is taken as the final output (Liaw and Wiener, 2002). Each regression tree choses the data based on bootstrap sampling, which is resampling with replacement. Unlike normal regression trees, where all the variables are used to decide the node split, random forest trees choose the node split based on random variables (Breiman, 2001). In this study, no pruning was performed for the trees. Hence, two parameters were considered for hyperparameter optimization of the random forest regression model. The minimum number of observations per trees, *No*, and the number of sample variables at each node, *Nv*, were optimized using the validation error as the objective function. The validation technique, '*out of box (oob)*', is based on the average error in outcomes of samples not chosen as the part of bootstrap sampling. Parameters were optimized based on Bayesian optimization using the statistics and machine learning toolbox in MATLAB with 'expected improvement plus' as the acquisition function, which evaluates the expected amount of improvement in the function and also avoids the local minima (Snoek et al., 2012; Gelbart et al., 2014). Based on the optimized parameters, a random forest model was built to predict the cumulative recovery and evaluated on the 22 image features listed in Table 3.2. The soft sensor development using random forest regression is summarized in Table 3.4. A constraint has been implemented to ensure that the cumulative recovery (y_k) at any time step k is higher than the cumulative recovery at the previous time step $k-1$ (y_{k-1}).

Table 3.4: Image-based soft sensor development specifications for random forest regression.

Specification	Value
Input data and size	Image features
Target output	Cumulative recovery
Test set percentage	10
Number of trees	300
Range for tuning parameter, No	[1 20]
Range for tuning parameter, Nv	[1 21]
Optimization function	*Out of box* error
Optimization algorithm	Bayesian
Acquisition function	*Expected improvement plus*

3.3.2 Multiscale fundamental model

The detailed modeling framework from our previous work (Popli et al., 2015) considers the different states a particle can be in: attached to bubbles in pulp, free in the pulp or collected in the concentrate. In this work, we have modified the model to incorporate the effect of the particle size on the rate constants related to probabilities of collision, attachment and detachment. Equations 3.2, 3.3, and 3.4 represent the state equations for the particles and Equation 3.5 represents the recovery.

$$\frac{d}{dt}(\epsilon_p V_p x_b) = k_1(1-\epsilon_p)V_p x_p - k_2 \epsilon V_p x_b - Q_{air} x_b \quad (3.2)$$

$$\frac{d}{dt}((1-\epsilon_p)V_p x_p) = k_2 \epsilon_p] V_p x_b - k_1(1-\epsilon_p)V_p x_p - Q_E x_p \quad (3.3)$$

$$\frac{d}{dt}(V_f x_c) = -k_3 V_f x_c + Q_{air} x_b + Q_E x_p \quad (3.4)$$

$$y = \frac{V_f t_{samp} k_3 x_c}{m_{int}} \quad (3.5)$$

where x_b, x_p, and x_c denote the concentration of particles attached to the bubbles in the pulp, concentration of particles free in the pulp and concentration of the particles collected in the froth, respectively. k_1, k_2, and k_3 denote the attachment rate constant, detachment rate constant, and rate constant for removal into the concentrate, respectively. ϵ_p denotes the air volume fraction in the pulp. V_f and V_p denote froth phase and pulp phase volumes, respectively. Q_{air} and Q_E denote the air flow rate and the entrainment flow rate, respectively. m_{int} denotes the initial mass, t_{samp} denotes the sampling time, and y denotes the instantaneous recovery of the process.

This model can also be represented as

$$\dot{\mathbf{X}} = f(\mathbf{X},\mathbf{U}) \quad (3.6)$$

$$\mathbf{Y} = g(\mathbf{X},\mathbf{U}) \quad (3.7)$$

where $\mathbf{X}$ is the vector of state variables $[x_b \ x_p \ x_c]^T$, $\dot{\mathbf{X}}$ is its derivative with respect to time, $\mathbf{Y}$ is the output(recovery), $\mathbf{U}$ is the vector of inputs to the system, and $\mathbf{w}$ and $\mathbf{v}$ are process and measurement noises, respectively.

The attachment rate constant, k_1, and the detachment rate constant, k_2, are further dependent on various probabilities and can be represented using the following equations:

$$k_1 = Z_1 P_c P_a P_s \tag{3.8}$$

$$k_2 = Z_2 P_d \tag{3.9}$$

where Z_1, Z_2, P_c, P_a, P_s, and P_d, represent the collision frequency, detachment frequency, probability of bubble-particle collision, probability of bubble-particle attachment, probability of bubble-particle aggregate stability and probability of bubble-particle detachment, respectively, and are given by (Duan et al., 2003; Z. Dai S.S. Dukhin and Ralston, 1998; Dai et al., 2000; Tao, 2005; Dai et al., 1999):

$$Z_1 = 30 \frac{Q_{air}\sqrt{U_b^2 + {U_p}^2}}{\pi D_b^2 V_{cell} v_b} \left(\frac{D_p + D_b}{2}\right)^2 \tag{3.10}$$

$$Z_2 = \sqrt{2}\epsilon^{\frac{1}{3}} (D_p + D_b)^{-\frac{2}{3}} \tag{3.11}$$

$$P_c = 3\sin^2\theta_t \exp\left[3K_3\cos\theta_t\left(\ln\frac{D_b}{D_p} - 1.8\right) - \frac{9K_3\left(\frac{2}{3} + \frac{\cos^3\theta_t}{3} - \cos\theta_t\right.}{\frac{6D_p\sin^2\theta_t}{D_b}}\right]\frac{D_p}{D_b} \tag{3.12}$$

$$P_a = \sin^2\left(2\arctan\exp\left[-t_{ind}\frac{2(v_p + v_b) + v_b\left(\frac{D_b}{D_p + D_b}\right)^3}{D_p + D_b}\right]\right) \tag{3.13}$$

$$P_d = \frac{1}{1 + \frac{F_{at}}{F_{de}}} \tag{3.14}$$

$$P_s = 1 - P_d \tag{3.15}$$

where U_p and U_b are the relative turbulent fluctuating velocities of particles and bubbles, respectively, D_p and D_b are particle and bubble size, respectively, V_{cell} is the volume of the flotation cell, v_b is the bubble rise velocity, ϵ is the turbulent dissipation energy, K_3 is a dimensionless number, θ_t represents the contact angle, v_p is the particle settling velocity, and F_{at} and F_{det} are the total attachment and detachment forces, respectively.

It is observed that the effect of feed particle size (D_p) propagates to the recovery through the rate constants for attachment (k_1) and detachment (k_2), and the model for recovery is nonlinear with respect to D_p.

The variation in probability with an increase in the particle size is shown in Figure 3.5 for the flotation experiments that were performed. The probability of collision, P_c, shows a maximum at an intermediate value of particle size. While the probability of attachment, P_a, decreases with an increase in the particle size, the probability of stability, P_s, remains constant with respect to particle size. In the terms defining the attachment rate constant (k_1), an increase in particle diameter leads to an increase in P_c up to a maximum, followed by a decrease in P_c at higher particle sizes; an increase in Z_1, and a decrease in P_a and P_s. For k_2, both P_d and Z_2 increase with increasing particle size. The variation of the attachment rate constant, k_1, and the detachment rate constant, k_2, with particle size is shown in Figure 3.6. It can be seen that an increase in the particle size leads to an increase in the detachment rate constant, k_2, and shows a maximum with respect to the attachment rate constant, k_1. This indicates that the effect of particle size on flotation is nonmonotonic and justifies the requirement of an optimal particle size range for efficient flotation.

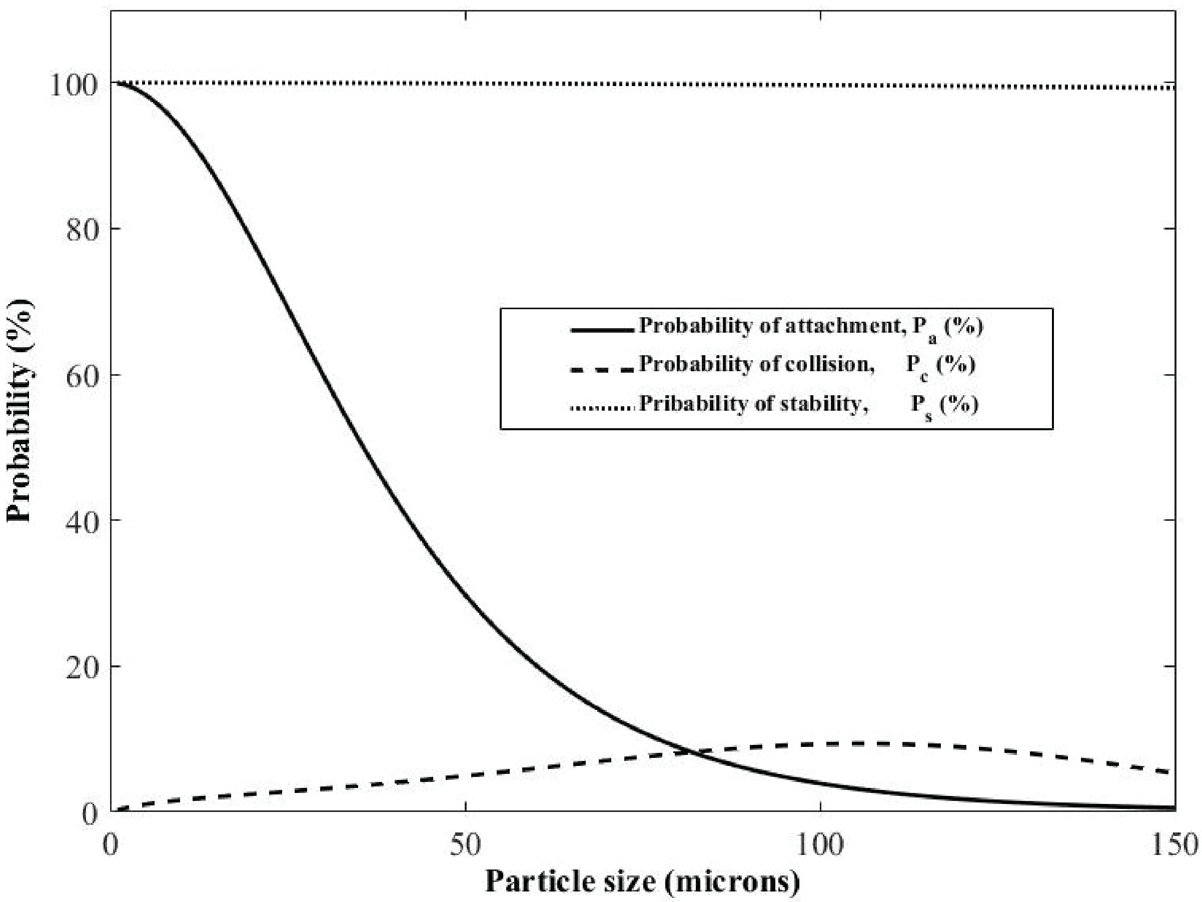

Figure 3.5: Variation in probabilities of collision, attachment and stability with an increase in the particle size.

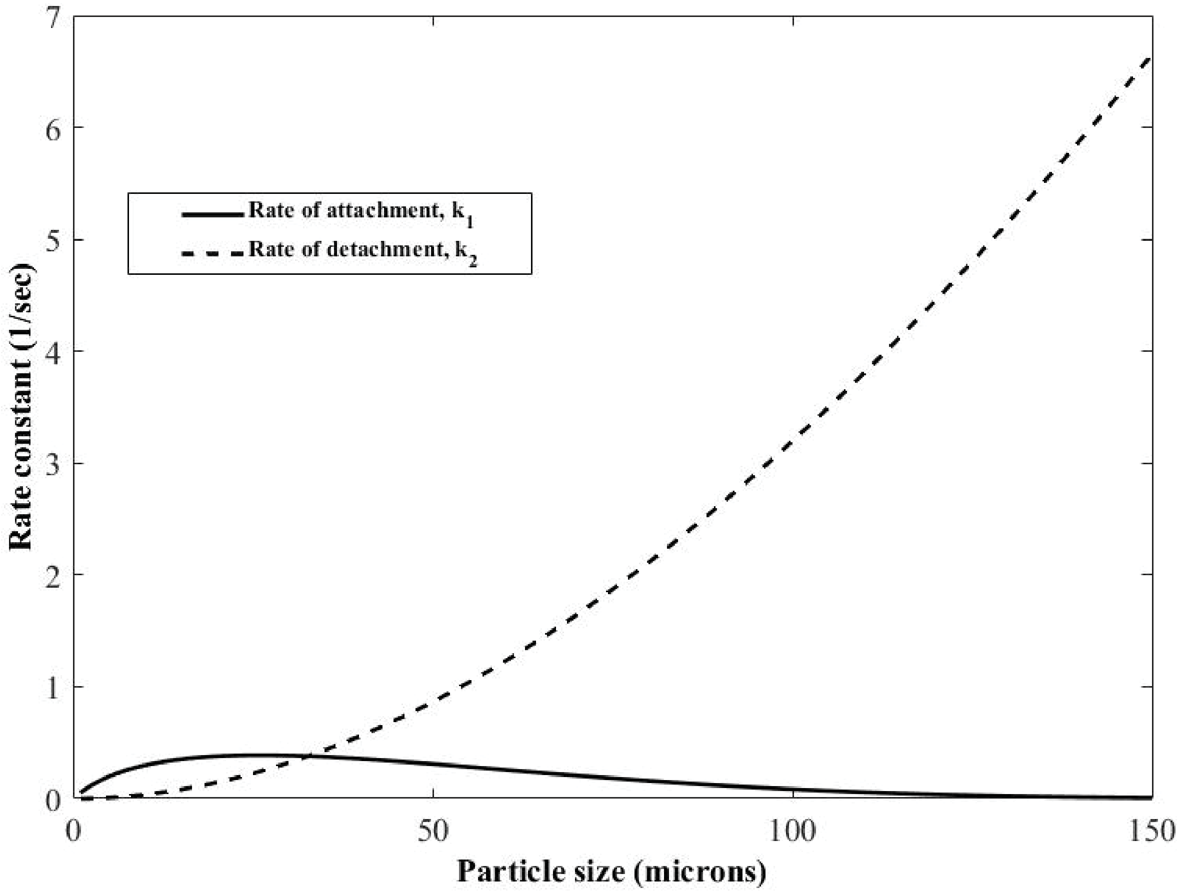

Figure 3.6: Variation in the rates of attachment and detachment with an increase in the particle size.

3.3.3 State and parameter estimation

Model states and parameters were estimated based on real-time measurements using the extended Kalman filter (EKF). It is based on minimizing the error covariance between the predicted output and its measurement. Fundamentally, the EKF is based on two steps: model prediction and measurement update. In the prediction step, the model is integrated in time to provide an estimate at the next time step, and in the measurement update that follows, the state estimates are updaetd based on the error between model predictions of the output (recovery) and the measured output value (Kalman, 1960; Welch and Bishop, 1995; Popli et al., 2015). The nonlinear model (equations 3.6 and 3.7) can be linearized using Taylor series expansion to obtain the following linear state space model:

$$\dot{\mathbf{X}} = \mathbf{AX} + \mathbf{BU} + \mathbf{w} \tag{3.16}$$

$$\mathbf{Y} = \mathbf{CX} + \mathbf{DU} + \mathbf{v} \tag{3.17}$$

where $\mathbf{w}$ and $\mathbf{v}$ are process and measurement noises, respectively, $\mathbf{A}$, $\mathbf{B}$, $\mathbf{C}$ and $\mathbf{D}$ are Jacobian matrices defined as:

$$\mathbf{A} = \frac{\partial f(X,U)}{\partial X} \quad \mathbf{B} = \frac{\partial f(X,U)}{\partial U} \quad \mathbf{C} = \frac{\partial g(X,U)}{\partial X} \quad \mathbf{D} = \frac{\partial g(X,U)}{\partial U}$$

Parameters were estimated by augmenting the state space matrix with a certain number of model parameters as a state (Popli et al., 2015). Based on observability analysis, only one parameter could be estimated by augmenting it with the states. Three choices of parameters to estimate, k_1, k_2, and D_p, were investigated. Initial parameter conditions for the EKF were obtained from a combination of evaluating fundamental rate equations (k_1, k_2) and nonlinear optimization (k_3) with an objective function based on the error between the recovery predicted by the model and the image-based soft sensor.

Indirect estimation of particle size

As seen from equations 3.8 and 3.9, both the rate constants are functions of D_p. Since only one parameter can be estimated using the EKF, both cases were considered separately, i.e., estimation of k_1 and k_2, and D_p was estimated indirectly by back-calculating it from these estimates. Also, the variation of the estimated k_1 and k_2 was studied for different feed particle size distributions.

Direct estimation of particle size

D_p can be estimated directly by expanding the functions f(**X**,**U**) and g(**X**,**U**) in equations 3.6 and 3.7 explicitly in terms of D_p by using equations 3.8 and 3.9 with D_p as the parameter. Matrices **A**, **B**, **C**, and **D** were evaluated using Taylor series expansion with D_p as an augmented state. This procedure was performed for all the three distributions with initial conditions obtained from the mean particle size. However, for the test distribution, no prior knowledge of its particle size was used in the estimation, and D_p was treated as being unknown. The conditions for Distribution III were used as the initial conditions for the estimation of the unknown test distribution, and the particle size was estimated using the image-based soft sensor and the EKF.

3.4 Results and discussion

3.4.1 Batch flotation experiments

Batch flotation was performed for all the four feed particle size distributions. The flotation dynamics are summarized in Figure 3.7 in the form of cumulative recovery versus time. It can be seen that distribution III, with the largest feed particle size, has the slowest dynamics and lowest recovery (92%), followed by 96%, 98.3% and 98.6% for distributions II, I and the test distribution, respectively. This is a clear indication that an increase in the particle size of galena lowered the recovery (y) and the attachment rate constant (k_1). Also, the recovery curves at the initial stages look similar for all the distributions and it is very difficult to monitor the particle size as well to isolate the fault in particle size among other recovery-reducing factors at these early stages of the flotation.

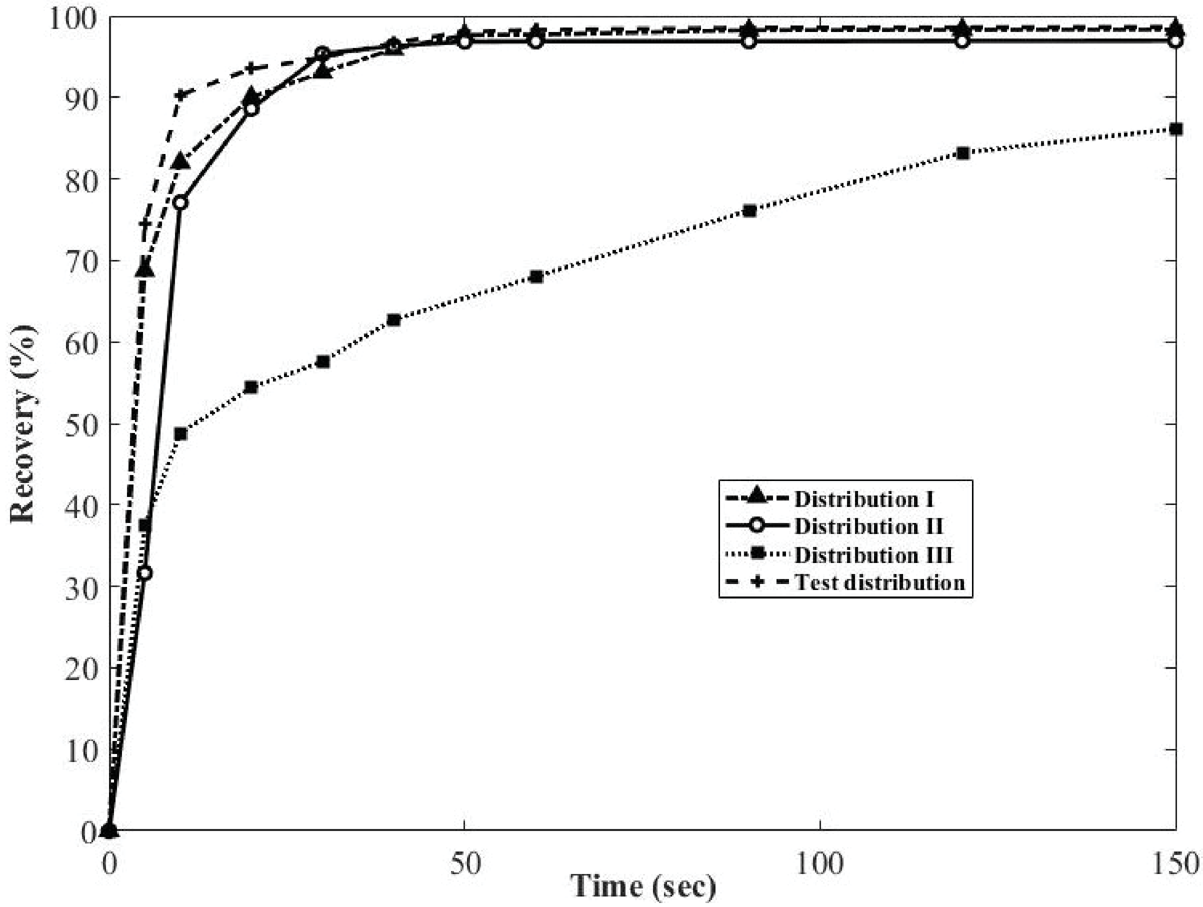

Figure 3.7: Flotation dynamics: cumulative recovery for all the distributions.

3.4.2 Image based soft sensor - Random forest

The experimental data from the flotation runs was used to develop the random forest-based soft sensor for prediction of the recovery at each sampling time (i.e., 5 s). Two sample images are shown in Figure 3.8 for distribution II at 5 s and 25, and we see that the colour changes significantly in this period. The image features listed in Table 3.2, including the colour, are used as inputs for the soft sensor. The random forest model parameters *No* and *Nv* were selected based on Bayesian optimization with minimum prediction error. Optimization results in Figure 3.9 show the variation of the 'out of box' (oob) error with *Nv* and *No*. It is shown that the oob error increases with *No* and *Nv* after reaching a minimum at No = 1 and Nv = 2 for oob error = 3.6917.

Figure 3.8: Froth images for distribution II at 5 s (left) and 25 s (right).

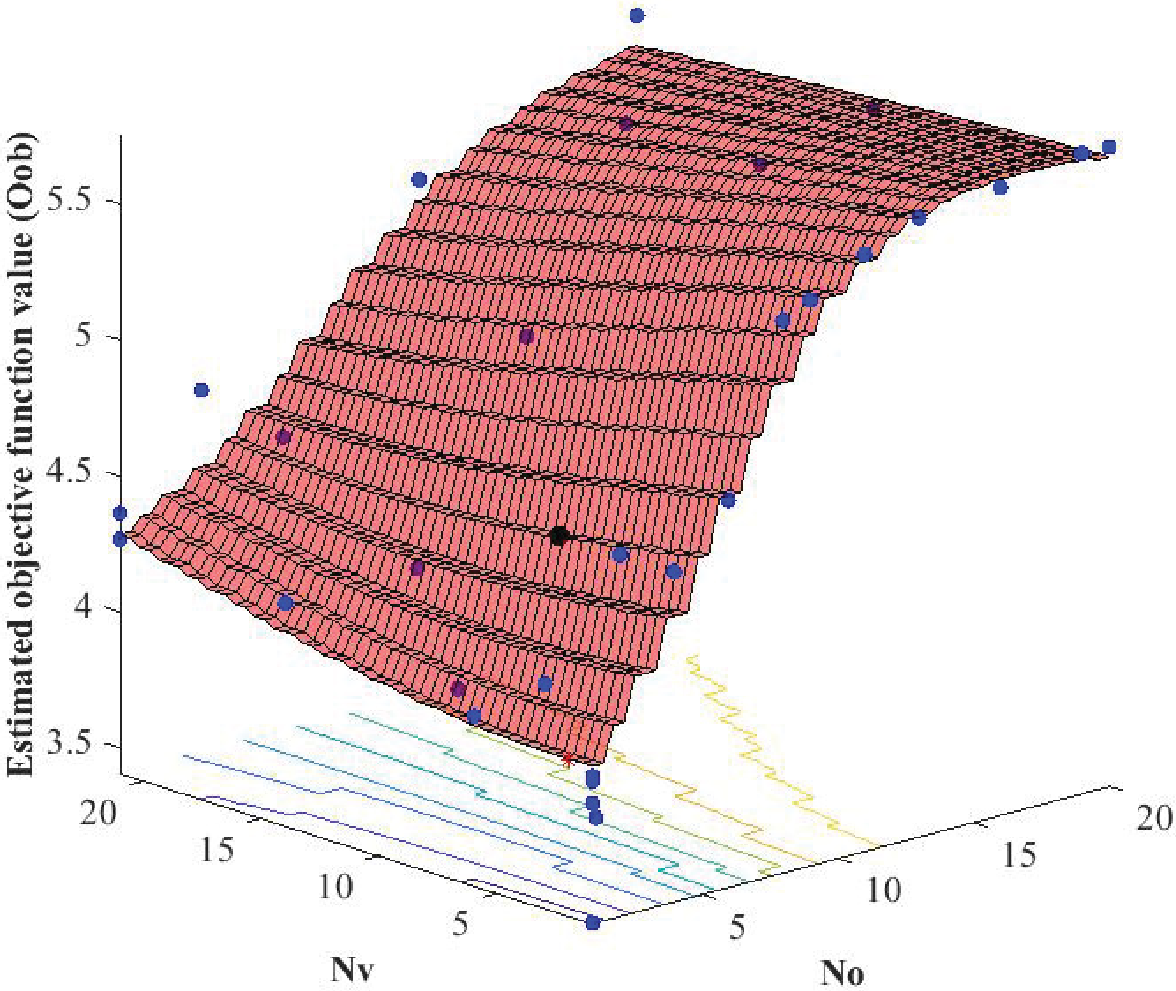

Figure 3.9: Hyperparameter optimization for random forest model using 'out of box' error.

The image-based soft sensor developed based on these optimized parameters performed well with a coefficient of determination $R^2 = 0.94$ on validation data. Prediction results for particle size distribution II are presented in Figure 3.10, showing that the recovery is successfully predicted at each sampling time using the soft sensor. In the following sections, the output of the soft sensor will be used and referred to as the measured real-time experimental recovery.

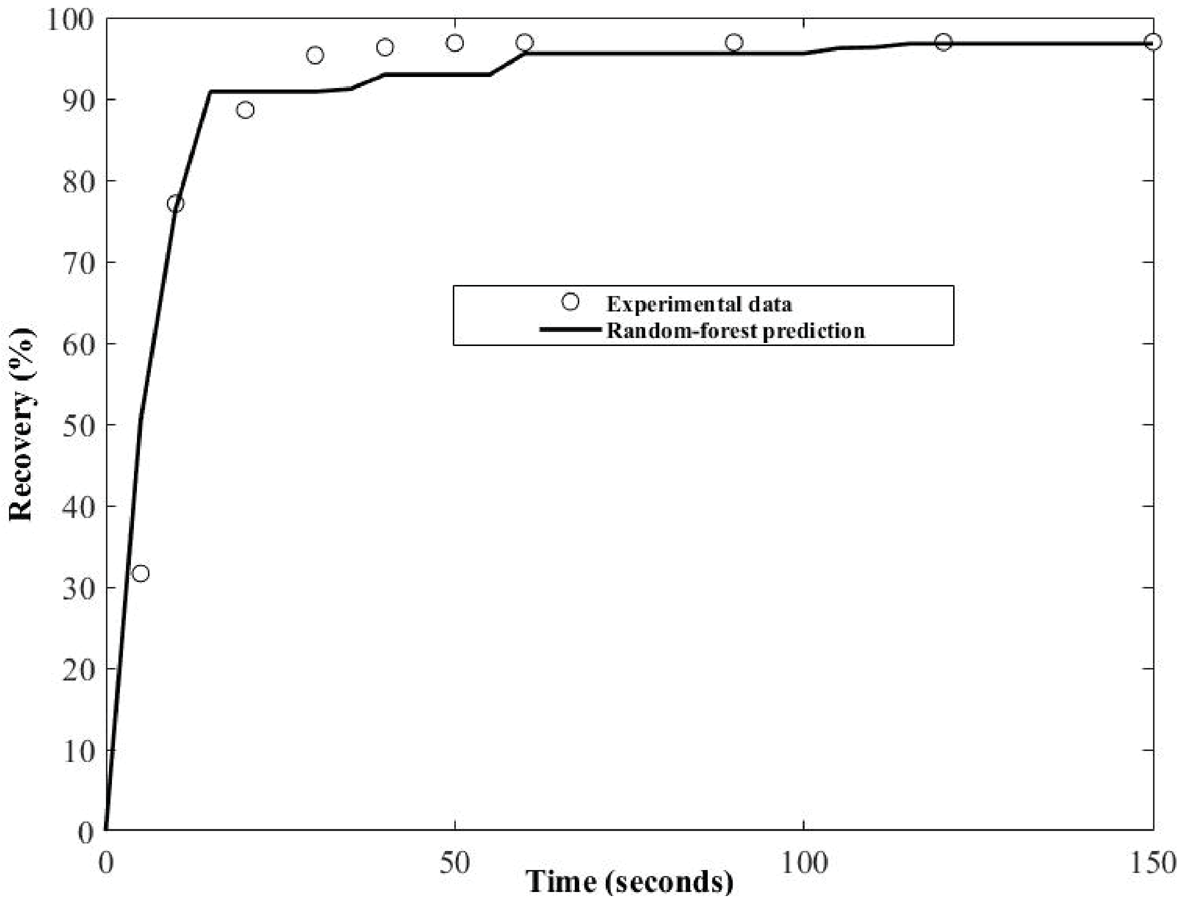

Figure 3.10: Comparison between the experimental recovery and the recovery predicted by the random forest-based soft sensor for particle size distribution II.

3.4.3 Qualitative analysis of induction time variation with particle size

The induction time was measured for all the four distributions with varying collector concentrations to maintain the same amount of collector per m^2 of the surface of galena. The probability of attachment in this case is defined as the fraction of attachment attempts in the induction timer that were successful for a specific contact time between a bubble and the particles in the bed. The induction time and the corresponding mean particle size are summarized in Table 3.5 for all the distributions, and the induction time increases as the particle size increases. The increase in individual particle size leads to an increase in its weight that should be carried by the bubbles. Additionally, the time required for stable attachment through TPC expansion increases for a larger particle size. This is in agreement with the relation (Equation 3.13 and Figure 3.5) that the probability of attachment (P_a) decreases with an increase in the particle size. These results are used to qualitatively understand the increase in induction time (and, decrease in P_a) with increase in particle size. However, these values are not used in the real-time dynamic model, as the conditions for the induction time measurement are not similar to those in the flotation cell. The induction time function used for modeling purpose is given below:

$$t_{ind} = 100({D_p}^{0.99}) \tag{3.18}$$

where t_{ind} is the induction time, and D_p is the particle mean size.

Table 3.5: Induction time measurements for all particle size distributions.

Distribution	Mean particle size (μ)	Induction time (ms)
Distribution I	12	7
Distribution II	28	23
Distribution III	113	86
Test distribution	45.4	45

3.4.4 Estimation and monitoring

The initial values for all the rate constants were estimated using offline nonlinear optimization (k_3) and fundamental equations for the attachment rate constant, k_1, and the detachment rate constant, k_2 (Equations 3.8 and 3.9). Nonlinear optimization results for recovery are presented in Figure 3.11 for distribution I. It demonstrates the model fit based on least squares regression. Initial conditions that were evaluated for all three distributions are summarized in Table 3.6. However, for the test distribution, initial conditions were chosen to be the same as that of distribution III, since the estimation should be tested without knowledge of the true distribution.

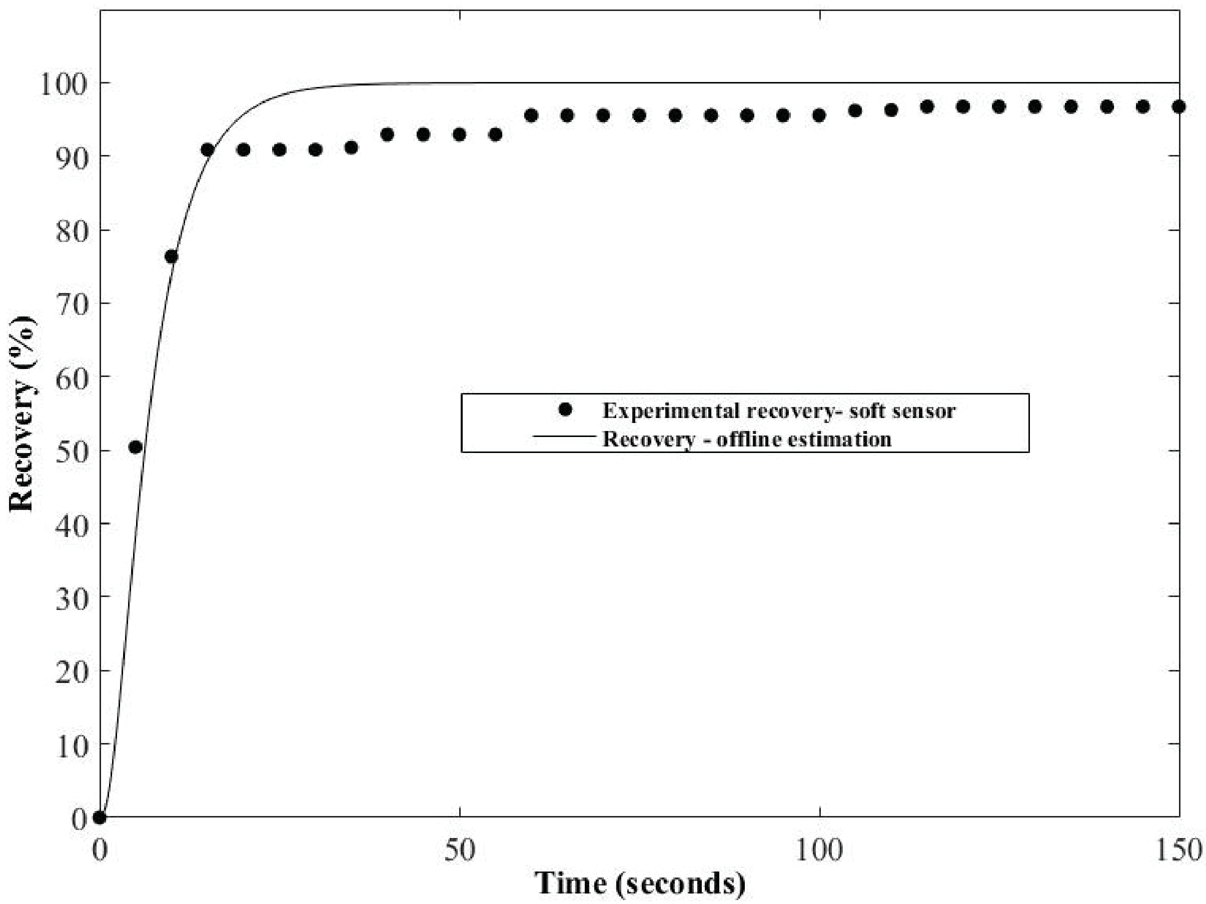

Figure 3.11: Comparison between experimentally measured recovery and the recovery estimated offline for particle size distribution I with an optimized initial value for k_3, the rate constant for removal into the concentrate.

EKF-based state estimation was performed to update the model online using the real-time experimental values of recovery at each time step. Figures 3.12, 3.13 and 3.14 show the online recovery predictions along with parameter estimation for particle size distribution I while Figure 3.15 shows the corresponding real-time estimation of the states

Table 3.6: Initial estimates for model parameters in the extended Kalman filter (EKF).

Distribution	Variable	Initial value (1/sec)
I	k_1	0.324
	k_2	0.050
	k_3	5.10
II	k_1	0.388
	k_2	0.281
	k_3	2.25
III	k_1	0.051
	k_2	3.99
	k_3	3.12

(x_b, x_p and x_c). The EKF model was initialized using the values given in Table 3.6. The parameter estimation converges and captures the real recovery successfully for all the particle size distributions studied. Parameter estimation concludes that attachment rate constant, k_1, has a maximum value for optimum particle size range while detachment rate constant, k_2, increases with the increase in particle size (D_p) in the range studied. These trends are in agreement with the trends based on fundamental relations (section 3.3.2).

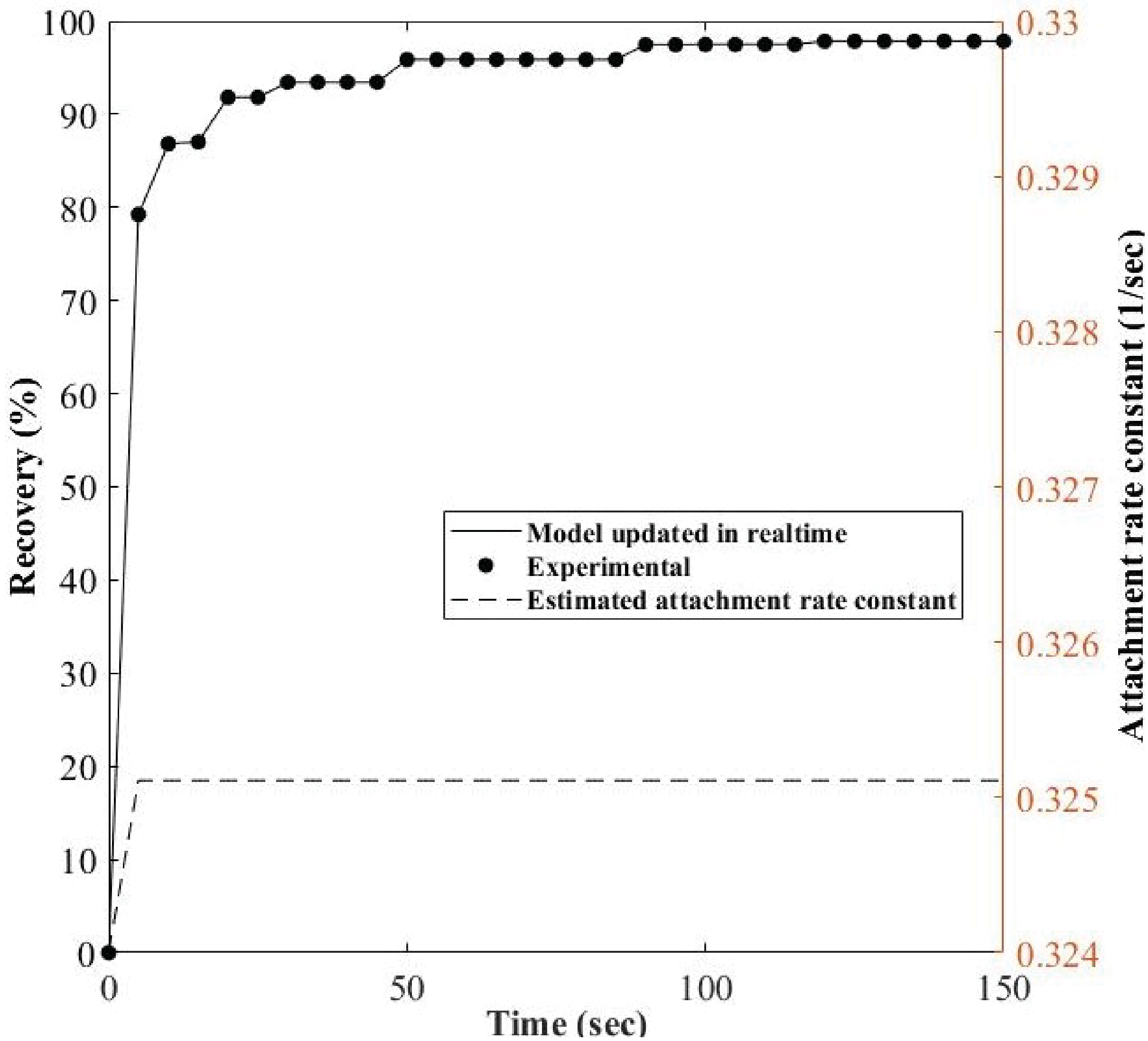

Figure 3.12: Estimation of the parameter k_1 along with prediction of the online recovery for particle size distribution I using the extended Kalman filter.

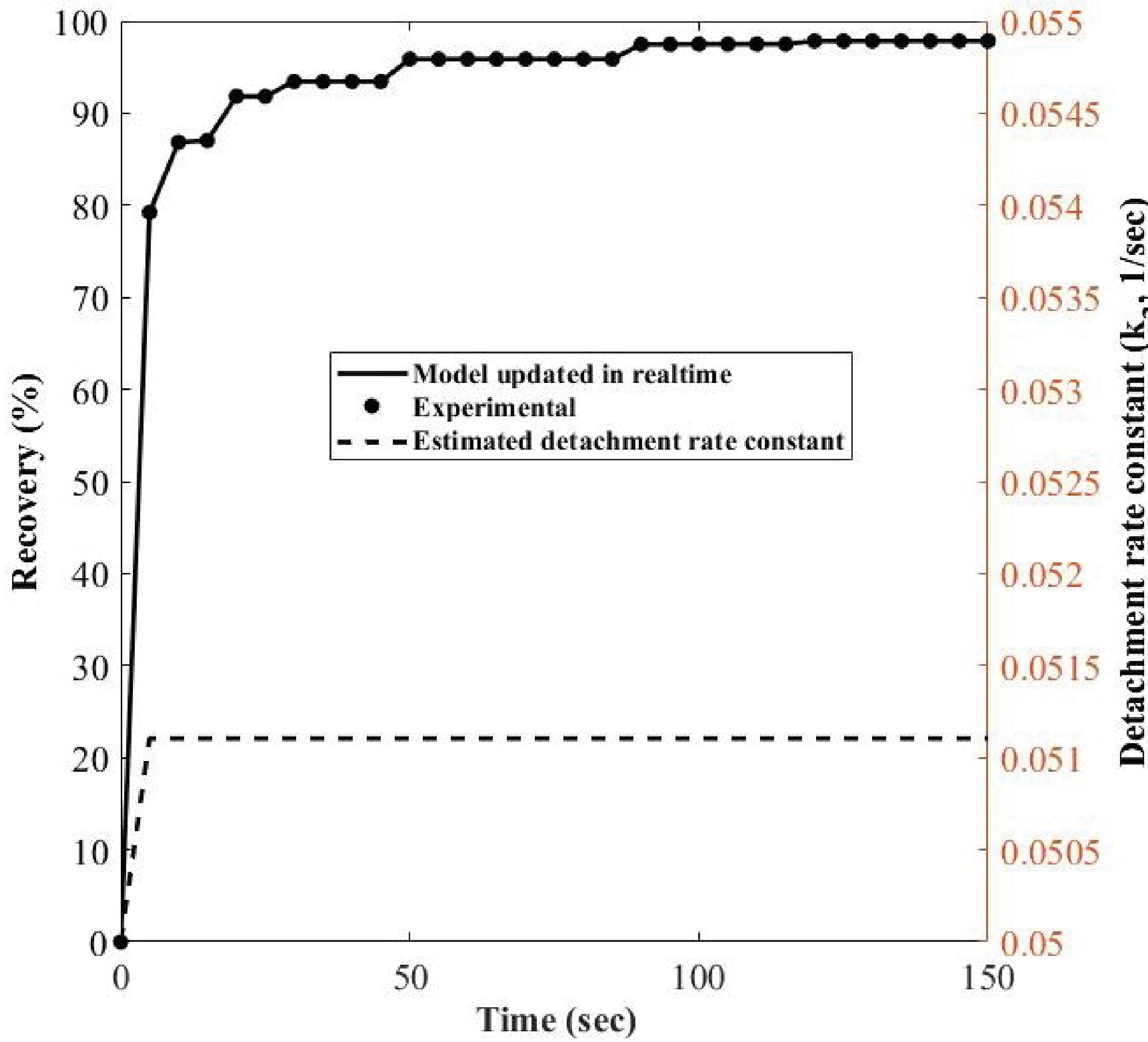

Figure 3.13: Estimation of the parameter k_2 along with prediction of the online recovery for particle size distribution I using the extended Kalman filter.

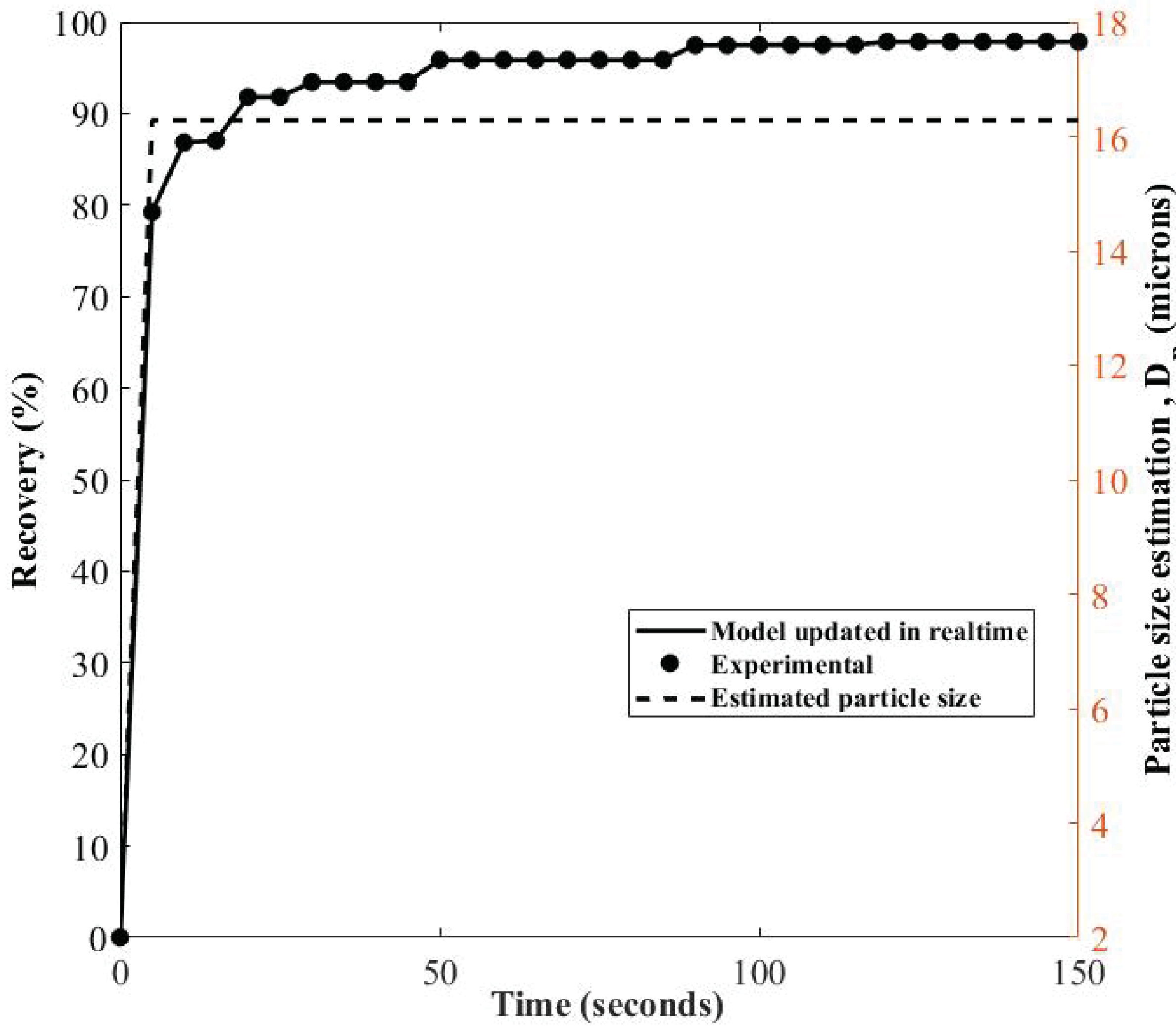

Figure 3.14: Direct estimation of particle size (D_p) along with online recovery prediction using the extended Kalman filter for particle size distribution I.

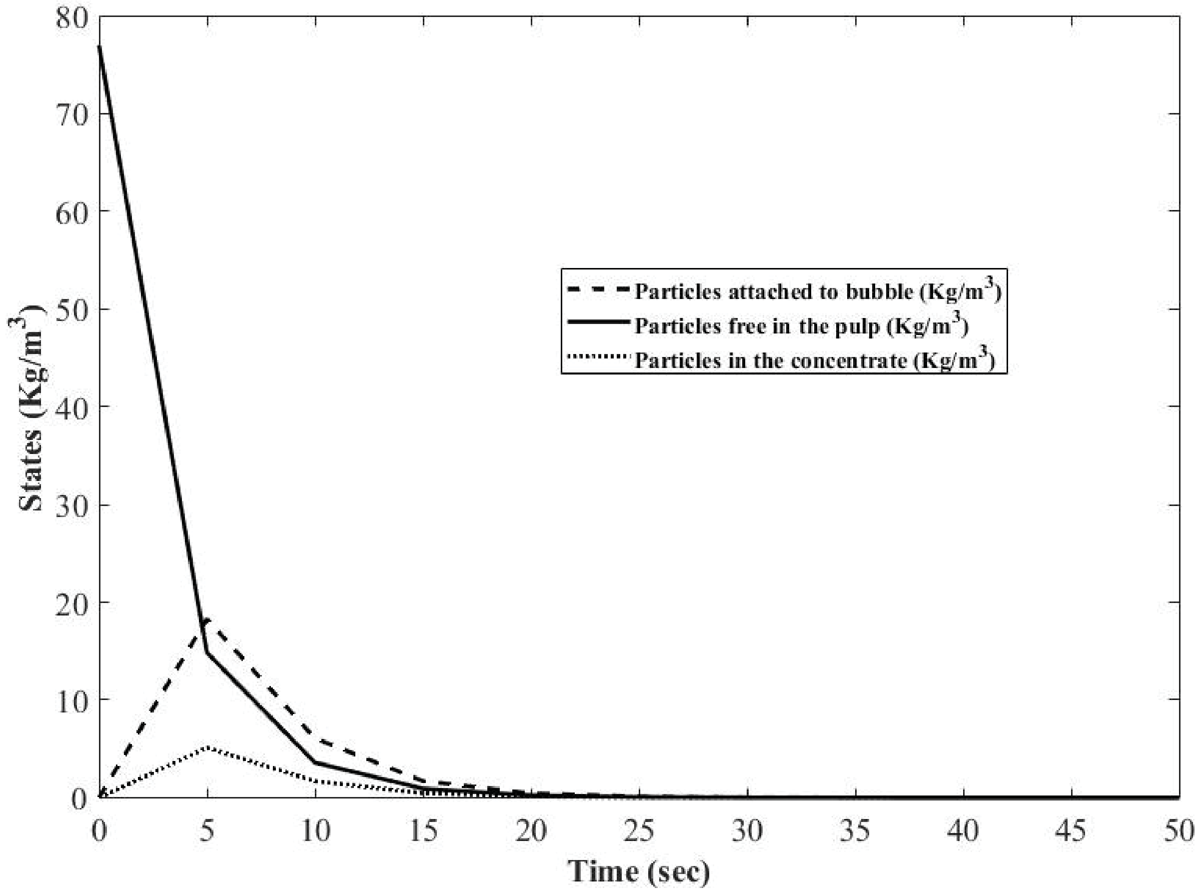

Figure 3.15: Estimation for all the system states using the extended Kalman filter for particle size distribution I.

Indirect particle size monitoring is presented in Figure 3.16 where estimation of k_1 was performed for both distribution III and the test distribution, with the same initial conditions. Indirect D_p estimation was performed by back-calculating D_p using the equations for k_1 and k_2 (Equations 3.8 and 3.9). Direct estimation of D_p for distribution III and the test distribution is presented in Figure 3.17, with the same initial conditions in both the cases. These values are summarized in Table 3.7. It was observed that D_p is estimated more accurately using the direct estimation, where the estimate converges closer to the true value. Indirect estimation does not work accurately; this is because D_p

influences both k_1 and k_2, but only one of those two parameters can be updated using the EKF, and this leads to inconsistency and inaccuracy in the back-calculation of the particle size. Therefore, we recommend using the direct estimation of D_p for monitoring the particle size.

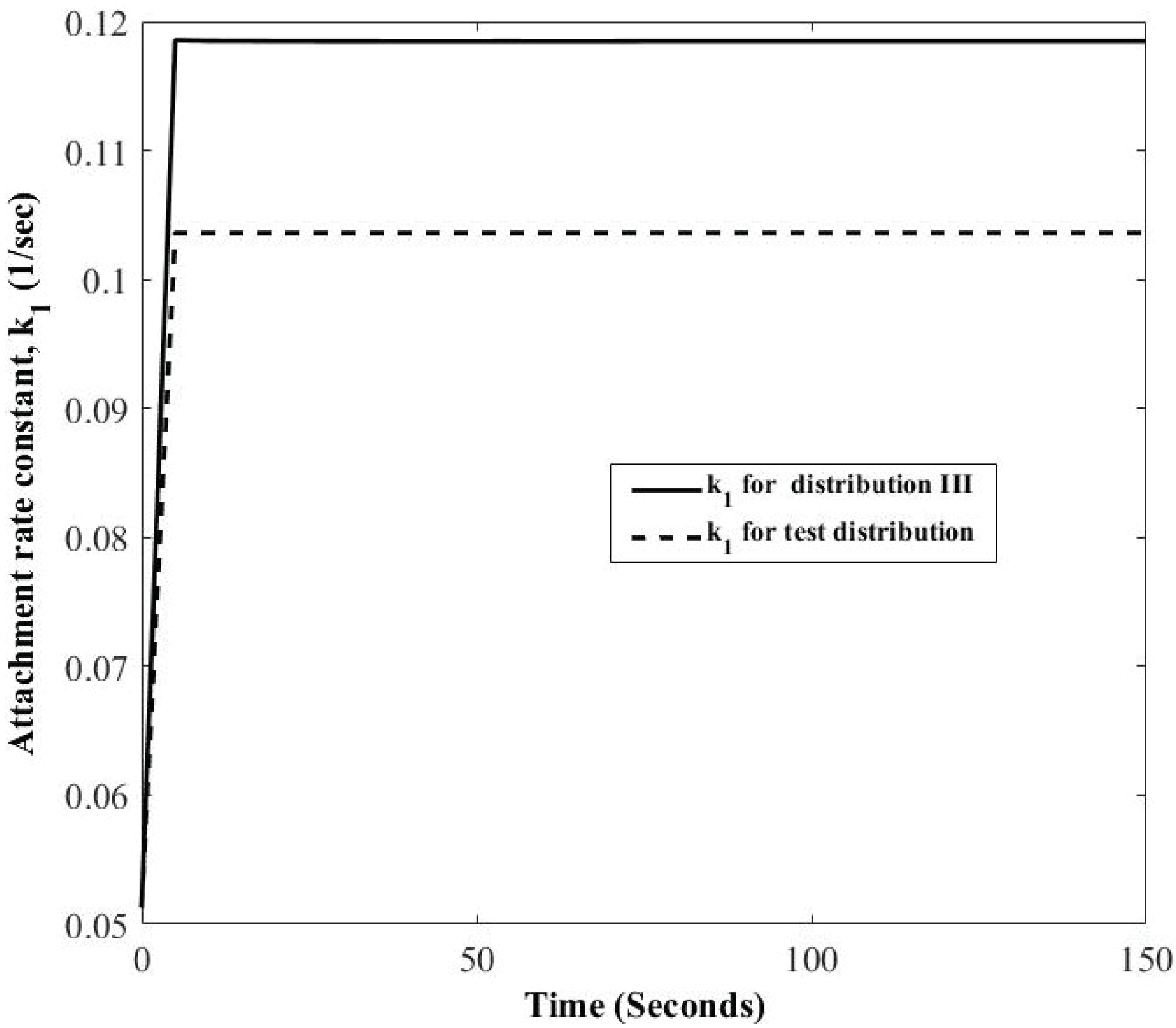

Figure 3.16: Indirect estimation of the particle size (D_p): monitoring of the rate of attachment (k_1) for the test distribution.

Table 3.7: Particle size estimation using indirect and direct estimation for the test distribution.

Estimation method	Particle size estimate, D_p (microns)
Indirect using k_1	94
Indirect using k_2	81
Direct	50
Measured value	45.4

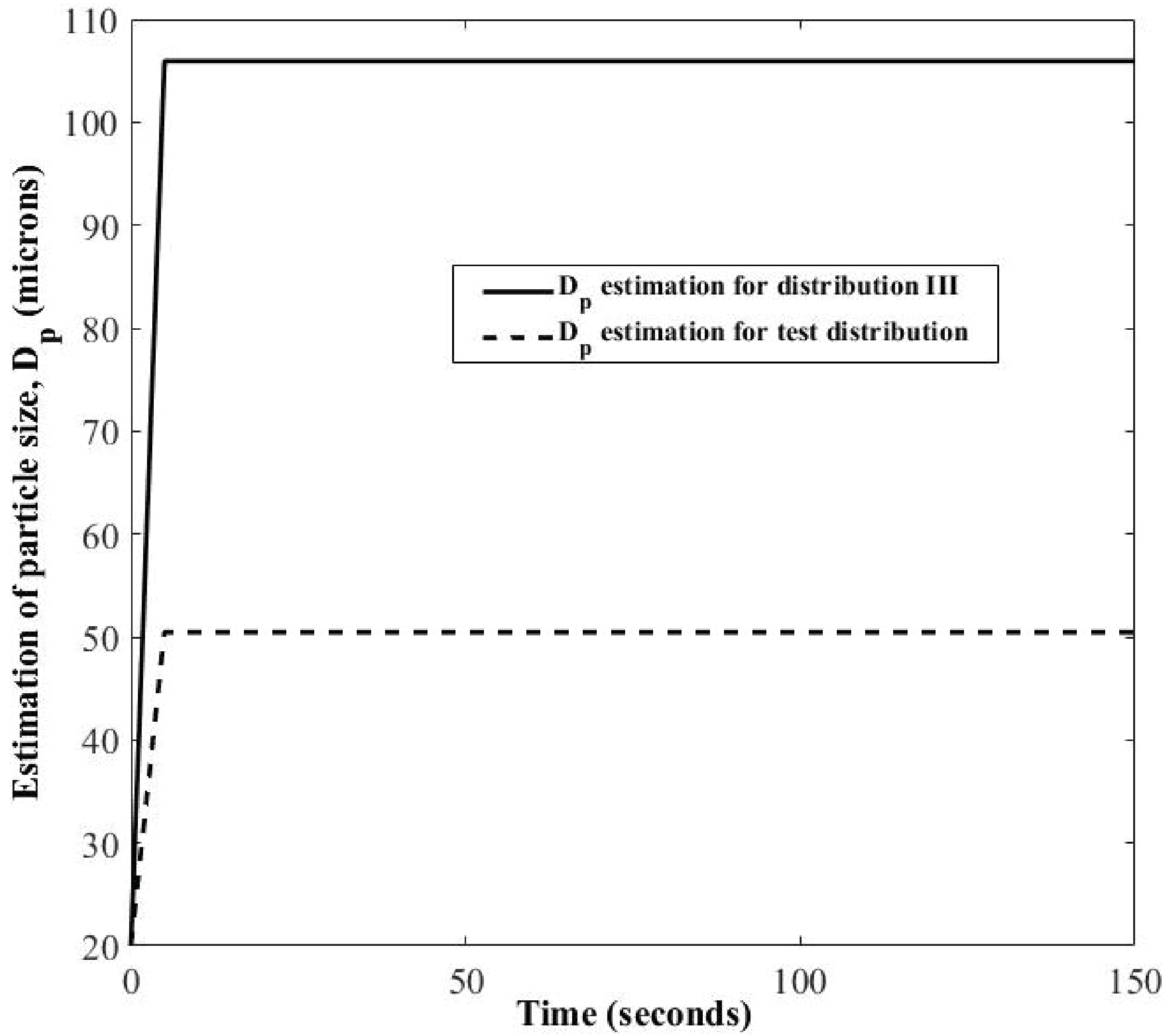

Figure 3.17: Direct estimation of the particle size (D_p) for the test distribution (true D_p = 45.4 microns).

3.5 Conclusions

This work proposed a methodology to monitor the feed particle size in the flotation process in real time. Four different galena particle size distributions, including one test distribution were considered for the development and testing of the monitoring scheme. The monitoring scheme consisted of a fundamental dynamic model, a soft sensor based on image processing and random forest regression for online estimation of recovery, and an extended Kalman filter-based real time estimation scheme to update estimates of the particle size.

We have provided validation for the random forest-based soft sensor for recovery and the particle size estimation using the extended Kalman filter (EKF). The fundamental model with real-time measurements and parameter estimation can be used to monitor the flotation process and understand different sub-processes and their dynamics. This scheme can be used in an industrial-scale flotation circuit, where the soft sensor and the EKF can be used on each flotation cell. Real-time monitoring of flotation sub-processes and the particle size distributions in each cell can be used for real-time fault detection and diagnosis to identify possible disturbances in the particle size distribution of the feed to the various cells in the flotation circuit and enable quick corrective action.

3.6 References

Aldrich, C., Marais, C., Shean, B.J., Cilliers, J.J., 2010. Online monitoring and control of froth flotation systems with machine vision: A review. International Journal of Mineral Processing 96, 1–13.

Aldrich, C., Moolman, D.W., Bunkell, S.J., Harris, M.C., Theron, D.A., 1997. Relationship between surface froth features and process conditions in the batch otation of a sulphide ore. Minerals Engineering 10, 1207–1218.

Bouchard, J., Desbiens, A., del Villar, R., 2005. Recent advances in bias and froth depth control in flotation columns. Minerals Engineering 18, 709–720.

Breiman, L., 2001. Random forests. Machine Learning 45, 5–32.

Brown, N., Bourke, P., Ronkainen, S., van Olst, M., 2001. Improving flotation plant performance at Cadia by controlling and optimizing the rate of froth recovery using Outokumpu Frothmaster, in: 33rd Annual Meeting of Canadian Mineral Processors, Ottawa, Canada. pp. 25–36.

Cipriano, A., Guarini, M., Vidal, R., Soto, A., Sepulveda, C., Mery, D., Griseno, H., 1998. A real time visual sensor for supervision of flotation cells. Minerals Engineering 11, 489–499.

Dai, Z., Fornasiero, D., Ralston, J., 1999. ParticleBubble Attachment in Mineral Flotation. Journal of Colloid and Interface Science 217, 70–76.

Dai, Z., Fornasiero, D., Ralston, J., 2000. Particlebubble collision models a review. Advances in Colloid and Interface Science 85, 231–256.

Duan, J., Fornasiero, D., Ralston, J., 2003. Calculation of the flotation rate constant of chalcopyrite particles in an ore. International Journal of Mineral Processing 72, 227–237.

Gaudin, A.M., Groh, J.O., Henderson, H.B., 1931. Effect of particle size on flotation. The American Institute of Mining, Metallurgical, and Petroleum Engineers 414, 3–23.

Gelbart, M.A., Snoek, J., Adams, R.P., 2014. Bayesian Optimization with Unknown Constraints. Technical Report.

Glembotsky, V.A., 1953. The time of attachment of air bubbles to mineral particles in flotation and its measurement. Izvestiya Akademii Nauk SSSR (OTN) 11, 1524–1531.

Gu, G., Xu, Z., Nandakumar, K., Masliyah, J., 2003. Effects of physical environment on induction time of airbitumen attachment. International Journal of Mineral Processing 69, 235–250.

Haddad, A., 1976. Applied optimal estimation. volume 64. The MIT Press, Cambridge.

K. Runge R. Crosbie, T.R.J.M., 2010. An evaluation of froth recovery measurement techniques. XXV International Mineral Processing Congress, Brisbane, Australia XXV.

Kaartinen, J., Koivo, H., 2002. Machine vision based measurement and control of zinc otation circuit. Studies in Informatics and Control 11, 97–105.

Kalman, R.E., 1960. A New Approach to Linear Filtering and Prediction Problems .

Kawatra, S.K., 2002. Froth Flotation - Fundamental Principles. Technical Report. Michigan Technical University.

King, R., 2012. Modeling and Simulation of Mineral Processing Systems. Society for Mining, Metallurgy and Exploration Inc, USA. 2 edition.

Liaw, A., Wiener, M., 2002. Classification and Regression by randomForest. R News 2, 18–22.

Liu, J.J., MacGregor, J.F., 2008. Froth-based modelling and control of otation processes. Minerals Engineering 21, 642–651.

Moolman, D.W., Eksteen, J.J., Aldrich, C., van Deventer, J.S.J., 1996. The significance of flotation froth appearance for machine vision control. International Journal of Mineral Processing 48, 135–158.

Neethling, S.J., Cilliers, J.J., 2002. Solids motion in flowing froths. Chemical Engineering Science 57, 607–615.

Neethling, S.J., Cilliers, J.J., 2009. The entrainment factor in froth flotation: Model for particle size and other operating parameter effects. International Journal of Mineral Processing 93, 141–148.

Neethling, S.J., Lee, H.T., Cilliers, J.J., 2003. Simple relationships for predicting the recovery of liquid from flowing foams and froths. Minerals Engineering 16, 1123–1130.

Popli, K., Sekhavat, M., Afacan, A., Dubljevic, S., Liu, Q., Prasad, V., 2015. Dynamic modeling and real-time monitoring of froth flotation. Minerals 5, 570–591.

Prasad, V., Schley, M., Russo, L.P., Bequette, B.W., 2002. Product property and production rate control of styrene polymerization. Journal of Process Control 12, 353–372.

Schwarz, S., Alexander, D., 2006. JKSimFloat V6.1 Plus: improving flotation circuit performance by simulation, in: Mineral Process Modelling, Simulation and Control Conference Proceedings, Sudbury. pp. 35–48.

Snoek, J., Larochelle, H., Adams, R.P., 2012. Practical Bayesian optimization of machine learning algorithms. Technical Report. University of Toronto.

Tao, D., 2005. Role of Bubble Size in Flotation of Coarse and Fine Particles: A Review. Separation Science and Technology 39, 741–760.

Trahar, W.J., 1981. A rational interpretation of the role of particle size in flotation. International Journal of Mineral Processing 8, 289–327.

Welch, G., Bishop, G., 1995. An Introduction to the Kalman Filter. Technical Report. University of North Carolina.

Ye, Y., Khandrika, S.M., Miller, J.D., 1989. Induction-time measurements at a particle bed. International Journal of Mineral Processing 25, 221–240.

Yoon, R.H., Yordan, J.L., 1991. Induction time measurements for the quartzamine flotation system. Journal of colloid and interface science 141, 374–383.

Z. Dai S.S. Dukhin, D.F., Ralston, J., 1998. The inertial hydrodynamic interaction of particles and rising bubbles with mobile surfaces. J. Colloid Interface Sci. 197, 275–292.

Chapter 4

Real-time Monitoring of Entrainment using Fundamental Models and Froth Images[1]

In this study, entrainment monitoring algorithms were developed, trained and implemented on the batch flotation of three synthetic mixtures of galena and quartz with different particle size ranges for the quartz mineral. An online image-based soft sensor framework was developed to estimate product grade and recovery using support vector regression. A dynamic fundamental model was developed with emphasis on the entrainment and drainage sub-processes. The model was reconciled with online soft sensor measurements and was updated in real-time by estimating the states and parameters using an extended Kalman filter. Along with the online measurements of quartz entrainment recovery, measurements of entrainment and the true flotation contribution for galena particles were obtained in real-time. The proposed monitoring framework was shown to be effective in monitoring entrainment for reducing entrainment while maximizing the grade and recovery of the desired minerals.

[1]A version of this chapter is submitted as Popli, K.; Liu, Q.; Afacan, A.; Prasad, V., 2017 "Real-time Monitoring of Entrainment using Fundamental Models and Froth Images ". Minerals Engineering

4.1 Introduction

The most commonly used mineral separation technique in mineral processing, froth flotation, is based on the principle of selective attachment of mineral particles to gas bubbles. In the majority of flotation processes, the desired mineral is induced with surface hydrophobicity, thus the propensity to attach to gas bubbles, in order to achieve separation from other non-desired (gangue) minerals. With the depletion of good quality (i.e., easily separable) ores, efforts are being made to achieve the desired separation from low quality (i.e.difficult to separate) ores. To process low quality ores, minerals liberation is achieved through fine grinding. However, fine particle flotation causes two major problems: reduction in the attachment of hydrophobic value mineral particles, leading to low recovery, and an increase in the quantity of hydrophilic particles in the concentrate through entrainment, leading to low grade.

Entrainment is a phenomenon wherein the solid particles suspended in the pulp enter the froth phase and the concentrate stream purely by mechanical or hydraulic means rather than by genuine flotation. It is considered a two-step process: upward transfer of particles from the top of the pulp phase to the froth phase, and transfer of these particles from froth phase to the concentrate (Seaman et al., 2006; Wang, 2016; Gorain et al., 1998). the literature reports three ways suspended particles can be entrained and transferred to the froth phase: (Wang, 2016; Smith and Warren, 1989; Gong, 2011; Gaudin, 1957; Moys, 1978; Hemmings, 1981; Bascur and Herbst, 1982; Yianatos et al., 1988)

- **Bubble swarm theory:** Bubbles are crowded just below the pulp-froth interface and the trapped water along with the suspended particles flows downwards. Buoyancy from the bubble swarm pushes some of the water and suspended particles over the interface. (Smith and Warren, 1989; Gong, 2011)

- **Boundary layer theory:** The water layer surrounding the bubbles is used to carry the suspended particles to the froth phase. (Gaudin, 1957; Moys, 1978; Hemmings, 1981; Bascur and Herbst, 1982; Wang, 2016)

- **Bubble wake theory:** Wake generated by the flowing bubbles is used to transfer the suspended particles to the froth phase. (Yianatos et al., 1988; Wang, 2016)

Bubble swarm theory is generally accepted as the dominant mechanism for mechanical entrainment of suspended particles(Wang, 2016; Gong, 2011). Entrained particles, along with the particles detached in the froth phase, can be transferred back to the pulp phase by drainage (Cutting et al., 1986). Plateau borders are formed by the assembly of the water layer surrounding the bubble consists of the liquid in froth zone as shown in Figure 4.1. They provide passage for the drainage of the water and entrained solids, and encourage their settling (Neethling and Cilliers, 2002b). Entrainment to the concentrate stream is the net upward motion of the suspended particles. The entrained particles are part of the water in the plateau border. Many researchers have studied the relationship between water recovery and entrainment recovery (Trahar, 1981; Engelbrecht and Woodburn, 1975; Hemmings, 1981; Lynch, 1981; Johnson, 2005; Laplante et al., 1989). Most of the entrained minerals follow a linear relationship with entrained recovery and water recovery, and the slope is approximated as the degree of entrainment (Wang, 2016; Trahar, 1981; Zheng et al., 2006; Warren, 1985; Jowett, 1966). The entrainment is dependent on various feed parameters such as particle size (Wang, 2016; Smith and Warren, 1989; Lynch, 1981) and particle density (Wang, 2016; Johnson, 2005; Maachar A. & Dobby, 1992), and operational parameters such as pulp density (Zheng et al., 2006; Johnson, 2005), impeller speed (Wang, 2016; Akdemir and Sönmez, 2003), and gas flow rate (Wang, 2016; Zheng et al., 2006).

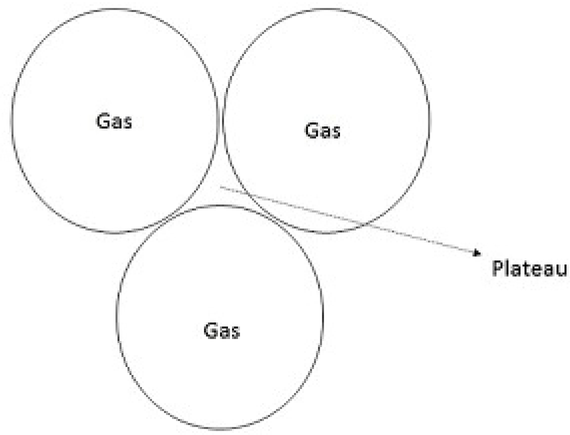

Figure 4.1: Plateau border description

Entrainment is non-selective and affects both hydrophilic and hydrophobic particles. The presence of hydrophilic particles in the froth phase reduces the grade of the desired minerals. It reduces the efficiency of the flotation process for the separation of fine ground ore. Several methods have been suggested to reduce entrainment in froth flotation. These methods can be grouped into the following categories: reducing the water recovery, increasing the drainage (Gong, 2011), and direct reduction in the particle suspension by selective flocculation (Gong, 2011; Liu et al., 2006; Gong et al., 2010). A washwater stream has been introduced in flotation to wash the froth and increase the drainage of particles by providing counter current flow (Gong, 2011; Mulleneers et al., 2002).

To improve the product grade, entrainment needs to be minimized, monitored, and controlled. Real-time entrainment needs to be measured for effective monitoring and control. Since, a reduction in the overall entrainment also reduces the amount of hydrophobic (desired) minerals (the entrainment contribution), entrainment needs to be measured for hydrophilic and hydrophobic minerals individually. Entrainment of hydrophilic minerals is usually measured off-line by timed weight measurements (with a long sampling time), followed by X-ray fluorescence (XRF) measurements (which also have longer sampling times). It is difficult to measure the entrainment contribution of the hydrophobic minerals. Recovery obtained by various methods provides the sum of true flotation and mechanical entrainment contributions. Three common methods are proposed in the literature (Trahar, 1981; Warren, 1985; Ross, 1988). Trahar (Trahar, 1981) suggested that two flotation tests, one in the presence of collector and frother (true flotation and entrainment), and the other in the presence of only the frother (entrainment), can be used to quantify entrainment. Differences in solid recovery between the two tests can be attributed to the true flotation, through which entrainment can be quantified. This method is not suitable for naturally hydrophobic minerals that have the capability of attachment even in the absence of a collector, or even in cases where the frother demonstrates collecting capabilities. Also, different reagents in both tests would influence the froth structure, and further affect the drainage and entrainment in both runs (Wang, 2016; Ross, 1989). Warren (Warren, 1985) explored the linear relationship between solids recovery and the water recovery as described in the following equation:

$$R(t) = R_f(t) + KR_w(t) \tag{4.1}$$

where R(t), R_f(t), K and R_w(t) represent overall recovery at time t, true flotation recovery at time t, degree of entrainment, and water recovery at time t, respectively. Recovery due to entrainment is represented as KR_w(t) at time t. Various experiments need to be conducted at different water recoveries obtained by varying the froth height, froth, pulp height, or the rate of froth removal (Warren, 1985; Pita, 2015). The true flotation recovery (R_f(t)) and the degree of entrainment (K) can be calculated using a linear regression relation between the overall mineral recovery and water recovery. However, varying the froth height, pulp height or the rate of froth removal also disturbs the froth structure and consequently, the drainage and entrainment rates. Hence, this method does not give an accurate measurements of the entrainment contribution. Also, it should be noted that the degree of entrainment changes with time and its variation is not considered in this method. Along with these drawbacks, this method requires numerous test runs, making it time consuming and economically infeasible. Another method, based on a single flotation test, was proposed by Ross and Van Deventer (Ross, 1988). It is based on the calculation of two timed functions X(t) and Y(t):

$$X(t) = \frac{E(t).C_w(t)}{W(t).C_m(t)} \tag{4.2}$$

$$Y(t) = \frac{R(t).C_w(t)}{W(t).C_m(t)} \tag{4.3}$$

where E(t), R(t), W(t) C_w(t), and C_m(t) represent the total mass of entrained solids at time t, the total mass of recovered solids (true flotation and entrained) at time t, the total mass of water recovered at time t, the concentration of water in the pulp at time (t), and the concentration of solids in the pulp at time t, respectively. This method is based on three assumptions: a) the recovery at the end (t = ∞) of batch flotation is solely due to entrainment, b) the timed function X(t) decreases linearly with flotation time, and c) the pulp is homogeneous. At t = ∞, X(t) can be approximated by using the assumption X(t) = Y(t), and Y(t) is calculated based on the total mass recovered. Based on the X(t) points towards the end, the X(t) line is extrapolated towards time t = 0, such that it increases linearly while moving from time t = ∞ to t = 0. It is critical to run the batch process until the optimum time where all the solids recovered are due to entrainment (Ross, 1988; Pita, 2015). Using the above simplification, the entrained mass E(t) can be calculated by measuring the mass of water recovered (M(t)) and the concentration of the specific mineral in the pulp (C_m(t)):

$$E(t) = M(t)C_m \tag{4.4}$$

This method provides inaccurate results for hydrophobic species, as their concentration in the pulp changes due to both true flotation and entrainment. In other words, hydrophobic minerals in the pulp are available for attachment to the bubbles as well as entrainment. Furthermore, all of these methods require a number of batch flotation tests to be completed before calculating the contribution from entrainment. In addition to the potential inaccuracies, these methods cannot be used to obtain real-time measurement of the entrainment contribution for the minerals floated. Hence, there is a critical need for a method to measure the entrainment contribution in real-time.

Several authors have proposed models for entrainment recovery. These models can be classified as empirical (Maachar A. & Dobby, 1992; Ross, 1989; Bisshop J.P. & White, 1976; Savassi et al., 1998; Yianatos and Contreras, 2010; Gulsoy, 2005; Çilek and Ylmazer, 2003; Alford, 1990; Uribe et al., 1999; Cilek and Umucu, 2001) or steady-state fundamental models (Moys, 1978; Neethling and Cilliers, 2002a; Bisshop J.P. & White, 1976; Neethling and Cilliers, 2003; Stevenson, 2007). Empirical models are usually valid only in a small range of certain process conditions. Fundamental models, on the other hand are general and provide valuable understanding of the entrainment process; however, the models cited cannot be used for dynamic monitoring or control since they are valid only at steady-state. A few compartment-based models that are dynamic in nature, have also been introduced for the flotation process (Dobby and Savassi, 2005; Fuerstenau et al., 2007; Bascur, 2000; Popli et al., 2015; Alves dos Santos et al., 2014; Hanumanth and Williams, 1992). These models divide the flotation process into various compartments such as pulp and froth, and apply the mass conservation principle to define various sub-processes for inter- and intra-compartment transfers. A fundamental understanding of the sub-processes of attachment, detachment, entrainment, and drainage can be incorporated to develop these models. The lack of direct entrainment-based dynamic models encourages the use of compartment-based models. We have previously used a similar model framework to monitor the attachment and detachment sub-processes in batch flotation (Popli et al., 2015).

The objectives of this study are to develop a froth image-based method to measure online grade and recovery for minerals, and to monitor the entrainment and drainage through online state and parameter estimation with a detailed compartment-based dynamic fundamental model using an extended Kalman filter. Furthermore, a method is proposed to estimate the entrainment and true flotation recovery for hydrophobic minerals separately in real-time using the developed monitoring algorithm.

4.2 Experimental Section

4.2.1 Materials: Minerals and reagents

Synthetic mixtures were prepared using pure galena (lead sulfide, PbS) and pure quartz (silicon dioxide, SiO_2). Galena and quartz were chosen to represent a mixture of hydrophobic and hydrophilic particles. Galena was obtained from Boreal Sciences, Canada and quartz was obtained from U.S. Silica, United States. In this study, three different types of quartz were used: MIN-U-SIL 15 (Q1, under 15 μm), MIN-U-SIL 40 (Q2, under 40 μm) and MIN-U-SIL 90 (Q3, under 90 μm). XRF was used to confirm the 99.8% and 99.6% mineral purity for galena and quartz, respectively. The three quartz types represented by Q1, Q2, and Q3 correspond to 98% under 15 μm, 40 μm, and 90 μm, respectively. Galena was dry ground using a jaw crusher and disc pulverizer to obtain solids under 110 μm. Three uniform samples of 50 g crushed galena were obtained using a RETSCH sample splitter. Particle size distributions were obtained for galena samples using a Mastersizer 3000. The particle sizes of D10, D50, and D90 were obtained as 3.95 μm, 21.6 μm, and 66.5 μm, respectively. A total of 450 g of each quartz type was mixed with 50 g of galena to form three types of mixtures, as summarized in Table 4.1. Variations in the quartz particle size were used to determine the effect of particle size on entrainment recovery and to monitor the process at different particle size conditions in the feed. Flotation experiments were conducted with quartz as a hydrophilic tracer. Potassium ethyl xanthate ($C_3H_5KOS_2$, KEX) and methyl isobutyl carbinol ($C_6H_{14}O$, MIBC) were used as the collector and frother, respectively.

Table 4.1: Types of synthetic feed mixtures

Type	Composition
1	50 g galena + 450 g Q1 quartz
2	50 g galena + 450 g Q2 quartz
3	50 g galena + 450 g Q3 quartz

4.2.2 Batch flotation

Batch flotation was performed using a 1.5L JKTech flotation cell. A VisioFroth imaging system by Metso® Minerals consisting of an IP camera, and laser was installed on the batch cell. Full details of the setup are given in our previous work (Popli et al., 2015).

Batch flotation experiments were conducted for the three different feeds as given in Table 4.1 and the flotation conditions for the batch experiments are summarized in Table 4.2. The same experimental conditions were maintained for the three runs to isolate the effects of quartz particle size amongst the different runs. Feed solids (Feed 1, 2, or 3) were mixed with water to make a slurry with the required volume and density (see Table 4.2 for detailed flotation conditions). It was transferred to the flotation cell, followed by the addition of the collector. The impeller was turned on and the slurry was mixed for

6 minutes at 1100 rpm. Subsequently, the desired amount of frother was added and the solution was mixed for 2 more minutes. Also, the make-up water was prepared with the same frother dosage to avoid disturbances in the frother concentration in the process. Air flow was initiated to start the flotation process and this time was defined as t=0. Make-up water was added during the process to maintain the pulp level. Froth was collected into different collection pans at time intervals: 10, 20, 30, 40, 50, 60, 90, 290, and 300 seconds. The collected froth was weighed in the presence of water, dried, and weighed again to obtain water and solid weights individually. Dried solid samples were then analyzed using X-ray fluorescence to determine the silica and galena content.

Table 4.2: Flotation conditions for the batch experiments

Variable	Value
Volume of slurry (l)	1.35
Solids weight % in feed (%)	29.8
Air flow rate (lpm)	6
Impeller speed (rpm)	1100
Frother dosage (ml/l)	0.1
Collector dosage (mol/l)	10^{-3}

4.3 Image based soft sensor: Data and modeling

The VisioFroth package was used to measure and analyze the real-time froth images along with various additional features as listed in Table 4.3. Detailed measurements algorithms were highlighted in our previous work (Popli et al., 2015). A sampling time of 10 seconds was chosen for image capture and calculations. Image-based models, named soft sensor A and soft sensor B, were developed for online galena grade and solids (sum of galena and quartz) cumulative recovery, respectively using support vector regression. The overall objective for the soft sensor model as illustrated in Figure 4.2 was to use the image data as an input to measure the online grade and recovery for galena and quartz.

Outputs from the image based soft sensors A and B were further used as inputs for mass balance equations.

Table 4.3: Image features extracted using VisioFroth system on top of the cell

Image features	Image features
Velocity	Green component
X velocity	Purity
Y velocity	Load
Froth height	Luminance
D50 (Bubble size)	Red component
D80 (Bubble size)	RBG
Brightness	Stability
Blue component	Tint
Collapse rate	Texture
Cell value	a- component lab model
Dispersion	b- component lab model

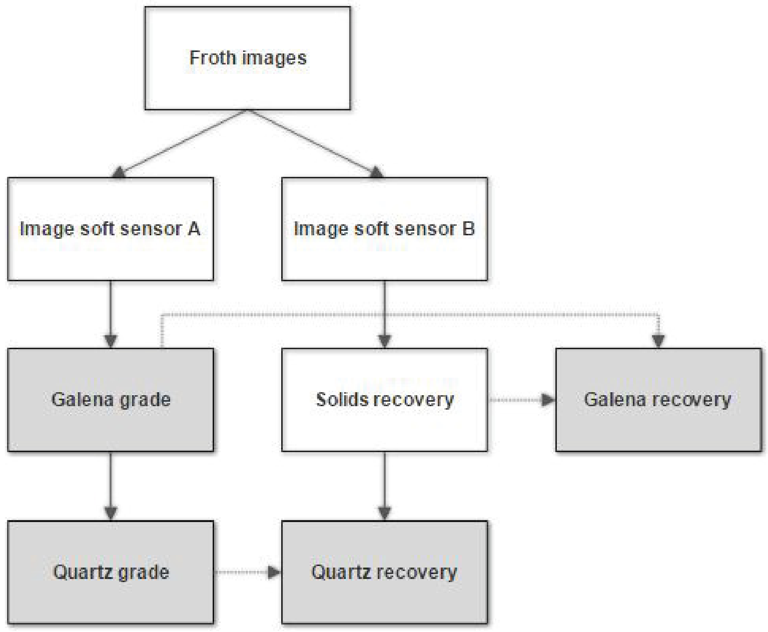

Figure 4.2: Overall framework for soft-sensor network: Online measurement of grade and recovery for quartz and galena

4.3.1 Soft-sensor A and soft-sensor B

Froth image features in real-time were used to inferentially measure galena grade (%) and solids cumulative recovery (%) using machine learning based regression models. Various researchers have stated that the froth features are indicative of the quality of the recovered sample (Moolman et al., 1996; Runge et al., 2007; Aldrich et al., 2010). We have also demonstrated machine learning methods to relate image features to recovery for pure mineral flotation in our previous work(Popli et al., 2015). In this work, XRF-based measurements were used to train and calibrate the machine learning regression models.

Model and algorithm

Support vector regression (SVR) is based on the principles of support vector machines (SVM), which were initially developed for classification problems (Vapnik, 1995; Boser et al., 1992). The SVR utilizes a kernel trick to transform the data in the feature space (R^m) to higher dimension space using a function, $\Phi(x)$. The nonlinear problem in the feature space is now linear in the higher-dimensional space using the kernel trick. Unlike other regression techniques, the SVR is based on structural risk minimization and reduces the model complexity alongwith the training data error. We have used the ϵ-SVR, which allows the training error up to a threshold ϵ. Hence, no cost is applied to the points where the error is less than ϵ. For a given set of training data, $(x_1, y_1), (x_2, y_2), ...(x_n, y_n)$, with $x \in R^m$, and $y \in R$, the prediction model is formulated as:

$$f = \mathbf{W}^T \Phi(\mathbf{x}) + \mathbf{b} \tag{4.5}$$

where $\mathbf{W}$ is the parametrized weight vector and $\mathbf{b}$ is the model bias. A constrained optimization problem was structured to minimize the empirical error and model complexity (Smola and Scholkopf, 2003):

$$\begin{cases} \underset{w,b,\xi,\xi'}{\text{minimize}} \ \frac{1}{2}\mathbf{w}^T\mathbf{w} + C\Bigg(\sum_{i=1}^{n} \xi_i + \sum_{i=1}^{n} \xi_i' \Bigg) \\ \text{subject to (i = 1,2,....n):} \\ y_i - \mathbf{w}^T\Phi(x_i) - b \leq \epsilon + \xi_i \\ \mathbf{w}^T\Phi(x_i) + b - y_i \leq \epsilon + \xi_i' \\ \xi_i \geq 0 \\ \xi_i' \geq 0 \end{cases} \tag{4.6}$$

where ξ_i and ξ_i' denote the slack variables to allow for the infeasible constraints with maximum error range of ϵ. C, also called the box constraint, is used to trade-off between two components of the objective function: model complexity ($\frac{1}{2}\mathbf{w}^T\mathbf{w}$) and error tolerance ($\sum_{i=1}^{n}\xi_i + \sum_{i=1}^{n}\xi_i'$).

The objective function and the constraints were used to design a dual optimization problem by presenting dual variables (α_i, α_i') and Lagrange multipliers as illustrated in equation 4.7 (Smola and Scholkopf, 2003). It is to be noted that the training points are used as inner products, which allows the use of the kernel trick. The optimal values of **w** and **b** were calculated based on saddle point conditions (Kuhn-Tucker conditions) and represented in equations 4.8 and 4.9 (Smola and Scholkopf, 2003). The optimal value of **w** is the support vector expansion, a linear combination of support vectors. The types of kernel functions used are summarized in Table 4.4 along with the function parameters.

$$\begin{cases} \underset{\alpha,\alpha'}{\text{maximize}} \sum_{i=1}^{n} y_i(\alpha_i - \alpha_i') - \epsilon \sum_{i=1}^{n}(\alpha_i + \alpha_i') - \\ \frac{1}{2}\sum_{i,j=1}^{n}(\alpha_i - \alpha_i')(\alpha_j - \alpha_j')\Phi(x_i)^T\Phi(x_j) \\ \text{subject to: } \sum_{i=1}^{n}(\alpha_i - \alpha i') = 0 \\ C \geq \alpha_i, \alpha_i' \geq 0, i = 1, 2, \ldots.., n \end{cases} \tag{4.7}$$

$$\mathbf{w} = \sum_{i=1}^{l}(\alpha_i - \alpha_i')\Phi(x_i) \tag{4.8}$$

$$\mathbf{b} = y_j - \Phi(x_j)^T\mathbf{w} + \epsilon, \ \ , s.t. \ \ 0 \leq \alpha_i' \leq \frac{C}{n} \tag{4.9}$$

Hyperparameter optimization : SVM model parameters selection

The SVM model parameters are very crucial in the sensor development process. The box constraint, C, is the contribution of the empirical error to the overall objective

Table 4.4: Common kernel functions used in support vector machines

Type of kernel	Function
Linear	$x_i^t x_j$
Polynomial	$(x_i^T x_j + 1)^p$
Radial basis function (rbf, Gaussian)	$e^{-\gamma \|\|x_i - x_j\|\|^2}$

function and decides the tradeoff between model accuracy and complexity. Half the width of the insensitive band (error allowance), ϵ is used to control the ϵ-sensitive loss function, and it's optimal value decides the number of support vectors. Kernel parameters such as the choice of kernel function, and respective function parameters are critical in the model selection and were also selected based on the hyperparameter optimization. These parameters and their design range are summarized in Table 4.5. Optimization was performed using the grid search technique, where random samples were evaluated based on uniform sampling without replacement. A 10-fold cross validation technique was applied for model selection where training data was randomly divided into 10 parts and the model was developed using 9 of these parts and validated with the 10^{th} part of the initial training data.

Table 4.5: Parameter range for hyperparameter optimization using grid search technique

Parameter	Range	Scale
C	$[10^{-3}\ 10^{3}]$	log
ϵ	[0.0062 623.7583]	log
Kernel function	[linear, gaussian, polynomial]	NA (categorical)
γ (gaussian kernel scale)	$[10^{-3}\ 10^{3}]$	log
p (polynomial kernel order)	[2,4]	linear

Data selection and preparation

Froth images were collected at every second. However, a sampling time of 10 seconds was chosen based on the froth collection time and requirements of model accuracy. Certain froth samples collected from all three experiments were used in the development of the soft sensor. A sampling point (k) consists of a 10 second interval. For example, k = 1, 2, and 3 correspond to the time 10, 20, and 30 seconds respectively. Specific data selection for soft sensor models A and B is discussed below:

Soft sensor A (Galena grade)

- **Input data for kth sample**: average image features of all the images from time *10(k-1)+1* to *10k* seconds
- **Output variable for kth sample**: the overall grade for the sample collected between *10(k-1)+1* and *10k* seconds.

Soft sensor B (Cumulative solids recovery)

- **Input data for kth sample (10k seconds)**: average image features of all the images from time 1 to *10k* seconds
- **Output variable at kth sample (10k seconds)**: Cumulative solids recovery at *10k* seconds

4.3.2 Galena and quartz recoveries

The outputs from these soft sensors (galena grade and solids recovery) were then used to evaluate quartz grade, galena recovery, and quart recovery based on mass balances. Since the synthetic mixture contained two minerals, the quartz grade was obtained from the galena grade using equation 4.10, where $G_{q,k}$ and $G_{g,k}$ are quartz grade (%) and galena grade (%), respectively, at time step k. The cumulative solids recovery at step k and step k-1 was used to find the recovery for the range of k seconds as shown in equation 4.11, where CR_s is the cumulative solids recovery (%) and $R_{s,k}$ is the solids recovery(%)

for that time range of 10 seconds at time step k. The amount of solids mass recovered in 10 seconds was calculated using equation 4.12. The denominator in equation 4.12 represents the initial solids mass in the feed stream (500 g). The masses of recovered quartz and galena were calculated using equations 4.13 and 4.14, respectively. Finally, galena ($R_{g,k}$) and quartz ($R_{q,k}$) recovery (%) were calculated using equations 4.15 and 4.16 based on their initial amounts in the feed stream (50 g and 450 g, respectively) and the grade measurements. Their cumulative recoveries were then calculated based on the sum of recovery values until the required time.

$$G_{q,k} = 100 - G_{g,k} \tag{4.10}$$

$$R_{s,k} = CR_{s,k} - CR_{s,k-1} \tag{4.11}$$

$$M_{s,k} = 500\frac{R_{s,k}}{100} \tag{4.12}$$

$$M_{q,k} = \frac{G_{q,k}M_{s,k}}{100} \tag{4.13}$$

$$M_{g,k} = \frac{G_{g,k}M_{s,k}}{100} \tag{4.14}$$

$$R_{g,k} = \frac{M_{g,k}}{50}100 \tag{4.15}$$

$$R_{q,k} = \frac{M_{q,k}}{450}100 \tag{4.16}$$

4.4 Fundamental model and real-time estimation

The monitoring and estimation scheme is presented in Figure 4.3 to update the model in real time. The fundamental model, reconciled with online measurements (from the image based soft sensor), was updated online using an extended Kalman filter that estimates states and parameters (augmented states) of the model.

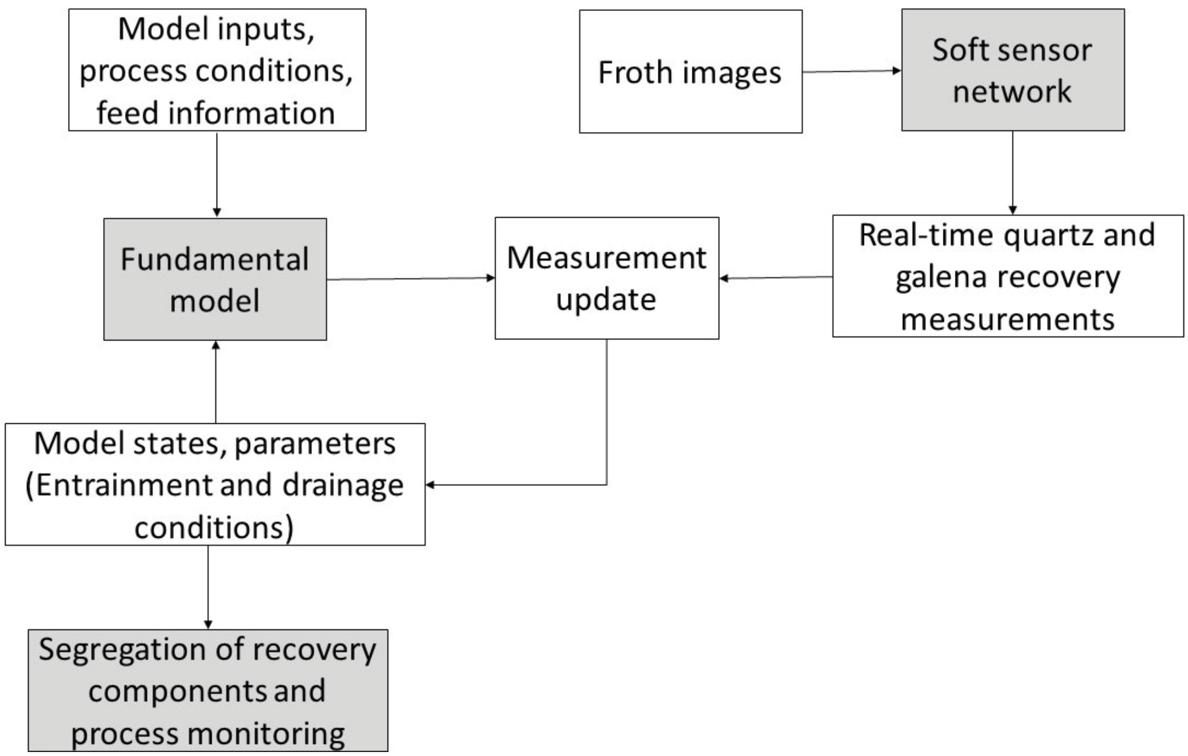

Figure 4.3: Developed scheme for entrainment monitoring and estimation

4.4.1 Fundamental modeling framework

Various structures for compartmental models for froth flotation have been proposed in the literature (Dobby and Savassi, 2005; Fuerstenau et al., 2007; Bascur, 2000; Popli et al., 2015; Alves dos Santos et al., 2014; Hanumanth and Williams, 1992). In this study, the model structure shown in Figure 4.4 divides the flotation precess into four compartments:

1. Gas phase in the pulp section
2. Slurry phase in the pulp section
3. Gas phase in the froth section
4. Slurry phase in the froth section

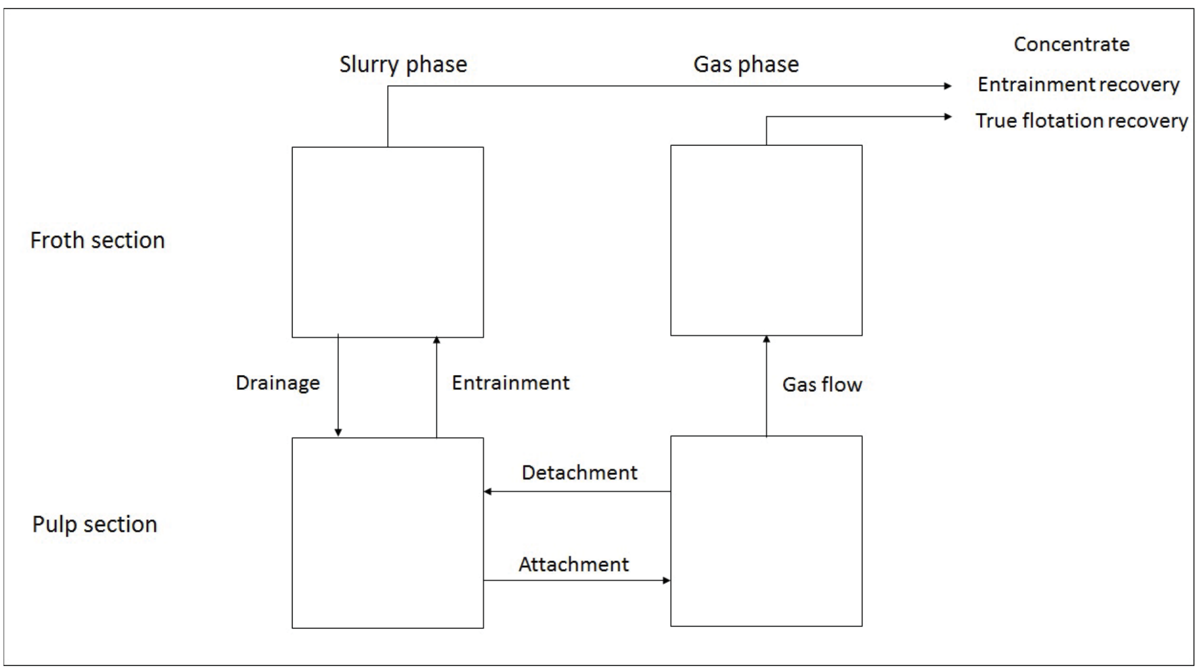

Figure 4.4: Model structure for the compartment-based dynamic fundamental modeling

A solid particle can be in any of the four compartments based on its state, i.e., attached to bubbles (gas phase) in the pulp or froth, or detached (free) in the slurry phase in the pulp or froth. The various sub-processes for the transport between the compartments are attachment, detachment, entrainment, and drainage (Bascur, 2000).

Attachment and detachment In this study, it was assumed that the attachment and detachment were first order processes and occur only in the pulp section (Popli et al., 2015). Therefore, a particle maintains its state (attached or detached) while moving from the pulp to the froth section. Attachment and detachment rate constants (k_a and k_d respectively) are defined in equations 4.17 and 4.18, where Z_1, Z_2, P_c, P_a, P_s, and P_d represent collision frequency, detachment frequency, probability of bubble-particle collision, probability of bubble-particle attachment, probability of bubble-particle aggregate stability and probability of bubble-particle detachment (Duan et al., 2003; Z. Dai S.S. Dukhin and Ralston, 1998; Tao, 2005; Dai et al., 1999, 2000; Popli et al., 2015) . It was assumed that the quartz mineral has no hydrophobic properties (even in the presence of a xanthate collector) and attachment and detachment sub-processes only impact galena. Therefore, quartz always remains in the detached state (slurry phase in the pulp and froth sections)

$$k_a = Z_1 P_c P_a P_s \tag{4.17}$$

$$k_d = Z_2 P_d \tag{4.18}$$

Entrainment and drainage The entrainment sub-process is used to carry the slurry phase (free particles) from the pulp section to the froth section. The drainage sub-process is the settling process of the slurry in the froth compartment to the pulp compartment. Their net effect is the contribution of the entrainment mechanism to the overall flotation. Entrainment and drainage flowrates are defined in equations 4.19 and 4.20, where k_e and k_r are entrainment and drainage parameters, respectively, Q_a is the air flow rate, V_{Sf} is the volume of slurry phase in froth compartment, σ is the surface tension, A is the cross-sectional area, and d_{Bp} and d_{Bf} are the bubble diameters in the pulp and froth compartments, respectively (Fuerstenau et al., 2007).

$$Q_E = \frac{k_e Q_a}{d_{Bp}^{0.75}} \tag{4.19}$$

$$Q_R = k_R \frac{(\frac{Q_a}{A})^{0.53} V_{Sf}^{0.56} A^{0.4}}{\sigma^{0.24} d_{Bf}^{1.92}} \tag{4.20}$$

Equations 4.21, 4.22, 4.23, 4.24, 4.25, and 4.26 describe the sub-processes in a dynamic flotation process, where ϵ_p and ϵ_f are volumetric gas-phase fractions for pulp and froth respectively, V_p and V_f are the pulp and froth volume respectively, $k_r g$ and $k_r q$ are the solid drainage constant for galena and quartz respectively, and k_w and k_{gf} are the residence time of liquid and gas phase in the froth, respectively. Various particle states used in the model are summarized in Table 4.6.

$$\frac{d}{dt}((1-\epsilon_p)V_p x_{g1}) = -k_a(1-\epsilon_p)V_p x_{g1} + k_d \epsilon_p x_{g2} - Q_E x_{g1} + k_{rg} Q_R x_{g3} \tag{4.21}$$

$$\frac{d}{dt}(\epsilon_p V_p x_{g2}) = k_a(1-\epsilon_p)V_p x_{g1} - k_d \epsilon_p x_{g2} - Q_a x_{g2} \tag{4.22}$$

$$\frac{d}{dt}((1-\epsilon_f)V_f x_{g3}) = Q_E x_{g1} - k_{rg} Q_R x_{g3} - k_w(1-\epsilon_f)V_f x_{g3} \tag{4.23}$$

$$\frac{d}{dt}(\epsilon_f V_f x_{g4}) = Q_a x_{g2} - k_g \epsilon_f V_f x_{g4} \tag{4.24}$$

$$\frac{d}{dt}((1-\epsilon_p)V_p x_{q1}) = k_{rq} Q_R x_{q3} - Q_E x_{q1} \tag{4.25}$$

$$\frac{d}{dt}((1-\epsilon_f)V_f x_{q3}) = Q_E x_{q1} - k_{rq} Q_R x_{q3} - k_w (1-\epsilon_f) V_f x_{q3} \tag{4.26}$$

Table 4.6: Descriptions of the particle states used in the compartmental model

State	Description
x_{g1}	Concentration(kg/m^3) of galena particles free in the pulp (compartment 1)
x_{g2}	Concentration(kg/m^3) of galena particles attached in the pulp (compartment 2)
x_{g3}	Concentration(kg/m^3) of galena particles free in the froth (compartment 3)
x_{g4}	Concentration(kg/m^3) of galena particles attached in the froth (compartment 4)
x_{q1}	Concentration(kg/m^3) of quartz particles free in the pulp (compartment 1)
x_{q3}	Concentration(kg/m^3) of quartz particles free in the froth (compartment 2)

The entrainment and drainage rates described in equations 4.19 and 4.20 are substituted into equations 4.21, 4.22, 4.23, 4.24 ,4.25, 4.26 to obtain the detailed compartment based fundamental model (equations 4.27, 4.28, 4.29, 4.30, 4.31, 4.32), which can be used for dynamic monitoring and/or control purposes. The measurements (galena and quartz recovery) are given in equations 4.33 and 4.34, where t_s is the sampling time, and M_{gi} and M_{qi} are the initial feed mass (kg) of galena and quartz, respectively. The first term in equation 4.33 is the entrainment contribution to the recovery, while the second term corresponds to the true flotation component of the overall recovery. The literature on the effects of density on entrainment indicates that the degree of entrainment is comparable for quartz and galena minerals (Maachar A. & Dobby, 1992; Wang et al., 2015). Therefore, in this work, it was assumed that the solid drainage constants $k_r g$ and $k_r q$ are equal, and can be denoted by a single parameter, $k_r qg$.

A new parameter $k_r\prime$, the product of $k_r qg$ and k_R can be used to represent the net drainage parameter in the following set of differential equations (Equation 4.27, 4.28, 4.29, 4.30, 4.31, and 4.32). This simplification reduces the number of parameters to be estimated in the model.

$$\frac{dx_{g1}}{dt} = -\left(k_a + \frac{k_e Q_a}{d_{Bp}^{0.75}(1-\epsilon_p)V_p}\right)x_{g1} + \left(\frac{k_d \epsilon_p}{1-\epsilon p}\right)x_{g2} + \left(\frac{k_r\prime(\frac{Q_a}{A})^{0.53}(V_f(1-\epsilon_f))^{0.56}A^{0.4}}{\sigma^{0.24}d_{Bf}^{1.92}(1-\epsilon_p)V_p}\right)x_{g3} \tag{4.27}$$

$$\frac{dx_{g2}}{dt} = \left(\frac{k_a(1-\epsilon_p)}{\epsilon_p}\right)x_{g1} - \left(k_d + \frac{Q_a}{\epsilon_p V_p}\right)x_{g2} \tag{4.28}$$

$$\frac{dx_{g3}}{dt} = -\left(\frac{k_e Q_a}{d_{Bp}^{0.75}(1-\epsilon_f)V_f}\right)x_{g1} - \left(k_w + \frac{k_r\prime(\frac{Q_a}{A})^{0.53}(V_f(1-\epsilon_f))^{0.56}A^{0.4}}{\sigma^{0.24}d_{Bf}^{1.92}(1-\epsilon_f)V_f}\right)x_{g3} \tag{4.29}$$

$$\frac{dx_{g4}}{dt} = \left(\frac{Q_a}{\epsilon_f V_f}\right)x_{g2} - (k_g)x_{g4} \tag{4.30}$$

$$\frac{dx_{q1}}{dt} = -\left(\frac{k_e Q_a}{d_{Bp}^{0.75}(1-\epsilon_p)V_p}\right)x_{q1} + \left(\frac{k_r\prime(\frac{Q_a}{A})^{0.53}(V_f(1-\epsilon_f))^{0.56}A^{0.4}}{\sigma^{0.24}d_{Bf}^{1.92}(1-\epsilon_p)V_p}\right)x_{q3} \tag{4.31}$$

$$\frac{dx_{q3}}{dt} = \left(\frac{k_e Q_a}{d_{Bp}^{0.75}(1-\epsilon_f)V_f}\right)x_{q1} - \left(k_w + \frac{k_r\prime(\frac{Q_a}{A})^{0.53}(V_f(1-\epsilon_f))^{0.56}A^{0.4}}{\sigma^{0.24}d_{Bf}^{1.92}(1-\epsilon_f)V_f}\right)x_{q3} \tag{4.32}$$

$$y_g = \left(\frac{(1-\epsilon_f)V_f k_w x_{g3}}{M_{gi}} + \frac{\epsilon_f V_f k_g x_{g4}}{M_g}\right)100 \tag{4.33}$$

$$y_q = \left(\frac{(1-\epsilon_f)V_f k_w x_{q3}}{M_{qi}}\right)100 \tag{4.34}$$

4.4.2 Extended Kalman Filter: State and parameter estimation

An extended Kalman filter (EKF) was used to estimate the state and parameters (augmented states) of the model using online measurements from the developed image-based soft sensor (Prasad et al., 2002; Kalman, 1960; Popli et al., 2015). The EKF is essentially a nonlinear version of the Kalman filter, which estimates the states based on minimization of the error covariance between the predicted output and the online measurements (Kalman, 1960; Welch and Bishop, 1995). Consider the nonlinear difference equation

$$X_k = f(X_{k-1}, U_{k-1}, W_{k-1}) \tag{4.35}$$

$$Z_k = h(X_k, V_k) \tag{4.36}$$

where X represents the vector of states, u is the input vector, Z is the measurement vector, and W and V are the process and measurement noise, respectively. W and V follow normal distributions with covariance Q and R, respectively. The Taylor series is used to linearize the model by using a Jacobian matrix to evaluate A and H:

$$A = \frac{\partial f}{\partial X}(\widehat{X}_{k-1}, U_{k-1}, 0) \tag{4.37}$$

$$H = \frac{\partial f}{\partial Z}(X_{k-1}, 0) \tag{4.38}$$

where, $\widehat{X}_{k-1}$ is the posteriori estimate of the state vector at time step k. The Linear form of the model is presented below using the calculated Jacobian matrices. In this work, differential equations 4.27, 4.28, 4.29, 4.30, 4.31 and 4.32 are used to represent the state space equation 4.39 where X vector is [x_{g1}, x_{g2}, x_{g3}, x_{g4}, x_{q1}, x_{q3}], and the measurements (y_g and y_q) in equations 4.33 and 4.34 are used in the equation 4.40 with $Z = [y_g \ y_q]$.

$$X_k = AX_{k-1} + BU_{k-1} + W_{k-1} \tag{4.39}$$

$$Z_k = HX_k + V_k \tag{4.40}$$

The EKF algorithm is based on two fundamental steps: predictor and corrector (Kalman, 1960; Welch and Bishop, 1995).

Prediction step State and covariance estimates from time step *k-1* are projected to time step k:

$$\widehat{X}_k^- = f(\widehat{X}_{k-1}, U_{k-1}, 0) \tag{4.41}$$

$$P_k^- = A_k P_{k-1} A_k^T + W_k Q_{k-1} W_k^T \tag{4.42}$$

Correction step In this step, state and covariance estimates are corrected using the real-time measurements and calculated Kalman gain (K_k):

$$K_k = P_k^- H_k^T (H_k P_k^- H_k^T + V_k R_k V_k^T)^{-1} \tag{4.43}$$

$$\widehat{X}_k = \widehat{X}_k^- + K_k(z_k - h(\widehat{X}_k^-, 0)) \tag{4.44}$$

$$P_k = (I - K_k H_k) P_k^- \tag{4.45}$$

These series of predictor and corrector steps are continued to estimate the states of the model. Model parameters were estimated by using them as augmented states in the state-space equations. States and parameters that can be estimated depend on the observability of the system. In this system of augmented states, observable parameters other than the states (x_{g1}, x_{g2}, x_{g3}, x_{g4}, x_{q1}, x_{q3}) are the attachment rate constant, k_a, the net drainage parameter, $k_{r'}$, and the entrainment parameter, k_e.

The model was updated for all three experiments and was used to evaluate the dynamic effect of quartz particle size on the estimated $k_{r'}$ and k_e. Estimated states and parameters were used to evaluate the dynamic contribution of true flotation and entrainment on the overall galena recovery using equation 4.33.

4.5 Results and discussion

4.5.1 Batch flotation experiments

Froth samples were collected at 10, 20, 30, 40, 50, 60, 90, 290, and 300 seconds for three different feed samples. Galena and quartz content were obtained using XRF, and used with dried weight measurements to determine the recovery for quartz and galena. Water content was obtained based on the difference in the wet and dried froth samples that were collected. Water recovery was calculated based on the initial water present in the flotation cell. Figures 4.5 and 4.6 show the experimental galena recovery as a function of time for feed 1,2 and 3. The final galena recovery is 92% $\pm$1% for all three feed samples. It can be seen that galena recovery was not highly dependent on the variation of quartz particle size. However, the experiment with feed 3, which contained quartz particles under 90 μm shows a relatively lower galena recovery in comparison to feed types 1 and 2, which contain finer quartz particle sizes. Quartz recovery, on the other hand, showed clear variation with changes in quartz particle size, and decreased with an increase in the particle size. Type 1 (under 15 μm) flotation resulted in the highest quartz recovery with final recovery of 25%. It was followed by type 2 (under 45 μm) and type 3 (under 90 μm) with ultimate quartz recovery of 17% and 12%, respectively.

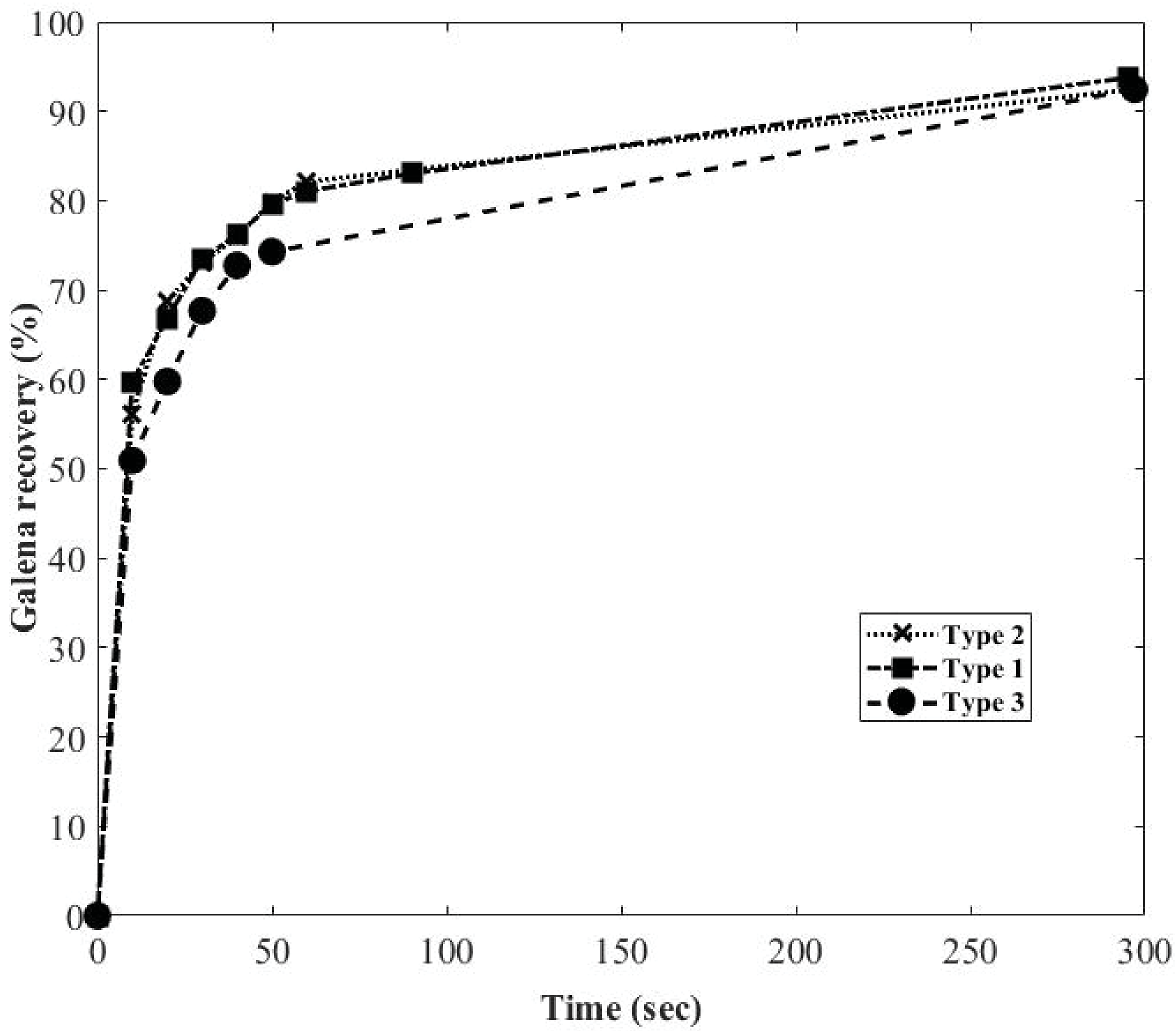

Figure 4.5: Galena recovery for batch flotation calculated using XRF

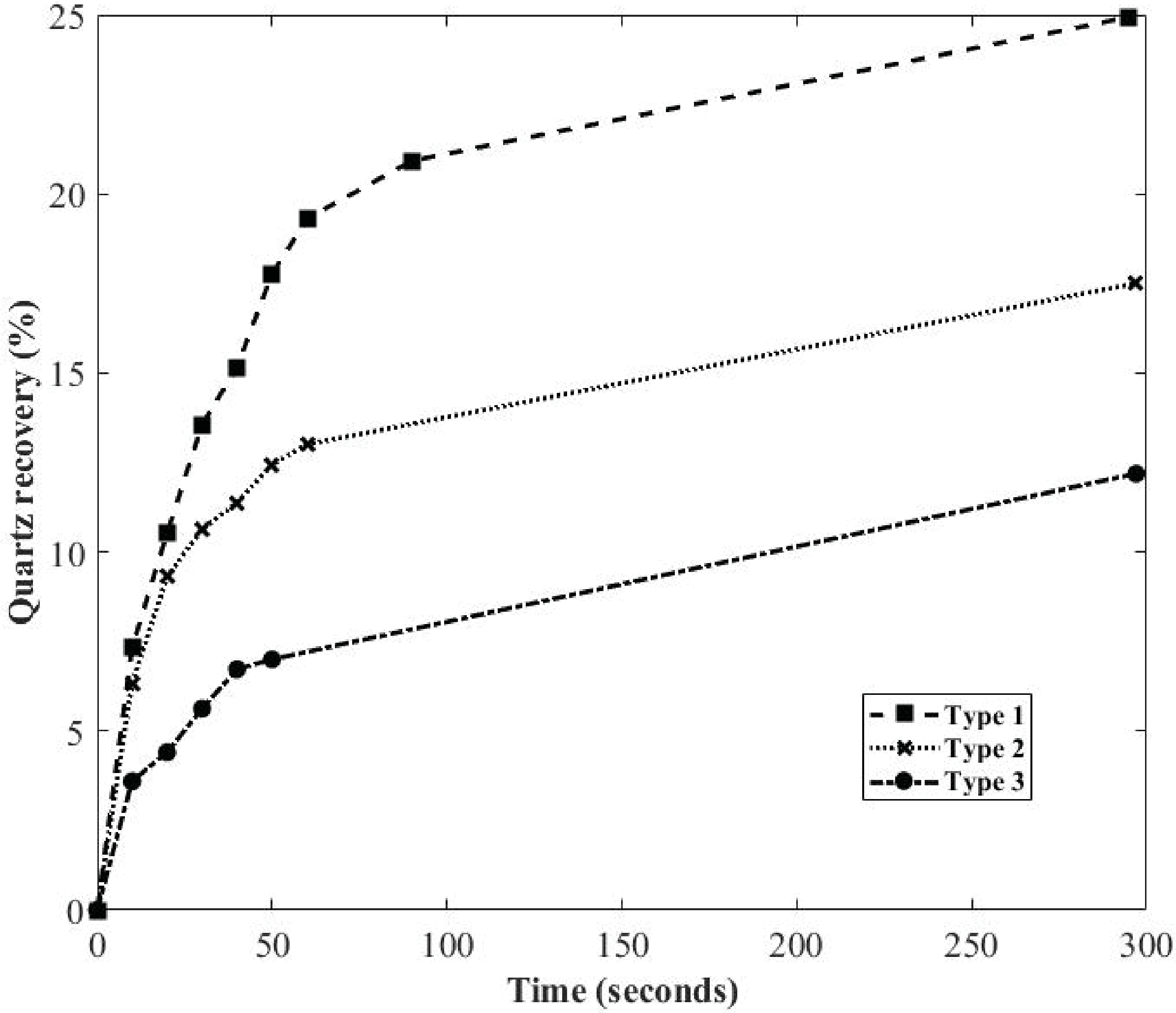

Figure 4.6: Quartz recovery for batch flotation calculated using XRF

Figure 4.7 shows the quartz recovery (entrainment) as a function of water recovery for three different feed stream types. It can be seen that there is a linear relationship between quartz and water recovery for all three feed streams. These trends agree with reported literature trends (Trahar, 1981; Gong et al., 2010). It can also be deduced that the slope, known as the degree of entrainment, decreases with an increase in the quartz particle size, which is consistent with the results given in the literature (Wang et al., 2015; Bisshop J.P. & White, 1976). These experimental results were used to calibrate the image-based soft sensors.

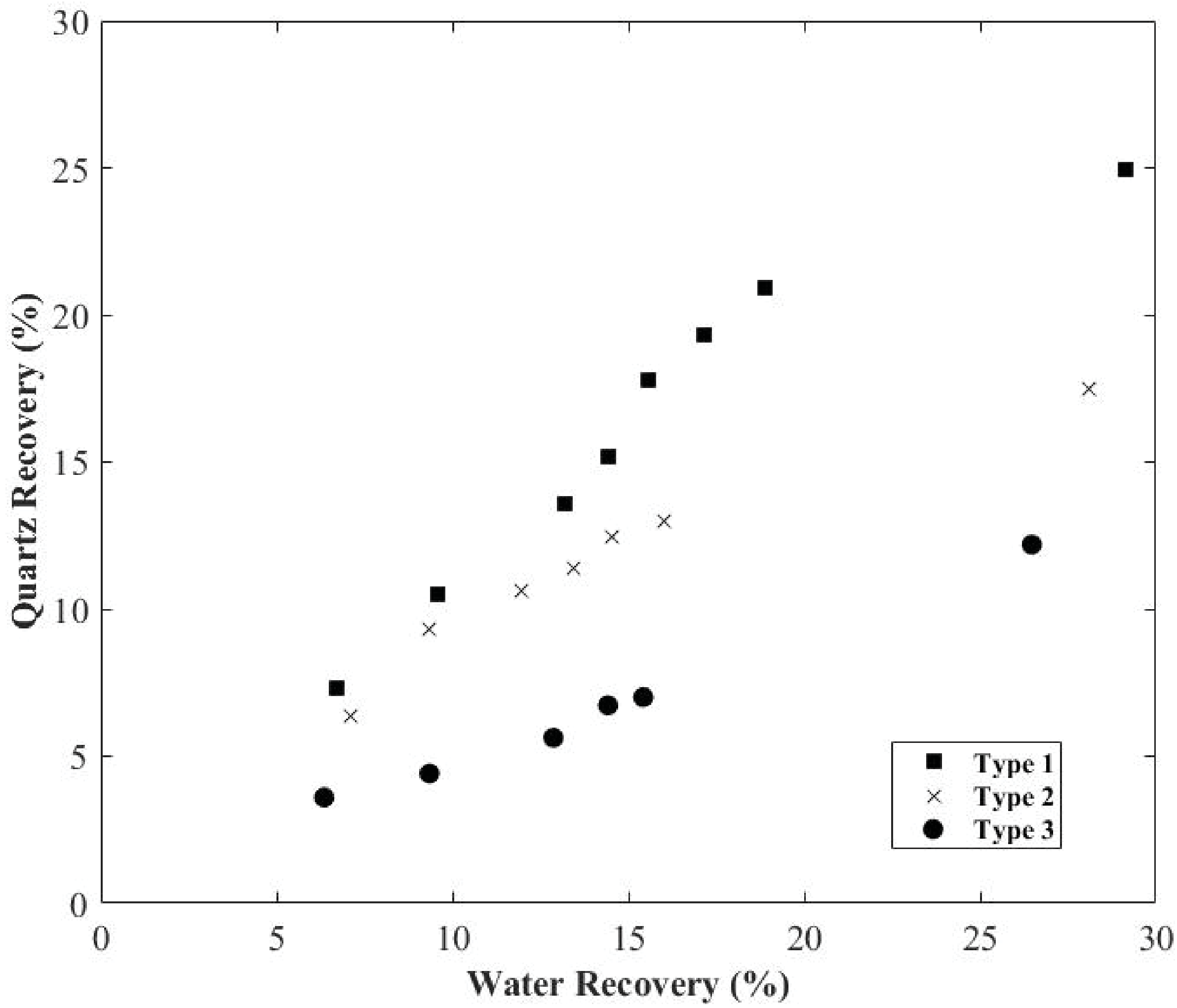

Figure 4.7: Quartz entrainment and water recovery for batch flotation experiments

4.5.2 Image-based soft sensor: Real-time grade and recovery measurements

Froth images are a good indication of the quality and quantity of product being floated. A sample set of time-based images are shown in Figure 4.8 for the Type 1 feed stream. A clear distinction is observed in the images with the increase in flotation time, and the developed soft sensors capture the relationship between the images and process outputs quantitatively. Real-time galena grade (image based soft sensor A) and solids recovery (image based soft sensor B) measurements were used to determine online grade and recovery for galena and quartz minerals.

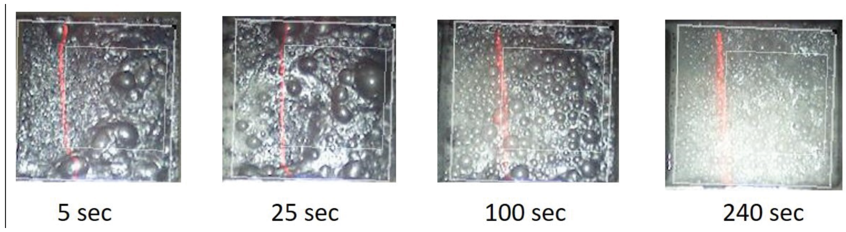

Figure 4.8: Variation in the froth images with time for the case of feed stream type 1

Soft sensors A and B

Support vector regression was used to develop image-based soft sensors and hyperparameter optimization was performed to obtain the optimal SVR model parameters. Results of the grid search algorithm are tabulated in Table 4.7. Due to the lack of training data between 200 and 300 seconds, soft sensors were implemented up to 200 seconds and capture the majority of the process dynamics. Figures 4.9 and 4.10 show the comparison between experimental and predicted galena grades (soft sensor A) and solids recoveries (soft sensor B), respectively, and the sensors predict the experimental grade and recovery accurately. The developed soft sensors A and B were then used to predict the galena grade and solids recovery to be used in mass balance-based inferential measurements of other process outputs.

Table 4.7: Hyper-parameter selection based on grid search optimization

Parameter	Soft-sensor A	Soft-sensor B
C	1000	215.44
ϵ	0.0191	0.0062
Kernel function	Gaussian	Gaussian
γ (Gaussian kernel scale)	10	10
p (polynomial kernel order)	n/a	n/a

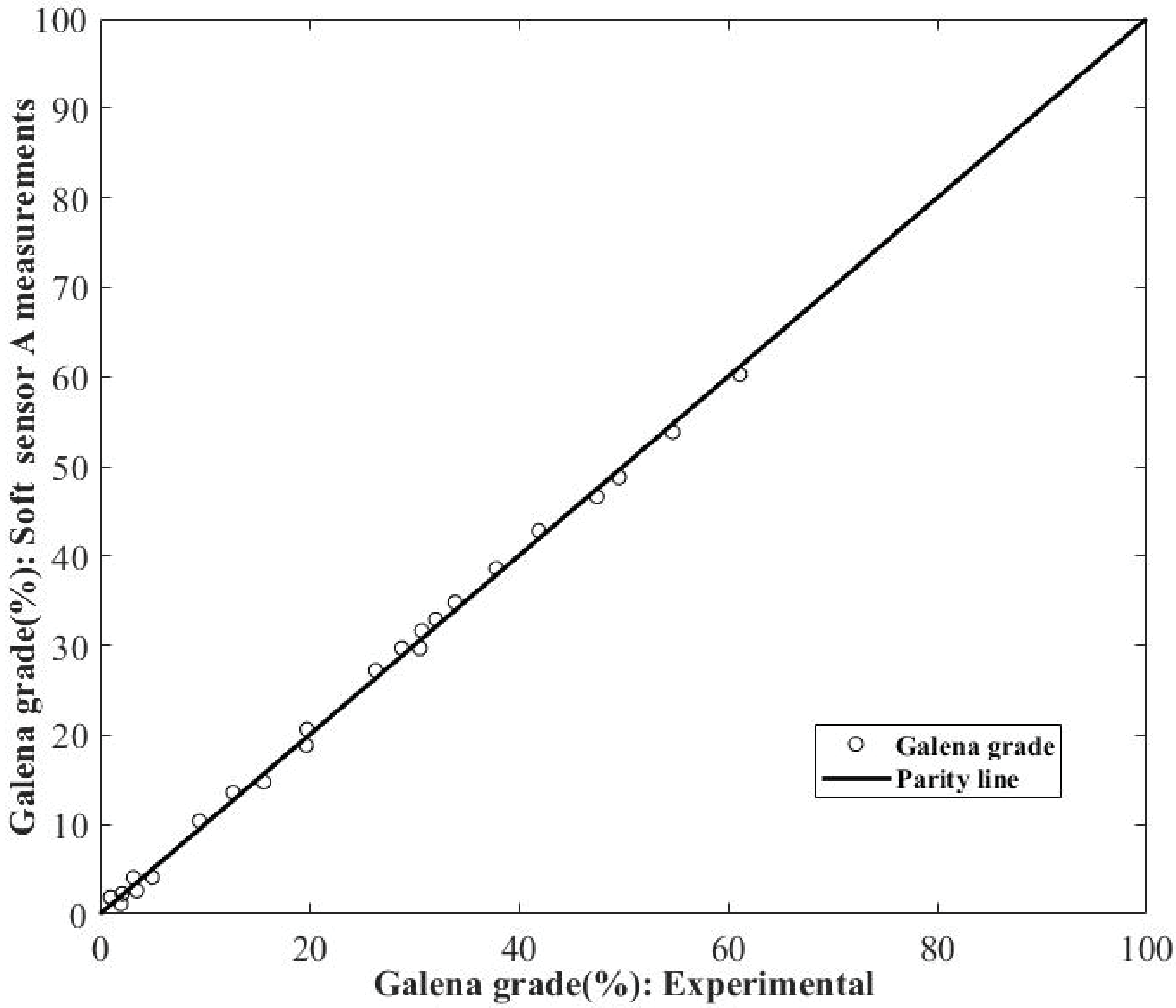

Figure 4.9: Parity plot of experimental (XRF based) measurements and online image-based soft sensor A estimates for galena grade

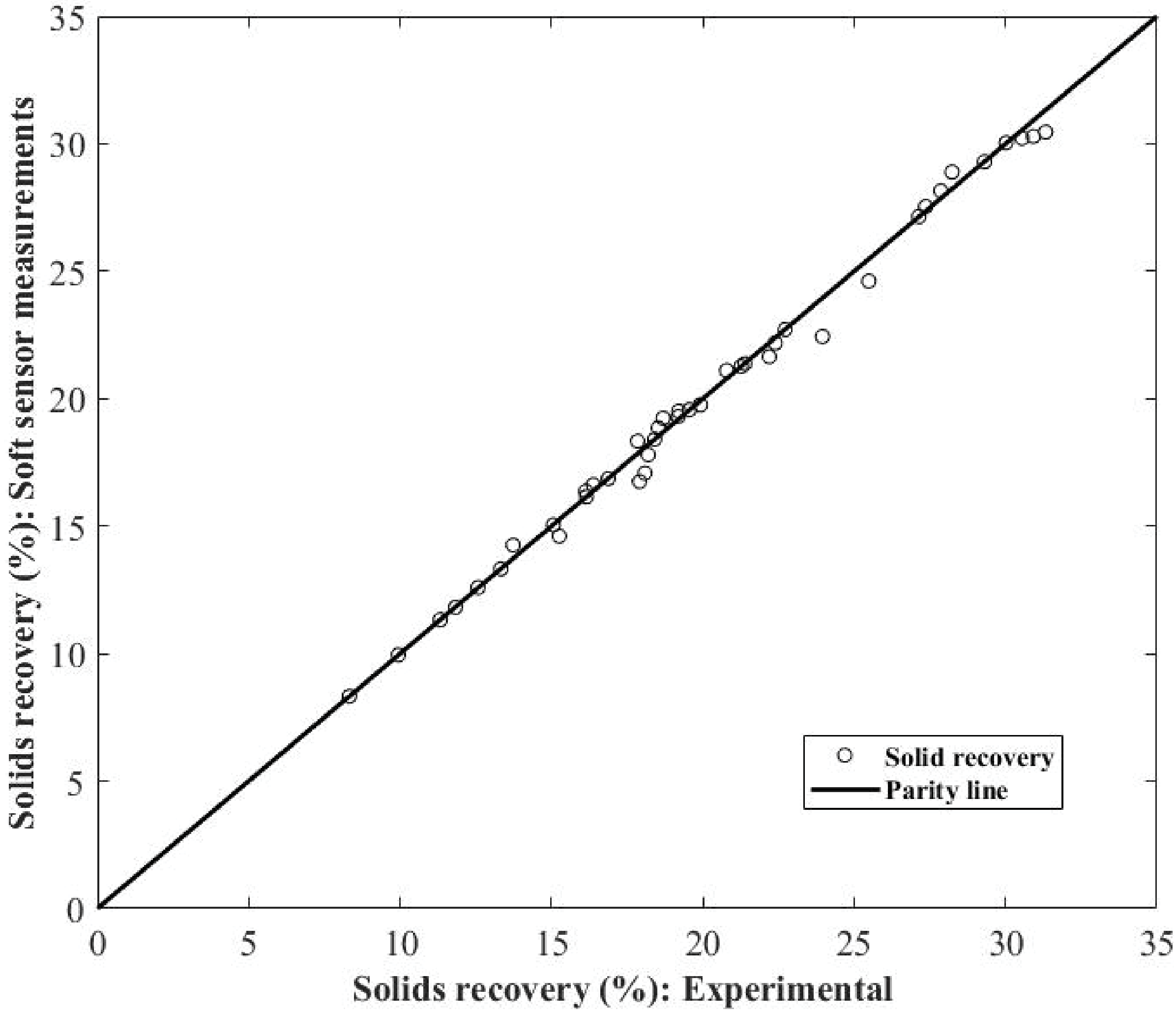

Figure 4.10: Parity plot of experimental measurements and online image-based soft sensor B estimates for solids recovery

Online estimates of the galena grade and solids recovery based on soft sensors A and B are shown along with the small number of offline XRF measurements in Figures 4.11 and 4.12, respectively, for feed stream Type 1. The soft sensor estimates show that the instantaneous grade reduces with time for 0-200 seconds. This trend is validated by the XRF-based grade measurements shown in Figure 4.11 and the XRF measurement of 3.2% for the sample collected between 290 and 300 seconds (not shown in the figure).

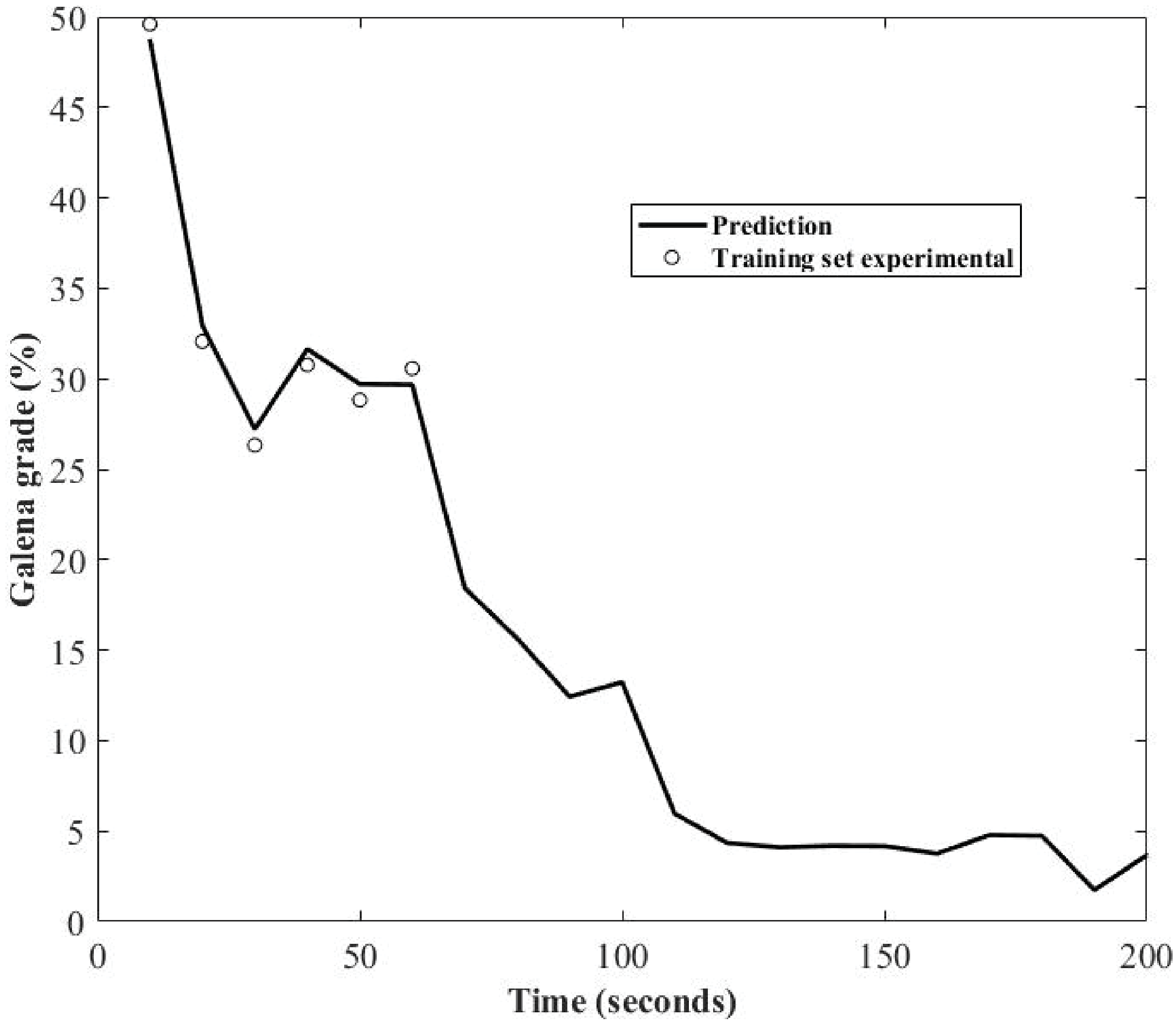

Figure 4.11: Soft sensor A-based galena grade prediction for feed Type 1

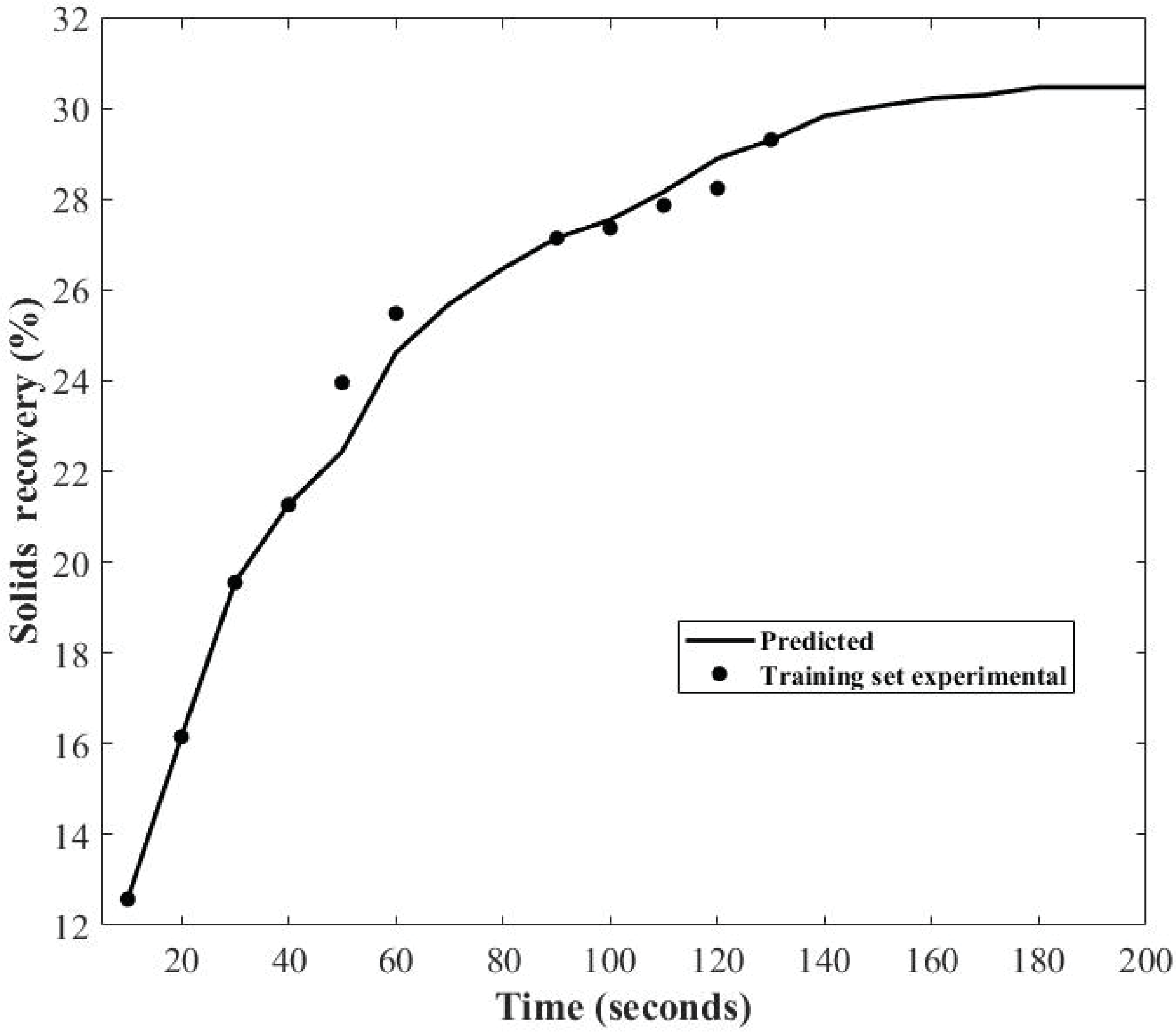

Figure 4.12: Soft sensor B-based solids recovery prediction for feed Type 1

Galena and quartz recovery are estimated using the image-based soft sensor outputs as a function of time, and are presented in Figures 4.13, 4.14, and 4.15 for Type 1, 2, and 3 feed streams, respectively. XRF-based experimental measurements for a few samples are also included in the figures for validation, which show that the complete sensor network provides accurate estimates in real-tie, and confirms that online froth images can be used to measure real-time process outputs such as grade and recovery under the flotation test conditions.

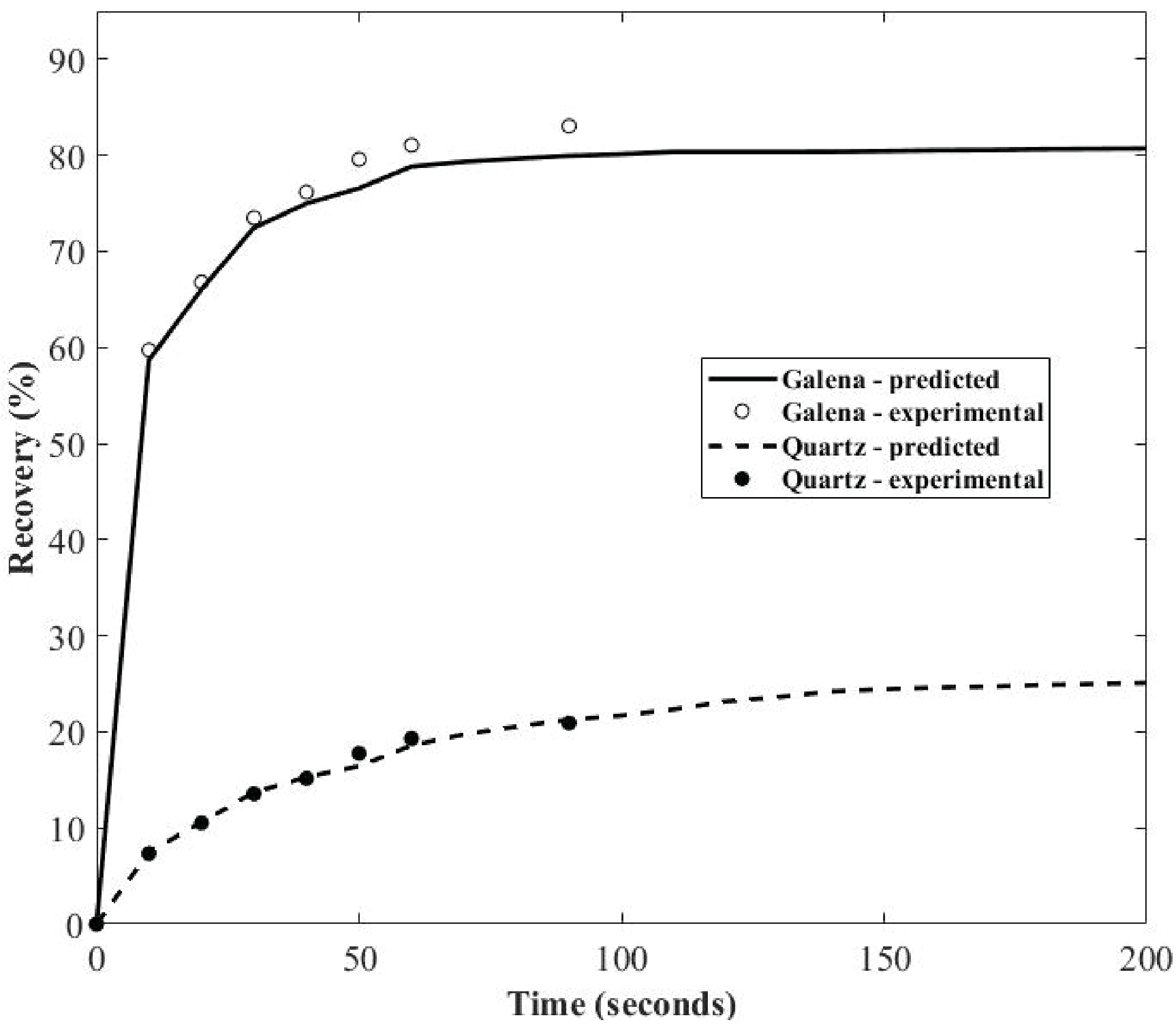

Figure 4.13: Soft sensor-based prediction for galena and quartz recovery for feed stream Type 1.

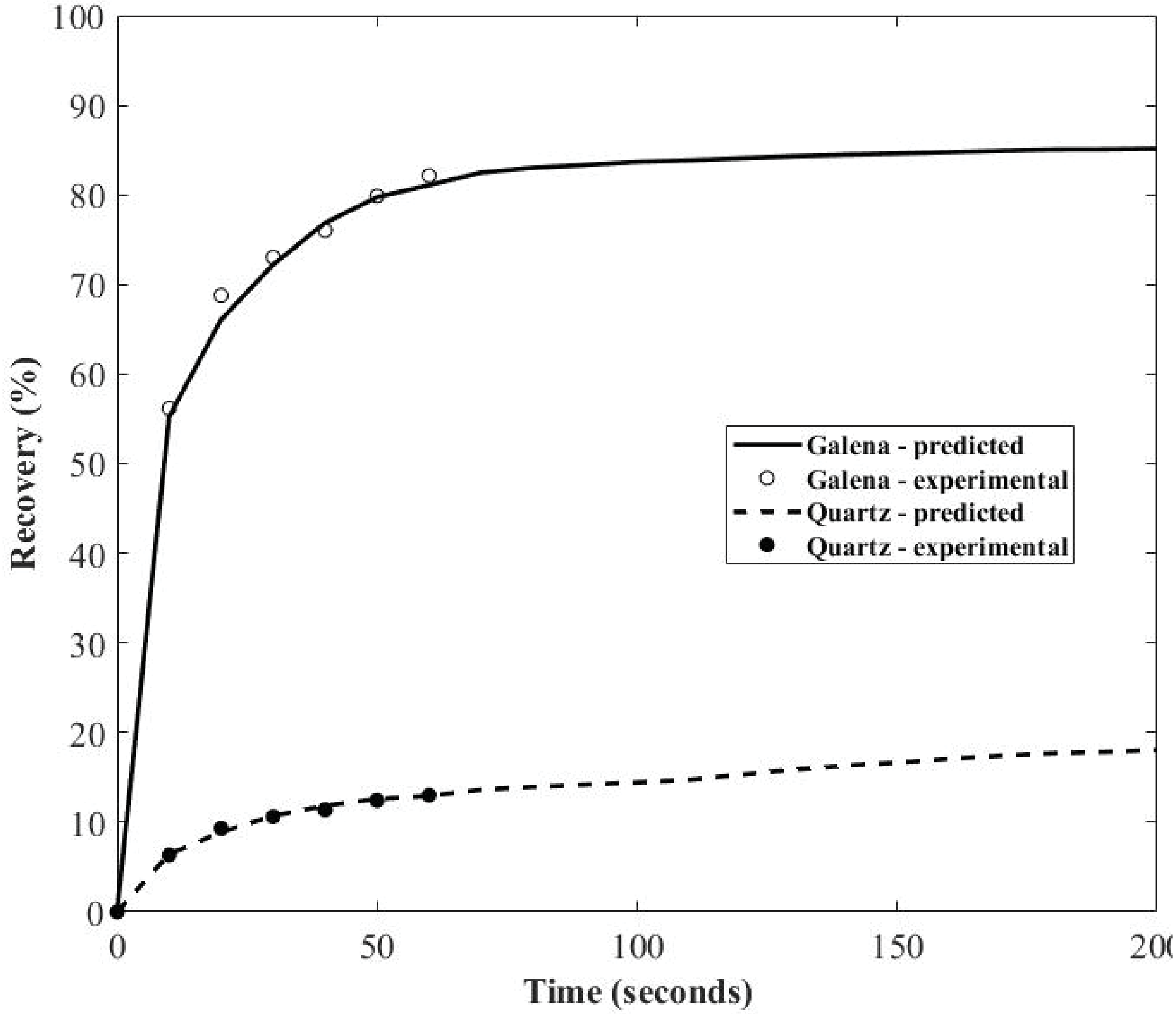

Figure 4.14: Soft sensor-based prediction for galena and quartz recovery for feed stream Type 2.

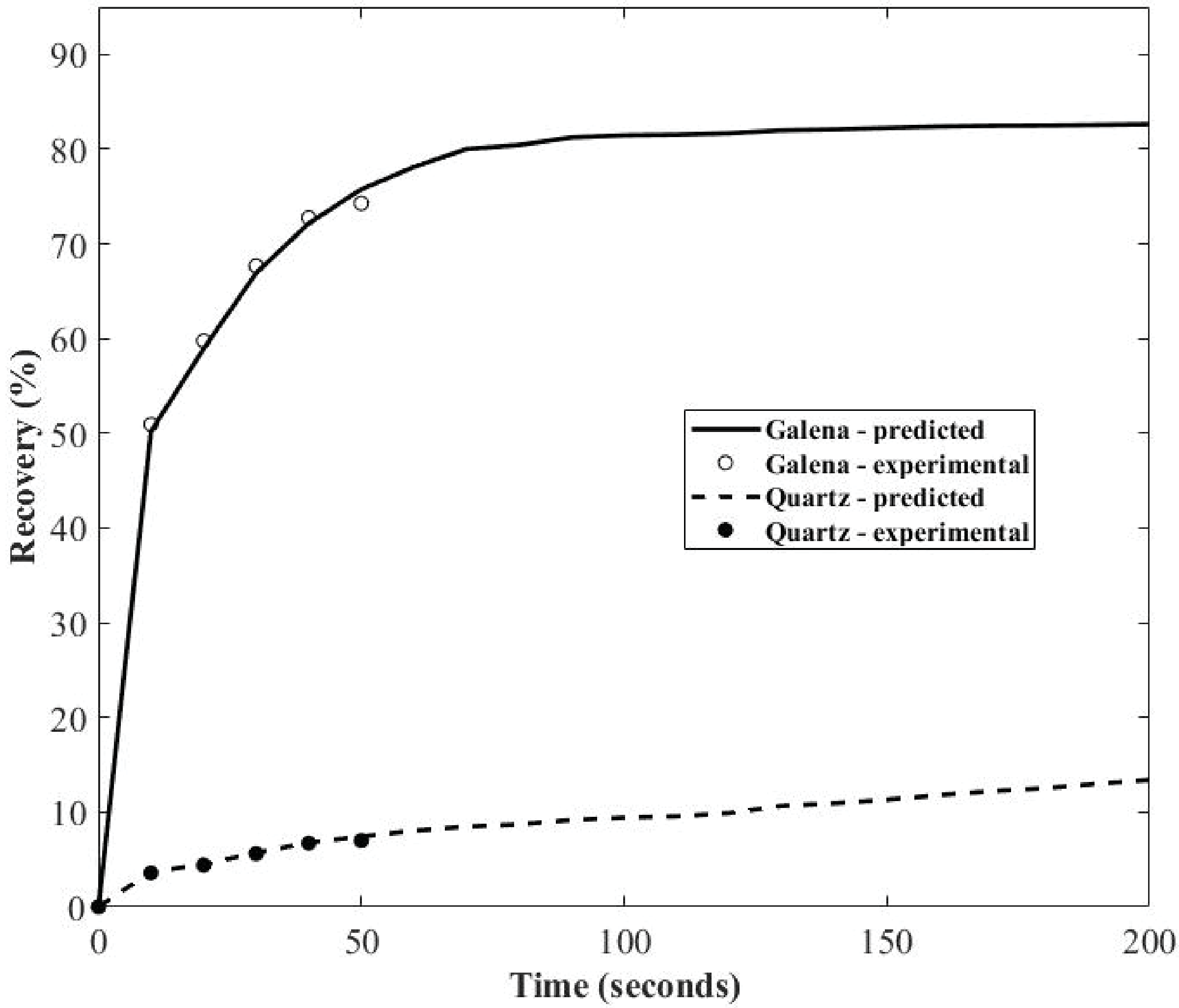

Figure 4.15: Soft sensor-based prediction for galena and quartz recovery for feed stream Type 3.

4.5.3 Model update: EKF based state and parameter estimation

The final measurements of galena and quartz recovery from the soft sensor framework were then provided to EKF to update the model by state and parameter estimation. Offline estimation was performed using nonlinear optimization to obtain the initial set of model parameters for the EKF. These parameters, along with other constants describing the hydrodynamic condition in the model are summarized in Table 4.8. The same initial values were maintained for EKF estimation for feed streams of type 1,2 and 3. This was done to track the real-time changes in net drainage and entrainment parameters caused by variation of quartz particle size in feed streams of Type 1, 2 and 3. The true flotation and entrainment contribution were isolated for the experiments through the estimated values of attachment rate constant (k_a), net drainage ($k_{r\prime}$), and entrainment parameter (k_e). Figures 4.16 and 4.17 show the updated fundamental model prediction for overall galena and quartz recovery, respectively, for feed stream Type 2, and compares it to the real-time estimates from the soft sensors. Additionally, Figure 4.16 shows the true flotation and entrainment recovery components for galena and provides estimates of true flotation and entrainment recovery with time.

Table 4.8: Model parameters for fundamental model structure

Parameter	Value	Method
d_{Bf}(cm)	0.8	VisioFroth
d_{Bp}(cm)(cm)	0.4	Assumption: Half of froth bubble size (Bouchard et al., 2014)
V_p (L)	1.1	Based on interface
V_f (L)	0.4	Based on interface
σ	0.05	Physical property
A_c (m^2)	0.0121	Measured
k_a	0.16	Least squares optimization
k_d	0.42	Least squares optimization
k_w	0.03	Least squares optimization
k_e	4.59	Least squares optimization
$k_a c$	0.143	Least squares optimization
$k_{r\prime}$	0.511	Least squares optimization
ϵ_p	0.50	Least squares optimization
ϵ_f	0.88	Least squares optimization

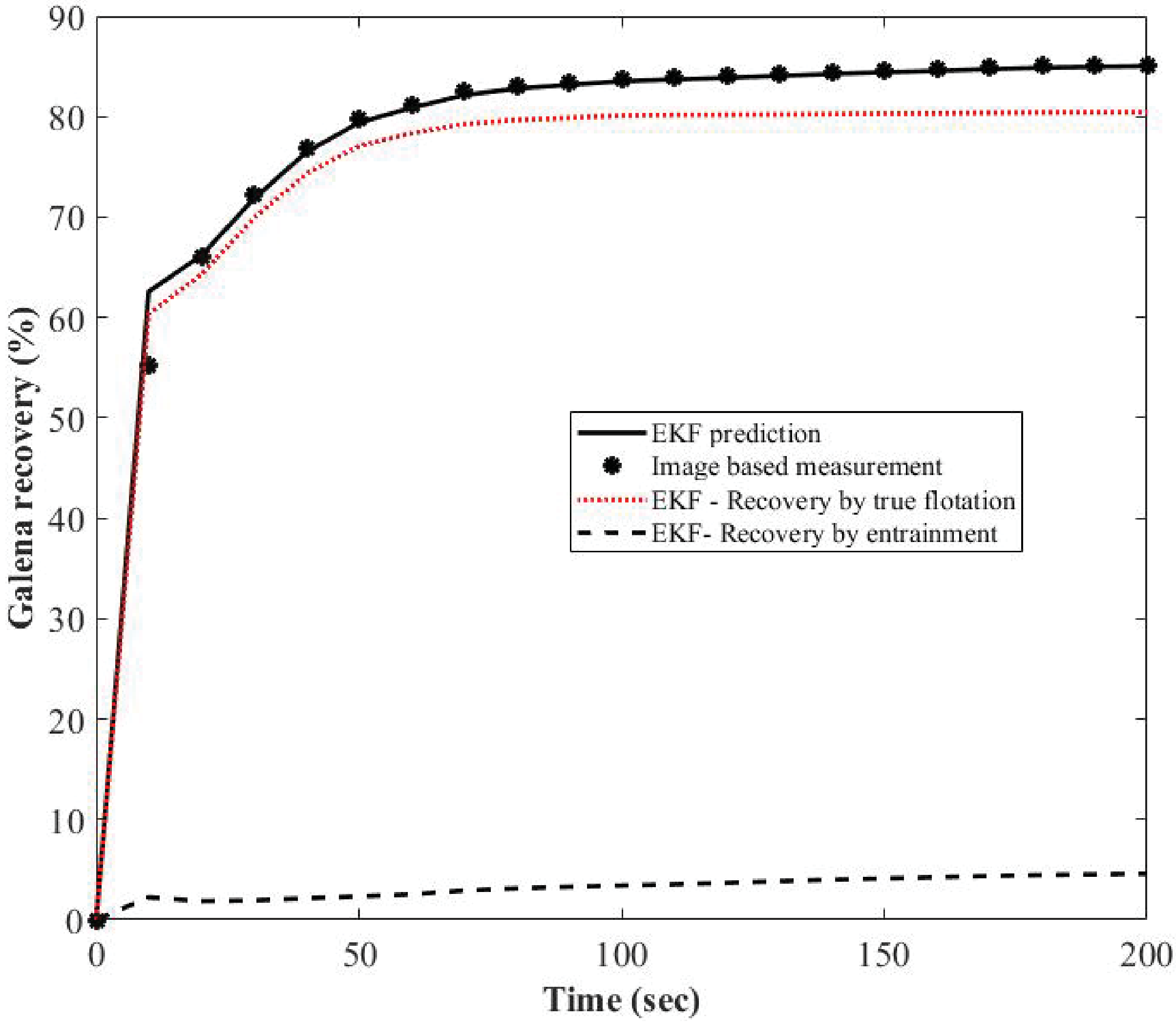

Figure 4.16: Prediction of the overall recovery of galena (and identification of the individual components of recovery) based on the updated fundamental model and its comparison with soft sensor-based measurements for flotation of Feed Type 2.

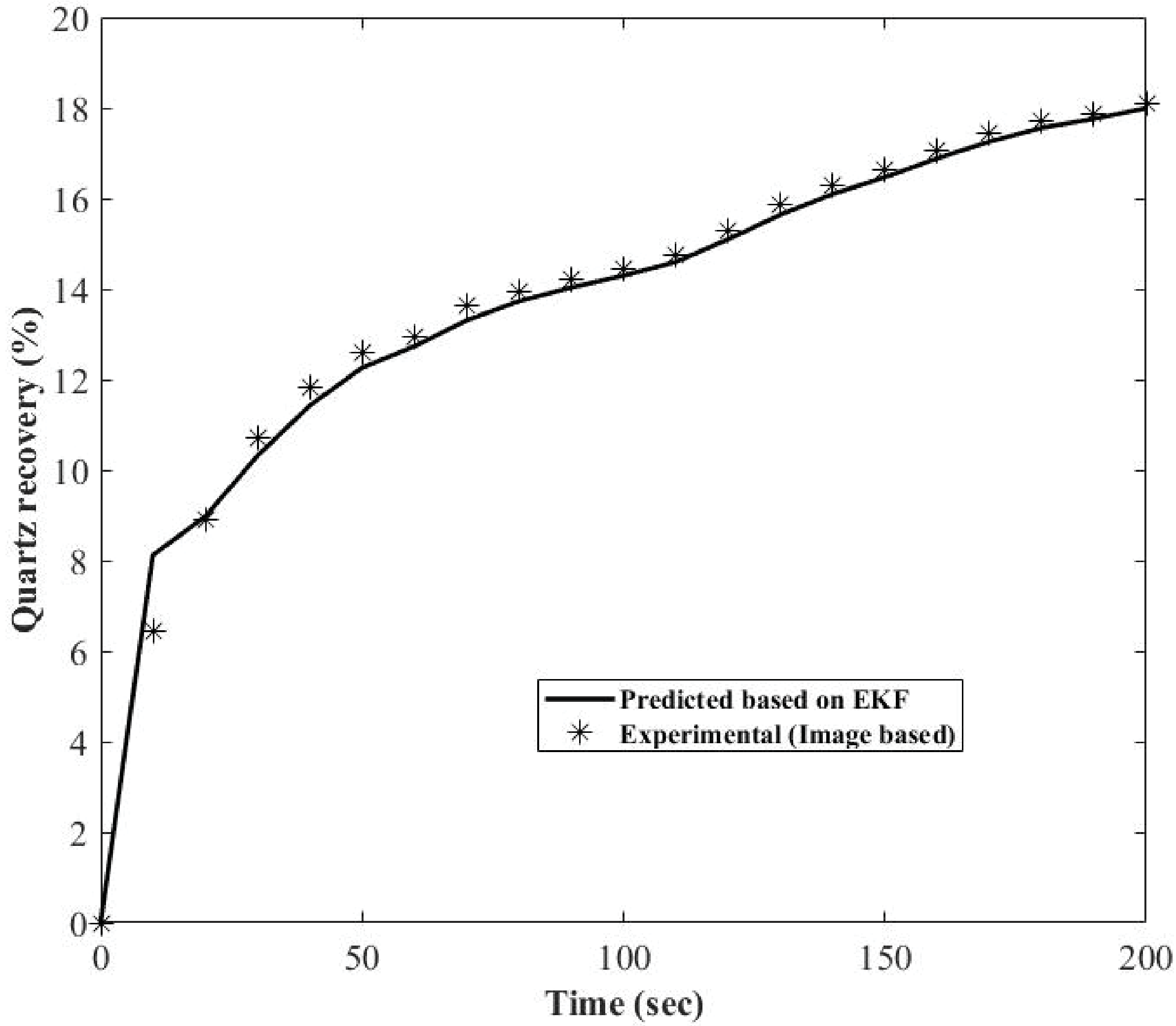

Figure 4.17: Quartz recovery prediction based on the updated fundamental model and its comparison with soft sensor-based measurements for flotation of feed Type 2.

Figures 4.18, 4.19, and 4.20 show the estimated k_a, k_e, and $k_{r'}$ parameters for different quartz particle sizes in feed stream Types 1,2 and 3. The estimated parameters obtained with the same initial conditions are able to track the dynamics of the flotation process for all three quartz particle sizes in feed streams of Type 1,2 and 3. It is observed that the change in quartz particle size does not have any effect on the estimated parameter k_a, which represents the attachment behavior of galena particles. Figure 4.20 shows the effect of quartz particle size on the estimated parameter $k_{r'}$, which represents the drainage behavior. $k_{r'}$ has its highest value in feed stream Type 3 (under 90 μm) followed by Type 2 (under 40 μm) and Type 1 (under 15 μm). However, Figure 4.19 shows the opposite trend. Feed stream Type 1, which contains smaller particles, has the highest estimated parameter value for k_e , which represents the entrainment process behavior. k_e increases with a decrease in quartz particle size, and this is in agreement with the reports of high entrainment for fine particles in the literature (Wang, 2016; Smith and Warren, 1989; Lynch, 1981).

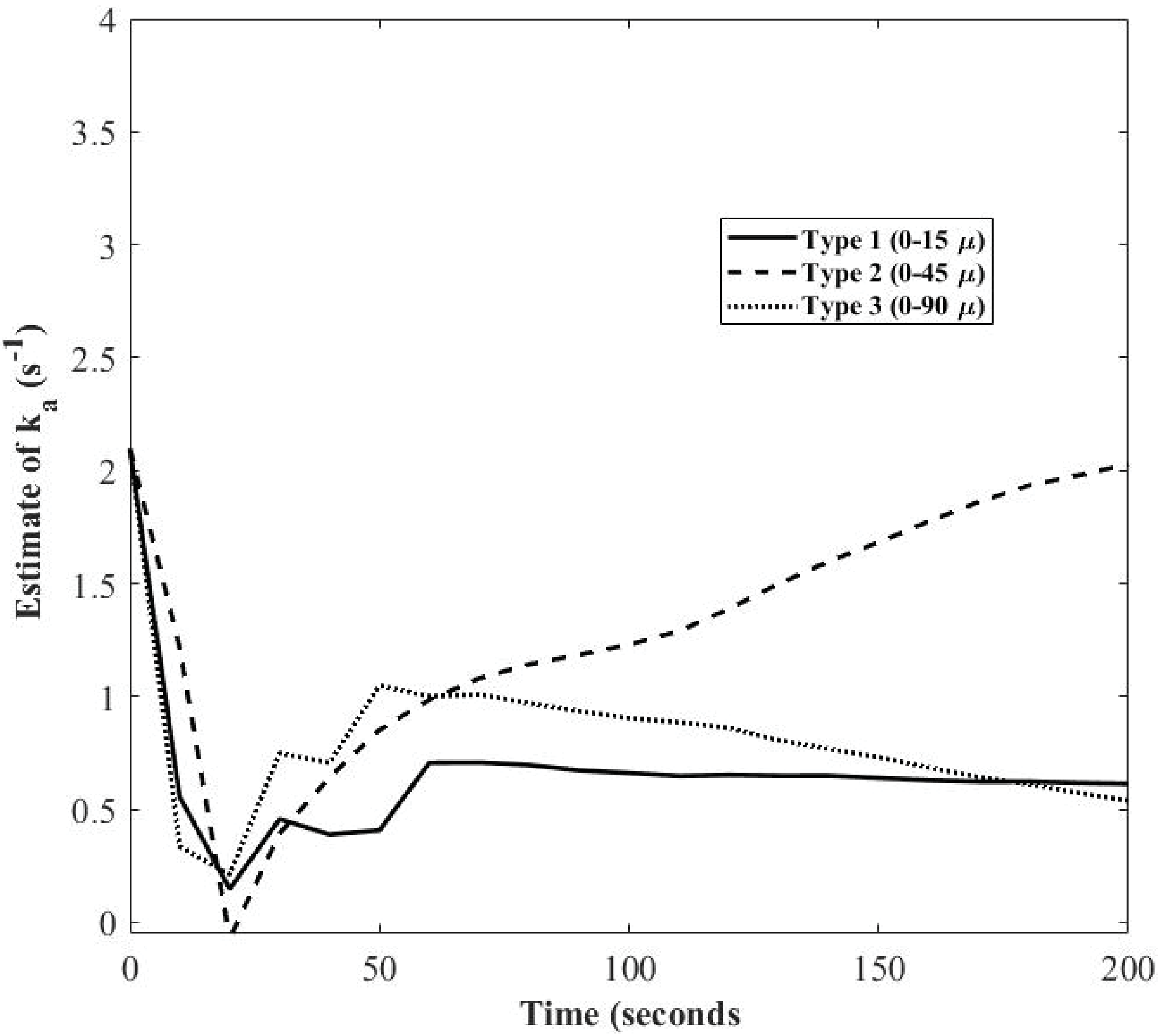

Figure 4.18: Estimate of attachment rate constant (k$_a$) for feed stream Types 1, 2, and 3

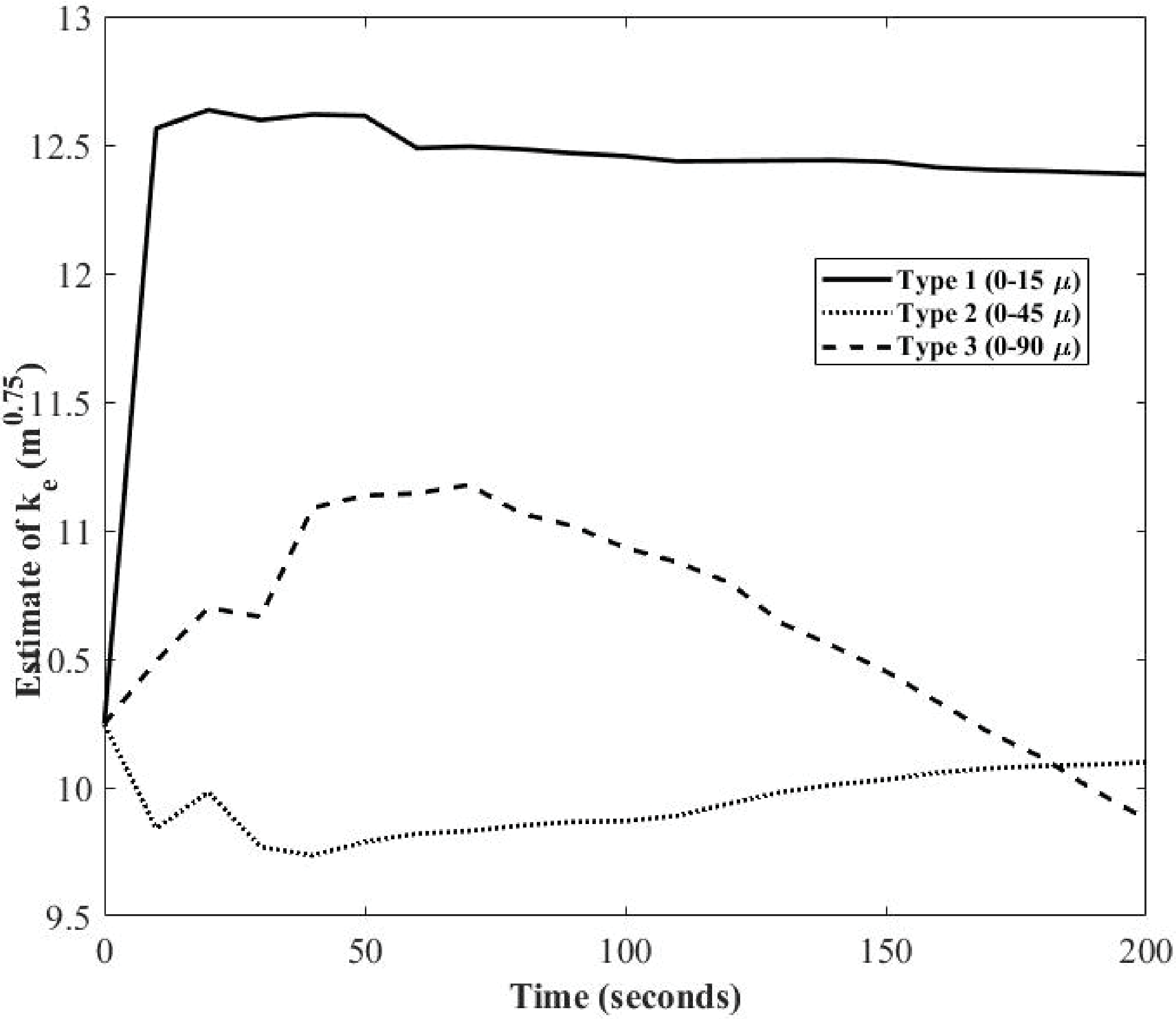

Figure 4.19: Estimate of entrainment parameter (k_e) for feed stream Types 1, 2, and 3

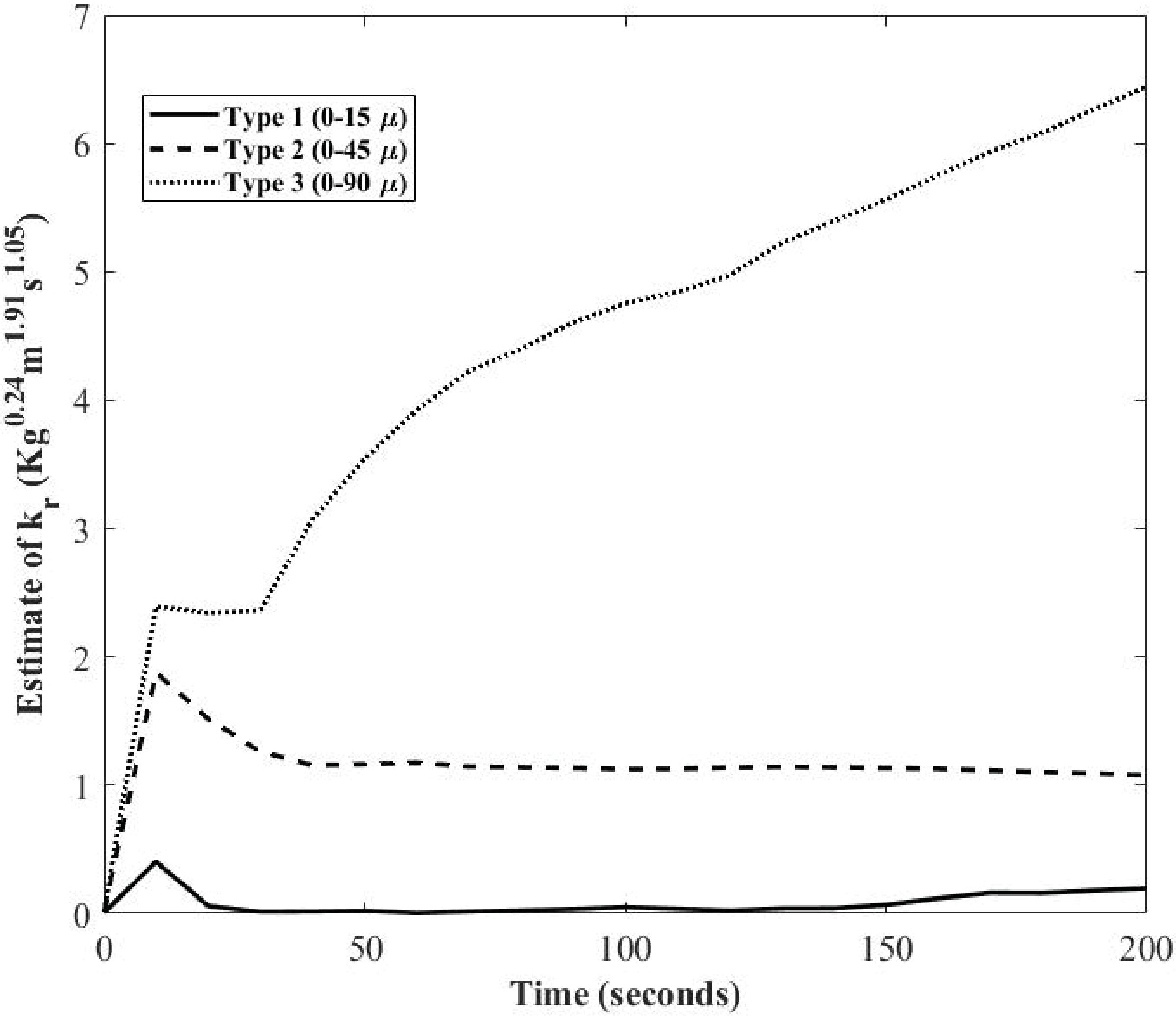

Figure 4.20: Estimate of drainage parameter ($k_{r'}$) for feed stream Types 1, 2, and 3

Entrainment recovery measurements were obtained based on estimated parameters for feed streams types 1 and 3. The trends in entrainment recovery based on the parameter estimates are shown in Figures 4.21 and 4.22. Galena entrainment, showed much less dependence on quartz particle size, which is possibly due to the assumption of same $k_{r'}$ for both the minerals. Low galena entrainment for feed stream Type 1 containing fine quartz could be due to high quartz entrainment. With the same plateau border area, less galena particles are entrained with the presence of a large amount of fine quartz particles.

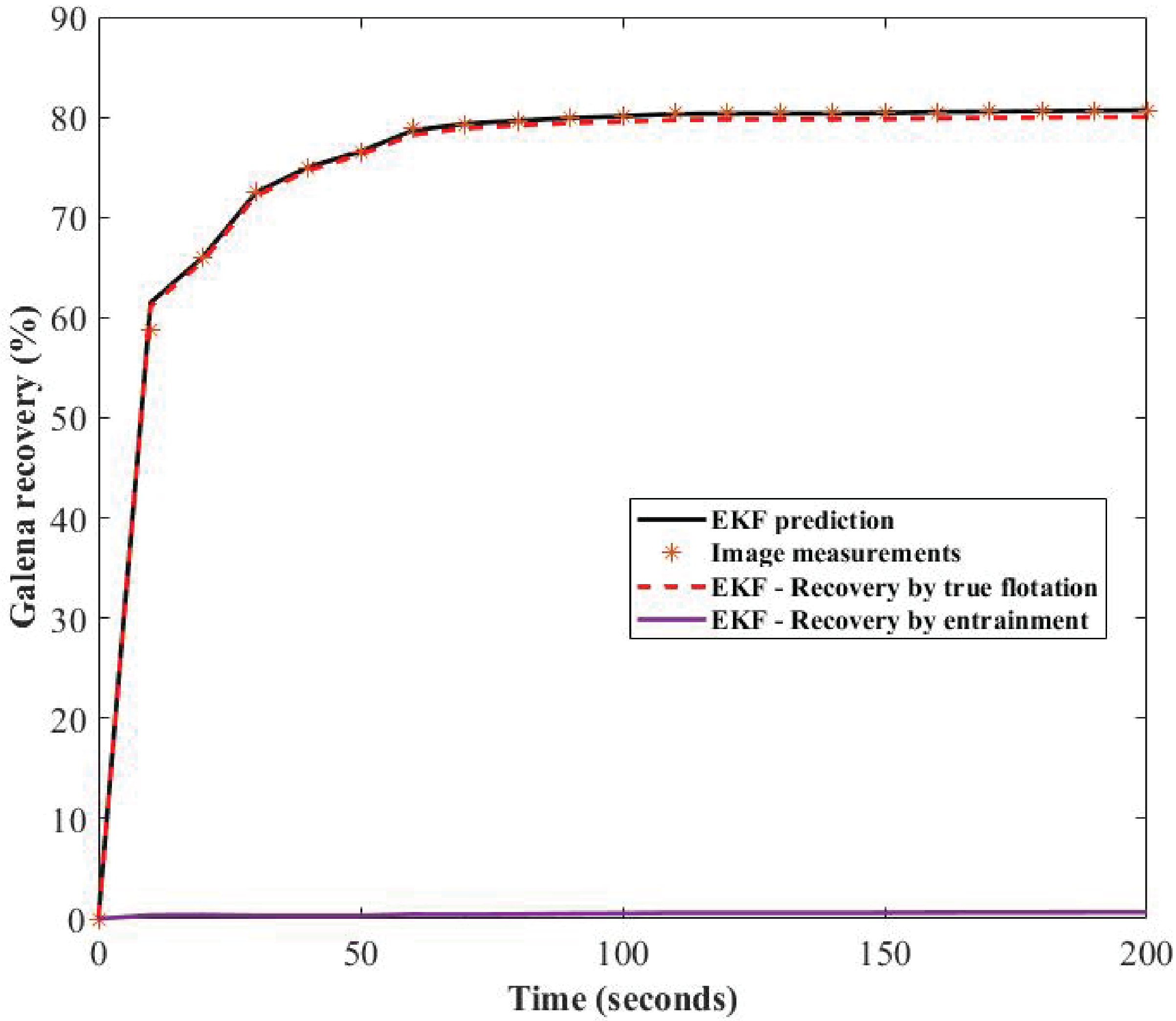

Figure 4.21: Prediction of the overall recovery of galena (and identification of the true flotation and entrainment components of recovery) based on the updated fundamental model and its comparison with soft sensor-based estimates for flotation of feed stream Type 1.

Apart from the identification of the true flotation and entrainment components of galena recovery, the estimated parameters can be used for process monitoring and identification of the disturbances causing an increase in entrainment recovery. Entrainment reduction methods can be studied and tested by using the real-time estimates of $k_{r'}$, and

k_e for the process.

4.6 Conclusions

In this paper, a framework was developed to monitor the entrainment and determine the contribution of true flotation and entrainment to the overall mineral recovery in real-time. Batch flotation experiments were designed and conducted with different sized quartz as a hydrophilic tracer. The SVR model was developed and trained to obtain online process estimates using images and the proposed soft sensor network. The soft sensor network was validated and showed the potential for being used to generate online estimates for entrainment. The fundamental model, combined with the online process measurements, was updated in real time using EKF-based state and parameter estimation. The updated model was used to obtain individual components of mineral recovery. Real-time monitoring showed that the net drainage parameter increased and the entrainment parameter decreased with increasing quartz particle size.

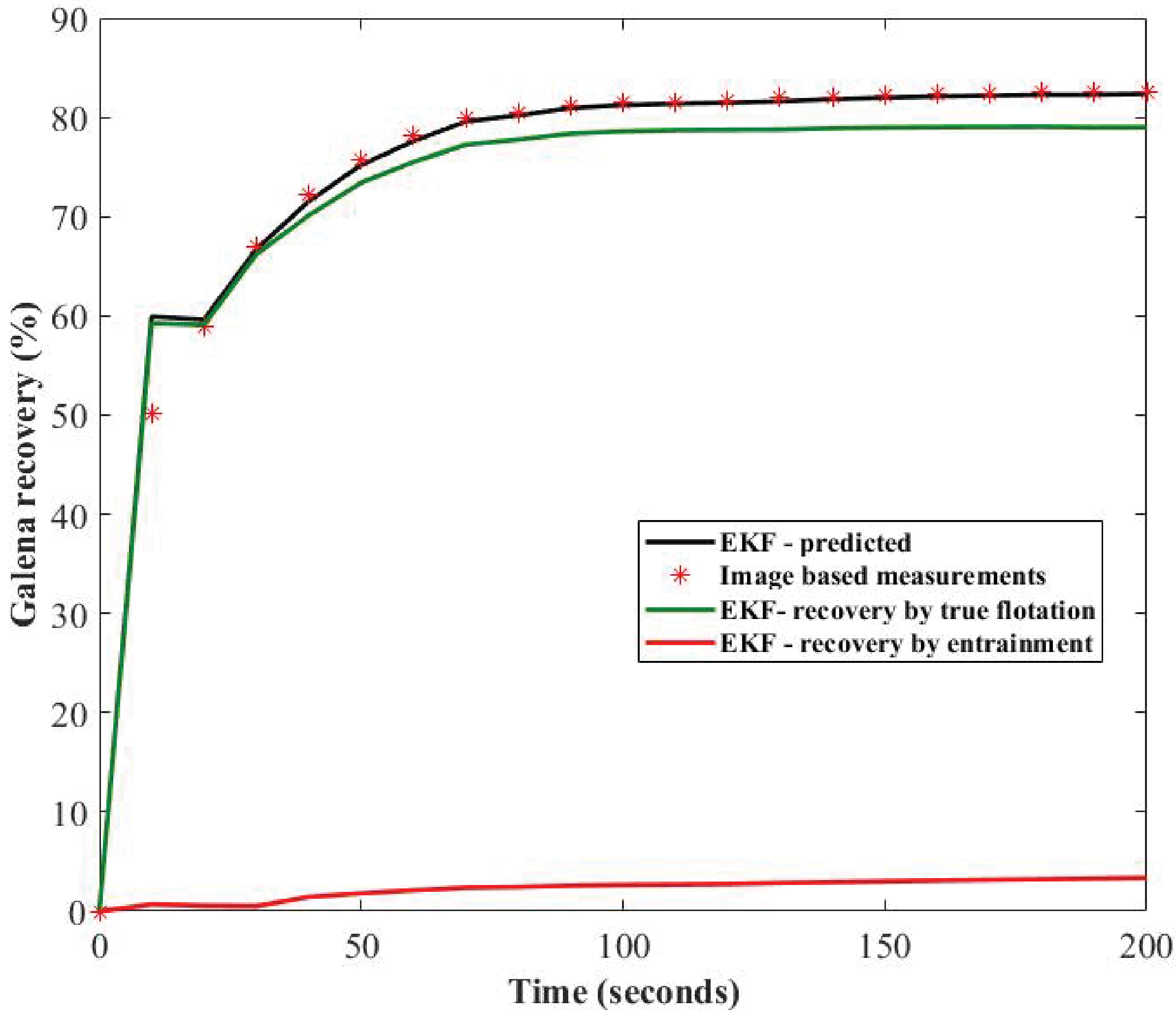

Figure 4.22: Prediction of overall recovery of galena (and identification of the true flotation and entrainment components of recovery) based on the updated fundamental model and its comparison with soft sensor-based measurements for flotation of feed Type 3.

4.7 References

Akdemir, Ü., Sönmez, ., 2003. Investigation of coal and ash recovery and entrainment in flotation. Fuel Processing Technology 82, 1–9.

Aldrich, C., Marais, C., Shean, B.J., Cilliers, J.J., 2010. Online monitoring and control of froth flotation systems with machine vision: A review. International Journal of Mineral Processing 96, 1–13.

Alford, R.A., 1990. Improved model for design of industrial column flotation circuits in sulphide applications. Springer Netherlands, Dordrecht. pp. 189–206.

Alves dos Santos, N., Savassi, O., Peres, A.E.C., Martins, A.H., 2014. Modelling flotation with a flexible approach Integrating different models to the compartment model. Minerals Engineering 66, 68–76.

Bascur, O., Herbst, J., 1982. Dynamic modeling of a otation cell with a view toward automatic control, in: IMPC Session III, pp. 17–23.

Bascur, O.A., 2000. An interactive dynamic flotation model framework. Developments in Mineral Processing 13, C8a–21–C8a–31.

Bisshop J.P. & White, M.E., 1976. Study of particle entrainment in flotation froths. Transactions of the Institution of Mining and Metallurgy 85.

Boser, B., Guyon, I., Vapnik, V., 1992. A training algorithm for optimal margin classifiers, in: Annual Conference on Computational Learning Theory, ACM Press. pp. 144–152.

Bouchard, J., Desbiens, A., del Villar, R., 2014. Column flotation simulation: A dynamic framework. Minerals Engineering 55, 30–41.

Çilek, E., Ylmazer, B., 2003. Effects of hydrodynamic parameters on entrainment and flotation performance. Minerals Engineering 16, 745–756.

Cilek, E.C., Umucu, Y., 2001. A statistical model for gangue entrainment into froths in flotation of sulphide ores. Minerals Engineering 14, 1055–1066.

Cutting, G., Barber, S., Newton, S., 1986. Effects of froth structure and mobility on the performance and simulation of continuously operated flotation cells. International Journal of Mineral Processing 16, 43–61.

Dai, Z., Fornasiero, D., Ralston, J., 1999. ParticleBubble Attachment in Mineral Flotation. Journal of Colloid and Interface Science 217, 70–76.

Dai, Z., Fornasiero, D., Ralston, J., 2000. Particlebubble collision models a review. Advances in Colloid and Interface Science 85, 231–256.

Dobby, G.S., Savassi, O.N., 2005. An Advanced Modelling Technique for Scale-Up of Batch Flotation Results to Plant Metallurgical Performance, in: Centenary of Flotation Symposium.

Duan, J., Fornasiero, D., Ralston, J., 2003. Calculation of the flotation rate constant of chalcopyrite particles in an ore. International Journal of Mineral Processing 72, 227–237.

Engelbrecht, J.A., Woodburn, E.T., 1975. The effects of froth height, aeration rate and gas precipitation on flotation. JS Afr.Inst.Min.Metall 76, 125–132.

Fuerstenau, M.C., Jameson, G.J., Yoon, R.H., 2007. Froth Flotation: A Century of Innovation. SME.

Gaudin, A.M., 1957. Flotation. Mcgraw - Hill, New York. 2nd edition.

Gong, J., 2011. The Role of High Molecular Weight Polyethylene Oxide in Reducing Quartz Gangue Entrainment in Chalcopyrite Flotation by Xanthate Collectors. Ph.D. thesis. University of Alberta.

Gong, J., Peng, Y., Bouajila, A., Ourriban, M., Yeung, A., Liu, Q., 2010. Reducing quartz gangue entrainment in sulphide ore flotation by high molecular weight polyethylene oxide. International Journal of Mineral Processing 97, 44–51.

Gorain, B.K., Harris, M.C., Franzidis, J.P., Manlapig, E.V., 1998. The effect of froth residence time of the kinetics of flotation. Minerals Engineering 11, 627–638.

Gulsoy, O.Y., 2005. A simple model for the calculation of entrainment in flotation. Korean Journal of Chemical Engineering 22, 628–634.

Hanumanth, G.S., Williams, D.J.A., 1992. A three-phase model of froth flotation. International Journal of Mineral Processing 34, 261–273.

Hemmings, C., 1981. On the significance of flotation froth liquid lamella thickness. Trans. Inst. Min. Met 90, 96–102.

Johnson, N., 2005. A Review of the Entrainment Mechanism and Its Modelling in Industrial Flotation Processes, in: Centenary of Flotation Symposium Australia, Brisbane.

Jowett, A., 1966. Gangue mineral contamination of froth. British Chemical Engineering 11, 330–333.

Kalman, R.E., 1960. A New Approach to Linear Filtering and Prediction Problems .

Laplante, A.R., Kaya, M., Smith, H.W., 1989. The Effect of Froth on Flotation Kinetics-A Mass Transfer Approach. Mineral Processing and Extractive Metallurgy Review 5, 147–168.

Liu, Q., Wannas, D., Peng, Y., 2006. Exploiting the dual functions of polymer depressants in fine particle flotation. International Journal of Mineral Processing 80, 244–254.

Lynch, A., 1981. Mineral and coal flotation circuits : their simulation and control. Elsevier Scientific, Amsterdam.

Maachar A. & Dobby, G.S., 1992. Measurement of feed water recovery and entrainment solids recovery in flotation columns,. Canadian Metallurgical Quarterly 31, 167–172.

Moolman, D.W., Eksteen, J.J., Aldrich, C., van Deventer, J.S.J., 1996. The significance of flotation froth appearance for machine vision control. International Journal of Mineral Processing 48, 135–158.

Moys, M., 1978. A study of a plug-flow model for flotation froth behaviour. International Journal of Mineral Processing 5, 21–38.

Mulleneers, H., Koopal, L., Bruning, H., Rulkens, W., 2002. Selective Separation of Fine Particles by a New Flotation Approach. Separation Science and Technology 37, 2097–2112.

Neethling, S., Cilliers, J., 2002a. The entrainment of gangue into a flotation froth. International Journal of Mineral Processing 64, 123–134.

Neethling, S.J., Cilliers, J.J., 2002b. Solids motion in flowing froths. Chemical Engineering Science 57, 607–615.

Neethling, S.J., Cilliers, J.J., 2003. Modelling flotation froths. International Journal of Mineral Processing 72, 267–287.

Pita, F.A., 2015. True Flotation and Entrainment of Kaolinitic Ore in Batch Tests. Mineral Processing and Extractive Metallurgy Review 36, 213–222.

Popli, K., Sekhavat, M., Afacan, A., Dubljevic, S., Liu, Q., Prasad, V., 2015. Dynamic modeling and real-time monitoring of froth flotation. Minerals 5, 570–591.

Prasad, V., Schley, M., Russo, L.P., Bequette, B.W., 2002. Product property and production rate control of styrene polymerization. Journal of Process Control 12, 353–372.

Ross, V., 1988. Mass transport in flotation froths. Ph.D. thesis. University of Stellenbosch.

Ross, V., 1989. No TitleDetermination of the contributions by true otation and entrainment during the otation process, in: Int. Colloquium: Developments in Froth Flotation. Southern African Institute of Mining and Metallurgy, Gordon's Bay.

Runge, K., McMaster, J., Wortley, M., Rosa, D.L., Guyot, O., 2007. A Correlation Between Visiofroth Measurements and the Performance of a Flotation Cell. Ninth Mill Operators' Conference , 79–86.

Savassi, O.N., Alexander, D.J., Franzidis, J.P., Manlapig, E.V., 1998. An empirical model for entrainment in industrial flotation plants. Minerals Engineering 11, 243–256.

Seaman, D.R., Manlapig, E.V., Franzidis, J.P., 2006. Selective Transport of attached Particles Across the Froth Phase. Minerals Engineering 19, 841–851.

Smith, P., Warren, L., 1989. Entrainment of Particles into Flotation Froths. Mineral Processing and Extractive Metallurgy Review 5, 123–145.

Smola, A.J., Scholkopf, B., 2003. A tutorial on support vector regression. Statistics and Computing 14, 199–222.

Stevenson, P., 2007. Hydrodynamic theory of rising foam. Minerals Engineering 20, 282–289.

Tao, D., 2005. Role of Bubble Size in Flotation of Coarse and Fine Particles: A Review. Separation Science and Technology 39, 741–760.

Trahar, W.J., 1981. A rational interpretation of the role of particle size in flotation. International Journal of Mineral Processing 8, 289–327.

Uribe, S., Vazquez, V., Perez, G., Nava, A., 1999. A statistical model for the concentrate water in flotation columns - ScienceDirect. Minerals Engineering 12, 937–948.

Vapnik, V., 1995. The Nature of Statistical Learning Theory. Springer-Verlag New York, New York.

Wang, L., 2016. Entrainment of Fine Particles in Froth Flotation. Ph.D. thesis. The University of Queensland.

Wang, L., Peng, Y., Runge, K., Bradshaw, D., 2015. A review of entrainment: Mechanisms, contributing factors and modelling in flotation. Minerals Engineering 70, 77–91.

Warren, L.J., 1985. Determination of the contributions of true flotation and entrainment in batch flotation tests. International Journal of Mineral Processing 14, 33–44.

Welch, G., Bishop, G., 1995. No Title. An introduction to the Kalman filter .

Yianatos, J., Contreras, F., 2010. Particle entrainment model for industrial flotation cells. Powder Technology 197, 260–267.

Yianatos, J., Finch, J., Laplante, A., 1988. Selectivity in column flotation froths. International Journal of Mineral Processing 23, 279–292.

Z. Dai S.S. Dukhin, D.F., Ralston, J., 1998. The inertial hydrodynamic interaction of particles and rising bubbles with mobile surfaces. J. Colloid Interface Sci. 197, 275–292.

Zheng, X., Johnson, N., Franzidis, J.P., 2006. Modelling of entrainment in industrial flotation cells: Water recovery and degree of entrainment. Minerals Engineering 19, 1191–1203.

Chapter 5

Development of Online Soft Sensors and Dynamic Fundamental Model-Based Process Monitoring for Complex Sulfide Ore Flotation[1]

Complex sulfide ores are difficult to process and often require multi-stage sequential flotation. Process outputs such as grade and recovery in each stage are affected by various sub-processes in the system, and it is crucial to monitor the performance in order to maximize the production. In this work, we have proposed and implemented a dynamic monitoring scheme using fundamental modeling and an online soft sensor network for real-time measurements of grade and recovery. Dynamic fundamental models for lead and zinc recovery were developed to represent the multi-stage rougher flotation for lead-zinc sulfide ores. A soft sensor network was built to measure the grade and recovery in real-time using support vector machine classification and regression on multivariate image data. A factorial design with feed particle size, collector dosage in the lead rougher flotation stage, and collector dosage in the zinc rougher flotation stage as the design variables was used to obtain diverse process conditions for validation. Successful validation at the entire

[1]A version of this chapter is submitted as Popli, K.; Liu, Q.; Afacan, A.; Prasad, V., 2017 "Development of Online Soft Sensors and Dynamic Fundamental Model-Based Process Monitoring for Complex Sulfide Ore Flotation ". Minerals Engineering

range of process conditions demonstrates the potential of the technique for use in process control and monitoring applications. Changes in the collector dosage were monitored in the lead and zinc rougher flotation stages using state and parameter estimates of the fundamental model structure. The process monitoring framework can be extended to monitor other key variables in the process.

5.1 Introduction

Froth flotation is the most used separation process in the mineral industry (Nguyen and Schulze, 2003; Wu et al., 2016) and is used to separate the ore into valuable mineral concentrates and tailings (gangue minerals) based on physicochemical principles(Yalcin and Kelebek, 2011; Kawatra, 2002; Wang et al., 2016). The process is driven by the difference in the surface hydrophobicity between the value and gangue minerals. In most cases, the value mineral is rendered hydrophobic using a chemical reagent known as the collector, which has a direct impact on the process outputs (grade and recovery). Froth flotation is a multi-phase process with gas flowing through the slurry to initiate the attachment of hydrophobic particles to the bubbles (Kawatra, 2002; Finkelstein and Lovell, 1972).

Flotation has been practiced for the beneficiation of sulfide ores for over 100 years (Somasundaran, 1980). With the recent advances in the technology, it is now possible to concentrate poor quality complex sulfide ores through fine grinding (Kohad, 1998). Most of the research has been focused on improving the types and dosage of reagents used in sulfide ore flotation (Barbaro, 2000). Thiol-type collectors (e.g., xanthates) have generally been accepted and employed for the separation of complex sulfide ores (Barbaro, 2000). Various researchers have studied the adsorption effects of Xanthates on the minerals (Barbaro, 2000; Little et al., 1961; Page and Hazell, 1989). It was found that the Xanthates can float all sulfide minerals and are thus not selective towards specific minerals found in the sulfide ores, and hence, the process requires the use of other reagents such as modifiers or depressants to achieve the differential flotation of different sulfide minerals (Barbaro, 2000; Finkelstein and Alllison, 1976). Lead-zinc sulfide ores are among the common sulfide ores that use flotation for beneficiation. Flotation of these sulfide ores is accomplished using multi-stage differential flotation. Several flotation cells are used to separate and recover galena (lead sulfide, PbS), followed by floating sphalerite (ZnS) in a sequential manner (Basilio et al., 1996). Various disturbances may be present and cause the separation process to deviate from its desired state of maximum possible grade and recovery. For instance, kinetic studies for the lead-zinc sulfide ore flotation have reported that the sphalerite shows certain floatability towards the end of galena flotation, and reduces the lead concentrate grade and zinc concentrate recovery (Basilio et al., 1996). The presence of copper activates sphalerite during the grinding (Fisher and Tokich, 1943), thus reducing the separation efficiency further. Depressants are added to inhibit the sphalerite activation. Bubble-particle attachment, dependent on these chemical reagents, is an important process for the ultimate objective of mineral separation, and any disturbance in collector or reagent addition or its quality has a direct impact on the concentrate grade and recovery by affecting the bubble-particle attachment. Other than the chemistry-based factors, there are several operational and feed-based variables that need to be manipulated and monitored to achieve the desired separation (Kawatra, 2002; Popli et al., 2015). Disturbances in feed particle size, feed density, feed grade, air flow rate, or pH are relatively common during operation. These disturbances influence the process and can degrade the product quality and move the operation away from the optimized state. It is therefore of great importance to develop in-depth fundamental process knowledge and monitor the attachment, detachment and transport sub-processes to maximize the grade and recovery without upsetting the operation. It is also important to understand the importance of these operational variables and their relationship to lead and zinc recovery to achieve effective process control.

Various attempts have been made to model the flotation processes and develop an accurate mathematical treatment. The majority of the studies deal with fitting first order kinetic models to the experimental data (Asghar et al., 2015; Kracht et al., 2005; Wills, 1997). First principles models have also been studied for the flotation process. The early first principles models were based solely on the pulp phase; later, many models were proposed for the froth phase by considering it as an important component (Arbiter and Harris, 1962; Harris et al., 1963; Harris and Rimmer, 1966; Lynch et al., 1974). Ventura-Medins and Celiers (Ventura-Medina and Cilliers, 2002) introduced the plateau border to describe the froth in the flotation process. Compartment-based models divide the process into various compartments and develop mathematical relations for inter-compartment processes (Fuerstenau et al., 2007; Bascur, 2000; Popli et al., 2015; Alves dos Santos et al., 2014). Some of these sub-processes include attachment between a bubble and particles to form an aggregate, detachment of a particle from the bubble-particle aggregate, entrainment of a particle from the pulp phase to the froth phase without being attached to a bubble and drainage of a detached particle from the froth to the pulp phase (Bascur, 2000; Popli et al., 2015; Alves dos Santos et al., 2014). The majority of these models are valid only at steady-state and their inability to connect various sub-processes has made them unsuitable for the control and monitoring purposes. In this study, we propose a compartment-based model that includes theoretical dependence of various operational and feed variables to sub-processes in both the lead and zinc rougher flotation stages of flotation for a Pb-Zn sulfide ore. These sub-processes were further connected to the lead and zinc concentrate recovery by developing dynamic equations for those relations.

Real-time or online process measurements are another vital component to complete a monitoring and control framework. Grade and recovery are the key measurements for the flotation processes. Traditional offline procedures of obtaining the grade measurements using analytical methods in the laboratory are not suitable for the dynamic operations due to their long sampling and measurement times. Recently developed online sample analyzers (online X-ray Fluorescence) have been implemented in various plants to measure the grade with better response time. However, their high maintenance, high initial cost, inaccurate data, and difficulty in calibration demand a better solution for the process control purposes (Duchesne, 2010; Popli et al., 2015). Additionally, experienced operators also rely on the qualitative assessment of the visual features of the froth such as color, texture, and stability. However, this assessment is not quantitative, and it is difficult for the operators to understand the process conditions or the root-cause for certain setbacks in the operations (Aldrich et al., 2010; Popli et al., 2015). However, it is known that two similar looking froth images can have different extracted features using machine vision, unnoticeable by even the experienced operators (Aldrich et al., 2010). In the last 25 years, several researchers have exploited the relationship between the froth image structure and corresponding mineral grade (Pryor, 1965; Aldrich et al., 2010; Barbian et al., 2007; Bonifazi et al., 2000; Holtham and Nguyen, 2002; Leiva et al., 2012; Moolman et al., 1996; Popli et al., 2015). Image processing algorithms have been applied to extract various static (color, texture, etc.) and dynamic features (froth mobility, speed, stability, etc.) followed by their application in control systems (Brown et al., 2001). Most of the research in flotation control and implementation in the industry is focused on using single variables such as froth velocities or color to control the product quality (Runge et al., 2007). Recently, multivariable analysis has been proposed for the flotation control and information extraction using image features (Duchesne, 2010). Modern developments in machine vision for flotation have led to the development of various commercial packages to extract and measure the image features. These packages include METCAM

FC (SGS), VisioFroth (Metso® Minerals), FrothMaster^{TM} Outotec), and PlantVision^{TM} (KnowledgeScape Inc) (Popli et al., 2015). We have previously attempted to correlate the image features obtained by VisioFroth to key process measurements for pure minerals and synthetic mixtures (Popli et al., 2015). In this work, we extend our studies to a real complex sulfide ore with multi-stage flotation. The concentrate grade is inferred with image features and supplied to a mass balance framework for inference of recovery. A robust structure is proposed to be implemented for multi-stage flotation circuits. VisioFroth is chosen for the studies due to its common usage in the Canadian mining and oil industries.

The objective of this work is to develop a process monitoring scheme using fundamental models and online measurements from a soft sensor network for complex lead-zinc sulfide ores. The fundamental model was updated in real-time using online process measurements and state and parameter estimation. Factorial design of experiments (DOE) was used to generate a set of multi-stage flotation operating conditions using two levels of each of three factors: the dosage of Xanthate collector in the lead stage of flotation, the dosage of Xanthate collector in the zinc stage of flotation, and the particle size distribution of the feed. The monitoring framework was used to estimate the rate of attachment in real-time and identify the disturbances introduced in the collector dosage. Furthermore, to demonstrate other applications of the image-based soft sensor network, results from factorial DOE were used to analyze the effects of design variables on online process measurements.

5.2 Experimental methods

5.2.1 Materials: Feed sample and reagents

Feed samples in the form of lead-zinc sulfide ore were obtained in the crushed form from the Red Dog Mine, Alaska. X-ray diffraction was used to analyze the feed ore and identify the minerals present as galena (lead sulfide), sphalerite (zinc sulfide), pyrite (iron sulfide), quartz (silicon dioxide), and barium oxide. Galena and sphalerite were the value minerals to be recovered while pyrite and quartz were identified as the gangue minerals. Lead and zinc content in the feed ore were found to be 3.52% and 18.12% respectively using atomic absorption spectroscopy (AAS) and classic zinc titration. A grinding circuit was designed for 500 g of the homogenized sample. A jaw crusher and wet ball mill (65% solid density) were used to obtain two types of feed streams with different particle size distributions of P_{80} at 35 μm and 75μm, respectively. Particle size distributions were measured using a Mastersizer 3000 and are presented in Figure 5.1. The feed streams have median particle sizes (P_{50}) of 18.4 μm and 47.1 μm, respectively.

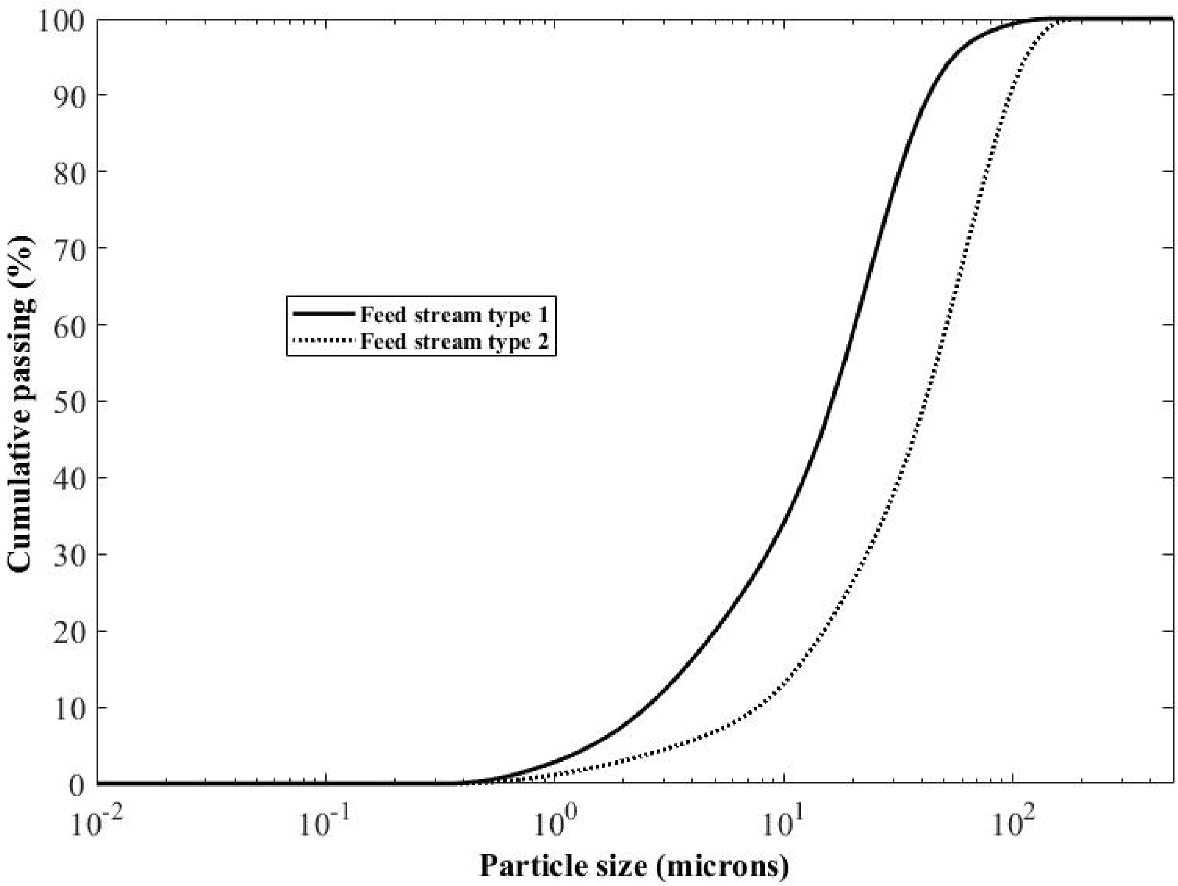

Figure 5.1: Particle size distributions for the two feed streams obtained using the Mastersizer 3000

Rougher flotation of lead and zinc ores requires several chemical reagents for efficient separation. Lime (CaO) was used to modify the pH of the slurry to the specific pH requirements. Potassium ethyl xanthate ($C_3H_5KOS_2$, KEX) was used as a sulfide collector for both lead and zinc stage flotation. Methyl isobutyl carbinol ($C_6H_{14}O$, MIBC) was used as a frother in both stages for stabilizing the froth. Depressants are the reagents that inhibit the flotation of certain minerals by controlling metal ion activation. Activators enhance the conditions for the interaction of the desired mineral with the collector (Bulatovic, 2007). Zinc sulfate ($ZnSO_4$) and sodium sulfite (Na_2SO_3) were used as sphalerite depressants for lead rougher flotation. Also, lime acts as a depressant for pyrite mineral. Copper sulfate ($CuSO_4$) was used as a sphalerite activator for zinc rougher flotation. All the reagent solutions were freshly prepared before being utilized in the grinding and flotation process.

5.2.2 Batch flotation: Lead and zinc stage

Flotation scheme Lead-zinc ore requires sequential flotation with galena being floated first, followed by the flotation of sphalerite. In a typical industrial flow-sheet (Bulatovic, 2007), the overall process is divided into two stages (lead and zinc flotation) with lead concentrate and zinc concentrate being the products. There is also a tailings stream. Sphalerite is initially depressed during the lead stage and then activated and floated in the zinc stage. Rejects from the lead rougher are passed to the zinc rougher through the lead scavenger. Rougher products from both lead and zinc stages are further passed through cleaners to improve the product quality. The objective of the scheme is to reduce the amount of lead and zinc in the tailing stream while maximizing their grade and recovery in respective stages. We have designed a laboratory scale procedure to mimic the rougher stages for lead and zinc flotation. Figure 5.2 presents the flow-sheet used in this work, focusing on the rougher stages of both desired minerals.

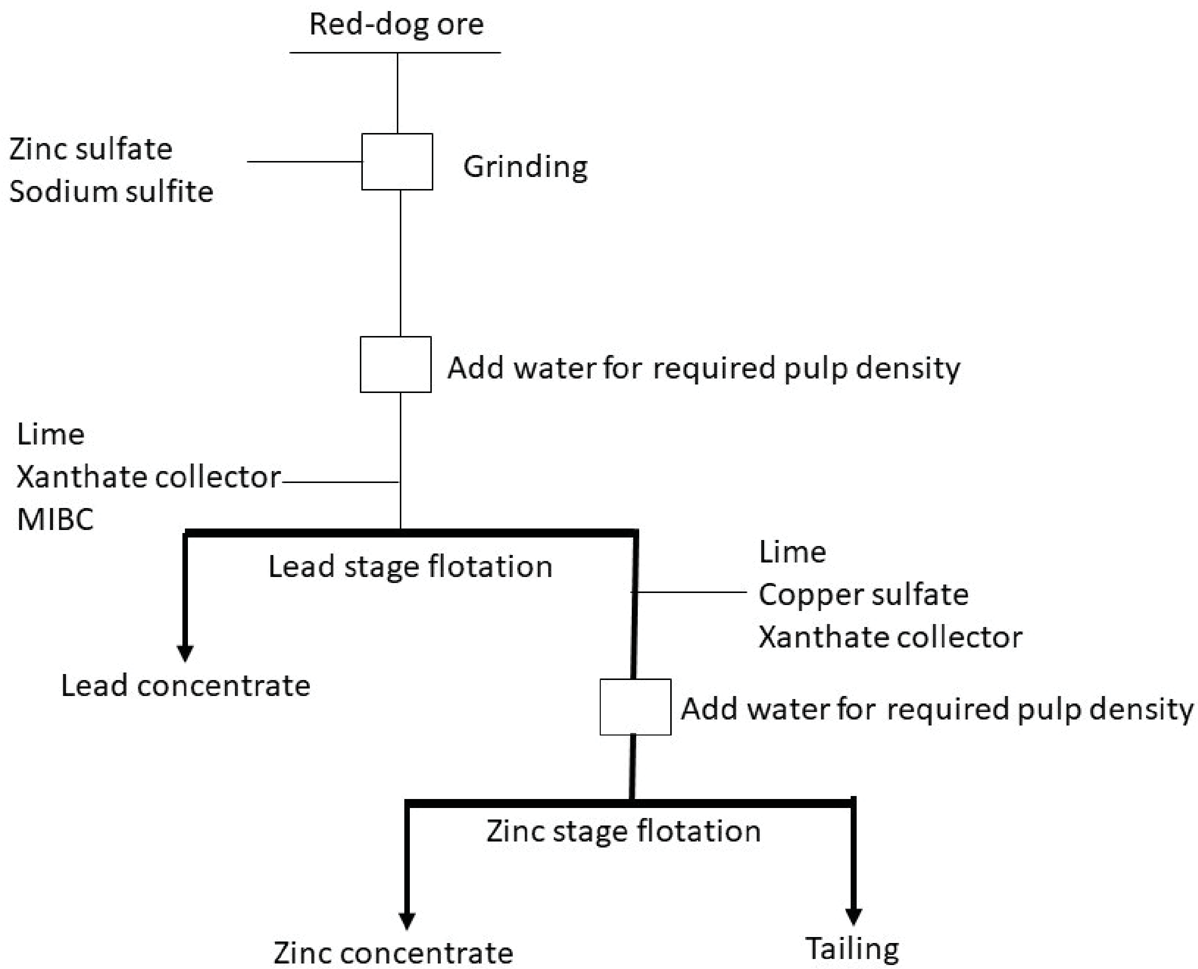

Figure 5.2: A schematic scheme to demonstrate the lab-scale flotation circuit used in this work.

Experimental set-up A 1.5 L JKTeck flotation cell was used for the batch flotation of lead and zinc ores, and was equipped with the VisioFroth package to acquire images of the froth (Popli et al., 2015). C Add-ons to the batch flotation cell include an LED light, laser light, and a froth IP camera. A laser beam was used to measure the height of the overflowing froth. Image features are summarized in Table 5.1, and various measurement algorithms are explained in our previous work (Popli et al., 2015). These measurements were further used for developing the image-based soft sensor network for process measurements.

Table 5.1: Image features extracted using Visiofroth system on top of the cell

Image features	Image features
Velocity	Green component
X velocity	Purity
Y velocity	Load
Froth height	Luminance
D50 (Bubble size)	Red component
D80 (Bubble size)	RBG
Brightness	Stability
Blue component	Tint
Collapse rate	Texture
Cell value	a- component lab model
Dispersion	b- component lab model

Flotation procedure Depressants for sphalerite during the flotation of galena were added to the grinding circuit with zinc sulfate and sodium sulfite dosages at 500g/t and 400g/t, respectively. The pulp solid density was fixed at 35% using 500 g of the feed ore and added water. Agitation was started at 1000 rpm to condition the pulp with the lime to maintain the required pH at 9. It was followed by adding required dosage of KEX and mixing for 2 minutes. MIBC with 0.1ml/L dosage was further added to the slurry and agitation was continued for 1 minute. Lead flotation was initiated with the addition of air at a controlled flow rate of 10 L/min using a rotameter. The concentrates were collected at every 10 seconds for 150 seconds, followed by collection at 270 seconds, 280 seconds, 290 seconds, 590 seconds, and 600 seconds. More frequent samples were collected at the beginning to capture the fast initial dynamics. The collected froth was dried, weighed, and stored for further analysis. After the lead rougher flotation is completed, makeup water is added to the slurry for the zinc rougher flotation to maintain the required slurry volume. The pH was again regulated and maintained at pH value of 10.5 using lime. The required dosage (400g/t) of copper sulfate was added to the pulp, followed by required dosage of KEX. The slurry was conditioned for 2 minutes with an agitation speed of 1000 rpm. Air was added with a flow rate of 10 L/min to start the zinc flotation. Froth samples were collected with the same sampling times described above for lead stage flotation. Image features were acquired with a sampling time of 5 sec. Make-up water, mixed with the required amount of MIBC, was used to maintain the froth height for both lead and zinc stages.

Table 5.2: Flotation conditions for the batch experiments

Variable	Value
Volume of slurry (l)	1.35
Solids weight % in feed (%)	29.8
Air flow rate (L/min)	10
Impeller speed (rpm)	800
Frother dosage (ml/l)	0.1
Sodium sulfite(g/t)	400
Zinc sulfate (g/t)	500
Copper sulfate (g/t)	400

Factorial design of experiments Lead and zinc flotation were characterized by fixed and variable process parameters. Fixed parameters are summarized in Table 5.2, and the variable process parameters (KEX for the lead stage, KEX for the zinc stage, and particle size for the feed stream) were designed using the factorial design of experiments. High and low level values for these process parameters are given in Table 5.3. Experiments were designed with two levels of 3 variables using factorial design. Table 5.4 presents the experimental conditions for $2^3 = 8$ runs obtained using the DOE technique. A 9^{th} run was used as a test run to validate the DOE model for zinc concentrate grade and recovery. Center values(zero) for X_2 and X_3 were 100g/t and 210g/t, respectively.

Table 5.3: Symbols, low level, and high level for design variables of full factorial design

Design parameter	Symbol	Low level (-1)	High level (+1)
Feed particle size (P50, microns)	X_1	18.4	47.1
KEX for lead flotation stage (g/t)	X_2	80	120
KEX for zinc flotation stage (g/t)	X_3	180	240

Table 5.4: Experiment conditions based on full factorial design.

Standard order	Run order	X_1	X_2	X_3
5	1	-1	+1	+1
8	2	+1	+1	+1
4	3	+1	+1	-1
1	4	-1	+1	-1
3	5	-1	-1	-1
2	6	+1	-1	-1
6	7	+1	-1	+1
7	8	-1	-1	+1
9	9	+1	0	0

5.3 Real-time monitoring: Image-based soft sensor, fundamental model, and estimation

The monitoring scheme shown in Figure 5.3 was implemented to monitor the performance of flotation in real-time. A similar scheme has been proposed and implemented in our previous work for pure mineral flotation (Popli et al., 2015). The main features include:

- An online soft sensor to measure process outputs.
- A fundamental model to describe various sub-processes and their relationship to process output measurements.
- State and parameter estimation to update the fundamental model in real-time using the online process measurements.

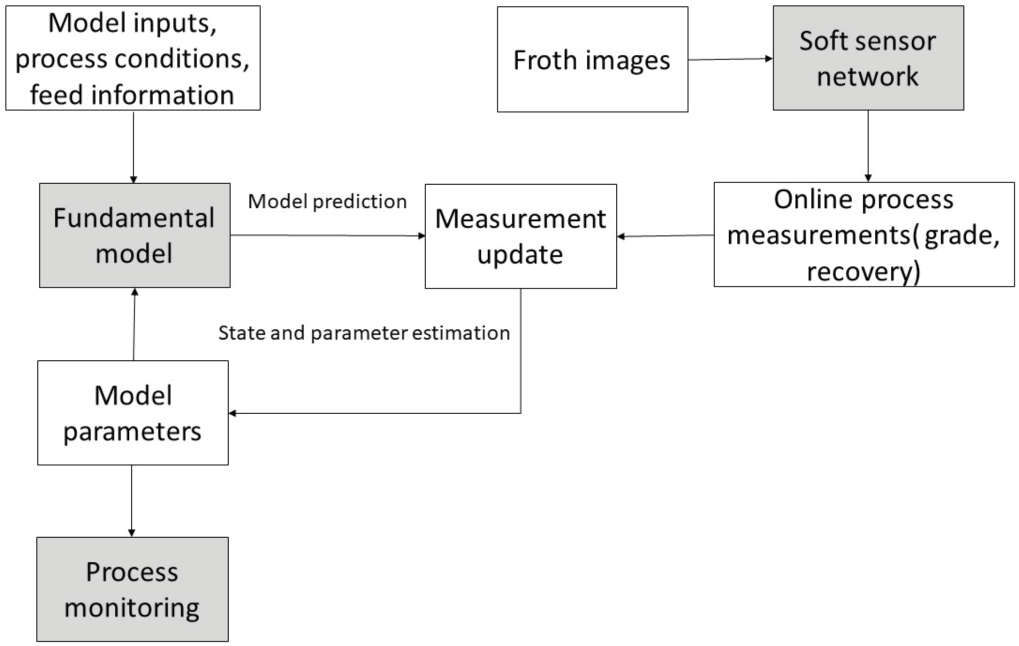

Figure 5.3: Proposed monitoring scheme for the sub-processes of flotation process

State and parameter estimates were then used to monitor the performance of the process. Disturbances in the process can be identified by the changes in these estimates.

5.3.1 Image-based soft sensor development

Image features (summarized in Table 5.1) are used to predict the mineral grade and solids recovery. A sampling time of 10 s was selected for the image-based models. Flotation experiments for each stage were conducted for 600 seconds; however, due to the lack of training data from 500 s to 600 s, online sensors were developed only for flotation times up to 500 s. The images and their features were considerably different for lead and zinc stages of flotation. Therefore, a single image-based soft sensor model cannot be developed to predict grade and recovery for both these stages with high accuracy. Therefore, different soft sensor models were developed for each stage of flotation. However, to automate the process, an image-based classifier was developed to classify any froth image to its respective flotation stage (lead or zinc) using a *support vector machine* for classification. The complete soft sensor network design is presented in Figure 5.4. The machine learning models were developed for the lead grade, zinc grade, and solid recovery separately for the lead and zinc concentrates. In total, there were six image-based regression models and a classification model as summarized in Table 5.5. Datasets of image features were converted to standard scores to remove the effects of different scaling in the algorithms. The converted dataset was characterized by zero mean and a standard deviation of 1. Grade and recovery for lead and zinc can be predicted for both stages using this design.

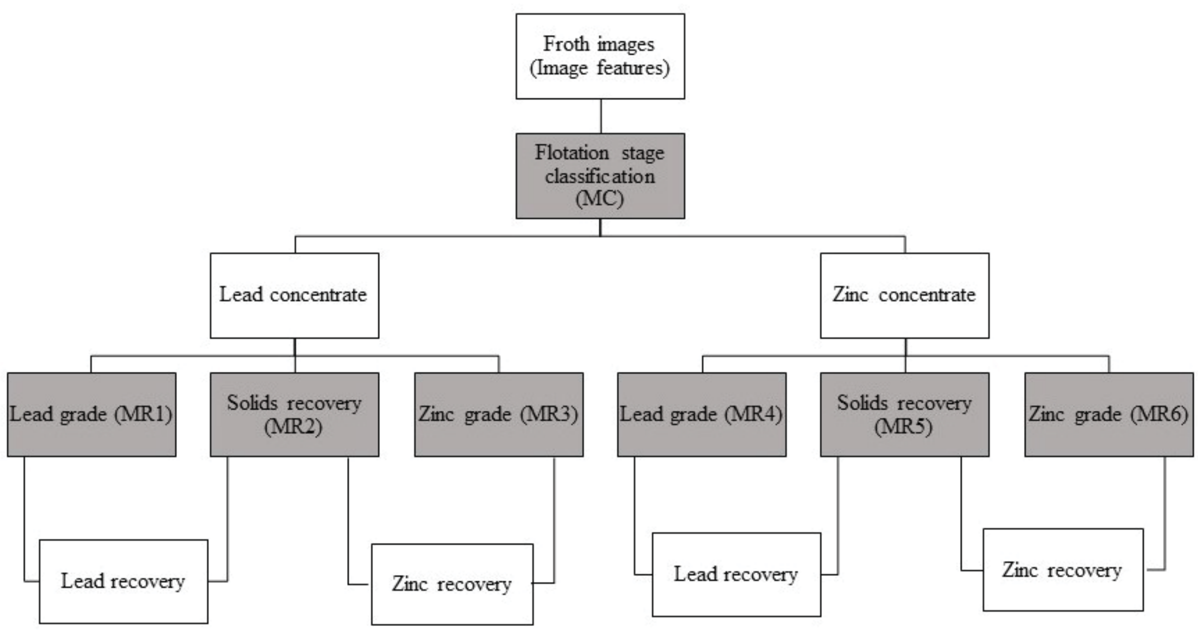

Figure 5.4: Soft sensor network based on the froth surface images to obtain real-time process measurements

Table 5.5: Summary of image-based machine learning models for soft sensor network

Model name	Type	Output	Flotation stage
MC	Classification	Flotation stage	Lead and zinc stage
MR1	Regression	Lead grade	Lead stage
MR2	Regression	Solids recovery	Lead stage
MR3	Regression	Zinc grade	Lead stage
MR4	Regression	Lead grade	Zinc stage
MR5	Regression	Solids recovery	Zinc stage
MR6	Regression	Zinc grade	Zinc stage

Image-based model for classification to lead and zinc stage flotation

Dataset and sampling A data set consisting of images from nine flotation tests was constructed with 22 image features as the inputs, and lead or zinc stage as the classes of outputs. The complete data set was divided into two parts: training and validation. The training data set contained 8896 sample points (chosen randomly), while the validation set contained 1569 randomly selected samples. Image features at any given discrete time sample 't' were used to predict the flotation stage for the corresponding sample point.

Classification model A support vector machine (SVM) was used to develop the image-based classification model. The SVM was chosen based on its robustness and ability to handle noisy data and outliers. Unlike other classifiers that are based on minimizing the error on prediction, the SVM algorithm minimizes the maximum allowed misclassification cases on the prediction (Gunn, 1998). It separates the training data into classes by constructing a hyperplane based on the maximum margin among two classes. Data points on the boundary of the margins are called support vectors.

Support vector machines use the kernel technique to handle the linearly non-separable problems. The kernel technique consists of transforming the data into higher dimension using a kernel function followed by construction of a linear hyperplane (Basak et al., 2007; Smola and Scholkopf, 2003). Detailed explanations of the SVM algorithm can be found in the literature (Basak et al., 2007; Smola and Scholkopf, 2003; Gunn, 1998; Hsu et al., 2010) and are omitted here. A grid search algorithm was used for the entire range of parameters given in Table 5.6 to develop the SVM classifier for the flotation stage. C is the box constraint that decides the trade-off between model accuracy and structure complication, and ϵ represents the maximum misclassification allowed by the model.

Table 5.6: Parameter range for hyperparameter optimization using grid search technique

Parameter	Range	Scale
C	$[10^{-3}\ 10^{3}]$	log
ϵ	[0.0062 623.7583]	log
Kernel function	[linear, gaussian, polynomial]	NA (categorical)
γ (kernel scale)	$[10^{-3}\ 10^{3}]$	log
p (polynomial kernel order)	[2,4]	linear

Image-based model for predicting mineral grade and solids recovery, for lead and zinc stage flotation

Model and methodology Regression models were developed using support vector regression (SVR). ϵ- sensitive loss functions were defined to allow the training error less than ϵ. The regression model with kernel transformation is formulated as

$$\mathbf{F} = \mathbf{W}^T \Phi(\mathbf{x}) + \mathbf{b} \tag{5.1}$$

Here $\mathbf{F}$ is the prediction model, $\mathbf{X}$ is the input data set, $\mathbf{W}$ is the weight vector, and $\mathbf{b}$ is the bias vector. Computation of $\mathbf{W}$ and $\mathbf{b}$ is based on structural loss minimization for the training dataset. Further details about the regression algorithm can be found in the reported literature (Basak et al., 2007; Smola and Scholkopf, 2003; Gunn, 1998). Regression models have similar model parameters to tune as the classification model. The Grid search was used for hyperparameter selection, and 5-fold cross-validation was used for the validation. A novel selection of input data consisting of dynamic image features and model outputs, mineral grade and solid recovery was utilized for the regression models.

Data selection for mineral grade The same data selection scheme was used for the mineral (lead and zinc) grade models for lead and zinc concentrates (ML1, MZ1, ML2, MZ2). Offline output measurements were obtained for flotation run 2 (defined in Table 5.4). Lead and zinc content was measured offline using AAS and zinc titration performed by a commercial laboratory. Image data was acquired from VisioFroth at intervals of every five seconds. However, the output for the training data set was obtained with a sampling time of 10 seconds due to experimental and testing constraints. The training data set consisted of 18 samples each for lead and zinc flotation. The grade output at any time t s was assumed to be dependent on the average image features of 10 images from *t-9* seconds to t seconds.

Data selection for solids recovery Solids recovery is defined as the percentage of solids in the feed that are collected in the concentrate. Offline measurements were obtained from all nine experiments (defined in Table 5.7) with a total of 180 samples for each lead and zinc stage of flotation. A total of 10% of the data was randomly selected as the test data to validate the developed models for image-based solid recovery, and the other 90% was used to train the models. It was observed that the cumulative recovery at each time t seconds was explained well with the average features of the images from beginning of the flotation test to the image at time t (Popli et al., 2015). Accordingly, the data scheme chosen was:

for t = 10, 20, 30,....500 sec

Input for time t: Average of features obtained from images from time one second to t *seconds*

Output for time t: Cumulative solids recovery at time t

Prediction of lead and zinc recovery

Finally, the results from the image-based soft sensors were used to predict lead and zinc recovery for both flotation stages. The cumulative solid recovery prediction (S_{CR}) was used to calculate solid recovery (S_R) using the difference between current and preceding cumulative recovery value.

$$S_R|_t = S_{CR}|_{t+10} - S_{CR}|_t \tag{5.2}$$

Solid recovery (S_R) was further used to compute the solid mass (S_M) collected for each 10 second time interval using the initial solid mass of 500 g.

$$S_M|_t = 100\frac{S_R|_t}{500} \tag{5.3}$$

The amount of lead (Pb_M) and zinc (Zn_M) collected at the concentrate was calculated by multiplying the solid amount (S_M) by the image-based prediction of lead and zinc grade, respectively.

$$Pb_M|_t = \frac{S_M|_t Pb_G|_t}{100} \tag{5.4}$$

$$Zn_M|_t = \frac{S_M|_t Zn_G|_t}{100} \tag{5.5}$$

Lead and zinc amounts were further used to calculate their recovery using feed content.

$$Pb_R|_t = 100\frac{Pb_M|_t}{17.6} \tag{5.6}$$

$$Zn_R|_t = 100\frac{Zn_M|_t}{90.6} \tag{5.7}$$

The same procedure was applied for lead and zinc stage flotation. It was assumed that there was no material loss, and mass balance was complete between feed, concentrates, and tailing for total solids, lead, and zinc content. The models trained using offline measurements from run number 2 (defined in Table 5.4) were used to predict mineral grade and recovery for lead and zinc stage flotation with different process conditions (Table 5.4).

5.3.2 Fundamental model for lead and zinc flotation

A dynamic modeling framework was previously proposed by us for single stage pure mineral flotation (Popli et al., 2015). The framework is extended in this work for a multi-stage flotation of complex sulfide ores. The modeling structure developed aims to satisfy the following requirements:

- Capture the dynamics of the process
- Describe micro-scale sub-processes in the flotation (attachment and detachment)
- Describe macro-scale sub-processes in the flotation (transfer of material from pulp to froth, and froth to the concentrate)
- Connect the micro-scale sub-processes to the macro-scale sub-processes

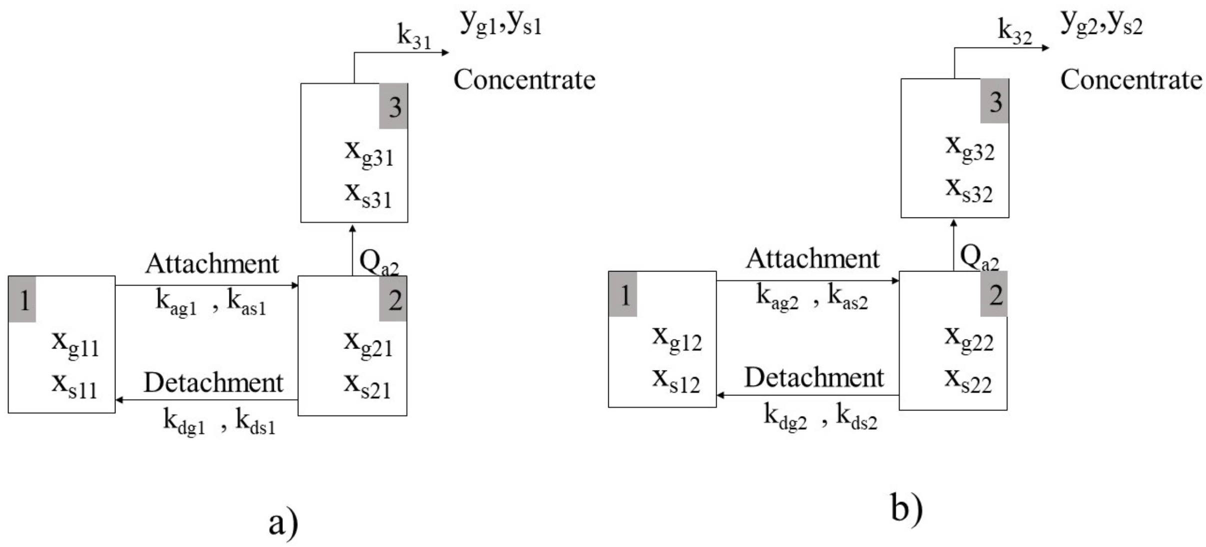

Figure 5.5: Compartment-based framework for multi-stage flotation: a) Lead stage flotation, b) Zinc stage flotation

The model framework is described in Figures 5.5a and 5.5b for lead and zinc stages of flotation, respectively. Three compartments (1, 2, 3) were proposed to represent the three states of the mineral particles: (1) particles free in the pulp , (2) particles attached in the pulp, and (3) particles attached in the froth (Popli et al., 2015; Bascur, 2000). The compartments depict the slurry phase in the pulp section, the gas phase in the pulp section, and the gas phase in the froth section. A mineral particle can be present in any of these three states during the flotation process. Modeling the mathematical equations for the proposed design involves mass transfer and kinetics-based relationships. Within the pulp section, particles are transferred from the slurry phase to the gas phase through attachment, and from the gas phase to the slurry phase by detachment. Attached particles present in the gas phase of pulp section are transferred to the froth section by upward motion of bubble-particle aggregates. Particles in the froth are collected in the concentrate as the final product. Kinetics for the attachment and detachment sub-processes were specified using the attachment rate constant (k_{amj}) and the detachment rate constant k_{dmi}, respectively. Here, m and j represent the mineral type (g: galena, and s: sphalerite) and stage (1: lead stage, and 2: zinc stage), respectively. The dynamic set of equations for lead and zinc flotation are given in equations (5.8, 5.9, 5.10) and (5.12, 5.13, 5.14) for galena and sphalerite, respectively. Galena and sphalerite recovery equations are presented in equations 5.11 and 5.15. Concentrations of minerals (kg/m^3) are represented by x_{mij}, where m denotes the mineral (galena or sphalerite), i denotes the compartment number (1, 2, 3) and j denotes the stage.

$$(1-\varepsilon_{pj})V_{p1}\frac{d}{dt}x_{g1j} = -k_{agj}(1-\varepsilon_{pj})V_{pj}x_{g1j} + k_{dgj}\varepsilon_{pj}V_{pj}x_{g2j} \tag{5.8}$$

$$\varepsilon_{pj}V_{pj}\frac{d}{dt}x_{g2j} = k_{agj}(1-\varepsilon_{pj})V_{pj}x_{g1j} - k_{dgj}\varepsilon_{pj}V_{pj}x_{g2j} - Q_{aj}x_{g2j} \tag{5.9}$$

$$\varepsilon_{fj}V_{fj}\frac{d}{dt}x_{g3j} = Q_{aj}x_{g2j} - k_{3j}x_{g3j}V_{fj}\varepsilon_{fj} \tag{5.10}$$

$$y_{gj} = \left(\frac{t_s\epsilon_{fj}V_{fj}k_{3j}x_{g3j}}{M_{g,feed}}\right)100 \tag{5.11}$$

$$(1-\varepsilon_{pj})V_{pj}\frac{d}{dt}x_{s1j} = -k_{asj}(1-\varepsilon_{pj})V_{pj}x_{s1j} + k_{dsj}\varepsilon_{pj}V_{pj}x_{s2j} \tag{5.12}$$

$$\varepsilon_{pj}V_{pj}\frac{d}{dt}x_{s2j} = k_{asj}(1-\varepsilon_{pj})V_{pj}x_{s1j} - k_{dsj}\varepsilon_{p1}V_{pj}x_{s2j} - Q_{aj}x_{s2j} \tag{5.13}$$

$$\varepsilon_{fj}V_{fj}\frac{d}{dt}x_{s3j} = Q_{aj}x_{s2j} - k_{3j}x_{s3j}V_{fj}\varepsilon_{fj} \tag{5.14}$$

$$y_{sj} = \left(\frac{t_s \epsilon_{fj} V_{fj} k_{3j} x_{s3j}}{M_{s,feed}} \right) 100 \tag{5.15}$$

where, ε_{pj} and ε_{fj} are the volume fraction of gas phase in pulp and froth, respectively, V_{pj} and V_{fj} are the pulp and froth volumes (m^3), respectively, k_{3j} is the froth residence time (1/s), t_s is the sampling time, $Q_a j$ is the air flow rate (m^3), $M_{g,feed}$ and $M_{s,feed}$ are the amount of galena and sphalerite, respectively, in the feed, and y_{gj} and y_{sj} are the galena and sphalerite recovery, respectively. All the variables are presented for lead (j=1) and zinc stage (j=2) of flotation.

Equations 5.16 and 5.17 explain the fundamental relationship between rate constants (k_{amj} and k_{dmj}) and the probabilities of attachment, detachment, and stability (Popli et al., 2015). These equations were used to calculate initial values of the kinetic parameters for estimation. Further details about the probability calculations are given in our previous work (Popli et al., 2015). k_{amj}, k_{dmj}, and k_{3j} represent the model parameters used in estimation.

$$k_{amj} = Z_{1,mj} P_{c,mj} P_{a,mj} P_{s,mj} \tag{5.16}$$

$$k_{dmj} = Z_{2,mj} P_{d,mj} \tag{5.17}$$

where, $Z_{1,m1}$, $Z_{2,m1}$, $P_{c,m1}$, $P_{a,m1}$, $P_{s,m1}$, and $P_{d,m1}$, represent the collision frequency, detachment frequency, probability of bubble-particle collision, probability of bubble-particle attachment, probability of bubble-particle aggregate stability and probability of bubble-particle detachment, respectively, for stage 1 and mineral m (galena or sphalerite).

5.3.3 Monitoring: State and parameter estimation

The dynamic fundamental models described in section 5.3.2 were updated in real-time using online measurements from the soft sensor network (described in section 5.3.1). The set of models can be written as:

$$X_k = f(X_{k-1}, W_{k-1}) \tag{5.18}$$

$$Z_k = h(X_k, V_k) \tag{5.19}$$

where, X_k and Z_k are the state and measurement vectors described in Table 5.7 for the four sets of models. W_{k-1} and V_k denote the process and measurement noise, respectively.

State estimation is a technique used to estimate the important physical variables of a system (states) that are not measurable using instrumentation. The Kalman filter (KF) and extended Kalman filter (EKF) have been applied for various industrial applications ranging from chemical industries to battery systems (Bressel et al., 2015; Popli et al., 2015; Prasad et al., 2002a; Bo et al., 2015). The KF provides the optimal state estimate in linear systems using the real-time information of the plant through online process measurements. The EKF is a nonlinear version of the KF that is based on the minimization of mean of the squared error.

The fundamental model framework can be converted to four sets of state-space equations, each with one output and three states. These are summarized in Table 5.7. Physical parameters used for the models were estimated based on the experimental conditions and machine specifications. Other parameters were obtained using offline estimation by least squares fitting against mineral recovery values. The initial values of states were based on feed pulp density for the lead stage and the initial pulp density for the zinc stage. Based on observability analysis for all the models given in Table 5.7, it was deduced that one parameter (k_{amj}, or k_{dmj}) can be augmented with the three states to perform state and parameter estimation.

Table 5.7: Summary of states and output measurements for different models

Model	States (kg/m^3)	Output measurement (%)	Stage
1	$[\mathrm{x}_{g11}\ \mathrm{x}_{g21}\ \mathrm{x}_{g31}]$	y_{g1}	Lead stage flotation
2	$[\mathrm{x}_{s11}\ \mathrm{x}_{s21}\ \mathrm{x}_{s31}]$	y_{s1}	Lead stage flotation
3	$[\mathrm{x}_{g12}\ \mathrm{x}_{g22}\ \mathrm{x}_{g32}]$	y_{g2}	Zinc stage flotation
4	$[\mathrm{x}_{s12}\ \mathrm{x}_{s22}\ \mathrm{x}_{s32}]$	y_{s2}	Zinc stage flotation

Extended Kalman filter

Model structure The general state-space model described in equations (5.18) and (5.19) is converted to a linear discrete state-space form as:

$$X_k = AX_{k-1} + W_{k-1} \tag{5.20}$$

$$Z_k = HX_k + V_k \tag{5.21}$$

where, W_{k-1} and V_k are the discrete process and measurement noise, respectively. Both process and measurement noise are assumed to be white Gaussian noise with covariance matrices as Q_k and R_k, respectively. X_k is the state vector that includes the augmented parameter.

Algorithm The EKF algorithm is an iteration of the following two steps (Welch and Bishop, 1995; Prasad et al., 2002b):

- **Predictor step.** This step projects the state and covariance estimates to next time step (from $k-1$ to k) (Welch and Bishop, 1995).

$$\widehat{X}_k^- = f(\widehat{X}_{k-1}, U_{k-1}, 0) \tag{5.22}$$

$$P_k^- = A_k P_{k-1} A_k^T + W_k Q_{k-1} W_k^T \tag{5.23}$$

- **Corrector step.** This is a measurement update step and uses the online measurement to correct (update) the estimates (Welch and Bishop, 1995).

$$K_k = P_k^- H_k^T (H_k P_k^- H_k^T + V_k R_k V_k^T)^{-1} \tag{5.24}$$

$$\widehat{X}_k = \widehat{X}_k^- + K_k(z_k - h(\widehat{X}_k^-, 0)) \tag{5.25}$$

$$P_k = (I - K_k H_k) P_k^- \tag{5.26}$$

Real-time process monitoring

The models were reconciled in real-time with the online data and updated using the EKF. The constant model parameters are summarized in Table 5.8 for Models 1 and 4, representing the lead and zinc stages of flotation, respectively (see Table 5.7). The process output measurements were galena recovery for the lead stage and sphalerite recovery for the zinc stage. Any change in the process conditions should be observed in the changes in the respective state or parameter estimates. It is known that changes in the collector dosage will have an impact on the recovery propagated through the change in the attachment sub-process. The attachment rate constant (k_{amj}) was used as a representative parameter of the attachment sub-process and augmented with the state vector for estimation. A disturbance was introduced to the collector dosage in the lead and zinc stages of flotation to evaluate the ability of the estimates to detect such disturbances.

Table 5.8: Parameters for Model 1 (lead stage) and Model 4 (zinc stage)

Parameter	Model 1	Model 4	Method
V_p (L)	1.1	1.1	Based on interface
V_f (L)	0.3	0.3	Based on interface
$k_a mj(s^{-1})$	0.015	0.086	Least square optimization
$k_d mj(s^{-1})$	0.09	3.575	Least square optimization
$k_3 j(s^{-1})$	4.9	4.97	Least square optimization
$\epsilon_p j$	0.2	0.21	Least square optimization
$\epsilon_f j$	0.95	0.734	Least square optimization

5.4 Results and discussion

5.4.1 Batch flotation: Offline measurements

Offline measurements were used to train (i.e. calibrate) the image-based soft sensor models for solids recovery, lead grade, and zinc grade. Solid recovery measurements were obtained for all the nine experiments. Lead and zinc grade measurements for both lead and zinc stages were measured for run 2 using AAS and classic zinc titration (defined in Table 5.4). Lead and zinc recoveries were obtained for run 2, and complete flotation results are summarized in Table 5.9. Variations of lead and zinc recoveries with time are presented in Figures 5.6 and 5.7, respectively, for both stages of batch flotation. The lead stage recovers 55.6 % of lead present in the feed and the zinc stage recovers 74.0% of the zinc present in the feed.

Table 5.9: Batch flotation results for run 2: Metal balance

Stream	Mass (%)	Pb (%)	Zn (%)	Pb recovery (%)	Zn recovery (%)
Feed ore	100	3.52	18.05	100	100
Lead concentrate	17.85	10.96	21.60	55.6	21.4
Zinc concentrate	30.32	1.04	44.24	9.0	74.3
Tailing	51.83	2.41	1.5	35.5	4.3

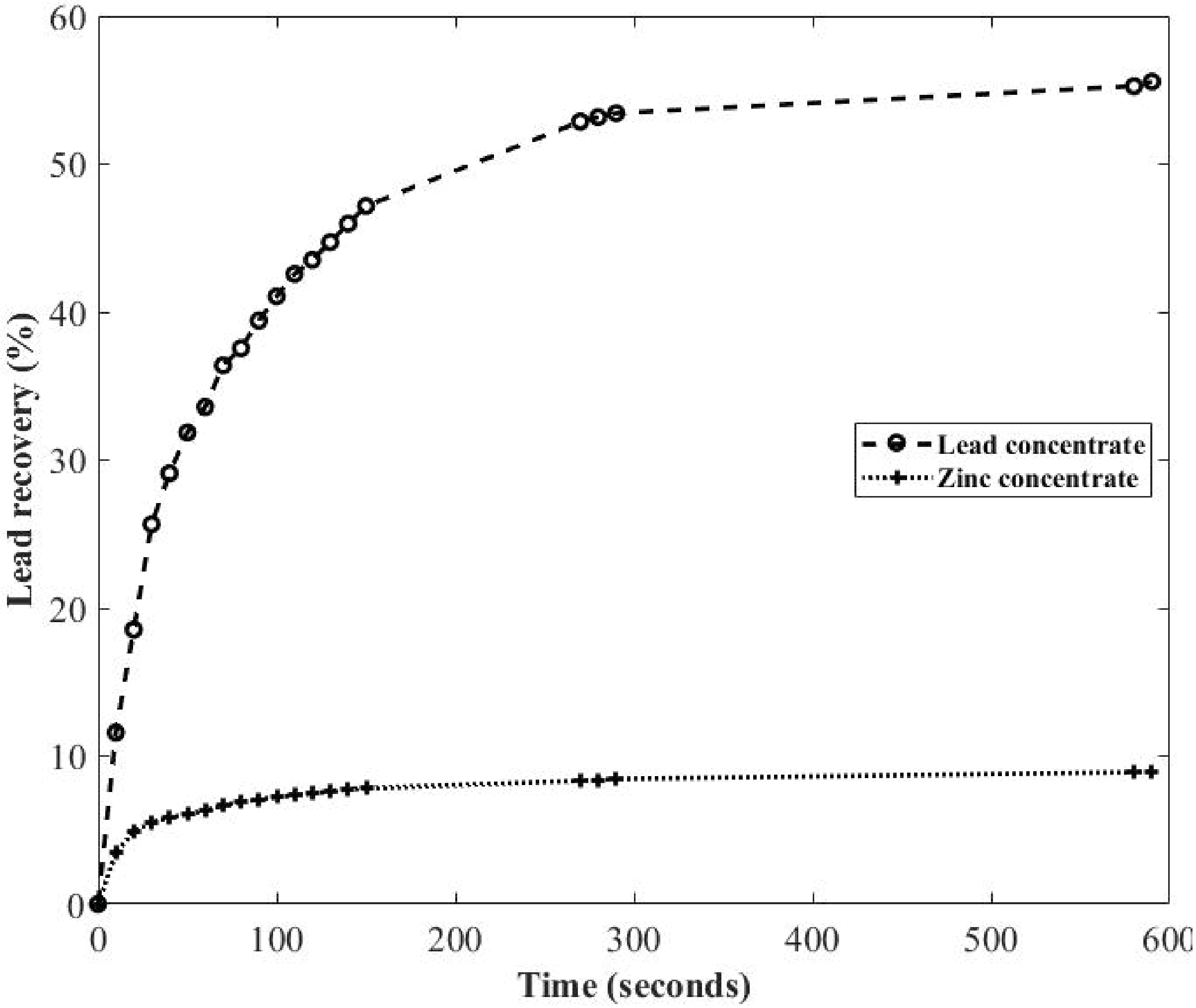

Figure 5.6: Variation of lead recovery with time for lead and zinc concentrate

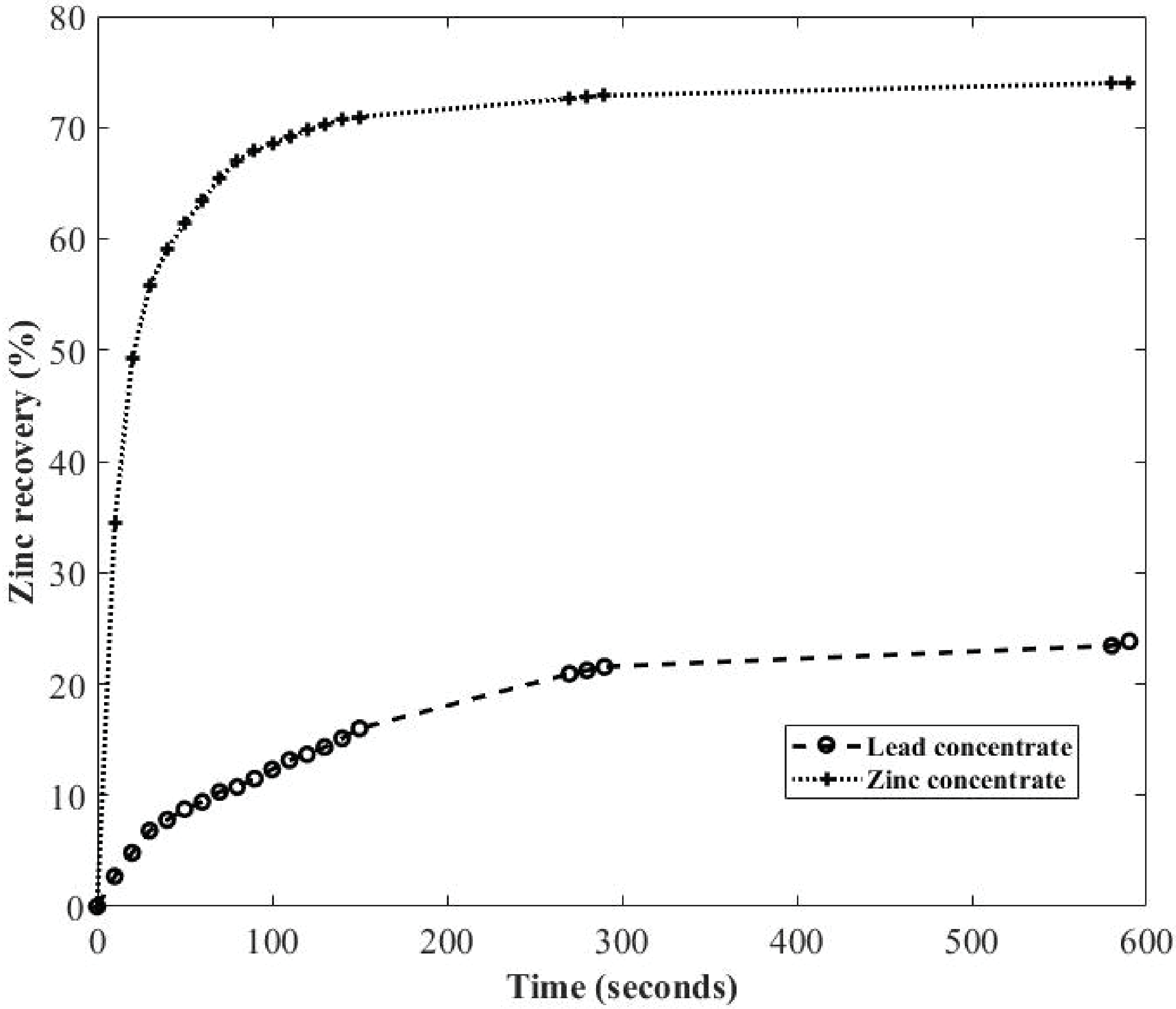

Figure 5.7: Variation of zinc recovery with time for lead and zinc concentrate

5.4.2 Image-based soft sensors

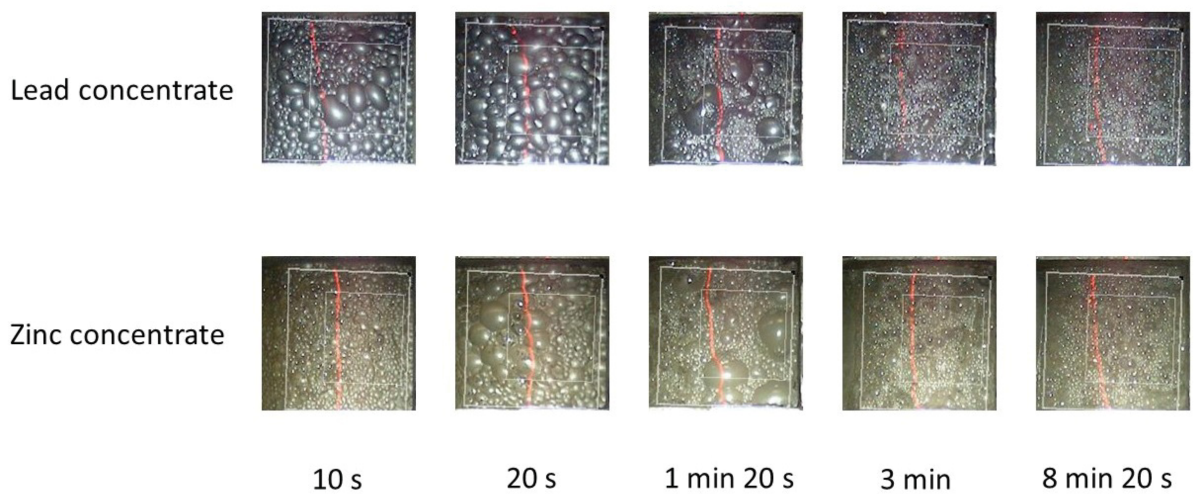

Figure 5.8: Representative images demonstrating variation in the top surface of the froth with time for lead and zinc concentrates

SVM classification of flotation stage Froth images were first used to classify the stage into lead or zinc flotation. Sample froth images are shown in Figure 5.8 for both lead and zinc stages of experiment number 2. It also demonstrates the variation of the froth images with the flotation time. Hyper-parameter selection was based on the grid search for selecting the best SVM parameters for the 2-class classification. Optimum SVM parameters are summarized in Table 5.10. The confusion matrix for the test data points is shown in Figure 5.9. It can be seen that the model developed was validated successfully with 100 % accuracy for the validation data-set. A clear difference in the colour between the froth images of both stages contributed to the success of the classification model (Figure 5.8).

Table 5.10: Hyperparameter selection based on grid search optimization for classification model MC

Parameter	Value
C	10
Kernel function	Linear
Kernel scale	0.1
polynomial kernel order	n/a

n = 1569		**Predicted**	
		Lead concentrate	Zinc concentrate
Actual	Lead concentrate	782	0
	Zinc concentrate	0	787

Figure 5.9: Confusion matrix for SVM bases flotation stage classifier for validation data

Lead and zinc grade - support vector regression Regression models for online lead and zinc grade measurements were developed for the individual stages of batch flotation. Results for the selection of SVM models parameters based on the grid search optimization are summarized in Table 5.11. The coefficient of determination (R^2) was used as a performance metric for the regression models and is also given in Table 5.11 for all the models. The comparison between off-line measurements and image-based prediction is shown in Figures 5.10 and 5.11 for lead and zinc grade, respectively. It was observed that the models perform better in the initial stages of flotation capturing the essential dynamic information. R^2 values and the comparison plots indicate that all the developed models have the potential for usage in real-time control applications. Online measurements of lead and zinc grade were obtained from all the nine experiment runs (see Table 5.4) and used for the prediction of lead and zinc recoveries.

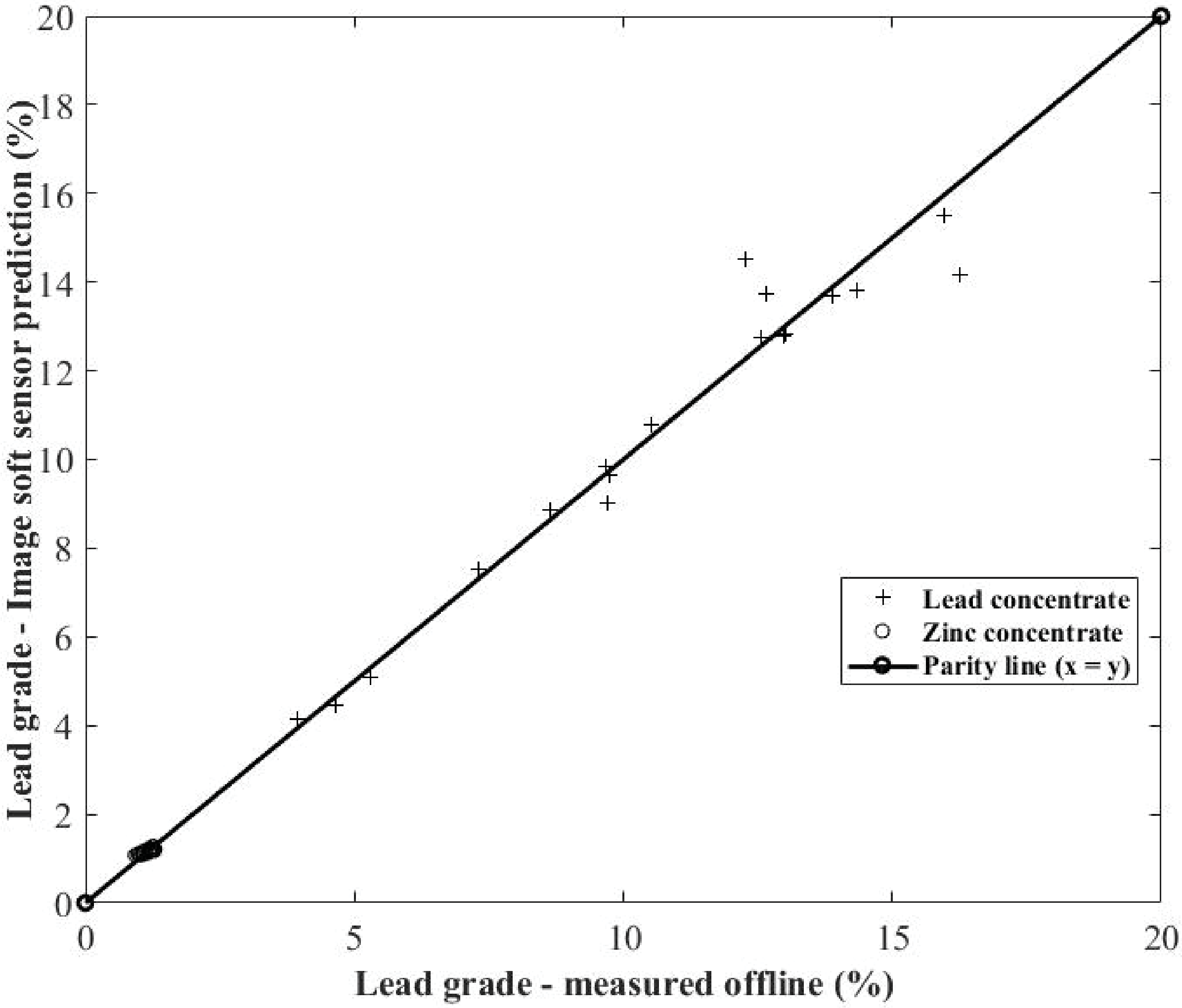

Figure 5.10: Image-based soft sensor prediction and off-line measurements for lead grade in lead and zinc stage flotation

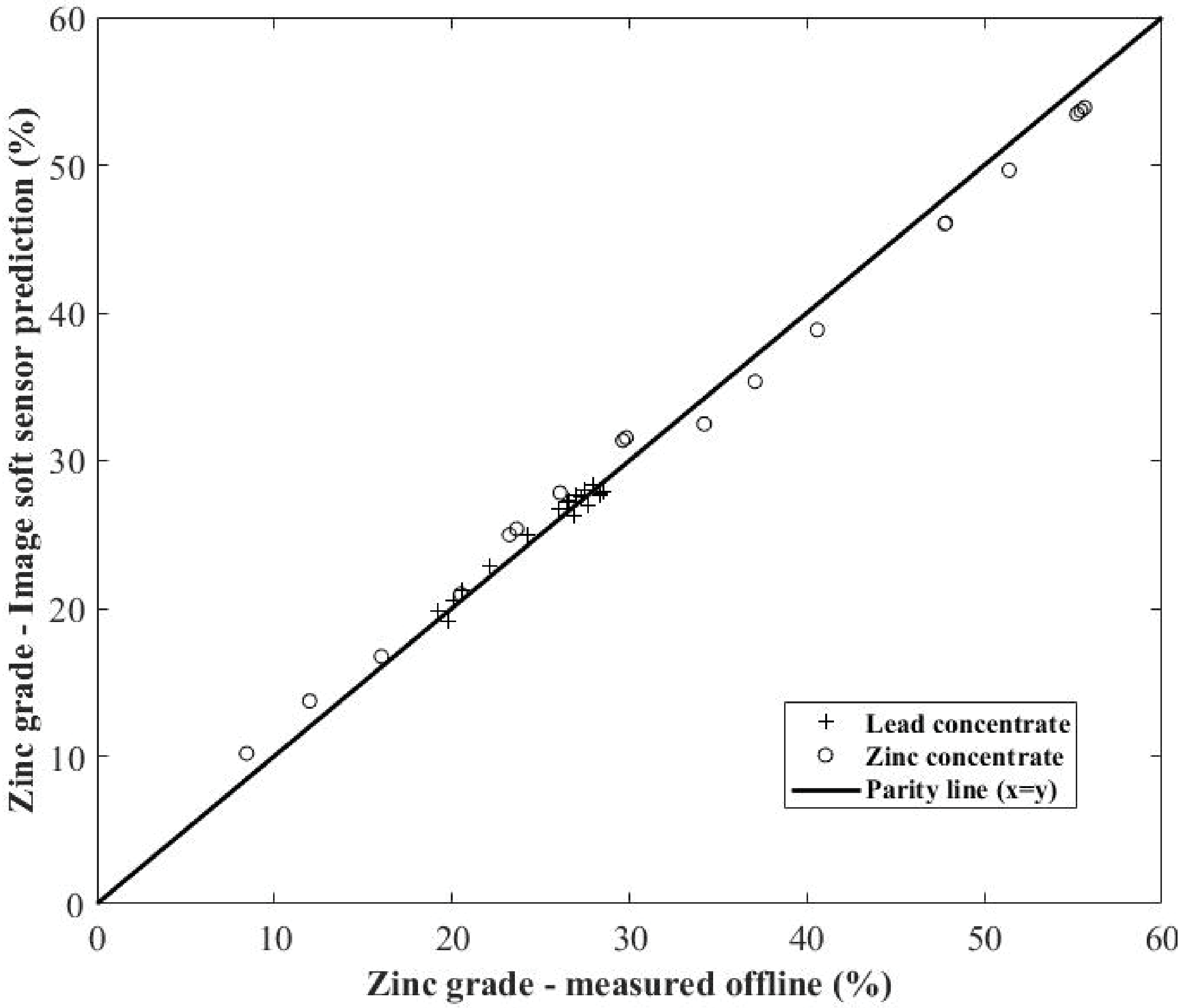

Figure 5.11: Image-based soft sensor prediction and off-line measurements for zinc grade in lead and zinc stage flotation

Table 5.11: Hyperparameter selection based on grid search optimization for all regression models

Parameter	Model-MR1	Model-MR2	Model-MR3	Model-MR4	Model-MR5	Model-MR6
C	1.0617	109.9924	114.7613	0.0115	804.5277	915.8475
ϵ	0.1927	0.2573	0.6592	0.0124	0.0086	1.7355
Kernel function	Linear	Linear	Polynomial	Linear	Linear	Polynomial
Polynomial kernel order	n/a	n/a	2	n/a	n/a	2
R^2	0.95	0.95	0.96	0.62	0.87	0.99

Solids recovery - support vector regression Offline solids recovery measurements from nine runs were used to train the support vector models for regression. Individual models were obtained for lead and zinc stages of the flotation. Model parameters obtained from the grid search algorithm are given in Table 5.11 for both the lead and zinc stages. The developed models were validated successfully against the test data with R^2 values of 0.95 and 0.87 for the lead and zinc stages, respectively. Figure 5.12 shows the comparison between offline measurements and image-based online estimates for the training and test data of the lead and zinc stage. It was seen that the model worked well for both the training and test data of both stages with the entire range of process conditions, and the model was used for online prediction of solid recovery. The model was applied to froth image data of all the runs for the entire time range with a sampling time of 10 s. The variation of online solids recovery values with time, predicted using the SVR models, are presented in Figure 5.13 for both the stages of flotation with their respective models against the offline measured data points, and the models are shown to be accurate. It was also noticed that the solids recovery was higher in the zinc stage compared to the lead stage, and this can be attributed to the higher zinc percentage in the feed.

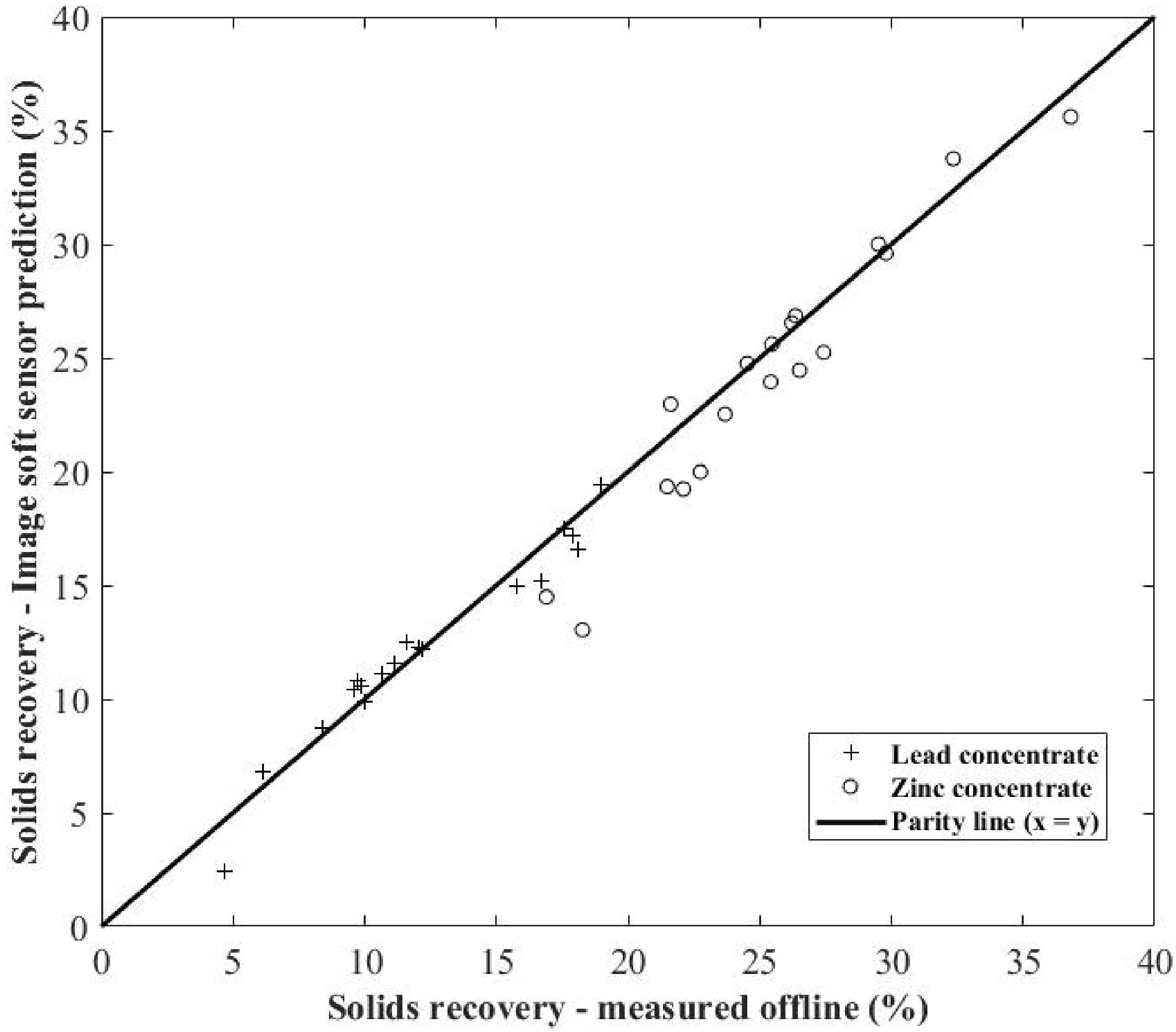

Figure 5.12: Image-based soft sensor prediction and offline measurements for solids recovery in lead and zinc stage flotation

Prediction of lead and zinc recovery Online predicted values of solids recovery, lead grade, and zinc grade were further used in the complete soft sensor network (Figure 5.4 and Table 5.8) to predict the lead and zinc recoveries for both stages of batch flotation. The soft sensor network was implemented on froth images of all nine experimental runs (see Table 5.4). The online predicted estimates of lead and zinc recovery with their

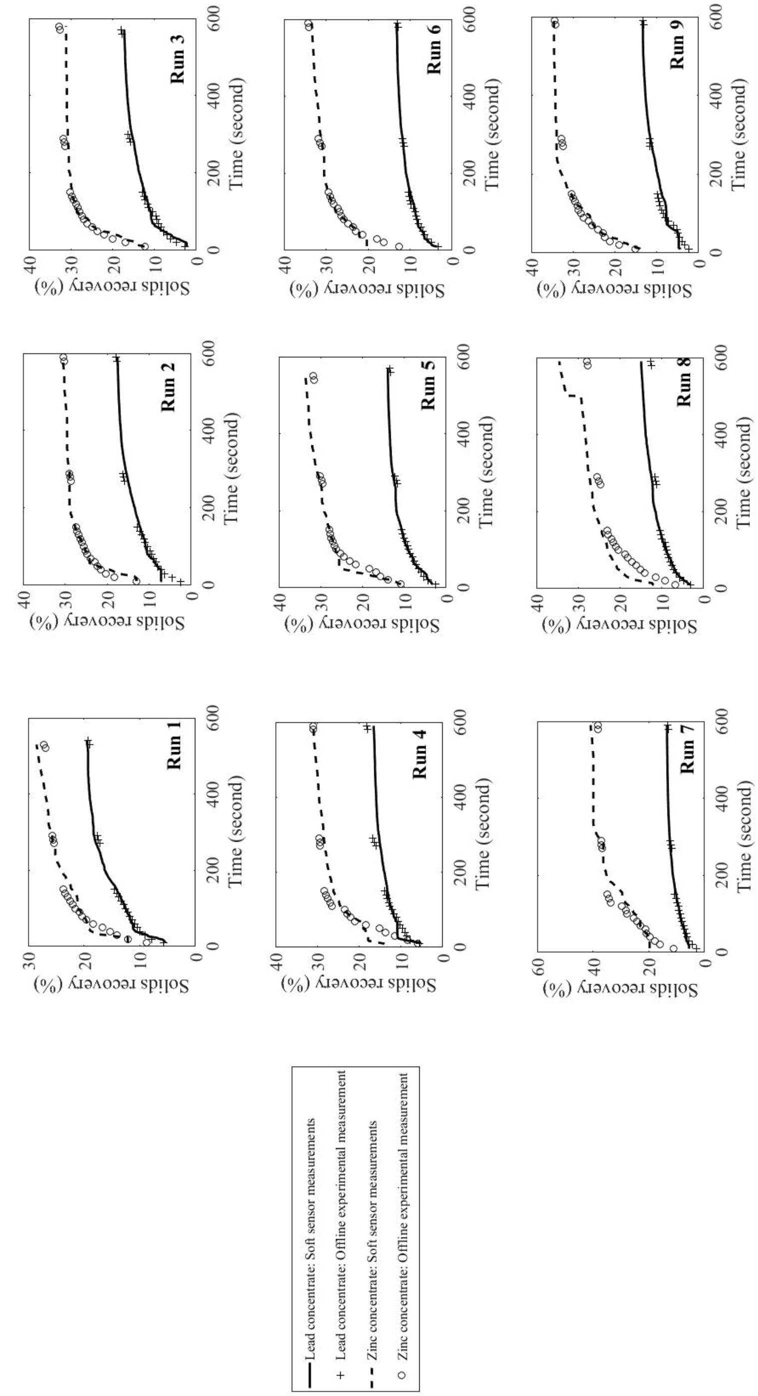

Figure 5.13: Dynamic variation of predicted measurements of solids recovery in lead and zinc stage flotation

variation in time, are given in Figures 5.14 and 5.15 for lead stage and zinc stage flotation, respectively. It can be seen that the soft sensor network was able to predict the process outputs across the diverse process conditions in the nine runs. The final lead and zinc recovery values from their respective concentrates are presented in Table 5.12 to summarize the DOE results. Since the values are based on image based prediction, there is a slight difference from the off-line measurements for the run 2. The ultimate recovery values were also used to calculate the final concentrate grades given in Table 5.12.

Table 5.12: Full factorial design results: Image based measurements of grade and recovery for lead and zinc concentrate.

Run order	Lead concentrate grade (%)	Lead concentrate recovery (%)	Zinc concentrate grade (%)	Zinc concentrate recovery (%)
1	14.37	78.61	43.25	67.24
2	11.59	56.90	44.13	73.35
3	9.85	47.63	41.57	71.34
4	14.99	69.14	39.91	66.83
5	8.42	33.13	37.75	69.30
6	8.06	29.79	34.74	63.15
7	7.85	29.75	30.46	67.05
8	7.56	31.08	44.64	72.24
9	4.01	36.07	36.38	69.25

DOE analysis Effects of the DOE design variables, feed particle size (P50), collector dosage in the lead stage, and collector dosage in the zinc stage, on the process outputs, lead recovery in the lead stage, lead grade in the lead stage, zinc recovery in the zinc stage, and zinc grade in the zinc stage are plotted in Figures 5.16 , 5.17, 5.18, and 5.19, respectively. It was observed that the particle size (P50) and collector dosage in the lead stage have predominant effects on lead concentrate grade and recovery. This is expected as theoretically, the collector dosage in the zinc concentrate has no effect on the lead concentrate grade and recovery. A small variation in the lead concentrate recovery could be due to experimental errors. Also, the lead concentrate recovery increases with a decrease in the feed particle size within the tested range, and an increase in the collector dosage in the lead stage. A similar effect was observed for the lead concentrate grade, but with smaller variation in the concentrate grade with changes in the design variables.

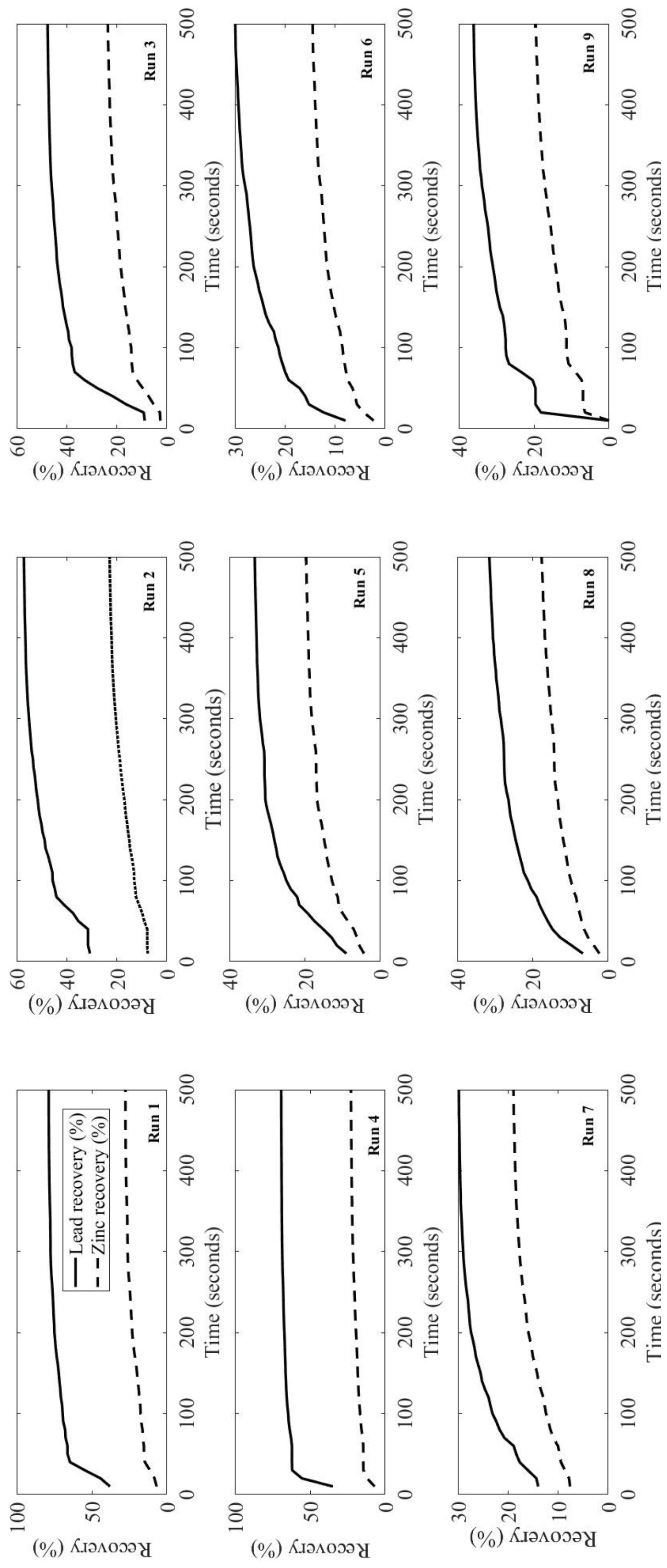

Figure 5.14: Dynamic variation of predicted estimates of lead and zinc recovery in the lead rougher stage of flotation

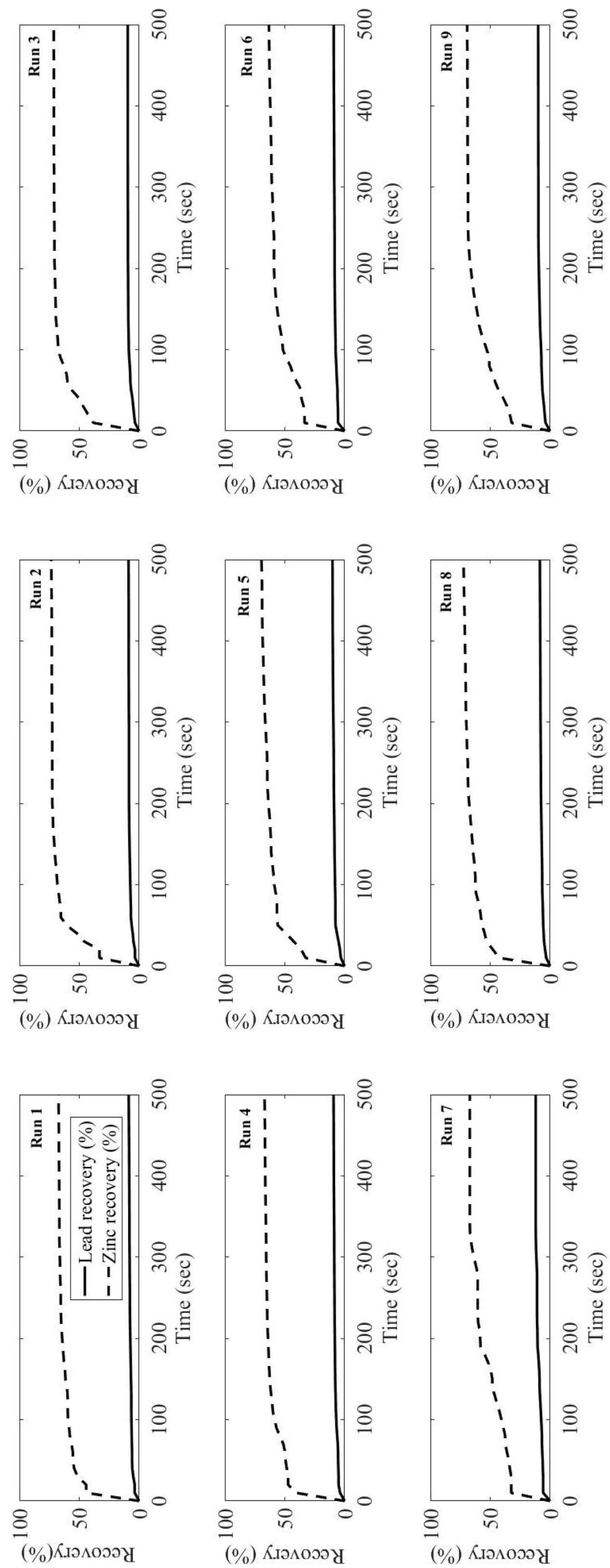

Figure 5.15: Dynamic variation of predicted estimates of lead and zinc recovery in the zinc rougher stage of flotation

Zinc concentrate grade and recovery, on the other hand, were affected by changes in all three design variables. However, it was observed that the changes in zinc concentrate grade and recovery with the variation in design variables were smaller than the changes in lead concentrate. It shows that the range chosen for the collector dosages could be higher than is optimum. Since zinc concentrate grade and recoveries were affected by all three design variables, they were chosen to develop DOE-based models using the data from the eight designed experiments. Zinc grade and recovery models for the zinc stage are given in equations 5.27 and 5.28, respectively.

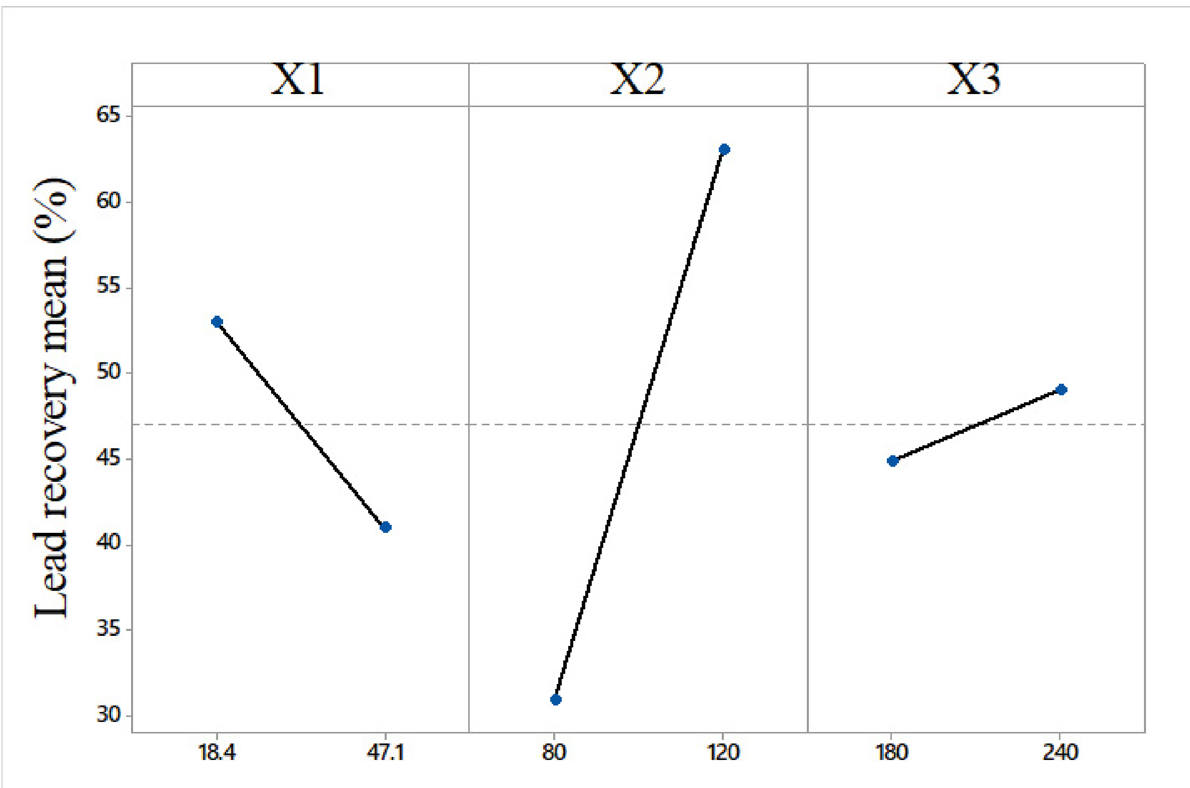

Figure 5.16: Effect of design variables on lead recovery in lead concentrate

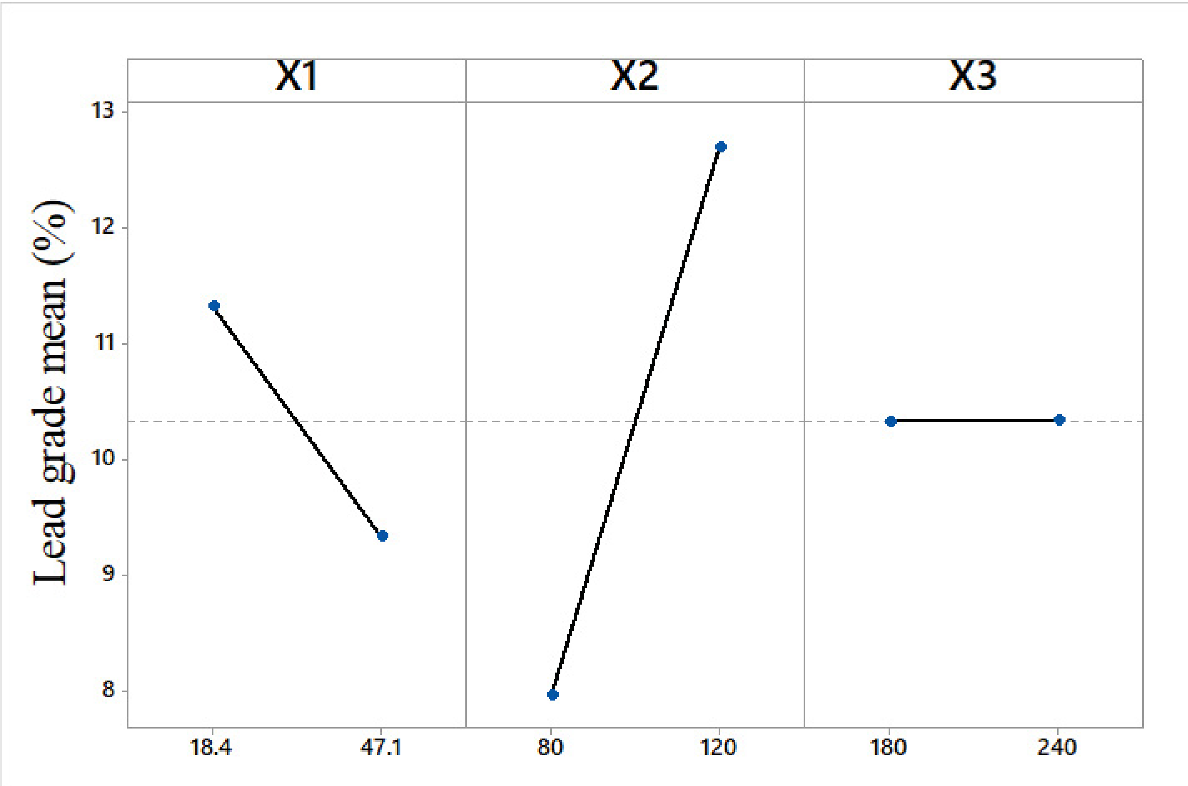

Figure 5.17: Effect of design variables on lead grade in lead concentrate

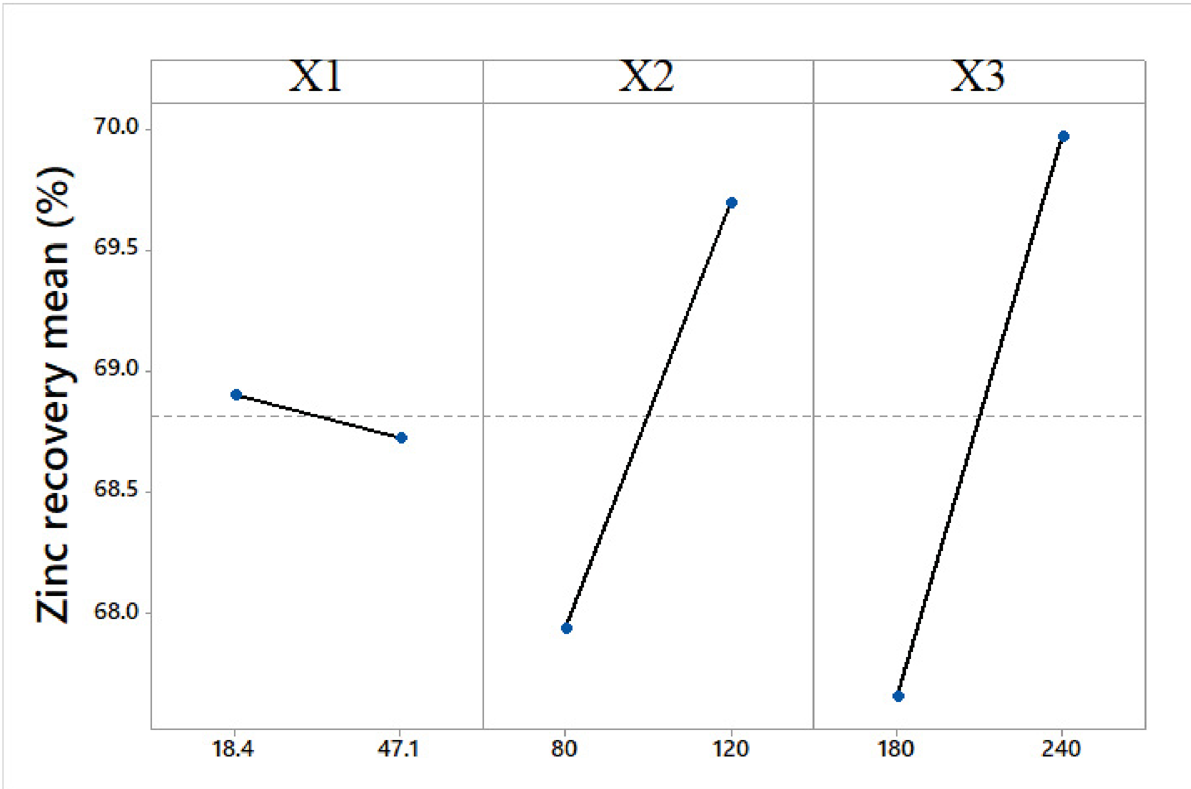

Figure 5.18: Effect of design variables on zinc recovery in zinc concentrate

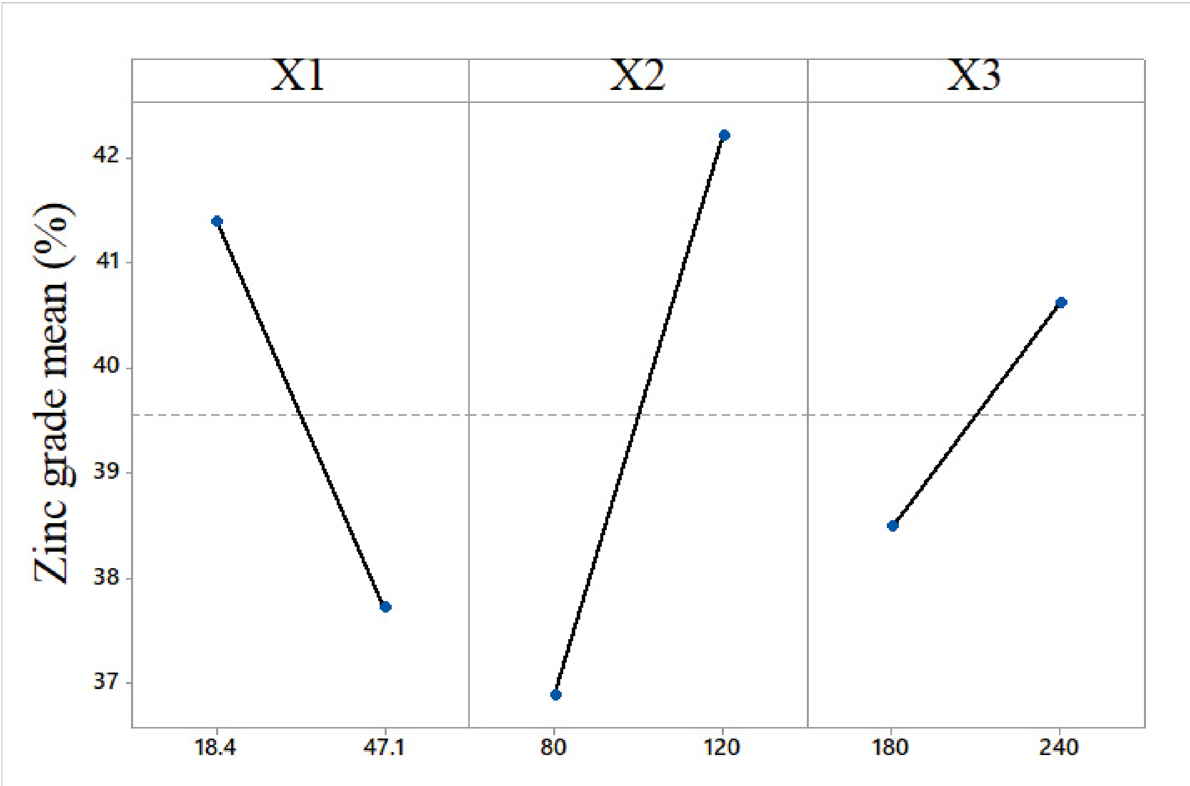

Figure 5.19: Effect of design variables on zinc grade in zinc concentrate

$$Zg(\%) = -62.04 + 2.909X_1 + 0.7450X_2 + 0.5744X_3 - 0.02309X_1 * X_2 \\ +0.01855X_1X_3 - 0.004255X_2X_3 \quad (5.27)$$

$$Zr(\%) = 67.36 - 0.9257X_1 + 0.01317X_2 + 0.1361X_3 - 0.007630X_1 * X_2 \\ +0.000176X_1X_3 - 0.001220X_2X_3 \quad (5.28)$$

where, Z_g and Z_r denote zinc concentrate grade and recovery. X_1, X_2, and X_3 are uncoded values for the design variables given in Table 5.4. Run 9 from Table 5.4 was used to validate the DOE models for the zinc concentrate. DOE model predictions were obtained using the values of designed variables as given in Table 5.4, with P50 of 47.1 μm, and collector dosages of 100 g/t in the lead concentrate and 210 g/t in the zinc concentrate. Table 5.13 compares the experimental (soft sensor network) estimates and DOE model predictions for zinc concentrate grade and recovery. The DOE model predictions were accurate for both the models and this validates the overall analysis for the designed experiments.

Table 5.13: Validation run (Run 9) results for DOE-based models for zinc concentrate

Output	Model prediction	Experimental (soft sensor network)
Zinc grade (%)	37.72	36.38
Zinc recovery (%)	68.72	69.25

5.4.3 Attachment monitoring and parameter estimation

Theoretical effects of collector dosage on attachment sub-process were used to monitor the attachment sub-process. Online lead and zinc recovery measurements obtained through the soft sensor network were used to update the fundamental models by state and parameter estimation. Online estimates of lead and zinc recoveries from the the soft sensor network were used as the measurements in the EKF algorithm.

1. Monitoring of the change in collector dosage in lead stage

   Online lead recovery was used as an online process measurement to estimate the attachment rate constant (k_{ag1}) by augmenting it to the state vector. Two experiments based on designed DOE (Table 5.4) were conducted with different collector dosages while other process conditions were kept constant. Process measurements from experiment run 8 (Table 5.4) with collector dosage of 80g/t, were used to update the model with state and parameter estimation. It was followed by the state and parameter estimation for experiment run 1 (Table 5.4) with collector dosage of

120 g/t. The initial values for state and parameter estimation for experiment run 1 were kept the same as the values used for the estimation for experiment run 8. Lead recovery predictions from the EKF-based updated model is compared with the online recovery measurements in Figure 5.20. The lead recovery was higher for experimental run 1 with higher collector dosage and shows the effect of collector dosage on the recovery. The model predictions were able to capture the dynamics of the lead concentrate flotation for both runs (run 8 and run 1). Real-time estimation of (k_{ag1}) is plotted in Figure 5.21 for both experiments. Parameter estimation were compared for both experiments in order to monitor the attachment sub-process with change in collector dosage. After starting from the same initial value of 0.015 s^{-1} , the estimate of (k_{ag1}) for run 1 with higher collector dosage is higher than its estimate for run 8 with a lower collector dosage. This shows that the parameter estimate monitors the attachment sub-process and directly indicates the change in collector dosage, as other experiment conditions were kept constant between these two runs.

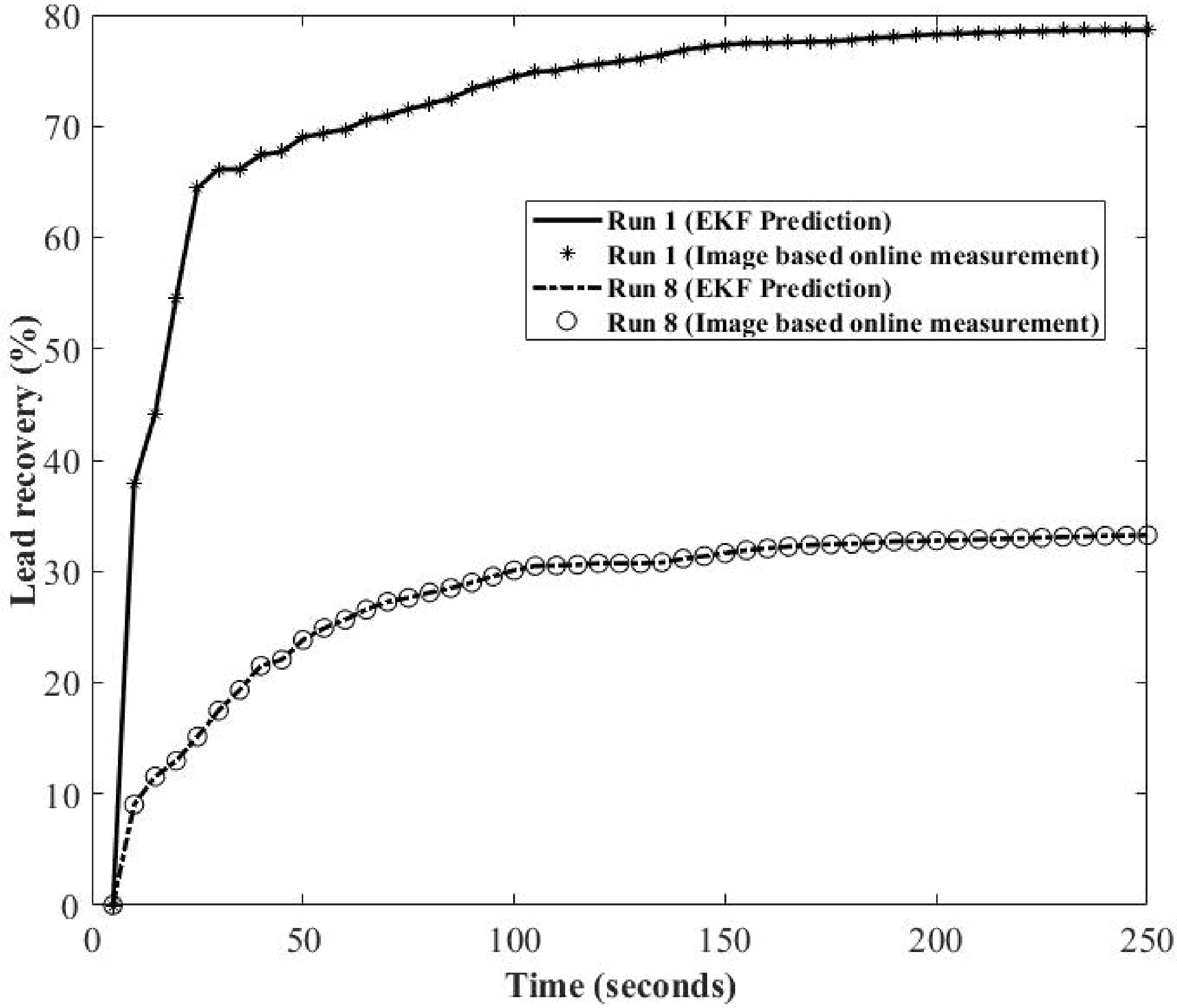

Figure 5.20: Comparison of lead concentrate recoveries for run 1 and run 8

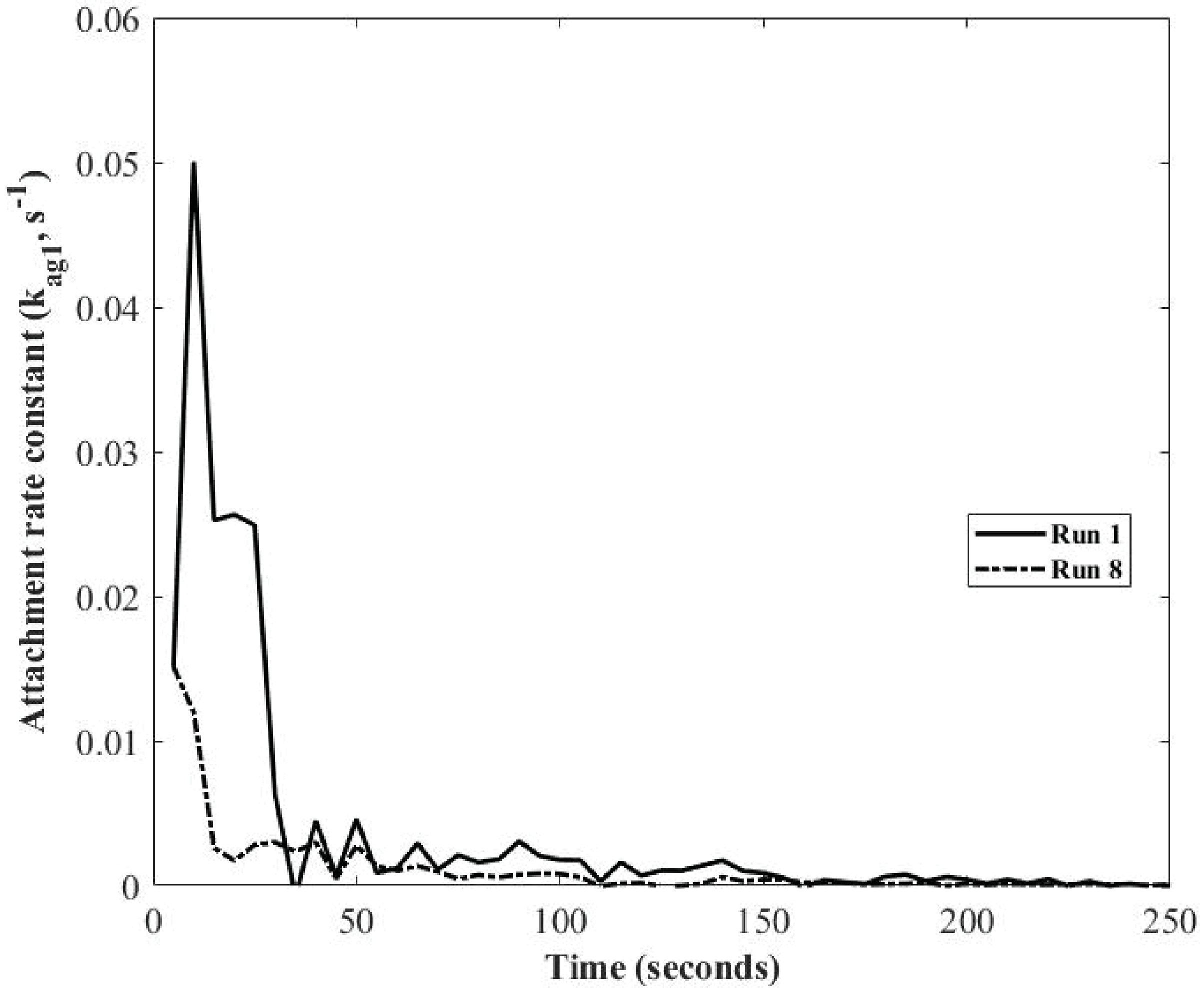

Figure 5.21: Comparison of estimated attachment rate constant (k_{ag1}) for run 1 and run 8

2. Monitoring of the change in collector dosage in zinc stage

   In this case, online process zinc recovery measurements were used for state and parameter estimation. The attachment rate constant for sphalerite mineral, k_{as2}, was used as a parameter augmented to the states for estimation. Two experiments, run 5 and run 8, with zinc concentrate collector dosages of 180g/t and 240g/t for zinc, respectively, were used for the estimation and real-time updating of the models. To monitor the attachment sub-process for zinc with the changes in collector dosage, the same initial conditions were maintained for the EKF-based estimation. Figure 5.22 plots the real-time model prediction with EKF update for zinc recovery and the online zinc recovery measurements for both experiments. Unlike the case of lead concentrate, there is a smaller change in recovery values between the two experiments. The parameter (k_{as2}) estimates are compared in Figure 5.23 for both experiments. Due to smaller variation in recovery values among the two experiments, the parameter estimates show a similar trend. However, there is a clear increase in the k_{as2} estimate for experiment 8 compared to experiment 1, especially in the beginning of the experiment, followed by a decrease towards the end. With other experiment conditions kept constant, monitoring the attachment sub-process through the increase in the estimate of k_{as2} in the initial time-frame is indicative of the change or increase in the collector dosage.

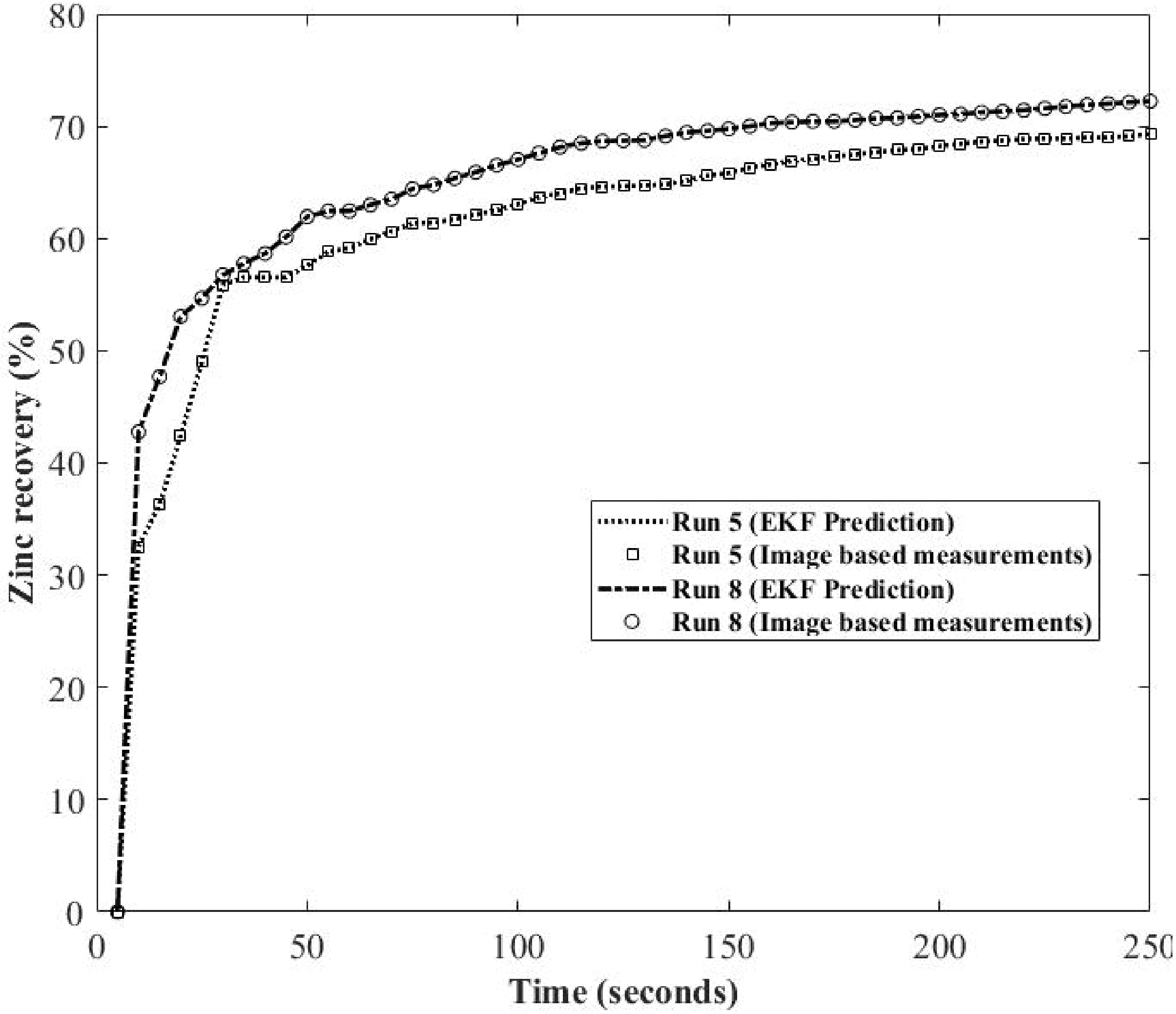

Figure 5.22: Comparison of zinc concentrate recoveries for run 5 and run 8

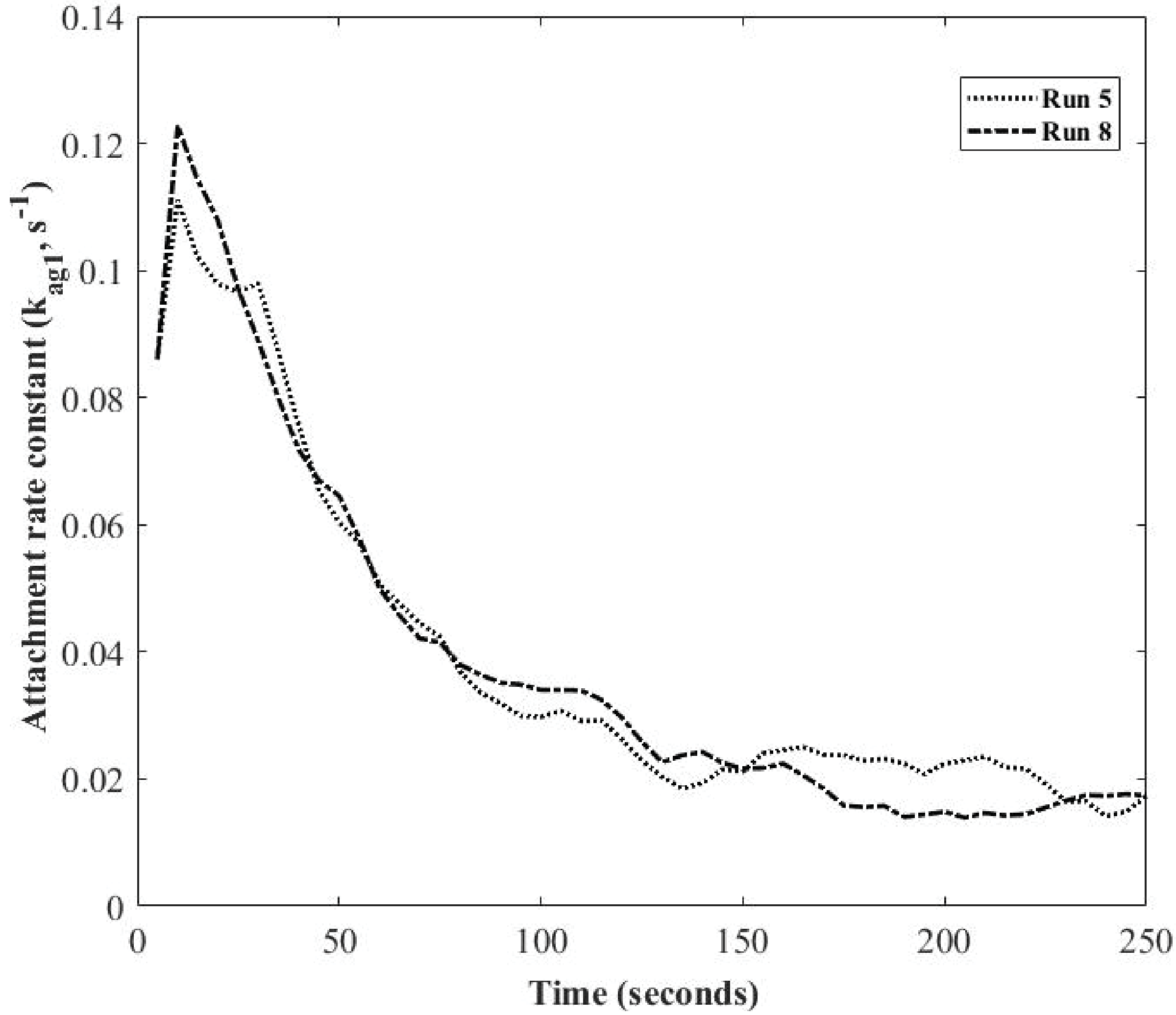

Figure 5.23: Comparison of the estimated attachment rate constant (k_{as1}) with time for run 5 and run 8

Thus, monitoring of the attachment sub-process through estimation of a fundamental model parameter (k_{ag1} or k_{as2}) was demonstrated successfully for lead and zinc concentrate. The framework can be extended to other sub-processes and used to monitor the performance and identify various disturbances or changes in the process.

5.5 Conclusions

A monitoring scheme was proposed to observe the performance of the Pb and Zn sulfide flotation process. A fundamental model framework was extended to be used in a multi-stage flotation process for flotation of a lead-zinc sulfide ore. Froth images were used to develop soft sensor models (support vector regression) for online measurements of solids recovery, lead grade, and zinc grade. Separate models were developed for lead and zinc concentrates. A classification model (SVM) was also developed to detect the flotation stage (lead or zinc concentrate) for automatic implementation of the respective concentrate regression models. Online estimates from the regression models were used to calculate online lead and zinc recovery using mass balances. A set of batch flotation experiments were designed to train and validate the soft sensor network. A 2-level factorial design was used with feed particle size, and collector dosage in the lead and zinc stages of flotation as design variables. Online data from the image-based soft sensor network was used to update the fundamental models in real-time by applying EKF for state and parameter estimation. The attachment rate constant was estimated in real-time to observe the attachment sub-process for lead and zinc concentrate. Finally, a disturbance in collector dosage was created for both lead and zinc concentrates to test the ability of the estimation and monitoring algorithm to capture the changes in attachment and their effect on the concentrate recoveries. It was observed that the attachment rate constants increase in real-time with the increase in collector dosage. It was demonstrated that the disturbances in process conditions can be identified using real-time estimation and used for process monitoring.

5.6 References

Aldrich, C., Marais, C., Shean, B.J., Cilliers, J.J., 2010. Online monitoring and control of froth flotation systems with machine vision: A review. International Journal of Mineral Processing 96, 1–13.

Alves dos Santos, N., Savassi, O., Peres, A.E.C., Martins, A.H., 2014. Modelling flotation with a flexible approach Integrating different models to the compartment model. Minerals Engineering 66, 68–76.

Arbiter, N., Harris, C., 1962. Flotation kinetic, in: Fuerstenau, D. (Ed.), Froth Flotation. AIME, New York, pp. 215–262.

Asghar, A., Ahmad, H., Behnam, F., 2015. Investigating the first-order flotation kinetics models for Sarcheshmeh copper sulfide ore. International Journal of Mining Science and Technology 25, 849–854.

Barbaro, M., 2000. Lead and zinc ores - flotation. Acadmieca Press Rome, Rome.

Barbian, N., Cilliers, J.J., Morar, S.H., Bradshaw, D.J., 2007. Froth imaging, air recovery and bubble loading to describe flotation bank performance. International Journal of Mineral Processing 84, 81–88.

Basak, D., Pal, S., Patranabis, D.C., 2007. Support Vector Regression. Neural Information Processing Letters and Reviews 11, 203–224.

Bascur, O.A., 2000. An interactive dynamic flotation model framework. Developments in Mineral Processing 13, C8a–21–C8a–31.

Basilio, C., Kartio, I., Yoon, R.H., 1996. Lead activation of sphalerite during galena flotation. Minerals Engineering 9, 869–879.

Bo, L., Xueqing, Y., Lin, Z., 2015. Li-ion battery SOC estimation based on EKF algorithm.

Bonifazi, G., Giancontieri, V., Meloni, A., Serranti, S., Volpe, F., Zuco, R., Koivo, H., Hätönen, J., Hyötyniemi, H., Niemi, A., Sipari, P., Kuopanporrti, H., Ylinen, R., Heikkila, I., Lahteenmaki, S., Miettunen, J., Stephasson, O., Wang, W., Carlsson, L.E., 2000. Characterization of the flotation froth structure and color by machine vision (ChaCo). Elsevier. volume Volume 13 of *Developments in Mineral Processing*. pp. C8a–39–C8a–49.

Bressel, M., Hilairet, M., Hissel, D., Bouamama, B.O., 2015. Fuel cells remaining useful life estimation using an extended Kalman Filter.

Brown, N., Bourke, P., Ronkainen, S., van Olst, M., 2001. Improving flotation plant performance at Cadia by controlling and optimizing the rate of froth recovery using Outokumpu Frothmaster, in: 33rd Annual Meeting of Canadian Mineral Processors, Ottawa, Canada. pp. 25–36.

Bulatovic, S.M., 2007. Handbook of flotation reagents : chemistry, theory and practice. Elsevier.

Duchesne, C., 2010. Multivariate Image Analysis in Mineral Processing, in: Sbarbaro, D., del Villar, R. (Eds.), Advanced Control and Supervision of Mineral Processing Plants. Springer, pp. 85–139.

Finkelstein, N., Alllison, S., 1976. The Chemistry of Activation, Deactivation and Depression in the Flotation of Zinc Sulfide: a Review, in: Fuerstenau, M.C. (Ed.), Flotation. AMIE, New York, pp. 414–457.

Finkelstein, N., Lovell, V., 1972. Fundamental studies of the flotation process : the work of the National Institute for Metallurgy. Journal of the Southern African Institute of Mining and Metallurgy 72, 328–342.

Fisher, T., Tokich, J., 1943. Concentration by flotation of a complex Galena –sphalerite –chalcopyrite ore from The nine mile district near missoula, Montana. Ph.D. thesis. Montana School of Mines.

Fuerstenau, M.C., Jameson, G.J., Yoon, R.H., 2007. Froth Flotation: A Century of Innovation. SME.

Gunn, S., 1998. Support Vector Machines for Classification and Regression. Technical Report. University of Southampton.

Harris, C., Jowett, A., Ghosh, S., 1963. Analysis of data from continuous flotation testing. Transactions of the American Institute of Mining and Metallurgical Engineers , 444–447.

Harris, C., Rimmer, H., 1966. Study of two-phase model of the flotation process. Transactions of the Institution of Mining and Metallurgy , 153–162.

Holtham, P.N., Nguyen, K.K., 2002. On-line analysis of froth surface in coal and mineral flotation using JKFrothCam. International Journal of Mineral Processing 64, 163–180.

Hsu, C.w., Chang, C.C., Lin, C.j., 2010. A practical guide to support vector classification. Technical Report. National Taiwan University. Taipei.

Kawatra, S.K., 2002. Froth Flotation - Fundamental Principles. Technical Report. Michigan Technical University.

Kohad, V., 1998. Flotation of sulfide Ores-HZL experience, in: Froth flotation: recent trends, Indian Institute of Mining Engineering, Jamshedpur. pp. 18–41.

Kracht, W., Vallebuona, G., Casali, A., 2005. Rate constant modelling for batch flotation, as a function of gas dispersion properties. Minerals Engineering 18, 1067–1076.

Leiva, J., Vinnett, L., Yianatos, J., 2012. Estimation of air recovery by measuring froth transport over the lip in a bi-dimensional flotation cell. Minerals Engineering 3638, 303–308.

Little, L.H., Poling, G.W., Leja, J., 1961. Infrared spectra of xanthate compounds: iii. Organic solvent effect on the C==S frequency. Canadian Journal of Chemistry 39, 1783–1786.

Lynch, A., Johnson, N., Mckee, D., Thorne, G., 1974. The behaviour of minerals in sulphide flotation processes with reference to simulation and control. Journal of the Southern African Institute of Mining and Metallurgy , 349–361.

Moolman, D.W., Eksteen, J.J., Aldrich, C., van Deventer, J.S.J., 1996. The significance of flotation froth appearance for machine vision control. International Journal of Mineral Processing 48, 135–158.

Nguyen, A., Schulze, H.J., 2003. Colloidal_Science_of_Flotation. Marcel Dekker Inc, New York.

Page, P., Hazell, L., 1989. X-ray photoelectron spectroscopy (XPS) studies of potassium amyl xanthate (KAX) adsorption on precipitated PbS related to galena flotation. International Journal of Mineral Processing 25, 87–100.

Popli, K., Sekhavat, M., Afacan, A., Dubljevic, S., Liu, Q., Prasad, V., 2015. Dynamic modeling and real-time monitoring of froth flotation. Minerals 5, 570–591.

Prasad, V., Schley, M., Russo, L.P., Bequette, B.W., 2002a. Product property and production rate control of styrene polymerization. Journal of Process Control 12, 353–372.

Prasad, V., Schley, M., Russo, L.P., Bequette, B.W., 2002b. Product property and production rate control of styrene polymerization. Journal of Process Control 12, 353–372.

Pryor, M., 1965. Mineral Processing. Elsevier Applied Science Publishers. third edition.

Runge, K., McMaster, J., Wortley, M., Rosa, D.L., Guyot, O., 2007. A Correlation Between Visiofroth Measurements and the Performance of a Flotation Cell. Ninth Mill Operators' Conference , 79–86.

Smola, A.J., Scholkopf, B., 2003. A tutorial on support vector regression. Statistics and Computing 14, 199–222.

Somasundaran, P., 1980. Role of Surface Chemistry of Fine Sulphides in their Flotation, in: Complex sulfide ores, Institute of Mining and Metallurgy, Rome. p. 118.

Ventura-Medina, E., Cilliers, J.J., 2002. A model to describe flotation performance based on physics of foams and froth image analysis. International Journal of Mineral Processing 67, 79–99.

Wang, X.l., Huang, L., Yang, P., Yang, C.h., Xie, Q.y., 2016. Online Estimation of the pH Value for Froth Flotation of Bauxite Based on Adaptive Multiple Neural Networks. IFAC-PapersOnLine 49, 149–154.

Welch, G., Bishop, G., 1995. An Introduction to the Kalman Filter. Technical Report. University of North Carolina.

Wills, B., 1997. Minerals Processing Technology. Pergamon Press, Oxford. 6 edition.

Wu, Z., Wang, X., Liu, H., Zhang, H., Miller, J.D., 2016. Some physicochemical aspects of water-soluble mineral flotation. Advances in Colloid and Interface Science 235, 190–200.

Yalcin, E., Kelebek, S., 2011. Flotation kinetics of a pyritic gold ore. International Journal of Mineral Processing 98, 48–54.

Chapter 6

Development of a Vision-Based Online Soft Sensor for Oilsands Flotation Using Support Vector Regression and its Application in the Dynamic Monitoring of Bitumen Extraction[1]

Extraction from oil sands is a crucial step in the industrial recovery of bitumen. It is challenging to obtain online measurements of process outputs such as bitumen grade and recovery. Online measurements are a prerequisite for innovating better process control solutions for process efficiency and cost reduction. We have developed a soft sensor to provide online measurements of bitumen grade and recovery in a flotation-based oil sand extraction process. Continuous froth images were captured using a VisioFroth camera system on a batch flotation unit. A support vector regression (SVR) model with a Gaussian kernel was constructed to develop a soft sensor for bitumen grade and recovery using froth image features as the inputs. The model was trained and validated for batch

[1] Popli, K.; Maries, Victor.; Afacan, A.; Liu, Q.; Prasad, V., 2017 ”Development of a Vision-Based Online Soft Sensor for Oilsands Flotation Using Support Vector Regression and its Application in the Dynamic Monitoring of Bitumen Extraction ”. The Canadian Journal of Chemical Engineering

flotation of different grades of oil sands ore at industry-relevant process conditions. A Dean-Stark analyzer was used to obtain offline grade and recovery measurements that were used to calibrate the soft sensor. Mean squared errors (MSE) of 62 and 74 were achieved for grade (%) and recovery (%), respectively, and this was obtained using 5-fold cross validation. The developed soft sensor model has been applied successfully in the real-time dynamic monitoring of flotation grade and recovery for different grades of ore and operating conditions.

6.1 Introduction

Oil sands ore is comprised of a mixture of mineral solids, water and bitumen. Ore is mined using open-pit mining and is further passed through the extraction process to recover bitumen. Most of the oil sands deposits contain bitumen ranging from 0-16 % by weight (Jia, 2010). The water-based extraction process for bitumen, proposed by Clark, is one of the standard commercial methods used since the 1960s (Masliyah et al., 2004; Clark and Pasternack, 1932). A typical process starts with crushing to disintegrate the oil sands ore lumps. The crushed ore is then mixed with warm water (about 50°C) and caustic soda to liberate the bitumen from the minerals. The slurry is pumped through hydrotransport pipelines to a primary separation vessel (PSV) where the liberated bitumen is aerated and floated off (Scramma et al., 2002; Masliyah et al., 2004). The froth stream from the PSV is deaerated and then sent to the froth treatment operations. The middlings stream from the PSV, containing unrecovered bitumen, is forwarded to the primary flotation units to further recover the bitumen. The tailings stream from the PSV and primary flotation is sent to the secondary flotation unit. Froth streams from primary flotation and secondary flotation units are recycled to the PSV in the feed stream, and the tailings stream from the secondary flotation unit is sent to tailings processing followed by its discharge in the tailing pond. The primary and secondary flotation units are conventional mechanical flotation cells. A final bitumen recovery up to approximately 90 % can be achieved with this process. The final bitumen froth typically contains 60 % bitumen, 30 % water, and 10 % solids by weight (Masliyah et al., 2004).

A batch extraction unit (BEU) was developed by Syncrude Canada Ltd to imitate the hot water extraction process in a laboratory environment (Sanford and Seyer, 1979). A conventional flotation machine is used to extract the bitumen from the oil sands ore in a single or multi-step flotation process, and the overall bitumen recovery from batch cells can be used to scale-up the parameters for commercial extraction of bitumen. Various oil sand extraction studies have been performed using BEUs to improve the overall understanding of the process (Kasongo et al., 2000; Liu et al., 2004), and this is the justification for our use of a batch flotation cell in our work.

With many factors such as water input rate, power input, different streams output flow-rate and temperature playing an important role, it is very crucial to control and monitor the overall extraction process. Even a 5% drop in grade or recovery in an hour can lead to losses of millions of dollars (Shao et al., 2012), and a good monitoring scheme is required to maintain overall quality and bitumen recovery. A lack of accurate online measurements makes it extremely challenging to monitor and control the product quality in extraction units. Currently, bitumen froth recovery estimation is based on the measurement of bitumen content in the tailings stream. Both offline (detailed laboratory analysis) and online (stream analyzer) measurements are obtained for bitumen content in tailings. Offline measurements are typically accurate with slow sampling times (of the order of a few hours), while online analyzers have fast sampling, but can be more inaccurate. A comparison of these methods is presented in Deng et al. (Deng et al., 2013), and they found that the online analyzer failed to provide accurate and dependable measurements for bitumen content. The Dean-Stark analysis, based on solvent extraction using toluene, is often used to characterize froth samples offline (Jia, 2010; Zhu, 2013) and provide the bitumen, water, and solids content. It takes $5-15h$ to complete the analysis of one sample and has a high maintenance cost for the solvents, and is thus unsuited for adaptation to real-time analysis. Due to unavailability of standard references, off-line measurements with Dean-Stark method can be used as reference measurements for accuracy. Inaccuracy of online analyzers has been studied with MSE values of bitumen content (%) ranging from 80 to 425 (Deng et al., 2013). Online measurement of recovery, which is usually calculated from bitumen content can be characterized with similar range of MSE values.

Inferential or soft sensors have been used extensively to estimate the non-measurable variables of various industrial processes (Fortuna et al., 2007; Kadleca et al., 2009; Sharmina et al., 2006; Liua and Chen, 2013; Khatibisepehr et al., 2013). A soft sensor is primarily a mathematical black box model for a key variable that is based on relations developed with other measurable process variables (Fortuna et al., 2007). Most of these soft sensors can work along with already installed hardware sensors to augment process information, and soft sensors can also be calibrated against offline measurements that may be available with delays.

There have been only a few soft sensors introduced in oil sands processes. A Bayesian method-based soft sensor was used to predict the water content in the conditioned slurry (Shao et al., 2012). Jampanaa et al. built a soft sensor to estimate the interface level in the PSV using a sight camera and particle filtering, which provided faster measurements than DP level transmitters (P.V. et al., 2010). Khatibisepehr et al. (Khatibisepehr et al., 2013) developed an inferential model for the bitumen recovery index based on partial least squares regression for bitumen content in the tailing. These inferential models identify the key process variables that are dependent on the target output and rely on adequate black-box modeling for the process and need to be re-trained for different operating conditions.

A lack of complete process understanding and different sampling times of variables present challenges for the development of these models. To the authors' knowledge, no robust soft sensor has been developed for direct prediction of output bitumen grade or recovery that does not depend on other key process measurements and yet provides accurate measurements in the entire range of operating conditions.

In our proposed solution, we have exploited the relationship between the visual characteristics of the froth surface and froth quality (Moolman et al., 1996). Various vision-based soft sensors have been developed for mineral flotation, where grade/recovery is predicted using the froth color or bubble size, amongst other features (Moolman et al., 1996; Runge et al., 2007; Aldrich et al., 2010; Popli et al., 2015). This relationship has not been utilized in oil sands flotation to determine froth quality directly from images of the froth. Various commercial packages such as VisioFroth (Metso® Minerals, Orleans Cedex, France), METCAM FC (SGS, Lakefield, ON, Canada), and FrothMaster^{TM} (Outotec, Burlington, ON, Canada) are available for image acquisition and analysis for the froth flotation process (Popli et al., 2015; Runge et al., 2007; Leiva et al., 2012). VisioFroth is used in this study because it is already installed in a few industrial operations in the oil sands and it provides a variety of image features such as color components, brightness, texture, and speeds through image analysis. Once calibrated, the image-based soft sensor does not rely on other process measurements and can operate in stand-alone fashion.

Machine learning and statistical algorithms (such as partial least square regression, artificial neural networks, random forest regression, principal component regression and support vector regression) can be useful to correlate image features to bitumen grade or recovery. We have used support vector regression (SVR) with Gaussian kernels in this work due to its higher accuracy and ability to handle the nonlinear relationship between image features and the target outputs of bitumen grade and recovery. The principle of support vector machines (SVMs) and regression was first proposed by Vapnik (Vapnik,

2006) and was proven to be a robust technique based on its ability to handle noisy data along with a higher variables-to-samples ratio in the data. Unlike other regression algorithms that are based on empirical risk minimization, this technique is based on more accurate structural risk minimization and shares various characteristics of artificial neural networks (ANNs) in this respect (Gunn et al., 1997).

We have used a batch extraction unit, the JKTech batch flotation cell, to mimic the commercial oil sands extraction. Different grades of Athabasca oil sands were processed in this flotation cell. VisioFroth was installed to acquire and analyze the froth images; this is explained in Section 6.2. Separate support vector-based models were trained and validated for grade and recovery prediction based on the average image features and offline results from Dean-Stark analysis. Hyperparameter optimization was performed for SVM parameters based on the minimization of the mean squared error with 5-fold cross-validation. The developed soft sensor was then applied at different operating conditions of the laboratory BEU process and for different grades of oil sands ore to validate its performance in a variety of cases. Section 6.2 outlines the experimental details along with data collection and formulation of the regression problem. SVM and its hyperparameter optimization is explained in Section 6.3. Section 6.4.1 describes the hyperparameter optimization results and 5-fold cross validation results for the developed SVM. Validation of the soft sensor for different cases is presented in Section 6.5.

6.2 Experimental section

6.2.1 Materials: Ore samples and characterization

Three different oil sands ore samples with different grades of Athabasca oil sands were obtained. Samples were homogenized and ground using a comil conical mill. Homogenized samples were then stored in a freezer to avoid aging effects that deteriorate the extraction performance (Schramm and Smith, 1987). Dean-Stark analysis (Jia, 2010; Zhu, 2013; Bulmer and Starr, 1979) was performed to characterize the composition of the oil sands. Table 6.1 presents the Dean-Stark analysis results for the three types of ore samples. Ores were classified based on the bitumen composition. Typically, high-grade ore contains bitumen in the range of 12-14 wt %, followed by medium and low grade ore in the ranges of 10-11 wt% and 6-9 wt % respectively (Pow et al., 1963).

Table 6.1: Dean-Stark analysis for oil sand ores: Weight % for bitumen, solids and water

Ore	Bitumen (%)	Solids (%)	Water (%)	Type
I	14.1	82.7	3.2	High grade
II	10.5	84	5.5	Medium grade
III	7	86.24	6.81	Low grade

6.2.2 Batch flotation : Methodology and set-up

The JKTech flotation machine was used to extract bitumen from the oil sands. It consists of a $1.5L$ cell with a bottom-driven impeller and a rotameter to measure and control the air flow into the cell. A VisioFroth package was used to acquire froth images and analyze their features. Image features are based on a selected area called 'region of interest' on the surface image. It includes a camera, laser and LED light that were installed $55cm$ above the froth surface. The laser was used to measure the froth width overflowing out of the cell (Popli et al., 2015). A schematic representation of the experimental set-up is given in Figure 3.2 (Chapter 3). Bitumen extraction required ore conditioning (to liberate the bitumen) and flotation. Table 6.2 summarizes the experimental conditions that were chosen based on industrial process conditions. $300g$ of homogenized oil sands ore was mixed with de-ionized water at $50°C$ to form $1.4L$ of slurry. The slurry was fed to the batch cell, and the impeller was turned on at $1500rpm$ for $12min$ for conditioning.

Unlike other flotation processes where collectors and frothers are added, bitumen flotation utilizes the natural surfactants present in the oil sands. After the conditioning, the air flow was turned on at $4.5lpm$ to start the flotation. Image acquisition was initiated at this time. Froth samples were collected in the collection pan at time intervals of $30s$, $60s$, $150s$, $300s$ and $600s$. These samples were analyzed using the Dean-Stark method to estimate the amount of bitumen, sand, and water. Image measurements were continuously recorded up to $600s$ with a sampling time of $5s$, and the features of the images that are obtained are listed in Table 6.3; further information on these images features can be obtained from Popli et al. (Popli et al., 2015). These experiments were performed for all three types of oil sand ores.

Table 6.2: Experimental conditions for batch flotation of oil sands ores

Parameter	Value
Cell Volume (l)	1.5
Feed density (g/l)	214
Air flow rate (lpm)	4.5
Impeller speed (rpm)	1500
Conditioning time (minutes)	12
De-ionized water temperature ($^{\circ}C$)	50

6.3 Soft sensor development: Support vector regression

The support vector machine (SVM) was designed initially for high-dimensional pattern recognition classification problems (Basak et al., 2007). Support vector algorithms were then used for regression after having been proposed by Vapnik et al. (Boser et al., 1992). While most regression algorithms compute in the same dimensional feature space, support vector regression (SVR) maps the training data to a higher space by using a

Table 6.3: Image features extracted using VisioFroth

Notation	Image feature
a	Froth velocity
b	Froth velocity x component
c	Froth velocity y component
d	Froth height for outlet stream
e	D80 - Bubble size
f	Bx color component
g	Blue color component - RGB model
h	Green color component - RGB model
i	D50- Bubble size
j	Lumen
k	Texture
l	Tint
m	Red color component - RGB model
n	Cell Value
o	RGB
p	Stability
q	Purity
r	Load
s	Dispersion
t	Brightness
u	Collapse
v	Ax color component

kernel feature space $\Phi(x)$ and kernel function K (Vapnik, 1995). The kernel trick allows the inner product calculation to be carried out implicitly without working in the higher dimension space. For a given set of data, $(x_1, y_1), (x_2, y_2), ...(x_n, y_n)$, with $x \in R^m$, and $y \in R$, the following function needs to be developed for the prediction of y:

$$f(\mathbf{x}) = \mathbf{w}^T \Phi(\mathbf{x}) + \mathbf{b} \tag{6.1}$$

where $\mathbf{w}$ is a vector of weights and $\mathbf{b}$ is the bias term.

SVR is based on the structural risk minimization (SRM) and aims to minimize generalization error instead of training error (Vapnik, 2006). It minimizes the complexity of the model along with the error loss function and avoids over-fitting of the data. SVR uses an ϵ-sensitive loss function that allows the predictive output to deviate as much as ϵ from the actual output. The ϵ-sensitive loss function and optimization scheme for finding the optimum values of **w** and **b** are defined in equations 6.2 and 6.3, respectively. SVR algorithm has been presented in literature and is summarized in equations 6.2, 6.3, 6.4, 6.5, 6.6, 6.7, 6.8, and 6.9 (Vapnik, 1995, 2006).

$$minimize \sum_{i=1}^{n} \epsilon_L(i) \tag{6.2}$$

$$\epsilon_L(i) = max(|(y_i - \mathbf{w}^T\Phi(x_i) + b| - \epsilon, 0) \tag{6.3}$$

The optimization problem is reformulated using slack variables, ξ and $\xi\prime$, as:

$$\begin{cases} \underset{w,b,\xi,\xi'}{\text{minimize}} \ \frac{1}{2}\mathbf{w}^T\mathbf{w} + C\left(\sum_{i=1}^{n} \xi_i + \sum_{i=1}^{n} \xi_i' \right) \\ \text{subject to (i = 1,2,....n):} \\ y_i - \mathbf{w}^T\Phi(x_i) - b \leq \epsilon + \xi_i \\ \mathbf{w}^T\Phi(x_i) + b - y_i \leq \epsilon + \xi_i' \\ \xi_i \geq 0 \\ \xi_i' \geq 0 \end{cases} \tag{6.4}$$

The first term of the objective function ($\frac{1}{2}\mathbf{w}^T\mathbf{w}$) captures the model complexity and improves the generalization ability of the model. Parameter C, the penalty cost, is introduced to maintain the tradeoff between model complexity and training errors by controlling the penalty assigned to slack variables. Constrained optimization is handled using Lagrangian method by incorporating Langrange multipliers (α_i, α_i') to reframe the objective function (Smith, 2004). The optimization problem in equation 6.4 can be converted to a dual problem by using the Lagrangian method to give:

$$\begin{cases} \underset{\alpha,\alpha'}{\text{maximize}} \sum_{i=1}^{n} y_i(\alpha_i - \alpha_i') - \epsilon \sum_{i=1}^{n} (\alpha_i + \alpha_i') - \\ \quad \frac{1}{2} \sum_{i,j=1}^{n} (\alpha_i - \alpha_i')(\alpha_j - \alpha_j')\Phi(x_i)^T \Phi(x_j) \\ \quad \text{subject to: } \sum_{i=1}^{n} (\alpha_i - \alpha i') = 0 \\ \quad C \geq \alpha_i, \alpha_i' \geq 0, i = 1, 2, ..., n \end{cases} \tag{6.5}$$

Equating the partial derivatives at the saddle point to zero provides estimates for $\mathbf{w}$ and f($\mathbf{x}$) represented by equations 6.6 and 6.7. The kernel trick can be used to evaluate the inner product in f($\mathbf{x}$) (Equation 6.8). The final function evaluation after incorporating the kernel trick is given in Equation 6.9. The optimal solution of $\mathbf{w}$ is the linear combination of the support vectors.

$$w = \sum_{i=1}^{l} (\alpha_i - \alpha_i')\Phi(x_i) \tag{6.6}$$

$$f(x) = \sum_{i=1}^{l} (\alpha_i - \alpha_i')(\Phi(x_i).\Phi(\mathbf{x})) \tag{6.7}$$

$$K(x_i, x) = \Phi(x_i).\Phi(x) \tag{6.8}$$

$$f(x) = \sum_{i=1}^{l} (\alpha_i - \alpha_i')K(x_i, x) \tag{6.9}$$

The kernel trick allows the nonlinear models to be treated by linear methods by transforming the training data points to a higher dimensional domain. Three common types of kernel functions are described in Table 6.4 (Wu et al., 2009). A standard kernel, rbf (Gaussian) was used in this work.

Table 6.4: Common kernel functions used in support vector machines

Type of kernel	Function
Linear	$x_i^t x_j$
Polynomial	$(\gamma x_i^T x_j + constant)^d, \gamma > 0$
Radial basis function (rbf, Gaussian)	$e^{-\gamma \|\|x_i - x_j\|\|^2}$

6.3.1 Hyperparameter optimization: Parameter selection

It is very critical to choose an optimum set of parameters for SVR. C, penalty cost, which affects the trade-off between training errors and model complexity. A higher value of C constructs a complex model with very little error on training points, whereas a lower value flattens the model response by allowing higher training error. Epsilon (ϵ) also affects the complexity of the model as it influences the number of support vectors by controlling the ϵ-sensitive loss function (Ito and Nakano, 2003). An increase in the value of ϵ decreases the number of support vectors required for the development of the model. The other parameter that has an effect is the parameter for the kernel function (γ for the rbf kernel that was used in this work; see Table 6.4). A grid-search mechanism was used to find an optimal set for C, γ and ϵ based on 5-fold cross-validation, which means that the data was divided into five parts, and each part was used for validating the model obtained by the training of the remaining four parts. Grid search, in this case, was not computationally heavy due to less number of training instances. Moreover, grid-search is commonly used for hyperparameter selection for similar SVR problems (Zhang et al., 2014; Hsu et al., 2010). 5-fold cross-validation has been commonly employed for industrial soft sensors (Hua and Sun, 2001; Shokri et al., 2016; Gholami et al., 2015; Yang and Shieh, 2010). Also, 5- fold cross validation was chosen over higher fold validations, such as 10-fold, to retain more data points for testing fold in this scenario, with lesser number of instances. The mean squared error (MSE) reported is the average over all of the 5-folds. The parameters and their ranges are summarized in Table 6.5 for the SVR models for both grade and recovery.

Table 6.5: Parameter range for hyperparameter optimization using grid-search technique

Parameter	Range
C	$[10^{-3}\ 10^{3}]$
ϵ	$[0.107\times10^{-3}\ 0.107\times10^{2}]$
γ	$[10^{-3}\ 10^{3}]$

The SVR models for recovery were constrained to ensure that estimates of cumulative recovery increased monotonically with time.

6.4 Results and Discussion

6.4.1 Batch flotation

Froth samples collected at different flotation times were analyzed using the Dean-Stark apparatus for all three types of oil sand ores, and the results are summarized in Table 6.6, where the grade reported has been calculated on a water-free basis. Recovery measurements for the different ores are summarized in Figure 6.1. The highest recovery of 82.3% was obtained for the high grade ore, followed by 74% and 49.2% for medium grade and low grade ore, respectively. This recovery is slightly lower than that obtained in industry, possibly because caustic soda was not used in our process. However, that is not a serious concern since the aim in this work is to show that the soft sensor can be used to monitor processes over a large range of grade and recovery values.

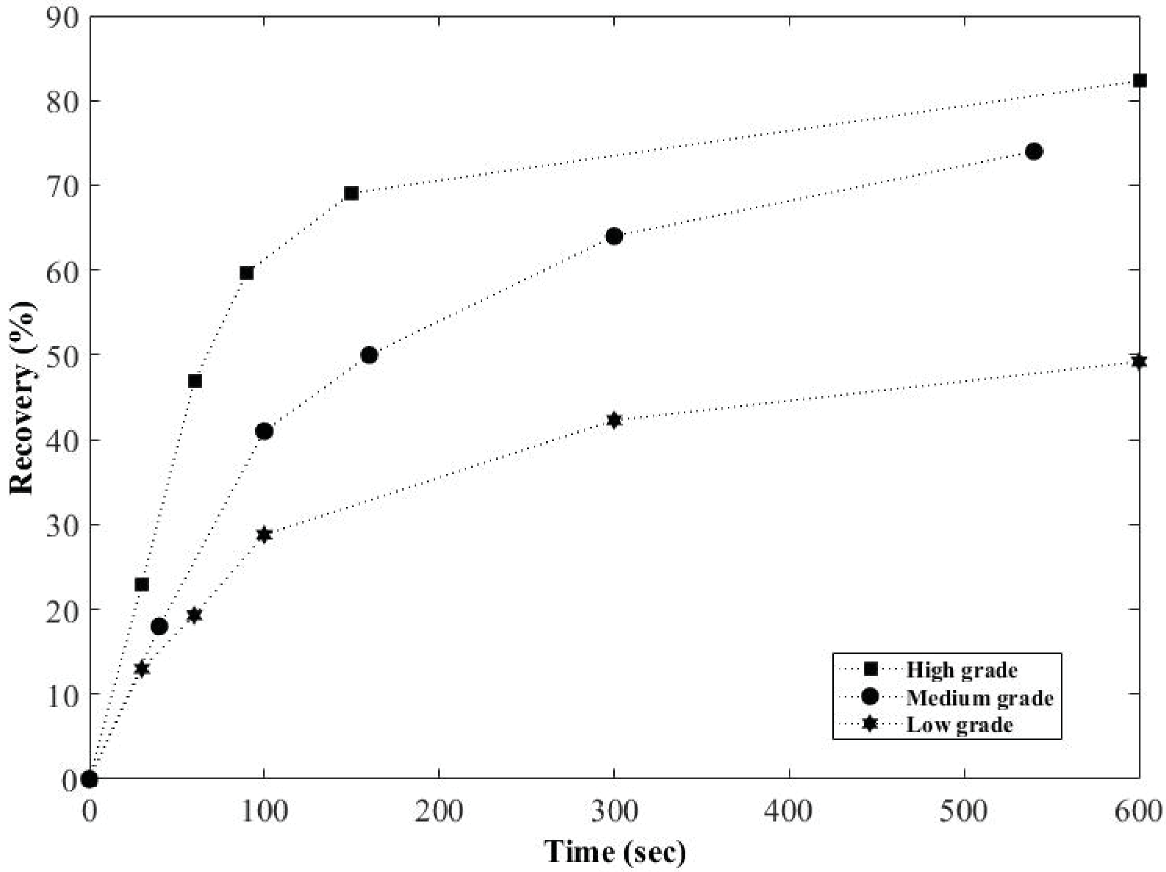

Figure 6.1: Experimental measurements of bitumen recovery for batch flotation

Representative real-time images of the top surface of the froth for the flotation of medium grade ore are shown in Figure 6.2 (from 5s to 500s). The overall image color gets lighter with time as the amount of bitumen decreases in the cell. The laser-produced red line indicated on the image and its horizontal movement were used to measure the froth width for the outlet stream. The image features were normalized before using them for the soft sensor development. All the 22 variables obtained from VisioFroth, representing image features, were used as the soft sensor inputs, and grade and recovery were the target outputs. Samples were collected for offline analysis and used for calibration of the soft sensor, and image features were averaged over the time of sample collection when developing the calibration relations.

Table 6.6: Batch flotation results for all three types of ores based on Dean-Stark analysis. Experimental conditions are summarized in Table 6.2. Grade is reported on a water-free basis

Ore type	Time (sec)	Cumulative grade (%)	Cumulative recovery (%)
High grade	30	29.94	22.97
	60	34.9	46.9
	90	31.3	59.7
	150	24.3	69.1
	600	18.9	82.3
Medium grade	40	42	18
	100	57	41
	160	40	50
	300	43	64
	540	31	74
Low grade	30	16	13
	60	24.7	19.3
	100	35.6	28.8
	300	26.7	42.3
	600	19.77	49.2

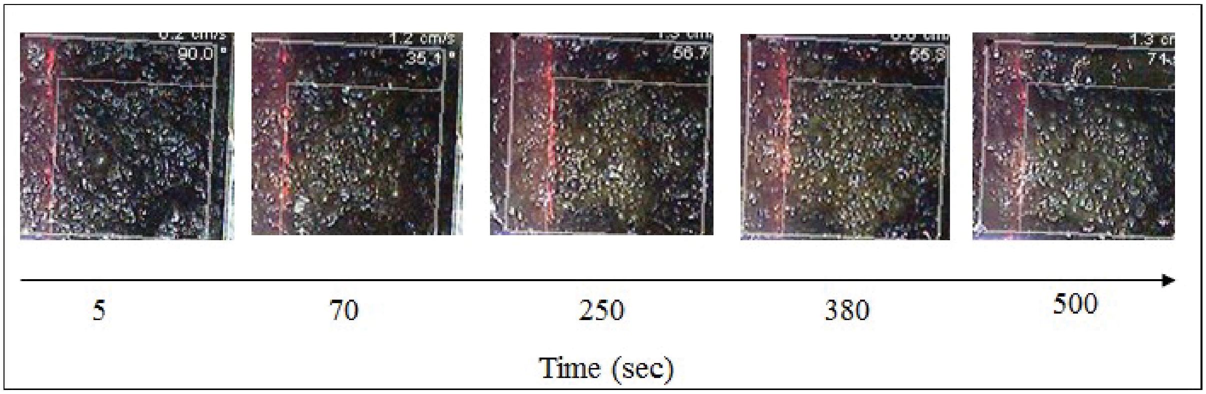

Figure 6.2: Variation of froth images for flotation of medium grade ore with time

6.4.2 Soft sensor development: Hyperparameter optimization

The soft sensor was developed for bitumen grade and recovery, since models for bitumen content and solids content were not accurate enough. Models were selected based on the minimum values of mean square error (MSE) for 5-fold cross-validation. A grid search was performed to find the optimal set of model parameters. The variation of 5-fold validated MSE with the SVR parameters C, ϵ, and γ is shown in Figure 6.3 and Figure 6.4 for grade and recovery as the output, respectively. It demonstrates the selection of hyperparameters based on minimum MSE value. Round points in both the figures represent MSE values corresponding to the respective parameter grids. A wide distribution of MSE values justifies the requirement of optimization for hyperparameter selection. Figure 6.3 shows that the MSE value is low at the grids representing lower values of C, ϵ and γ. The lowest MSE value of 62 was used to select model parameters as given in Table 6.7. Grid search results for recovery model in Figure 6.4 show a similar regions of low MSE values. Majority of the lower MSE values were observed at the intersection of low regions of C, ϵ and γ. Hyperparameters were selected based on lowest MSE value of 74 with ϵ value in this case higher than the optimum value for grade model (see Table 6.7).

Computations Matlab (version 9.1.0.441655 and release R2016b) with 'Statistics and Machine Learning Toolbox' was used to develop and implement the SVR models. Computational times for hyperparameter selection using grid-search optimization was 19.15 and 22.15 minutes for grade and recovery models, respectively. However, once the parameters were selected, SVR model development was faster with computational times of 0.55 and 0.26 seconds, respectively.

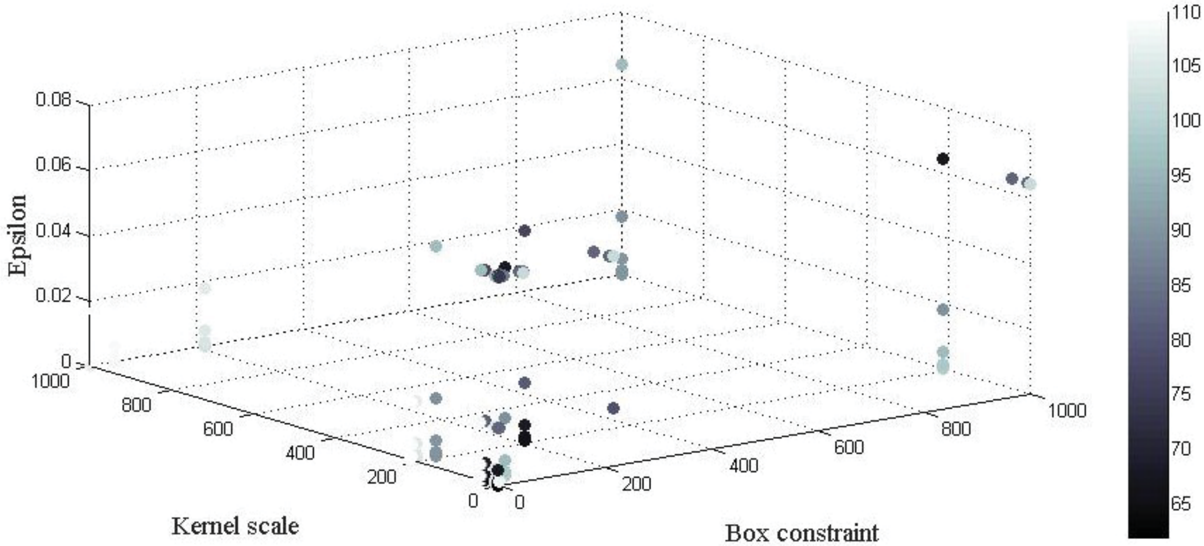

Figure 6.3: Variation of MSE for grade model with SVR parameters C, ϵ and γ

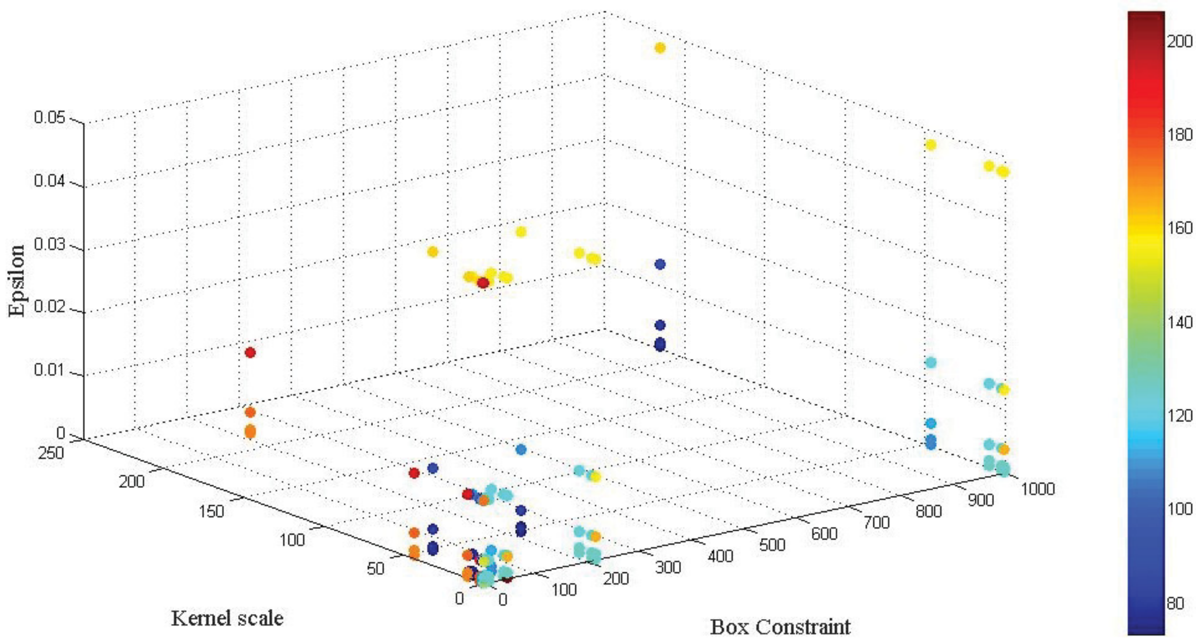

Figure 6.4: Variation of MSE for recovery model with SVR parameters C, ϵ and γ

Table 6.7: Optimal SVR parameter set for grade and recovery models

Model output	Minimum MSE	C	ϵ	γ
Grade(%)	62	0.001	0.000107	0.46416
Recovery(%)	74	0.02	0.00029	0.46415

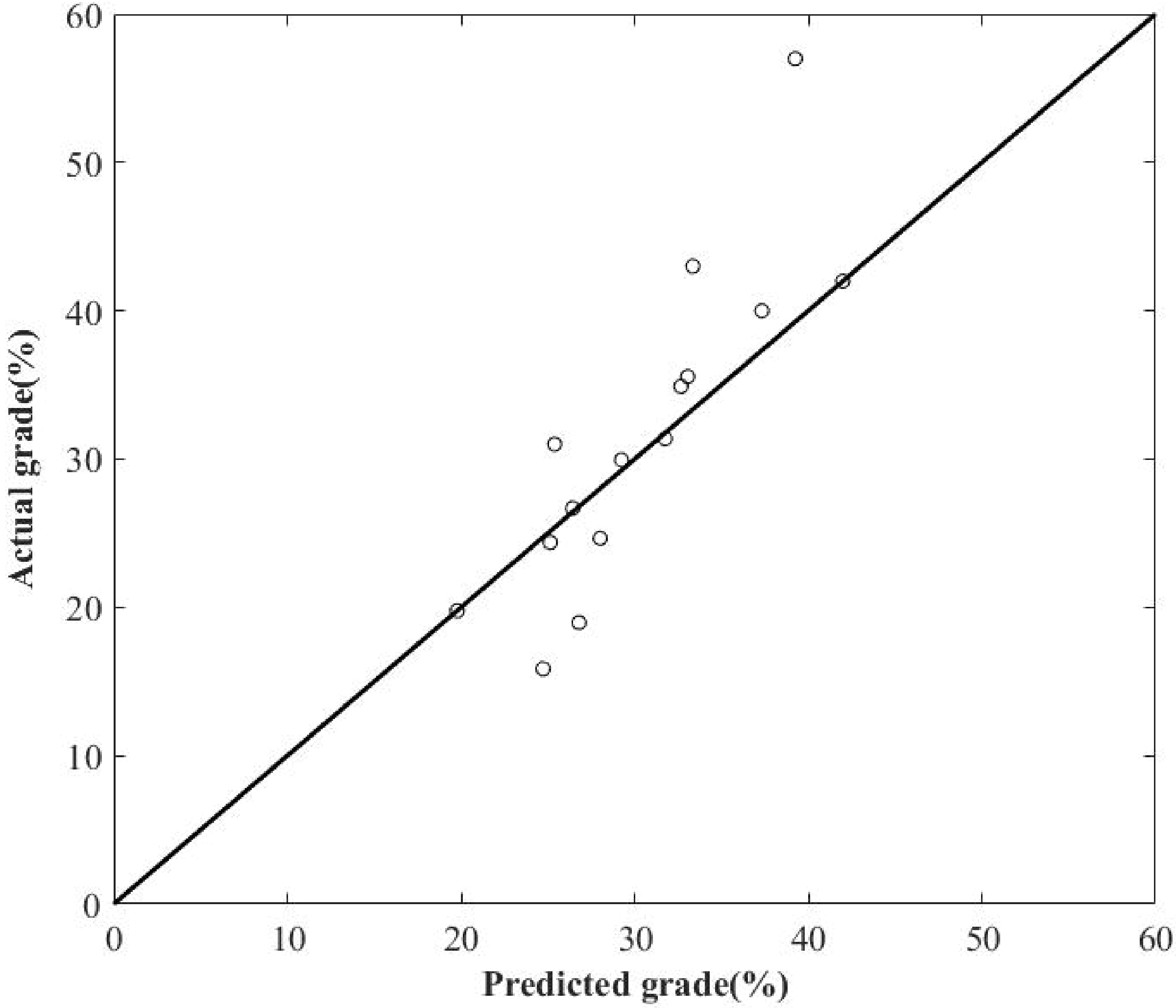

Figure 6.5: Comparison of online SVR model for prediction of grade with offline experimental values

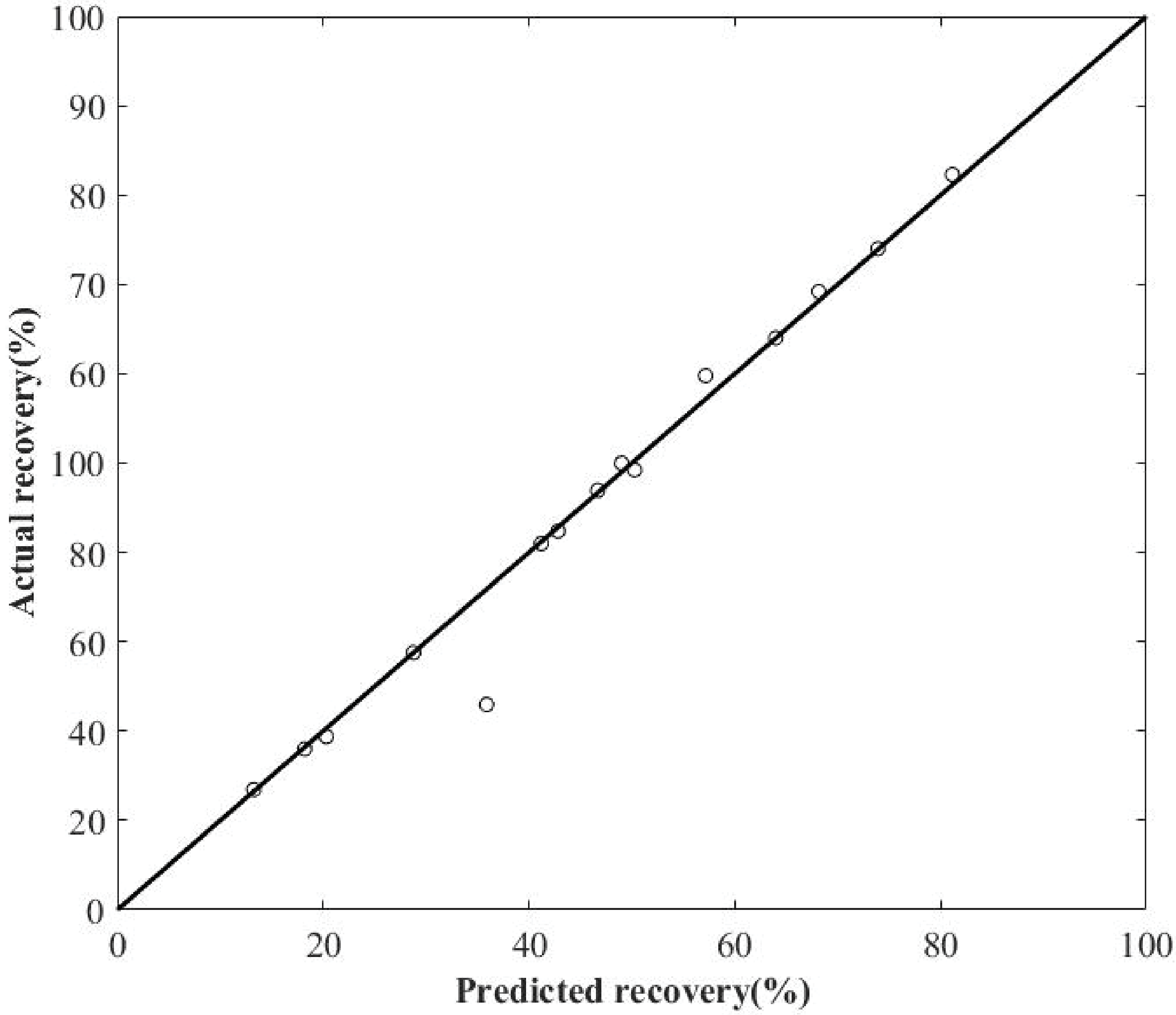

Figure 6.6: Comparison of online SVR model for prediction of recovery with off-line experimental values

The predictions of the SVR-based soft sensor are compared with the results of offline analysis using the Dean-Stark method. Figures 6.5 and 6.6 present comparison of offline and SVR-estimated grade and recovery, respectively. The Dean-Stark measurements have a delay of approximately $15h$ for analysis, while the soft sensor estimates are available every $5s$. Proximity of points to the 45° line in the figures represents good prediction performance. Both the grade and recovery models perform reasonably well for the three types of ores that were used as the feed. Root-mean square error (RMSE), which is square root of MSE, was calculated for both the models according to the equation 6.10.

$$RMSE = \sqrt{\frac{\sum_{i=1}^{n}(y_{exp,i} - y_{pred,i})^2}{n}} \tag{6.10}$$

Here, $y_{exp,i}$ is the experimental value of the observation, $y_{pred,i}$is the predicted value of the observation, and n is the number of observations. RMSE for training data set was found to be 6.4% and 3.4% for grade and recovery model, respectively. However, recovery model with lower RMSE value performs better than the grade model which is also seen in Figures 6.5 and 6.6. The outlier point in the Figure 6.6 corresponds to the 22.97 % recovery for high grade ore at 30 seconds. The prediction gap could be attributed to the faster flotation rate compared to other grade ores and slightly different image features. It can be improved by improving experimental capabilities to collect more training data between zero and 30 seconds of flotation. Also, a single model was developed and validated for different operating conditions for each of grade and recovery, which means that the developed model is robust to the feed type and operating conditions of the process. As the model only relies on froth images, it can potentially be used to monitor the performance of various units in the industrial extraction process where images can be obtained, such as the primary separation vessel (PSV) and primary and secondary flotation cells to obtain real-time grade and recovery measurements. However, model needs to be re-calibrated for its use in different part of the overall extraction circuit. The developed soft sensor can be used for optimizing process conditions, developing process control strategies, fault diagnosis and process monitoring. In particular, multi-objective optimization can be used to find the conditions that maintain an optimal trade-off between higher grade and recovery.

6.5 Implementation of soft sensor at other process conditions

In this section, we present results for the use of the soft sensor for real-time monitoring of grade and recovery at operating conditions that are different from those at which it was developed. A systematic approach using a stuctured design of experiments (e.g., factorial or response surface designs) would require a significant amount of experimental effort, and is the basis for future work. The results of two flotation runs are presented for the high grade ore, and one run each for the low and medium grade ores. Figure 6.7 presents the predicted grade and recovery using the soft sensor for the two runs performed with the high grade ore, and Figure 6.8 shows representative images of the froth surface at different times during the flotation runs along with the cumulative recovery and the instantaneous grade. Run 1 for the high grade ore is performed at an air flow rate of $4.5lpm$, initial temperature of $25°C$ and impeller speed of $1500rpm$, and Run 2 is performed at an air flow rate of $6.0lpm$, initial temperature of $50°C$ and impeller speed of $1100rpm$, i.e., Run 1 has a different temperature than the conditions listed in Table 6.2 and run 2 has different temperature and impeller speed. The flotation for the low grade ore was carried out at an air flow rate of $6.0lpm$, initial temperature of $25°C$ and impeller speed of $1100rpm$, and the predicted grade and recovery are shown in Figure 6.9, and representative froth images are shown in Figure 6.10. Finally, flotation of the medium grade ore was performed at an air flow rate of $4.5lpm$, initial temperature of $50°C$ and impeller speed of $1100rpm$, and Figure 6.11 presenting the change in grade and recovery with time and Figure 6.12 showing representative froth images. High grade ore demonstrates the faster process dynamics due to better liberation and attachment rate for higher bitumen and lesser solids content. From the results, it is clear that the soft sensor is able to predict the grade and recovery in different regions of operation and for different grades of ore. Thus, it can be used as a basis for the optimization of grade and recovery by manipulating processing conditions.

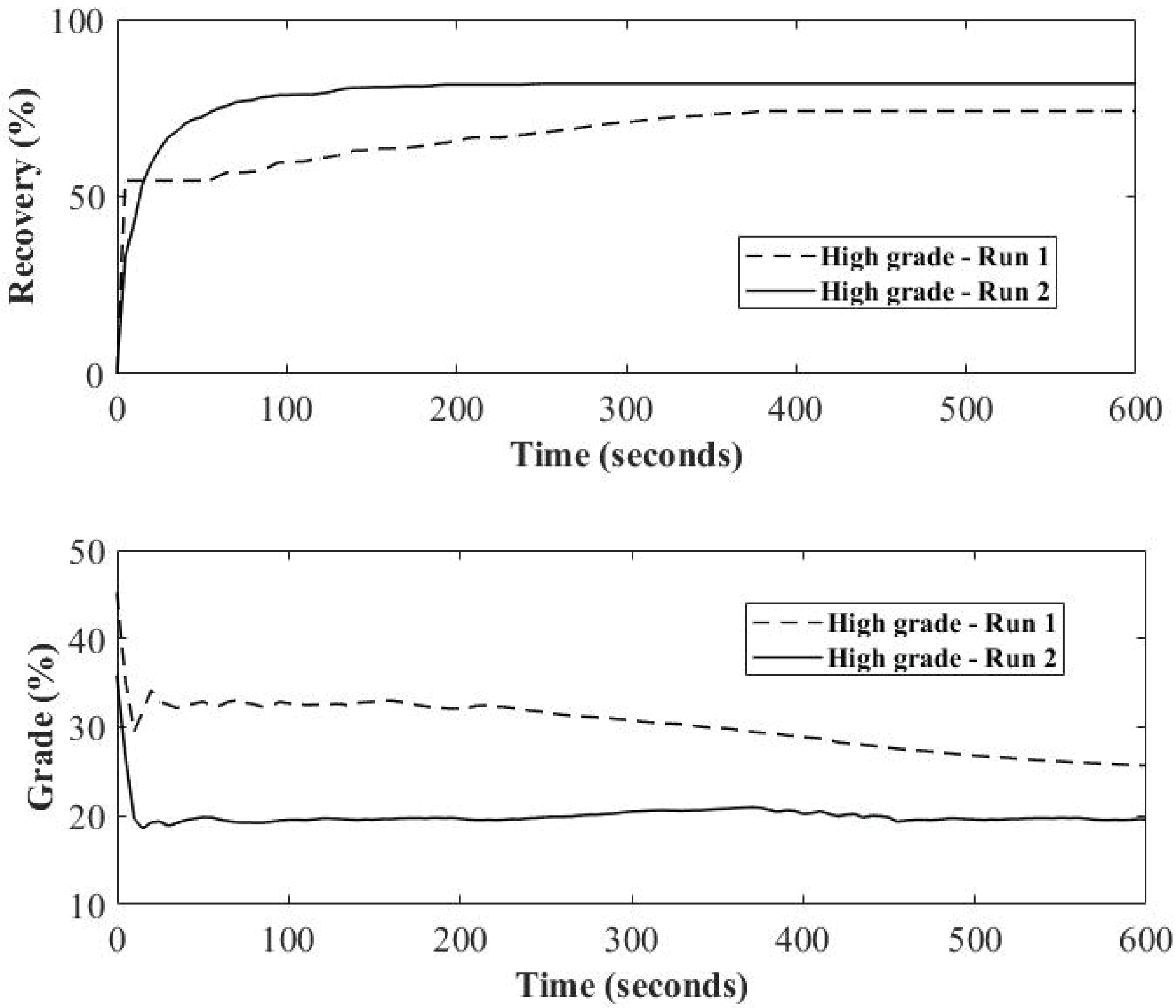

Figure 6.7: SVR model predictions of grade and recovery for high grade ore

Time (sec)	0	40	250	600
Cumulative Recovery (%)	0	54.20	68.02	74.01
Grade	-	33.4	16.37	0.8

Figure 6.8: Images at different flotation times for the high grade ore and predicted grade and cumulative recovery

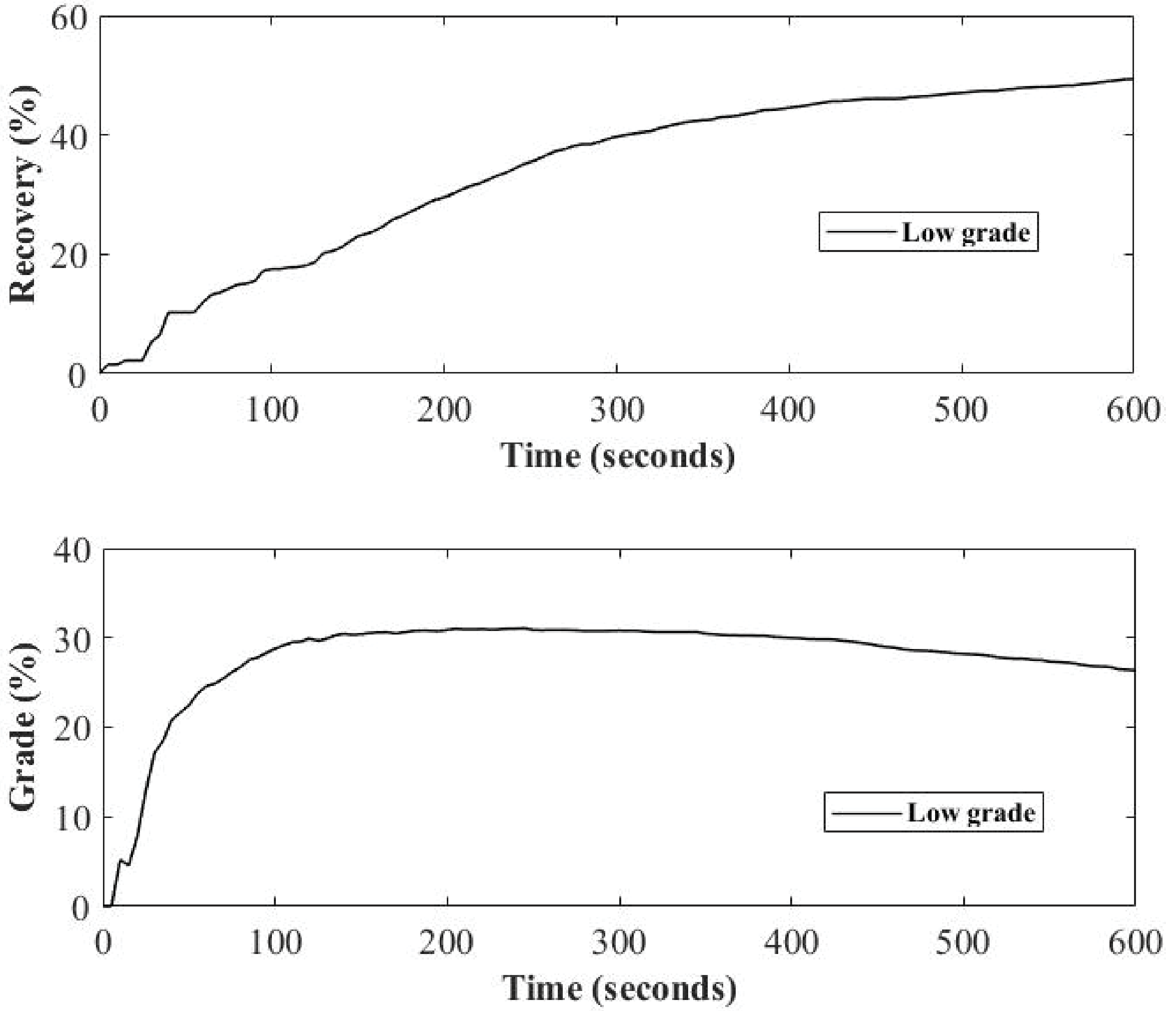

Figure 6.9: SVR model predictions of grade and recovery for low grade ore

Time (sec)	0	40	390	600
Cumulative Recovery (%)	0	10.52	44.18	49.36
Grade	-	20.12	5.59	1.28

Figure 6.10: Images at different flotation times for the low grade ore and predicted grade and cumulative recovery

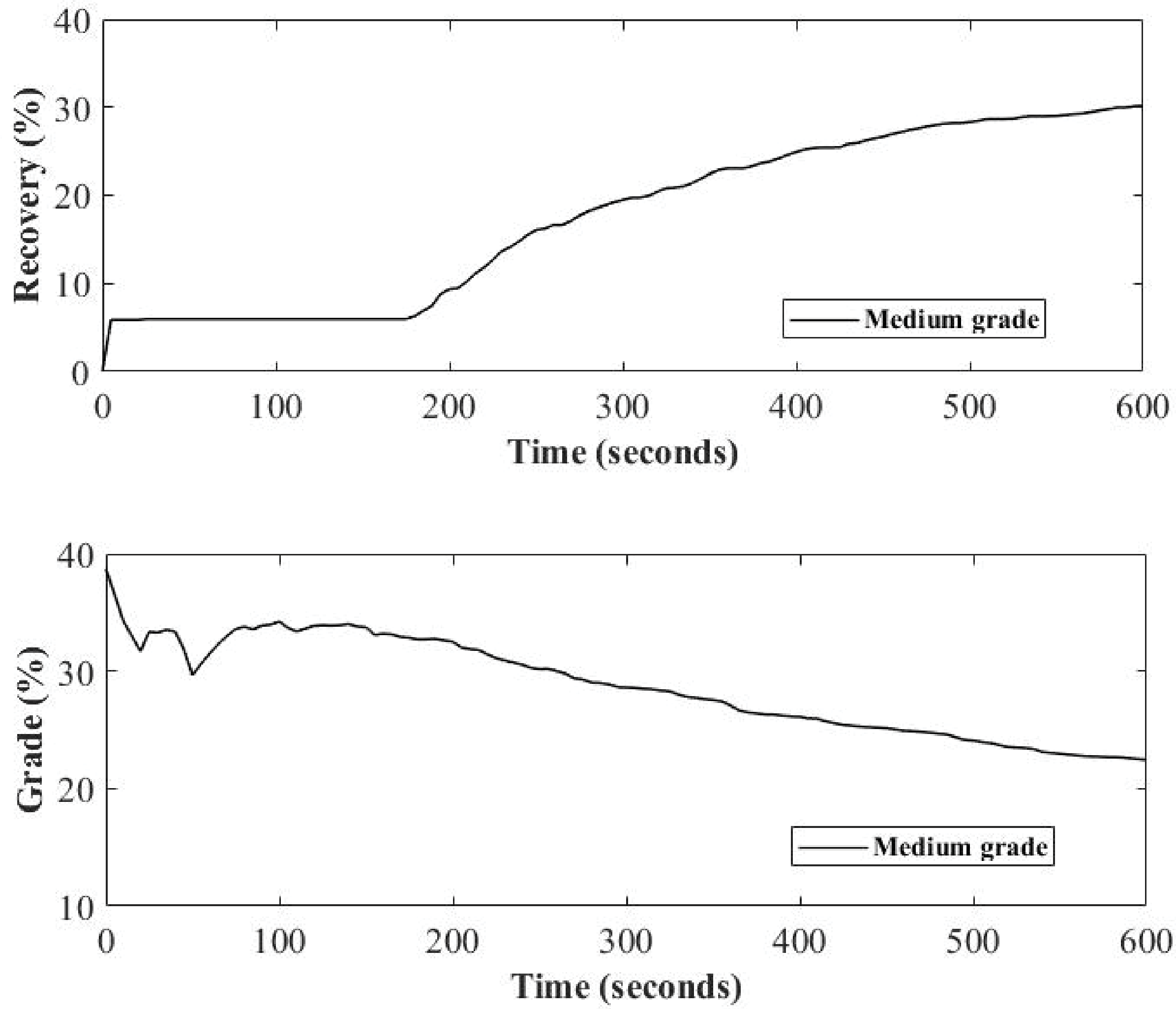

Figure 6.11: SVR model predictions of grade and recovery for medium grade ore

Time (sec)	0	40	315	600
Cumulative Recovery (%)	0	5.95	20.42	30.12
Grade	-	33.33	24.66	2.20

Figure 6.12: Images at different flotation times for the medium grade ore and predicted grade and cumulative recovery

6.6 Conclusions

In this work, a soft sensor was developed to measure the real-time grade and recovery for batch flotation of bitumen using real-time image data for the top surface of the froth along with support vector regression models. The soft sensor was calibrated against offline estimates of grade and recovery obtained using Dean-Stark analysis. Good model performance, with the mean squared error of prediction for grade being 0.62% and that for recovery being 0.74%, suggested that visual features are good indicators for flotation performance. 5-fold cross-validation was used in the development of the soft sensor. In addition, the developed SVR soft sensor was tested at different operating conditions of air flow rate, temperature and impeller speed for the different grades of ore, and was shown to provide meaningful estimates of grade and recovery in all these cases. This makes it suitable for real-time process monitoring and multi-objective optimization performed using the relations that can be developed between processing conditions and grade and recovery.

6.7 References

Aldrich, C., Marais, C., Shean, B.J., Cilliers, J.J., 2010. Online monitoring and control of froth flotation systems with machine vision: A review. International Journal of Mineral Processing 96, 1–13.

Basak, D., Pal, S., Patranabis, D.C., 2007. Support Vector Regression. Neural Information Processing Letters and Reviews 11, 203–224.

Boser, B., Guyon, I., Vapnik, V., 1992. A training algorithm for optimal margin classifiers, in: Annual Conference on Computational Learning Theory, ACM Press. pp. 144–152.

Bulmer, J., Starr, J., 1979. Syncrude Analytical Methods for Oil Sand and Bitumen Processing;. Alberta Oil Sands Technology and Research Authority, Edmonton. 1 edition.

Clark, K., Pasternack, D., 1932. Hot Water Separation of Bitumen from Alberta Bituminous Sand. Industrial & Engineering Chemistry Research1 24, 1410–1416.

Deng, J., Xie, L., Chen, L., Khatibisepehr, S., Huang, B., Xu, F., Espejo, A., 2013. Development and industrial application of soft sensors with on-line Bayesian model updating strategy. Journal of Process Control 23, 317–325.

Fortuna, L., Graziani, S., Rizzo, A., Xibilia, M., 2007. Soft Sensors for Monitoring and Control of Industrial Processes. Springer-Verlag London, London. 1 edition.

Gholami, A., Shahbazian, M., Safian, G., 2015. Soft Sensor Development for Distillation Columns Using Fuzzy C-Means and the Recursive Finite Newton Algorithm with Support Vector Regression (RFN-SVR). Industrial & Engineering Chemistry Research 54, 12031–12039.

Gunn, S., Brown, M., Bossly, K., 1997. Network performance assessment for neuro-fuzzy data modeling. Intelligent Data Analysis 1208, 313–323.

Hsu, C.w., Chang, C.C., Lin, C.j., 2010. A practical guide to support vector classification. Technical Report. National Taiwan University. Taipei.

Hua, S., Sun, Z., 2001. Support vector machine approach for protein subcellular localization prediction. Bioinformatics 17, 721–728.

Ito, K., Nakano, R., 2003. Optimizing Support Vector regression hyperparameters based on cross-validation, in: International Joint Conference on Neural Networks, IEEE. pp. 2077–2082.

Jia, B., 2010. Distribution of Oil Sands Formation Water in Bitumen Froth. Master's. University of Alberta.

Kadleca, P., Gabrysa, B., Strandtb, S., 2009. Data-driven Soft Sensors in the process industry. Computers & Chemical Engineering 33, 795–814.

Kasongo, T., Zhou, Z., Xu, Z., Masliyah, J., 2000. Effect of Clays and Calcium Ions on Bitumen Extraction from Athabasca Oil Sands Using Flotation. The Canadian Journal of Chemical Engineering 78, 674–681.

Khatibisepehr, S., Huang, B., Domlan, E., Naghoosi, E., Zhao, Y., Miao, Y., Shao, X., Khare, S., Keshavarz, M., Feng, E., Xu, F., Espejo, A., Kadali, R., 2013. Soft sensor solutions for control of oil sands processes. The Canadian Journal of Chemical Engineering 91, 1416–1426.

Leiva, J., Vinnett, L., Yianatos, J., 2012. Estimation of air recovery by measuring froth transport over the lip in a bi-dimensional flotation cell. Minerals Engineering 3638, 303–308.

Liu, J., Xu, Z., Masliyah, J., 2004. Interaction between Bitumen and Fines in Oil Sands Extraction System: Implication to Bitumen Recovery. The Canadian Journal of Chemical Engineering 82, 655–666.

Liua, Y., Chen, J., 2013. Integrated soft sensor using just-in-time support vector regression and probabilistic analysis for quality prediction of multi-grade processes. Journal of Process Control2 23, 793–804.

Masliyah, J., Zhou, Z.J., Xu, Z., Czarnecki, J., Hamza, H., 2004. Understanding Water-Based Bitumen Extraction from Athabasca Oil Sands. The Canadian Journal of Chemical Engineering 82, 628–654.

Moolman, D.W., Eksteen, J.J., Aldrich, C., van Deventer, J.S.J., 1996. The significance of flotation froth appearance for machine vision control. International Journal of Mineral Processing 48, 135–158.

Popli, K., Sekhavat, M., Afacan, A., Dubljevic, S., Liu, Q., Prasad, V., 2015. Dynamic modeling and real-time monitoring of froth flotation. Minerals 5, 570–591.

Pow, J., Fairbanks, G., Zamora, W., 1963. Athabasca Oil SandsThe Karl A. Clark Volume. Research Council of Alberta, Edmonon. 1 edition.

P.V., J., Shah, S.L., Kadali, R., 2010. Computer vision based interface level control in a separation cell. Control Engineering Practice 18, 349–357.

Runge, K., McMaster, J., Wortley, M., Rosa, D.L., Guyot, O., 2007. A Correlation Between Visiofroth Measurements and the Performance of a Flotation Cell. Ninth Mill Operators' Conference , 79–86.

Sanford, E., Seyer, F., 1979. Processibility of Athabasca Tar Sand Using a Batch Extraction Unit: The Role of NaOH. CIM Bulletin 72, 164–169.

Schramm, L., Smith, R., 1987. Some Observations on the Ageing Phenomenon in the Hot Water Processing of Athabasca Oil SandsPart 1. The Nature of the Phenomenon. AOSTRA Journal of Research 3, 195–214.

Scramma, L., Stasiuk, E., Yarranton, H., Maini, B., Shelfantook, B., 2002. Temperature Effects in the Conditioning and Flotation of Bitumen From Oil Sands in Terms of Oil Recovery and Physical Properties, in: Canadian International Petroleum Conference, Petroleum Society of Canada, Calgary.

Shao, X., Xu, F., Huang, B., Espejo, A., 2012. Estimation of Bitumen Froth Quality Using Bayesian Information Synthesis: An Application to Froth Transportation Process. The Canadian Journal of Chemical Engineering 90, 1393–1399.

Sharmina, R., Sundararaj, U., Shah, S., Griendb, L.V., Sun, Y.J., 2006. Inferential sensors for estimation of polymer quality parameters: industrial application of a PLS-based soft sensor for a LDPE plant. Chemical Engineering Science 61, 6372–6384.

Shokri, S., Marvast, M.A., Sadeghi, M.T., Narasimhanc, S., 2016. Combination of data rectification techniques and soft sensor model for robust prediction of sulfur content in HDS process. Journal of the Taiwan Institute of Chemical Engineers 58, 117–126.

Smith, B.T., 2004. Lagrange Multipliers Tutorial in the Context of Support Vector Machines. Technical Report. Memorial University of Newfoundland.

Vapnik, V., 1995. The Nature of Statistical Learning Theory. Springer-Verlag New York, New York.

Vapnik, V., 2006. Estimation of Dependences Based on Empirical Data. Springer-Verlag New York, New York. 1 edition.

Wu, C.H., Tzeng, G.H., Lin, R.H., 2009. A Novel hybrid genetic algorithm for kernel function and parameter optimization in support vector regression. Expert Systems with Applications 36, 4725–4735.

Yang, C.C., Shieh, M.D., 2010. A support vector regression based prediction model of affective responses for product form design. Computers and Industrial Engineering 59, 682–689.

Zhang, H., Chen, L., Qu, Y., Zhao, G., Guo, Z., 2014. Support Vector Regression Based on Grid-Search Method for Short-Term Wind Power Forecasting. Journal of Applied Mathematics 2014.

Zhu, Q., 2013. Understanding the Role of Caustic Addition in Oil Sands Processing. Ph.D. thesis. University of Alberta.

Chapter 7

Conclusions and Future work

7.1 Concluding remarks

The complex nature of the froth flotation processes gives rise to various unidentified disturbances in the system. It is necessary to monitor the process in real-time with diagnostics of the various sub-processes taking part in the overall process. However, real-time monitoring in froth flotation is always limited by absence of online process measurements and an adequate modeling framework. Various challenges needs to be addressed before developing monitoring schemes and online sensing for process measurements. These challenges range from the development of dynamic fundamental models incorporating first principles knowledge of the sub-processes to robustness of the inferential sensing methods. The overall objective of the thesis was to develop a real-time monitoring scheme for froth flotation processes using fundamental modeling structure and image-based soft sensors for mineral grade and recovery. A multiscale model framework was developed to connect sub-processes to the overall process.

The overall scheme was developed for pure mineral flotation as a proof of concept and then extended to a synthetic mixture of two minerals and finally a real industrial sulfide ore. Furthermore, disturbances in various factors influencing flotation were studied and heuristics were developed for their tracking in real-time. The factors included air flow rate, impeller speed, feed particle size, and reagent dosages. Studies were also undertaken to obtain their influences on sub-processes in the system. A major contributor to the reduction in product quality, entrainment, was also studied and estimated by decoupling the overall recovery to its components of *true flotation* and *entrainment* recoveries. The concluding remarks for the thesis are discussed below with reference to the studies in different chapters.

Chapter 2 mainly dealt with the pure mineral (galena) flotation to provide proof of concept for the monitoring scheme. A set of models were developed with in-depth explanation of attachment and detachment sub-processes. An induction time machine was used to calculate the induction time which was further used as a offline measurement to the model to obtain the initial values for the parameters. Online measurements for the recovery were obtained using statistical methods, (principal component regression and partial least squares regression) on froth image features that were obtained through VisioFroth. Model was applied for diverse process conditions which were created based on fraction factorial design of experiments with air flow rate, impeller speed, frother dosage, and collector dosage as the design variables. The extended Kalman filter (EKF), a state and parameter estimation technique was used to update the fundamental model based on the online recovery values. The parameters estimated were the attachment rate constant, detachment rate constant, and froth residence time. These parameters were estimated parallely with *one at a time* estimation based on the observability analysis. Disturbances were induced in the batch flotation experiments by changing the air flow rate from 14 L/min to 8 L/min, and impeller speed from 500 rpm to 1100 rpm in the middle of the experiments. Models were updated in the presence of disturbances and captured the process dynamics. Successful tracking of the disturbances through the changes in parameter estimation led to the development of heuristics for identifying disturbances incurred through any changes in air flow rate and impeller speed. The proof of concept obtained in this chapter, was then extended to rest of the study to include more disturbances and increase in the complexity of process feed.

The effect of feed particle size was successfully studied in Chapter 3. Also, the soft sensor model for galena recovery based on froth image features was successfully upgraded using a *random forest* machine learning algorithm. A fundamental model for froth flotation was included with in-depth understanding of the particle size effect on the attachment and detachment sub-processes. Feed particle size was also included in the modeling structure. Batch flotation experiments were conducted with four different particle size distributions for galena. The mean particle size was in the range of 12.13 microns to 113 microns for the four distributions. Induction times were obtained for all the particle size ranges to study the particle size effects specifically on the bubble-particle attachment. A clear variation among the induction time values showed the high dependency of attachment on feed particle size. Models were updated through state and parameter estimation by using EKF. Two separate methods were proposed to monitor the feed particle size using online recovery measurements and parameter estimation. These methods were named direct and indirect estimation based on the parameters estimated. The direct method was based on estimating feed particle size as a parameter while the indirect method back-calculated the feed particle size based on the estimated attachment and detachment rate constants. The direct method showed better performance and was successful in estimating the feed particle size of an unknown test distribution. Hence, a drop in recovery because of, for example, issues in the grinding circuit and variation in feed particle size could now be captured with the proposed monitoring scheme.

In chapter 4, single mineral flotation was extended to bi-mineral flotation consisting of synthetic mixture of galena and quartz. Successful attempts were made to monitor the entrainment by decoupling the overall recovery to the recovery by *entrainment* and *true flotation*. The fundamental modeling structure was further upgraded to include detailed functions for entrainment and drainage sub-processes. Unlike previous single mineral flotations studies, both grade and recovery were measured online through froth image features. A complete network was developed using a machine learning algorithm based on support vector regression (SVR) and mass balance equations to inferentially estimate grade and recovery for galena and quartz in real-time. Galena grade and solids recovery were used as model outputs for image-based SVR machine learning models. An EKF-based model update was used to estimate model parameters for entrainment and drainage sub-processes. Different quartz sizes (under 15 microns, 40 microns, and 90 microns) were used for batch flotation to understand the effect of quartz particle size on entrainment. The monitoring scheme was successful in decoupling the overall recovery to obtain entrainment recoveries for both galena and quartz in real-time. It showed the potential of the developed entrainment monitoring scheme to be used for maintaining product grade and specifically target the reduction of the gangue entrainment recovery.

To accomplish the study for a full scale industrial flotation, Chapter 5 established monitoring algorithms for multi-stage flotation of a real industrial complex sulfide ore procured from Red Dog mine, Alaska. Batch flotation experiments were conducted for lead and zinc rougher cells to represent the industrial flotation by multiple stages of differential flotation. Experiments were designed using factorial-based DOE and collector dosages as the design variables. The soft sensor network was extended for a complex feed ore to measure grade and recovery in real-time for galena and sphalerite. Image-based SVR models were developed for galena grade, sphalerite grade, and solids recovery, with distinct models for lead and zinc rougher flotation. These measurements were further used in mass balance equations to measure galena and zinc recovery in real-time. Off-line laboratory measurements were obtained for mineral grade to calibrate the image-based models. A support vector machine classifier was constructed and calibrated to classify the froth images to two classes of lead rougher or zinc rougher that automated the entire process of obtaining online process measurements. The soft sensor network was successfully applied for diverse process conditions that were created using design of experiments. A fundamental dynamic model was developed for the multi-stage flotation network, keeping the connection between micro-scale and macro-scale sub-processes. An EKF was used for state and parameter estimation by reconciling soft sensor online measurements to the dynamic model. Disturbances were created in the process through variation in collector dosages in both the stages. The attachment rate constant was selected as the parameter to estimate based on its theoretical dependence on collector dosages. Estimates of attachment rate constant showed higher values for the cases with higher collector dosages. Successful monitoring was obtained for collector dosages through the trends observed in attachment rate constant estimation. The online sensing, modeling, and monitoring scheme for the real industrial ore with multi-stage flotation provides a promising application for the developed framework.

Chapters 2 to 5 showed a step-by-step method development for monitoring in froth flotation for mineral processing. Another study was performed with oil sands extraction as reported in Chapter 6, to demonstrate the potential of the image-based soft sensing in other applications that use froth flotation. Different types of oil sands ore were obtained from the Athabasca region for the study. Batch flotation was used to extract bitumen from the oil sands ore. Dean-Stark analysis was performed for the collected froth samples to obtain off-line measurements for bitumen grade, and consequentially recovery. Soft sensor models were obtained for the online measurements of bitumen grade and recovery using froth surface images. Training data was obtained for different types of oil sands ore to create diversity in the data-set. The developed model was validated and applied to diverse process conditions with wide ranges of bitumen content in the feed ore. The application demonstrated the robustness of the soft sensor and suggests that the model need not be re-calibrated for different types of oil sands ore as the feed. This establishes its potential in process monitoring and advanced process control for the oil sands industry. It also provides a method to the oil sands industry for real-time process measurements in the form of a soft sensor by reducing the previous sampling time of 10-15 hours for Dean Stark measurements to 10 seconds for image-based measurements. It should be noted that, apart from the VisioFroth installation, which is already available with many oil sands operators, this method does not require any additional capital cost.

7.2 Future Work

The proposed monitoring scheme, dynamical modeling framework, and online soft sensing present many research paths to enhance the understanding of the flotation process and improve the process control scenario for the industries using flotation. The following list presents the ideas and motivation for other studies that could be conducted based on the work in this thesis:

- Enhancement of the fundamental model

  The modeling framework developed in this study provides a good mechanism to connect various sub-processes to the mineral recovery. It can be extended to include the quantitative relationship between chemistry reagents and the sub-processes. For instance, a model for efficiency of a collector for the separation can be incorporated into the modeling framework for better understanding of the attachment process. This would also improve the detection of disturbances obtained through changes in reagent dosages. The model would also be useful in identifying new collectors for the specific flotation tasks. Additionally, bubble population models should be added to the framework to capture the dynamics of bubble breakage and bubble coalescence.

- New sensors for the online measurements of froth flotation variables

  The developed research proposes a robust method for inferential measurements of grade and recovery using froth images and machine learning algorithms. However, various other measurements could improve the observability and increase the parameters that can be estimated using EKF. These measurements for the variables could be obtained with the development of new soft or hard sensors. The variables may include of plateau border area, or dissipation energy in the mixing zone.

- Monitoring algorithm for the oil sands extraction

  Chapter 6 provides the soft sensor development for oil sands extraction for real-time measurements of bitumen grade and recovery. A detailed study can be carried out for developing a dynamic model for oil sands extraction processes in primary separation vessels (PSV) and mechanical flotation cells. It would be challenging and interesting to understand the dynamic behavior of these processes and their effects on the final bitumen recovery. Models and online measurements could then be used for advanced process control applications or real-time monitoring to improve bitumen content in the concentrate.

- Column flotation

  Column flotation, a recent development in flotation technology, has been widely used in the industry for beneficiation and final cleaning of the concentrates. It is therefore necessary to develop similar monitoring schemes for column flotation. This involves modification of the model and incorporating already developed dynamic models for column flotation that are available in the literature. Also, new soft sensor models should be developed to be applicable in continuous processes using column flotation. With continuous processes, it is easy to artificially create various disturbances in the feed streams to test the monitoring scheme. A column flotation circuit has already been developed for further study. Figure 7.1 shows the schematic diagram for the column cell that is designed and fabricated for further study. The column has been equipped with VisioFroth for image features and basic control using PI and PID control loops for flows and level in the column. With more states arising in the column operation, the EKF estimation method can be replaced with other methods such as the particle filter (PF) or Ensemble Kalman filter (EnKF) which could handle more states in the model. Additionally, dynamic models could be combined with black box models for developing model predictive control (MPC) algorithms. Once the image-based soft sensors are developed, on-line grade and recovery can be directly used as control variables instead of other secondary variables such as bias or froth height.

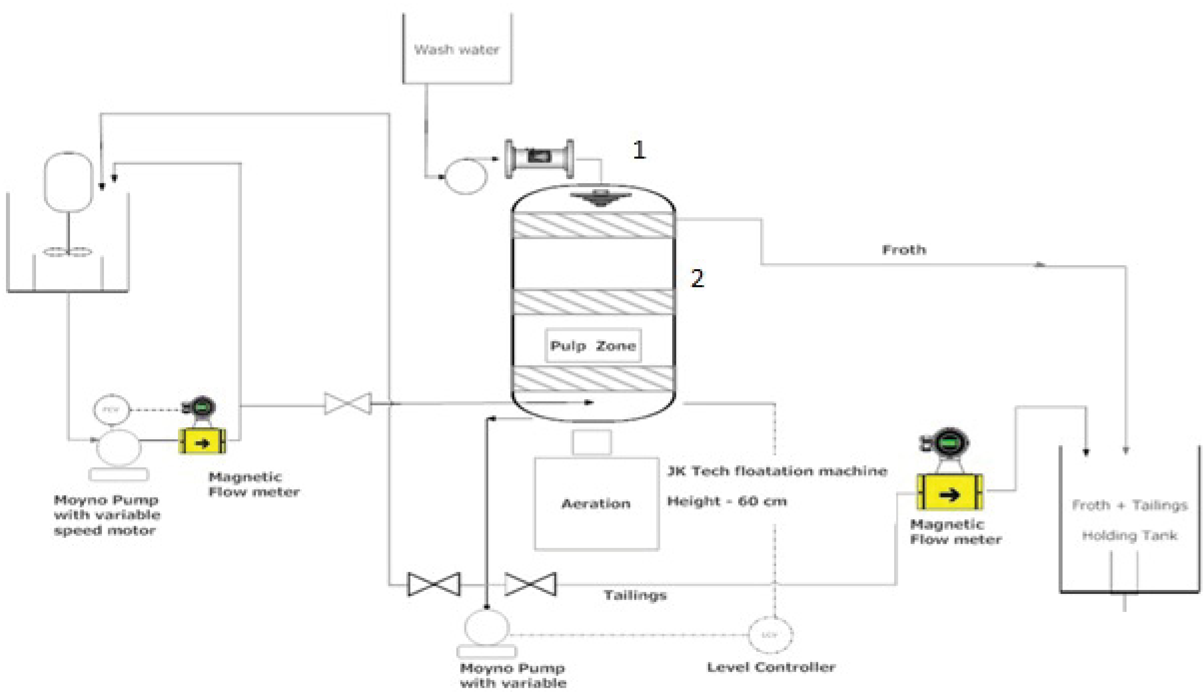

Figure 7.1: A schematic diagram for the column flotation set-up

Bibliography

Akdemir, Ü., Sönmez, ., 2003. Investigation of coal and ash recovery and entrainment in flotation. Fuel Processing Technology 82, 1–9.

Aldrich, C., Marais, C., Shean, B.J., Cilliers, J.J., 2010. Online monitoring and control of froth flotation systems with machine vision: A review. International Journal of Mineral Processing 96, 1–13.

Aldrich, C., Moolman, D.W., Bunkell, S.J., Harris, M.C., Theron, D.A., 1997. Relationship between surface froth features and process conditions in the batch otation of a sulphide ore. Minerals Engineering 10, 1207–1218.

Alford, R.A., 1990. Improved model for design of industrial column flotation circuits in sulphide applications. Springer Netherlands, Dordrecht. pp. 189–206.

Alves dos Santos, N., Savassi, O., Peres, A.E.C., Martins, A.H., 2014. Modelling flotation with a flexible approach Integrating different models to the compartment model. Minerals Engineering 66, 68–76.

Amand, F.J.S., 1999. Hydrodynamics of deinking flotation. International Journal of Mineral Processing 56, 277–316.

Arbiter, N., Harris, C., 1962. Flotation kinetic, in: Fuerstenau, D. (Ed.), Froth Flotation. AIME, New York, pp. 215–262.

Asghar, A., Ahmad, H., Behnam, F., 2015. Investigating the first-order flotation kinetics models for Sarcheshmeh copper sulfide ore. International Journal of Mining Science and Technology 25, 849–854.

Ata, S., 2012. Phenomena in the froth phase of flotation A review. International Journal of Mineral Processing 102-103, 1–12.

Barbaro, M., 2000. Lead and zinc ores - flotation. Acadmieca Press Rome, Rome.

Barbian, N., Cilliers, J.J., Morar, S.H., Bradshaw, D.J., 2007. Froth imaging, air recovery and bubble loading to describe flotation bank performance. International Journal of Mineral Processing 84, 81–88.

Bartolacci, G., Jr., P.P., Jr., J.T., Duchesne, C., Bossé, P.A., Fournier, J., 2006. Application of numerical image analysis to process diagnosis and physical parameter measurement in mineral processesPart I: Flotation control based on froth textural characteristics. Minerals Engineering 19, 734–747.

Basak, D., Pal, S., Patranabis, D.C., 2007. Support Vector Regression. Neural Information Processing Letters and Reviews 11, 203–224.

Bascur, O., Herbst, J., 1982. Dynamic modeling of a otation cell with a view toward automatic control, in: IMPC Session III, pp. 17–23.

Bascur, O.A., 2000. An interactive dynamic flotation model framework. Developments in Mineral Processing 13, C8a–21–C8a–31.

Basilio, C., Kartio, I., Yoon, R.H., 1996. Lead activation of sphalerite during galena flotation. Minerals Engineering 9, 869–879.

Benkouider, A.M., Buvat, J.C., Cosmao, J.M., Saboni, A., 2009. Fault detection in semi-batch reactor using the EKF and statistical method. Journal of Loss Prevention in the Process Industries 22, 153–161.

Bergh, L., Yianatos, J., 2011. The long way toward multivariate predictive control of flotation processes. Journal of Process Control 21, 226–234.

Bergh, L., Yianatos, J., 2013. Control of rougher flotation circuits aided by industrial simulator. Journal of Process Control 23, 140–147.

Bhole, M.R., Joshi, J.B., Ramkrishna, D., 2008. CFD simulation of bubble columns incorporating population balance modeling. Chemical Engineering Science 63, 2267–2282.

Bisshop J.P. & White, M.E., 1976. Study of particle entrainment in flotation froths. Transactions of the Institution of Mining and Metallurgy 85.

Bloom, F., Heindel, T.J., 1997. Mathematical modelling of the flotation deinking process. Mathematical and Computer Modelling 25, 13–58.

Bloom, F., Heindel, T.J., 2002. On the structure of collision and detachment frequencies in flotation models. Chemical Engineering Science 57, 2467–2473.

Bloom, F., Heindel, T.J., 2003. Modeling flotation separation in a semi-batch process. Chemical Engineering Science 58, 353–365.

Bo, L., Xueqing, Y., Lin, Z., 2015. Li-ion battery SOC estimation based on EKF algorithm.

Bonifazi, G., Giancontieri, V., Meloni, A., Serranti, S., Volpe, F., Zuco, R., Koivo, H., Hätönen, J., Hyötyniemi, H., Niemi, A., Sipari, P., Kuopanporrti, H., Ylinen, R., Heikkila, I., Lahteenmaki, S., Miettunen, J., Stephasson, O., Wang, W., Carlsson, L.E., 2000. Characterization of the flotation froth structure and color by machine vision (ChaCo). Elsevier. volume Volume 13 of *Developments in Mineral Processing*. pp. C8a–39–C8a–49.

Boser, B., Guyon, I., Vapnik, V., 1992. A training algorithm for optimal margin classifiers, in: Annual Conference on Computational Learning Theory, ACM Press. pp. 144–152.

Bouchard, J., Desbiens, A., del Villar, R., 2005. Recent advances in bias and froth depth control in flotation columns. Minerals Engineering 18, 709–720.

Bouchard, J., Desbiens, A., del Villar, R., 2014. Column flotation simulation: A dynamic framework. Minerals Engineering 55, 30–41.

Breiman, L., 2001. Random forests. Machine Learning 45, 5–32.

Bressel, M., Hilairet, M., Hissel, D., Bouamama, B.O., 2015. Fuel cells remaining useful life estimation using an extended Kalman Filter.

Brown, N., Bourke, P., Ronkainen, S., van Olst, M., 2001. Improving flotation plant performance at Cadia by controlling and optimizing the rate of froth recovery using Outokumpu Frothmaster, in: 33rd Annual Meeting of Canadian Mineral Processors, Ottawa, Canada. pp. 25–36.

Bulatovic, S.M., 2007. Handbook of flotation reagents : chemistry, theory and practice. Elsevier.

Bulmer, J., Starr, J., 1979. Syncrude Analytical Methods for Oil Sand and Bitumen Processing;. Alberta Oil Sands Technology and Research Authority, Edmonton. 1 edition.

Çilek, E., Ylmazer, B., 2003. Effects of hydrodynamic parameters on entrainment and flotation performance. Minerals Engineering 16, 745–756.

Cilek, E.C., Umucu, Y., 2001. A statistical model for gangue entrainment into froths in flotation of sulphide ores. Minerals Engineering 14, 1055–1066.

Cipriano, A., Guarini, M., Vidal, R., Soto, A., Sepulveda, C., Mery, D., Griseno, H., 1998. A real time visual sensor for supervision of flotation cells. Minerals Engineering 11, 489–499.

Clark, K., Pasternack, D., 1932. Hot Water Separation of Bitumen from Alberta Bituminous Sand. Industrial & Engineering Chemistry Research1 24, 1410–1416.

Cruz, E.B., 1997. A comprehensive dynamic model of the column flotation unit operation. Phd. Virginia Polytechnic Institute and State University.

Cutting, G., Barber, S., Newton, S., 1986. Effects of froth structure and mobility on the performance and simulation of continuously operated flotation cells. International Journal of Mineral Processing 16, 43–61.

Dai, Z., Fornasiero, D., Ralston, J., 1999. ParticleBubble Attachment in Mineral Flotation. Journal of Colloid and Interface Science 217, 70–76.

Dai, Z., Fornasiero, D., Ralston, J., 2000. Particlebubble collision models a review. Advances in Colloid and Interface Science 85, 231–256.

Deng, J., Xie, L., Chen, L., Khatibisepehr, S., Huang, B., Xu, F., Espejo, A., 2013. Development and industrial application of soft sensors with on-line Bayesian model updating strategy. Journal of Process Control 23, 317–325.

Derjaguin, B.V., Dukhin, S.S., 1993. Theory of flotation of small and medium-size particles. Progress in Surface Science 43, 241–266.

Dewitt, C.C., 1940. Froth Flotation Concentration. Industrial & Engineering Chemistry 32, 652–658.

Ding, L., Gustafsson, T., 1999. Modelling and control of a flotation process: Control and optimisation in minerals, metals and materials processing, in: Proceedings of an international symposium held at the 38th annual conference of metallurgists of CIM in Quebec, Canadian Institute of Mining, Metallurgy and Petroleum, Quebec. pp. 285–298.

Dobby, G.S., Finch, J.A., 1987. Particle size dependence in flotation derived from a fundamental model of the capture process. International Journal of Mineral Processing 21, 241–260.

Dobby, G.S., Savassi, O.N., 2005. An Advanced Modelling Technique for Scale-Up of Batch Flotation Results to Plant Metallurgical Performance, in: Centenary of Flotation Symposium.

Duan, J., Fornasiero, D., Ralston, J., 2003. Calculation of the flotation rate constant of chalcopyrite particles in an ore. International Journal of Mineral Processing 72, 227–237.

Duchesne, C., 2010. Multivariate Image Analysis in Mineral Processing, in: Sbarbaro, D., del Villar, R. (Eds.), Advanced Control and Supervision of Mineral Processing Plants. Springer, pp. 85–139.

Ek, C., 1992. Flotation kinetics. Innovation in Flotation Technology 5, 183–210.

Engelbrecht, J.A., Woodburn, E.T., 1975. The effects of froth height, aeration rate and gas precipitation on flotation. JS Afr.Inst.Min.Metall 76, 125–132.

F. Sawyerr D.A. Deglon, O'Connor, C.T., 1998. Prediction of bubble size distribution in mechanical flotation cells. Journal of The South African Institute of Mining and Metallurgy 98, 179–185.

Finkelstein, N., Alllison, S., 1976. The Chemistry of Activation, Deactivation and Depression in the Flotation of Zinc Sulfide: a Review, in: Fuerstenau, M.C. (Ed.), Flotation. AMIE, New York, pp. 414–457.

Finkelstein, N., Lovell, V., 1972. Fundamental studies of the flotation process : the work of the National Institute for Metallurgy. Journal of the Southern African Institute of Mining and Metallurgy 72, 328–342.

Fisher, T., Tokich, J., 1943. Concentration by flotation of a complex Galena –sphalerite –chalcopyrite ore from The nine mile district near missoula, Montana. Ph.D. thesis. Montana School of Mines.

Fortuna, L., Graziani, S., Rizzo, A., Xibilia, M., 2007. Soft Sensors for Monitoring and Control of Industrial Processes. Springer-Verlag London, London. 1 edition.

Fuerstenau, M.C., Jameson, G.J., Yoon, R.H., 2007. Froth Flotation: A Century of Innovation. SME.

Gaudin, A.M., 1957. Flotation. Mcgraw - Hill, New York. 2nd edition.

Gaudin, A.M., Groh, J.O., Henderson, H.B., 1931. Effect of particle size on flotation. The American Institute of Mining, Metallurgical, and Petroleum Engineers 414, 3–23.

Geetha, M., Kumar, P.A., Jerome, J., 2014. Comparative Assessment of a Chemical Reactor Using Extended Kalman Filter and Unscented Kalman Filter. Procedia Technology 14, 75–84.

Geladi, P., Kowalski, B.R., 1986. Partial least-squares regression: a tutorial. Analytica Chimica Acta 185, 1–17.

Gelbart, M.A., Snoek, J., Adams, R.P., 2014. Bayesian Optimization with Unknown Constraints. Technical Report.

Gholami, A., Shahbazian, M., Safian, G., 2015. Soft Sensor Development for Distillation Columns Using Fuzzy C-Means and the Recursive Finite Newton Algorithm with Support Vector Regression (RFN-SVR). Industrial & Engineering Chemistry Research 54, 12031–12039.

Glembotsky, V.A., 1953. The time of attachment of air bubbles to mineral particles in flotation and its measurement. Izvestiya Akademii Nauk SSSR (OTN) 11, 1524–1531.

Gong, J., 2011. The Role of High Molecular Weight Polyethylene Oxide in Reducing Quartz Gangue Entrainment in Chalcopyrite Flotation by Xanthate Collectors. Ph.D. thesis. University of Alberta.

Gong, J., Peng, Y., Bouajila, A., Ourriban, M., Yeung, A., Liu, Q., 2010. Reducing quartz gangue entrainment in sulphide ore flotation by high molecular weight polyethylene oxide. International Journal of Mineral Processing 97, 44–51.

Gorain, B.K., Harris, M.C., Franzidis, J.P., Manlapig, E.V., 1998. The effect of froth residence time of the kinetics of flotation. Minerals Engineering 11, 627–638.

Gu, G., Xu, Z., Nandakumar, K., Masliyah, J., 2003. Effects of physical environment on induction time of airbitumen attachment. International Journal of Mineral Processing 69, 235–250.

Gulsoy, O.Y., 2005. A simple model for the calculation of entrainment in flotation. Korean Journal of Chemical Engineering 22, 628–634.

Gunn, S., 1998. Support Vector Machines for Classification and Regression. Technical Report. University of Southampton.

Gunn, S., Brown, M., Bossly, K., 1997. Network performance assessment for neuro-fuzzy data modeling. Intelligent Data Analysis 1208, 313–323.

Haddad, A., 1976. Applied optimal estimation. volume 64. The MIT Press, Cambridge.

Hadler, K., Greyling, M., Plint, N., Cilliers, J.J., 2012. The effect of froth depth on air recovery and flotation performance. Minerals Engineering 3638, 248–253.

Hanumanth, G.S., Williams, D.J.A., 1992. A three-phase model of froth flotation. International Journal of Mineral Processing 34, 261–273.

Hargrave, J., Hall, S., 1997. Diagnosis of concentrate grade and mass flowrate in tin flotation from colour and surface texture analysis. Minerals Engineering 10, 613–621.

Harris, C., Jowett, A., Ghosh, S., 1963. Analysis of data from continuous flotation testing. Transactions of the American Institute of Mining and Metallurgical Engineers , 444–447.

Harris, C., Rimmer, H., 1966. Study of two-phase model of the flotation process. Transactions of the Institution of Mining and Metallurgy , 153–162.

Heindel, T.J., Bloom, F., 1999. Exact and Approximate Expressions for Bubble Particle Collision. Journal of colloid and interface science 213, 101–111.

Hemmings, C., 1981. On the significance of flotation froth liquid lamella thickness. Trans. Inst. Min. Met 90, 96–102.

Höckerdal, E., Frisk, E., Eriksson, L., 2011. EKF-based adaptation of look-up tables with an air mass-flow sensor application. Control Engineering Practice 19, 442–453.

Holtham, P.N., Nguyen, K.K., 2002. On-line analysis of froth surface in coal and mineral flotation using JKFrothCam. International Journal of Mineral Processing 64, 163–180.

Hsu, C.w., Chang, C.C., Lin, C.j., 2010. A practical guide to support vector classification. Technical Report. National Taiwan University. Taipei.

Hua, S., Sun, Z., 2001. Support vector machine approach for protein subcellular localization prediction. Bioinformatics 17, 721–728.

Ito, K., Nakano, R., 2003. Optimizing Support Vector regression hyperparameters based on cross-validation, in: International Joint Conference on Neural Networks, IEEE. pp. 2077–2082.

J. Ralston, S.S.D., Mischuk, N.H., 1999. Bubble-particle attachment and detachment in otation. International Journal of Mineral Processing 56, 133–164.

Jahedsaravani, A., Massinaei, M., Marhaban, M., 2017. Development of a machine vision system for real-time monitoring and control of batch flotation process. International Journal of Mineral Processing 167, 16–26.

Jameson, G.J., Nam, S., Young, M.M., 1977. Physical factors affecting recovery rates in flotation. Miner.Sci.Eng 9, 103–118.

Jia, B., 2010. Distribution of Oil Sands Formation Water in Bitumen Froth. Master's. University of Alberta.

Johnson, N., 2005. A Review of the Entrainment Mechanism and Its Modelling in Industrial Flotation Processes, in: Centenary of Flotation Symposium Australia, Brisbane.

Jolliffe, I., 2005. Principal Component Analysis. Encyclopedia of Statistics in Behavioral Science. .

Jowett, A., 1966. Gangue mineral contamination of froth. British Chemical Engineering 11, 330–333.

K. Runge R. Crosbie, T.R.J.M., 2010. An evaluation of froth recovery measurement techniques. XXV International Mineral Processing Congress, Brisbane, Australia XXV.

Kaartinen, J., Koivo, H., 2002. Machine vision based measurement and control of zinc otation circuit. Studies in Informatics and Control 11, 97–105.

Kadleca, P., Gabrysa, B., Strandtb, S., 2009. Data-driven Soft Sensors in the process industry. Computers & Chemical Engineering 33, 795–814.

Kalman, R.E., 1960. A New Approach to Linear Filtering and Prediction Problems .

Kasongo, T., Zhou, Z., Xu, Z., Masliyah, J., 2000. Effect of Clays and Calcium Ions on Bitumen Extraction from Athabasca Oil Sands Using Flotation. The Canadian Journal of Chemical Engineering 78, 674–681.

Kawatra, S.K., 2002. Froth Flotation - Fundamental Principles. Technical Report. Michigan Technical University.

Khatibisepehr, S., Huang, B., Domlan, E., Naghoosi, E., Zhao, Y., Miao, Y., Shao, X., Khare, S., Keshavarz, M., Feng, E., Xu, F., Espejo, A., Kadali, R., 2013. Soft sensor solutions for control of oil sands processes. The Canadian Journal of Chemical Engineering 91, 1416–1426.

King, R., 2012. Modeling and Simulation of Mineral Processing Systems. Society for Mining, Metallurgy and Exploration Inc, USA. 2 edition.

Kirjavainen, V.M., 1992. Mathematical model for the entrainment of hydrophilic particles in froth flotation. International Journal of Mineral Processing 35, 1–11.

Klimpel, R., 1995. The Influence of Frother Structure on Industrial Coal Flotation, in: HighEfficiency Coal Preparation (Kawatra, ed.), Society for Mining, Metallurgy, and Exploration, Littleton. pp. 141–151.

Kohad, V., 1998. Flotation of sulfide Ores-HZL experience, in: Froth flotation: recent trends, Indian Institute of Mining Engineering, Jamshedpur. pp. 18–41.

Kracht, W., Vallebuona, G., Casali, A., 2005. Rate constant modelling for batch flotation, as a function of gas dispersion properties. Minerals Engineering 18, 1067–1076.

Laplante, A.R., Kaya, M., Smith, H.W., 1989. The Effect of Froth on Flotation Kinetics-A Mass Transfer Approach. Mineral Processing and Extractive Metallurgy Review 5, 147–168.

Laplante, A.R., Toguri, J.M., Smith, H.W., 1983. The effect of air flow rate on the kinetics of flotation. Part 1: The transfer of material from the slurry to the froth. International Journal of Mineral Processing 11, 203–219.

Laurila, H., Karesvuori, J., Tiiili, O., 2002. Strategies for Instrumentation and Control of Flotation Circuits, in: Mineral processing plant design, practice, and control, Vancouver. pp. 2174–2195.

Leiva, J., Vinnett, L., Yianatos, J., 2012. Estimation of air recovery by measuring froth transport over the lip in a bi-dimensional flotation cell. Minerals Engineering 3638, 303–308.

Liaw, A., Wiener, M., 2002. Classification and Regression by randomForest. R News 2, 18–22.

Little, L.H., Poling, G.W., Leja, J., 1961. Infrared spectra of xanthate compounds: iii. Organic solvent effect on the C==S frequency. Canadian Journal of Chemistry 39, 1783–1786.

Liu, J., Xu, Z., Masliyah, J., 2004a. Interaction between Bitumen and Fines in Oil Sands Extraction System: Implication to Bitumen Recovery. The Canadian Journal of Chemical Engineering 82, 655–666.

Liu, J.J., MacGregor, J.F., 2008. Froth-based modelling and control of otation processes. Minerals Engineering 21, 642–651.

Liu, J.J., MacGregor, J.F., Duchesne, C., Bartolacci, G., 2004b. Monitoring of Flotation Processes Using Multiresolutional Multivariate Image Analysis (MR-MIA). IFAC Proceedings Volumes 37, 53–58.

Liu, Q., Wannas, D., Peng, Y., 2006. Exploiting the dual functions of polymer depressants in fine particle flotation. International Journal of Mineral Processing 80, 244–254.

Liua, Y., Chen, J., 2013. Integrated soft sensor using just-in-time support vector regression and probabilistic analysis for quality prediction of multi-grade processes. Journal of Process Control2 23, 793–804.

Lynch, A., 1981. Mineral and coal flotation circuits : their simulation and control. Elsevier Scientific, Amsterdam.

Lynch, A., Johnson, N., Mckee, D., Thorne, G., 1974. The behaviour of minerals in sulphide flotation processes with reference to simulation and control. Journal of the Southern African Institute of Mining and Metallurgy , 349–361.

Maachar A. & Dobby, G.S., 1992. Measurement of feed water recovery and entrainment solids recovery in flotation columns,. Canadian Metallurgical Quarterly 31, 167–172.

Maffei, A.C., de Oliveira Luz, I.L., 2000. Pulp-froth interface control in the flotation column. Developments in Mineral Processing 13, C3–1–C3–7.

Marais, C., Aldrich, C., 2010. The estimation of platinum flotation grade from froth image features by using artificial neural networks., in: International Platinum Conference, Platinum in transition Boom or Bust', The Southern African Institute of Mining and Metallurgy.

Masliyah, J., Zhou, Z.J., Xu, Z., Czarnecki, J., Hamza, H., 2004. Understanding Water-Based Bitumen Extraction from Athabasca Oil Sands. The Canadian Journal of Chemical Engineering 82, 628–654.

McFadzean, B., Marozva, T., Wiese, J., 2016. Flotation frother mixtures: Decoupling the sub-processes of froth stability, froth recovery and entrainment. Minerals Engineering 85, 72–79.

Mehrabi, A., Mehrshad, N., Massinaei, M., 2014. Machine vision based monitoring of an industrial flotation cell in an iron flotation plant. International Journal of Mineral Processing 133, 60–66.

Moolman, D.W., Eksteen, J.J., Aldrich, C., van Deventer, J.S.J., 1996. The significance of flotation froth appearance for machine vision control. International Journal of Mineral Processing 48, 135–158.

Moys, M., 1978. A study of a plug-flow model for flotation froth behaviour. International Journal of Mineral Processing 5, 21–38.

Mulleneers, H., Koopal, L., Bruning, H., Rulkens, W., 2002. Selective Separation of Fine Particles by a New Flotation Approach. Separation Science and Technology 37, 2097–2112.

Neethling, S., Cilliers, J., 2002a. The entrainment of gangue into a flotation froth. International Journal of Mineral Processing 64, 123–134.

Neethling, S.J., Cilliers, J.J., 2002b. Solids motion in flowing froths. Chemical Engineering Science 57, 607–615.

Neethling, S.J., Cilliers, J.J., 2003. Modelling flotation froths. International Journal of Mineral Processing 72, 267–287.

Neethling, S.J., Cilliers, J.J., 2009. The entrainment factor in froth flotation: Model for particle size and other operating parameter effects. International Journal of Mineral Processing 93, 141–148.

Neethling, S.J., Lee, H.T., Cilliers, J.J., 2003. Simple relationships for predicting the recovery of liquid from flowing foams and froths. Minerals Engineering 16, 1123–1130.

Nguyen, A., Schulze, H.J., 2003. Colloidal_Science_of_Flotation. Marcel Dekker Inc, New York.

Nguyen, A.V., Ralston, J., Schulze, H.J., 1998. On modelling of bubbleparticle attachment probability in flotation. International Journal of Mineral Processing 53, 225–249.

Page, P., Hazell, L., 1989. X-ray photoelectron spectroscopy (XPS) studies of potassium amyl xanthate (KAX) adsorption on precipitated PbS related to galena flotation. International Journal of Mineral Processing 25, 87–100.

Parkinson, L., Ralston, J., 2011. Dynamic aspects of small bubble and hydrophilic solid encounters. Advances in Colloid and Interface Science 168, 198–209.

Pita, F.A., 2015. True Flotation and Entrainment of Kaolinitic Ore in Batch Tests. Mineral Processing and Extractive Metallurgy Review 36, 213–222.

Popli, K., Sekhavat, M., Afacan, A., Dubljevic, S., Liu, Q., Prasad, V., 2015. Dynamic modeling and real-time monitoring of froth flotation. Minerals 5, 570–591.

Pow, J., Fairbanks, G., Zamora, W., 1963. Athabasca Oil SandsThe Karl A. Clark Volume. Research Council of Alberta, Edmonon. 1 edition.

Prasad, V., Schley, M., Russo, L.P., Bequette, B.W., 2002a. Product property and production rate control of styrene polymerization. Journal of Process Control 12, 353–372.

Prasad, V., Schley, M., Russo, L.P., Bequette, B.W., 2002b. Product property and production rate control of styrene polymerization. Journal of Process Control 12, 353–372.

Pryor, M., 1965. Mineral Processing. Elsevier Applied Science Publishers. third edition.

P.V., J., Shah, S.L., Kadali, R., 2010. Computer vision based interface level control in a separation cell. Control Engineering Practice 18, 349–357.

Rao, F., Liu, Q., 2013. Froth treatment in Athabasca oil sands bitumen recovery process: A review. Energy & Fuels 27, 7199–7207.

Rao, T., Govindarajan, B., Barnwal, J., 1995. A Simple Model for Industrial Coal Flotation Operation, in: High-Efficiency Coal Preparation (Kawatra, ed.), Society for Mining, Metallurgy, and Exploration, Littleton. pp. 177–185.

Ross, V., 1988. Mass transport in flotation froths. Ph.D. thesis. University of Stellenbosch.

Ross, V., 1989. No TitleDetermination of the contributions by true otation and entrainment during the otation process, in: Int. Colloquium: Developments in Froth Flotation. Southern African Institute of Mining and Metallurgy, Gordon's Bay.

Rubio, J., Souza, M., Smith, R., 2002. Overview of flotation as a wastewater treatment technique. Minerals Engineering 15, 139–155.

Runge, K., McMaster, J., Wortley, M., Rosa, D.L., Guyot, O., 2007. A Correlation Between Visiofroth Measurements and the Performance of a Flotation Cell. Ninth Mill Operators' Conference , 79–86.

Sanford, E., Seyer, F., 1979. Processibility of Athabasca Tar Sand Using a Batch Extraction Unit: The Role of NaOH. CIM Bulletin 72, 164–169.

Savassi, O.N., Alexander, D.J., Franzidis, J.P., Manlapig, E.V., 1998. An empirical model for entrainment in industrial flotation plants. Minerals Engineering 11, 243–256.

Schramm, L., Smith, R., 1987. Some Observations on the Ageing Phenomenon in the Hot Water Processing of Athabasca Oil SandsPart 1. The Nature of the Phenomenon. AOSTRA Journal of Research 3, 195–214.

Schulze, H.J., 1991. The fundamentals of flotation deinking in comparison to mineral flotation. .

Schulze, H.J., 1992. Probability of particle attachment on gas bubbles by sliding. Advances in Colloid and Interface Science 40, 283–305.

Schulze, H.J., Hecker, M., 1984. Physico-chemical elementary processes in flotation: an analysis from the point of view of colloid science including process engineering considerations. Elsevier Amsterdam.

Schwarz, S., Alexander, D., 2006. JKSimFloat V6.1 Plus: improving flotation circuit performance by simulation, in: Mineral Process Modelling, Simulation and Control Conference Proceedings, Sudbury. pp. 35–48.

Scramma, L., Stasiuk, E., Yarranton, H., Maini, B., Shelfantook, B., 2002. Temperature Effects in the Conditioning and Flotation of Bitumen From Oil Sands in Terms of Oil Recovery and Physical Properties, in: Canadian International Petroleum Conference, Petroleum Society of Canada, Calgary.

Seaman, D.R., Manlapig, E.V., Franzidis, J.P., 2006. Selective Transport of attached Particles Across the Froth Phase. Minerals Engineering 19, 841–851.

Sekhavat, M., 2014. Real-Time Updating of a Dynamic Fundamental Model for Froth Flotation Process.

Shao, X., Xu, F., Huang, B., Espejo, A., 2012. Estimation of Bitumen Froth Quality Using Bayesian Information Synthesis: An Application to Froth Transportation Process. The Canadian Journal of Chemical Engineering 90, 1393–1399.

Sharmina, R., Sundararaj, U., Shah, S., Griendb, L.V., Sun, Y.J., 2006. Inferential sensors for estimation of polymer quality parameters: industrial application of a PLS-based soft sensor for a LDPE plant. Chemical Engineering Science 61, 6372–6384.

Shean, B., Cilliers, J., 2011. A review of froth flotation control. International Journal of Mineral Processing 100, 57–71.

Shokri, S., Marvast, M.A., Sadeghi, M.T., Narasimhanc, S., 2016. Combination of data rectification techniques and soft sensor model for robust prediction of sulfur content in HDS process. Journal of the Taiwan Institute of Chemical Engineers 58, 117–126.

Singh, A., Louw, J., Hulbert, D., 2003. Flotation stabilization and optimization. South African Institute of Mining and Metallurgy 103, 581–588.

Smith, B.T., 2004. Lagrange Multipliers Tutorial in the Context of Support Vector Machines. Technical Report. Memorial University of Newfoundland.

Smith, P., Warren, L., 1989. Entrainment of Particles into Flotation Froths. Mineral Processing and Extractive Metallurgy Review 5, 123–145.

Smola, A.J., Scholkopf, B., 2003. A tutorial on support vector regression. Statistics and Computing 14, 199–222.

Snoek, J., Larochelle, H., Adams, R.P., 2012. Practical Bayesian optimization of machine learning algorithms. Technical Report. University of Toronto.

Somasundaran, P., 1980. Role of Surface Chemistry of Fine Sulphides in their Flotation, in: Complex sulfide ores, Institute of Mining and Metallurgy, Rome. p. 118.

Stevenson, P., 2007. Hydrodynamic theory of rising foam. Minerals Engineering 20, 282–289.

Supomo, A., Yap, E., Zheng, X., Banini, G., Mosher, J., Partanen, A., 2008. PT Freeport Indonesia's mass-pull control strategy for rougher flotation. Minerals Engineering 21, 808–816.

Tao, D., 2005. Role of Bubble Size in Flotation of Coarse and Fine Particles: A Review. Separation Science and Technology 39, 741–760.

Trahar, W.J., 1981. A rational interpretation of the role of particle size in flotation. International Journal of Mineral Processing 8, 289–327.

Tuteja, R.K., Spottiswood, D.J., Misra, V.N., 1994. Mathematical models of the column flotation process: A review. Minerals Engineering 7, 1459–1472.

Uribe, S., Vazquez, V., Perez, G., Nava, A., 1999. A statistical model for the concentrate water in flotation columns - ScienceDirect. Minerals Engineering 12, 937–948.

Vapnik, V., 1995. The Nature of Statistical Learning Theory. Springer-Verlag New York, New York.

Vapnik, V., 2006. Estimation of Dependences Based on Empirical Data. Springer-Verlag New York, New York. 1 edition.

Vazirizadeh, A., Bouchard, J., del Villar, R., 2015a. On the relationship between hydrodynamic characteristics and the kinetics of column flotation. Part I: Modeling the gas dispersion. Minerals Engineering 74, 207–215.

Vazirizadeh, A., Bouchard, J., del Villar, R., Ghasemzadeh Barvarz, M., Duchesne, C., 2015b. On the relationship between hydrodynamic characteristics and the kinetics of flotation. Part II: Model validation. Minerals Engineering 74, 198–206.

Ventura-Medina, E., Cilliers, J.J., 2002. A model to describe flotation performance based on physics of foams and froth image analysis. International Journal of Mineral Processing 67, 79–99.

Vera, M.A., Mathe, Z.T., Franzidis, J.P., Harris, M.C., Manlapig, E.V., O'Connor, C.T., 2002. The modelling of froth zone recovery in batch and continuously operated laboratory flotation cells. International Journal of Mineral Processing 64, 135–151.

Villar, R.D., Grégoire, M., Pomerleau, A., 1999. Automatic control of a laboratory flotation column. Minerals Engineering 12, 291–308.

Wang, L., 2016. Entrainment of Fine Particles in Froth Flotation. Ph.D. thesis. The University of Queensland.

Wang, L., Peng, Y., Runge, K., 2016a. Entrainment in froth flotation: The degree of entrainment and its contributing factors. Powder Technology 288, 202–211.

Wang, L., Peng, Y., Runge, K., Bradshaw, D., 2015. A review of entrainment: Mechanisms, contributing factors and modelling in flotation. Minerals Engineering 70, 77–91.

Wang, W., Bergholm, F., Yang, B., 2003. Froth delineation based on image classification. Minerals Engineering 16, 1183–1192.

Wang, W., Stephasson, O., 1999. A robust bubble delineation algorithm for froth images, in: International Conference on Intelligent Processing and Manufacturing of Materials, pp. 471–476.

Wang, X.l., Huang, L., Yang, P., Yang, C.h., Xie, Q.y., 2016b. Online Estimation of the pH Value for Froth Flotation of Bauxite Based on Adaptive Multiple Neural Networks. IFAC-PapersOnLine 49, 149–154.

Warren, L.J., 1985. Determination of the contributions of true flotation and entrainment in batch flotation tests. International Journal of Mineral Processing 14, 33–44.

Welch, G., Bishop, G., 1995a. An Introduction to the Kalman Filter. Technical Report. University of North Carolina.

Welch, G., Bishop, G., 1995b. No Title. An introduction to the Kalman filter .

Wills, B., 1997. Minerals Processing Technology. Pergamon Press, Oxford. 6 edition.

Woodburn, E.T., 1970. Mathematical modelling of flotation processes. Miner.Sci.Eng 2, 3–17.

Wu, C.H., Tzeng, G.H., Lin, R.H., 2009. A Novel hybrid genetic algorithm for kernel function and parameter optimization in support vector regression. Expert Systems with Applications 36, 4725–4735.

Wu, Z., Wang, X., Liu, H., Zhang, H., Miller, J.D., 2016. Some physicochemical aspects of water-soluble mineral flotation. Advances in Colloid and Interface Science 235, 190–200.

Xing, Y., Gui, X., Liu, J., Cao, Y., Lu, Y., 2015. Effects of Energy Input on the Laboratory Column Flotation of Fine Coal. Separation Science and Technology 50, 2559–2567.

Xing, Y., Gui, X., Pan, L., Pinchasik, B.E., Cao, Y., Liu, J., Kappl, M., Butt, H.J., 2017. Recent experimental advances for understanding bubble-particle attachment in flotation. Advances in Colloid and Interface Science 246, 105–132.

Yalcin, E., Kelebek, S., 2011. Flotation kinetics of a pyritic gold ore. International Journal of Mineral Processing 98, 48–54.

Yang, C.C., Shieh, M.D., 2010. A support vector regression based prediction model of affective responses for product form design. Computers and Industrial Engineering 59, 682–689.

Ye, Y., Khandrika, S.M., Miller, J.D., 1989. Induction-time measurements at a particle bed. International Journal of Mineral Processing 25, 221–240.

Yianatos, J., Contreras, F., 2010. Particle entrainment model for industrial flotation cells. Powder Technology 197, 260–267.

Yianatos, J., Contreras, F., Díaz, F., Villanueva, A., 2009. Direct measurement of entrainment in large flotation cells. Powder Technology 189, 42–47.

Yianatos, J., Finch, J., Laplante, A., 1988. Selectivity in column flotation froths. International Journal of Mineral Processing 23, 279–292.

Yoon, R.H., Mao, L., 1996. Application of Extended DLVO Theory, IV: Derivation of Flotation Rate Equation from First Principles. Journal of colloid and interface science 181, 613–626.

Yoon, R.H., Yordan, J.L., 1991. Induction time measurements for the quartzamine flotation system. Journal of colloid and interface science 141, 374–383.

Z. Dai S.S. Dukhin, D.F., Ralston, J., 1998. The inertial hydrodynamic interaction of particles and rising bubbles with mobile surfaces. J. Colloid Interface Sci. 197, 275–292.

Zhang, H., Chen, L., Qu, Y., Zhao, G., Guo, Z., 2014. Support Vector Regression Based on Grid-Search Method for Short-Term Wind Power Forecasting. Journal of Applied Mathematics 2014.

Zheng, X., Johnson, N., Franzidis, J.P., 2006. Modelling of entrainment in industrial flotation cells: Water recovery and degree of entrainment. Minerals Engineering 19, 1191–1203.

Zhu, Q., 2013. Understanding the Role of Caustic Addition in Oil Sands Processing. Ph.D. thesis. University of Alberta.